STRESSES AT THE ROOTS OF CRACKS, NOTCHES AND CAVITIES, AND MECHANISMS OF BRITTLE AND DUCTILE FRACTURE OF METALS

By

HERAMBA KUMAR DEY SARKER

ME
1979
D
SAR
STR

TH
ME/1979/D
Sa738

DEPARTMENT OF MECHANICAL ENGINEERING
INDIAN INSTITUTE OF TECHNOLOGY KANPUR
NOVEMBER, 1979

STRESSES AT THE ROOTS OF CRACKS, NOTCHES AND CAVITIES, AND MECHANISMS OF BRITTLE AND DUCTILE FRACTURE OF METALS

A Thesis Submitted
in Partial Fulfilment of the Requirements
for the Degree of
DOCTOR OF PHILOSOPHY

By
HERAMBA KUMAR DEY SARKER

to the
DEPARTMENT OF MECHANICAL ENGINEERING
INDIAN INSTITUTE OF TECHNOLOGY KANPUR
NOVEMBER, 1979

CERTIFICATE

This is to certify that the present work on 'STRESSES AT THE ROOTS OF CRACKS, NOTCHES AND CAVITIES, AND MECHANISMS OF BRITTLE AND DUCTILE FRACTURE OF METALS' by Heramba Kumar Dey Sarker has been carried out under my supervision and this work has not been submitted elsewhere for the award of a degree.

S N Bandyopadhyay
26/11/

(Dr. S. N. Bandyopadhyay)
Assistant Professor
Department of Mechanical Engineering
Indian Institute of Technology, Kanpur

I.I.T. KANPUR
ENTRAL LIBRARY
A 65898
APR 1981

ME-1979-D-SAR-STR

CERTIFICATE

This is to certify that the present work on 'STRESSES AT THE ROOTS OF CRACKS, NOTCHES AND CAVITIES, AND MECHANISMS OF BRITTLE AND DUCTILE FRACTURE OF METALS' by Heramba Kumar Dey Sarker has been carried out under my supervision and this work has not been submitted elsewhere for the award of a degree.

S N Bandyopadhyay 26/11/79

(Dr. S. N. Bandyopadhyay)
Assistant Professor
Department of Mechanical Engineering
Indian Institute of Technology, Kanpur.

ACKNOWLEDGEMENTS

Author wishes to express sincere gratitude to Dr. S. N. Bandyopadhyay, Assistant Professor, Department of Mechanical Engineering, Indian Institute of Technology, Kanpur for his supervision and constant guidance of this work. Dr. Bandyopadhyay has not only suggested these problems, but also has been immensely helpful in discussing the results and arriving at conclusions.

The author wishes to express his deep sense of gratitude to Dr. B. L. Dhooper, Professor and Head of the Department of Mechanical Engineering for his kind assistance and providing facilities needed for the work.

Thanks are due to Professor G. S. Murthy, Department of Metallurgical Engineering and Professor P. N. Murthy, Department of Aeronautical Engineering for their active co-operation and helpful discussion during the course of this work. The author is also indebted to Prof. N. C. Das Gupta, Regional Engineering College, Durgapur for his inspiration.

The author is very thankful to Messers, D. K. Sarkar, S. L. Srivastava, S. N. Yadav, B. L. Sharma, M. H. Rahman and K. P, Mukherjee for their kind help needed for

this work from time to time.

Thanks are due to Mr. S. S. Pethkar for typing and Mr. B. N. Srivastava for tracing of figures.

Lastly, the author wishes to record a deep sense of appreciation to his wife Bharati for her constant encouragement.

HERAMBA KUMAR DEY SARKER

TABLE OF CONTENTS

				Page
LIST OF TABLES				viii
LIST OF FIGURES				ix
SYNOPSIS				xix
CHAPTER	I	:	INTRODUCTION	1
	1.1	:	Griffith Criterion for Brittle Fracture of Elastic Solids	2
	1.2	:	Barenblatt's Hypothesis at the Tip of an Equilibrium Crack in a Brittle Solid	4
	1.3	:	Elastic Stresses at the Roots of Cracks and Notches	5
	1.4	:	Brittle Fracture at the root of a Crack Like Notch in an Elastic Solid	7
	1.5	:	Bowie's Problem and Stress Intensity Factor for Cracks Emanating from an Edge Notch	8
	1.6	:	Elastic-Plastic Stresses Ahead of Cracks and Notches Under a Plane Strain Condition	10
	1.7	:	Mechanism of Elastic-Plastic Fracture at the root of a Crack Like Notch	12
	1.8	:	Interaction Strain Field Between Spheroidal Cavities and Mechanism of Ductile Rupture Due to Shear Localization	16
	1.9	:	Objective of the Present Work	18

CHAPTER II : LITERATURE REVIEW 20

2.1 : Theories of Brittle Fracture 20

2.2 : Stress Intensity Factor for Cracks Emanating from Machined Notches 23

2.3 : Photoelastic Determination of SIF for a Crack 26

2.4 : Elastic-Plastic Fracture at the Roots of Cracks and Notches 30

2.5 : Ductile Fracture Due to Three Dimensional Hole Growth Inside a Plastically Yielded Material 36

CHAPTER III : STRESS INTENSITY FACTOR FOR A CRACK EMANATING FROM A SEMI-CIRCULAR EDGE NOTCH 43

3.1 : Finite Mellin Transforms of Stresses and Displacements in a Notched Plate 44

3.2 : Stress Intensity Factor for a Crack Radially Emanating from the Root of a Semi-Circular Edge Notched Tension Plate 47

CHAPTER IV : ELASTIC STRESSES AHEAD OF A CRACK LIKE NOTCH 55

4.1 : Elastic Stress Field Ahead of a Crack Like Notch 55

4.2 : Computed Results 65

CHAPTER V : DUCTILE FRACTURE DUE TO INTERACTION OF PROLATE SPHEROIDAL VOIDS 69

5.1 : Shear Localization and Ligament Instability between two Prolate Spheroidal Holes in an Incompressible Elastic Solid under Uniaxial Tension 70

5.2 : Computed Results 77

CHAPTER VI : DISCUSSION 80

6.1 : S.I.F. of a Crack Radially Emanating from Semi-Circular Edge Notch in a Tension Plate 81

6.2 : Elastic Stresses Ahead of a Crack Like Notch 83

6.3 : Mismatch Stresses and Misfit Energy for a Crack Like Notch 87

6.4 : Plane Strain Elastic-Plastic Stresses and Mechanism of Crack Extension at the Root of Yielded tip Crack Like Notch 90

6.5 : Ligament Instability and Shear-Localization Between two Prolate Spheroidal Voids Inside an Incompressible Medium 96

CHAPTER VII : CONCLUSIONS 99

Scope for Future Work 102

FIGURES 103

BIBLIOGRAPHY 201

APPENDIX A

APPENDIX B

APPENDIX C

LIST OF TABLES

Table No.		Page
3.1	Numerical Values of the Co-efficients in Eqns. (3.14), (3.25) and (3.26).	54
5.1	Critical Orientation Angle θ_c for Various Prolateness Ratios (Ref. Fig. 1.14) for an Incompressible Solid	79
B.1	First Few Real Roots of $\phi(z) = 0$, $Re(z) > \frac{1}{2}$ for three Different Flank Angles, $\alpha \leq 1^{\circ}$	B.4
B.2	First Few Real Roots of $\sin 2w(\pi-\alpha) + 2w \sin\alpha = 0$; $Re(w) > 1/2$ for notch opening angle $\alpha = 1^{\circ}$	B.11

LIST OF FIGURES

Figure No. — Page

1.1 An Infinitely Deep Crack-Like-Notch with a Finite Radiused Tip at the Vertex 103

1.2 An Elliptic Through Slit in a Tension Plate [1] 104

1.3 Wedge Loaded Crack -- An Example of a Crack in Stable Equilibrium [6]. Equilibrium Crack Length, $a = [3Eb^3 h^2/16\gamma]^{\frac{1}{4}}$ 105

1.4(a) Smooth Joining of Faces and Cohesive Forces at the Tip of Barenblatt's Equilibrium Crack [9] 106

1.4(b) Successive Expansion of the Crack Edge Under Increasing Extensional Load [9] 106

1.5 Schematic Representation of Stresses at the Root of Cracks and Notches [19, 20, 22] 107

1.6 Zones of Pure Distortion and High Dilatation Ahead of a Blunt Crack-Tip [28] 108

1.7 Bowie Problem for Cracks Radially Emanating from a Hole in a Tension Plate [32] 109

1.8 Cracks Emanating from the Root of (i) A Semi-Circular Edge Notch and (ii) An Infinitely Deep Radiused Tip Notch 110

1.9 Typical Observations on Crack Opening, Tip Blunting and Plasticity Spread Together with Load-Cod Record for a Short Edge-Cracked Flat Beam During Fracture Test of a Metal 111

1.10 Local Plane Strain Plastic Fields Around A Crack Tip (a) Prandtl Field in Region of Crack Tip [63], (b) Modification of Slip-Line Field Due to Crack-Tip Blunting [63], (c) Plot of Stress $\sigma_{\theta\theta}/\sigma_Y$ and Plastic Strain Around the Blunted Notch for $\sigma_Y/E = 1/300$ and Non-Strain Hardened Material [61]. 112

Figure No. Page

1.11 (a) Finite element analysis of stress below a deep charpy notch in pure bending showing the variation of maximum principal stress (σ_{11}) with distance below notch root for various applied loads (P/P_{GY}) [59],

(b) Schematic longitudinal Stress (σ_{yy}) distribution ahead of a rounded notch, radius, ρ , at general yield; rigid/ plastic slip-line field solution. ($\sigma_Y = 2k$, Tresca criterion, and $= \sqrt{3}k$, Mises criterion). 113

1.12 Growing Void Dimensions in the Near-Tip Field Against the Notch Width to Void Distance Ratio [61] 114

1.13 Overlapping Slip-Line Fields in the Ligament between a Pair of Cylindrical Holes [85] 115

1.14 Geometrical Configuration for Calculating the Exterior Strain Fields of two Prolate Spheroidal Holes in Space Under Tension Loading $a > b \ (= c)$. 116

2.1 Co-Ordinate Systems Near the Tip of a Crack in an Infinite Medium [22] 117

2.2 Possible Regions of Localized Flow and Subsequent Void Formation Ahead of a 45° Notched Crack-Tip [85] 118

2.3 Crack-tip Deformation, Plasticity Spread and Isochromatic Photoelastic Coating Observations Ahead of a Short Edge-cracked Mild Steel Beam [178]. 119

2.4 Cumulative Dilatational Ductile Fracture by the Growth and Coalescence of Holes, Discontinuous Plastic Flow Ahead of a Notch [55] 120

2.5 Contours of Stresses and Strains Showing Tension, Compression and Localized Shear: Computed Contours of (a) Axial Stress, (b) Mean Tensile Stress, and (c) Equivalent Plastic Strain [159] 121

Figure No. Page

2.6 Schematic Diagram of the Fracture Process in Aluminium Alloy Single Crystals Age Hardened by the Formation of GP Zones [153] 122

2.7 Strain Concentrated in Localized Shear Bands by large Voids in Copper, Tension Axis being Vertical [160] 123

3.1 Stresses at the Root of a Semi-Circular Edge Notch and a Crack Radially Emanating From its Root 124

3.2 Stress Intensity Factor for a Crack Emanating from the Root of a Semicircular Edge Notch 125

3.3 Isochromatic Fringe Pattern in Dark Field on Plane Transmission Photoelastic Model Specimen at the Tip of a Fine Razor Blade Slit-Cut Emanating from the Root of a Semi-Circular Edge Notch in a Tension Plate 126

3.4 Isochromatic Fringe Pattern in Light Field on Plane Transmission Photoelastic Model Specimen Emanating from the Root of a Semi-Circular Edge-Notch in a Tension Plate. 127

3.5 Isochromatic Fringe Pattern in Dark Field on Plane Transmission Photoelastic Model Specimen at the Tip of a Fine Razor Blade Slit-Cut Emanating from the Root of a Semi-Circular Edge Notch in a Tension Plate 128

4.1 Geometry of a Crack-Like-Notch and Loading on its Flat Faces. 129

4.2 Tangential and Radial Normal Stresses Near the Notch Root Region on 0° plane. Flank Angle , $\alpha = 1^{\circ}$ and Tip Root Radius, $a = 1/100$. 130

4.3 Tangential Normal Stress $\sigma_{\phi\phi}$ Ahead of a Crack-Like-Notch on $\phi = 0^{\circ}$ and 45° Planes, Flank Angle, $\alpha = 1^{\circ}$ and Tip Root Radius, $a = 1/100$. 131

Figure No.		Page
4.4	Tangential Normal Stress $\sigma_{\phi\phi}$ Ahead of a Crack-Like-Notch on $\phi = 0^{\circ}$ and Tip Root Radius, a = 1/100.	132
4.5	Tangential Normal Stress $\sigma_{\phi\phi}$ Ahead of a Crack-Like-Notch on $\phi = 0^{\circ}$ and 45° Planes, Flank Angle, $\alpha = 1o$ and Tip Root Radius, a = 1/100.	133
4.6	Tangential Normal Stress $\sigma_{\phi\phi}$ Ahead of a Crack-Like-Notch on $\phi = 20^{\circ}$ and 50° Planes Flank Angle, $\alpha = 1^{\circ}$ and Tip Root Radius, a = 1/100.	134
4.7	Tangential Normal Stress $\sigma_{\phi\phi}$ Ahead of a Crack-Like-Notch on $\phi = 20^{\circ}$ and 50° Planes. Flank Angle, $\alpha = 1^{\circ}$ and Tip Root Radius, a = 1/100	135
4.8	Tangential Normal Stress $\sigma_{\phi\phi}$ Ahead of a Crack-Like-Notch on $\phi = 20^{\circ}$ and 50° Planes. Flank Angle, $\alpha = 1^{\circ}$ and Tip Root Radius, a = 1/100.	136
4.9	Tangential Normal Stress $\sigma_{\phi\phi}$ Ahead of a Crack-Like-Notch on $\phi = 30^{\circ}$ Plane. Flank Angle, $\alpha = 1^{\circ}$ and Tip Root Radius, a = 1/100.	137
4.10	Tangential Normal Stress $\sigma_{\phi\phi}$ Ahead of a Crack-Like-Notch on $\phi = 30^{\circ}$ Plane. Flank Angle, $\alpha = 1^{\circ}$ and Tip Root Radius, a = 1/100.	138
4.11	Tangential Normal Stress $\sigma_{\phi\phi}$ Ahead of a Crack-Like-Notch on $\phi = 30^{\circ}$ Plane. Flank Angle, $\alpha = 1^{\circ}$ and Tip Root Radius, a= 1/100.	139
4.12	Tangential Normal Stress $\sigma_{\phi\phi}$ Ahead of a Crack-Like-Notch on $\phi = 60^{\circ}$ and 70° Planes. Flank Angle, $\alpha = 1^{\circ}$ and Tip Root Radius, a = 1/100.	140
4.13	Tangential Normal Stress $\sigma_{\phi\phi}$ Ahead of a Crack-Like-Notch on $\phi = 60^{\circ}$ and 70° Planes. Flank Angle, $\alpha = 1^{\circ}$ and Tip Root Radius, a = 1/100.	141

Figure No. Page

4.14 Tangential Normal Stress $\sigma_{\phi\phi}$ Ahead of a Crack-Like-Notch on $\phi = 60^{\circ}$ and 70° Planes. Flank Angle, $\alpha = 1^{\circ}$ and Tip Root Radius, $a = 1/100$. 142

4.15 Tangential Normal Stress $\sigma_{\phi\phi}$ Ahead of a Crack-Like-Notch $\phi = 80^{\circ}$ Plane. Flank Angle, $\alpha = 1^{\circ}$ and Tip Root Radius, $a = 1/100$ 143

4.16 Tangential Normal Stress $\sigma_{\phi\phi}$ Ahead of a Crack-Like-Notch on $\phi=80^{\circ}$ Plane. Flank Angle, $\alpha = 1^{\circ}$ and Tip Root Radius, $a = 1/100$. 144

4.17 Radial Normal Stress $\sigma_{\rho\rho}$ Ahead of a Crack-Like-Notch on $\phi = 0^{\circ}$, 30° and 60° Planes. Flank Angle, $\alpha = 1^{\circ}$ and Tip Root Radius, $a = 1/100$. 145

4.18 Radial Normal Stress $\sigma_{\rho\rho}$ Ahead of a Crack-Like-Notch on $\phi = 0^{\circ}$, 30° and 60° Planes. Flank Angle, $\alpha = 1^{\circ}$ and Tip Root Radius, $a = 1/100$. 146

4.19 Radial Normal Stress $\sigma_{\rho\rho}$ Ahead of a Crack-Like-Notch on $\phi = 0^{\circ}$ Plane. Flank Angle, $\alpha = 1^{\circ}$ and Tip Root Radius, $a = 1/100$. 147

4.20 Radial Normal Stress $\sigma_{\rho\rho}$ Ahead of a Crack-Like-Notch on $\phi = 30^{\circ}$ Plane. Flank Angle, $\alpha = 1^{\circ}$ and Tip Root Radius, $a = 1/100$. 148

4.21 Radial Normal Stress $\sigma_{\rho\rho}$ Ahead of a Crack-Like-Notch on $\phi = 60^{\circ}$ Plane. Flank Angle, $\alpha = 1^{\circ}$ and Tip Root Radius, $a = 1/100$. 149

4.22 Radial Normal Stress $\sigma_{\rho\rho}$ Ahead of a Crack-Like-Notch on $\phi = 20^{\circ}$ and 80° Planes. Flank Angle, $\alpha = 1^{\circ}$ and Tip Root Radius, $a = 1/100$ 150

4.23 Radial Normal Stress $\sigma_{\rho\rho}$ Ahead of a Crack-Like-Notch on ϕ 20° and 80° Planes. Flank Angle, $\alpha = 1^{\circ}$ and Tip Root Radius, $a = 1/100$. 151

4.24. Radial Stress $\sigma_{\rho\rho}$ Ahead of a Crack-Like-Notch on $\phi = 20^{\circ}$ Plane. Flank Angle, $\alpha = 1^{\circ}$ and Tip Root Radius, $a = 1/100$. 152

Figure No. Page

4.25 Radial Normal Stress $\sigma_{\rho\rho}$ Ahead of a Crack-Like-Notch on $\phi = 80^{\circ}$ Plane.Flank Angle, $\alpha = 1^{\circ}$ and Tip Root Radius, a = 1/100. 153

4.26 Radial Normal Stress $\sigma_{\rho\rho}$ Ahead of a Crack-Like-Notch on $\phi = 45^{\circ}$ Plane Flank Angle, $\alpha = 1^{\circ}$ and Tip Root Radius, a = 1/100. 154

4.27 Radial Normal Stress $\sigma_{\rho\rho}$ Ahead of a Crack-Like-Notch on $\phi = 45^{\circ}$ Plane. Flank Angle, $\alpha = 1^{\circ}$ and Tip Root Radius, a = 1/100. 155

4.28 Radial Normal Stress $\sigma_{\rho\rho}$ Ahead of a Crack-Like-Notch on $\phi = 45^{\circ}$ Plane. Flank Angle, $\alpha = 1^{\circ}$ and Tip Root Radius, a = 1/100. 156

4.29 Radial Normal Stress $\sigma_{\rho\rho}$ Ahead of a Crack-Like-Notch on $\phi = 50^{\circ}$ Plane Flank Angle, $\alpha = 1^{\circ}$ and Tip Root Radius, a = 1/100. 157

4.30 Radial Normal Stress $\sigma_{\rho\rho}$ Ahead of a Crack-Like-Notch on $\phi = 50^{\circ}$ Plane . Flank Angle, $\alpha = 1^{\circ}$ and Tip Root Radius, a = 1/100 158

4.31 Radial Normal Stress $\sigma_{\rho\rho}$ Ahead of a Crack-Like-Notch on $\phi = 50^{\circ}$ Plane. Flank Angle, $\alpha = 1^{\circ}$ and Tip Root Radius, a = 1/100. 159

4.32 Shear Stress $\sigma_{\rho\phi}$ Ahead of a Crack-Like-Notch on $\phi = 20^{\circ}$ and 30° Planes. Flank Angle, $\alpha = 1^{\circ}$, a = 0.01. 160

4.33 Shear Stress $\sigma_{\rho\phi}$ Ahead of a Crack-Like-Notch on $\phi = 20^{\circ}$ and 30° Planes. Flank Angle $\alpha = 1^{\circ}$, a = 0.01. 161

4.34 Shear Stress $\sigma_{\rho\phi}$ Ahead of a Crack-Like-Notch on $\phi = 20^{\circ}$ Plane. Flank Angle, $\alpha = 1^{\circ}$, a = 1/100. 162

4.35 Shear Stress $\sigma_{\rho\phi}$ Ahead of a Crack-Like-Notch on $\phi = 30^{\circ}$ Plane. Flank Angle, $\alpha = 1^{\circ}$, a = 1/100. 163

4.36 Shear Stress $\sigma_{\rho\phi}$ Ahead of a Crack-Like-Notch on $\phi = 45^{\circ}$ and 60° Planes. Flank Angle, $\alpha = 1^{\circ}$, a = 0.01. 164

Figure No. Page

4.37 Shear Stress $\sigma_{\rho\phi}$ Ahead of a Crack-Like-Notch on $\phi = 45^\circ$ and 60° Planes. Flank Angle, $\alpha = 1^\circ$, a = 1/100 165

4.38 Shear Stress $\sigma_{\rho\phi}$ Ahead of a Crack-Like-Notch on $\phi = 45^\circ$ Plane. Flank Angle, $\alpha = 1^\circ$, a = 1/100. 166

4.39 Shear Stress $\sigma_{\rho\phi}$ Ahead of a Crack-Like-Notch on $\phi = 60^\circ$ Plane. Flank Angle, $\alpha = 1^\circ$, a = 0.01 167

4.40 Shear Stress $\sigma_{\rho\phi}$ Ahead of a Crack-Like-Notch on $\phi = 50^\circ$ and 70° Planes. Flank Angle, $\alpha = 1^\circ$, a = 1/100. 168

4.41 Shear Stress $\sigma_{\rho\phi}$ Ahead of a Crack-Like-Notch on $\phi = 50^\circ$ and 70° Planes. Flank Angle $\alpha = 1^\circ$, a = 0.01. 169

4.42 Shear Stress $\sigma_{\rho\phi}$ Ahead of a Crack-Like-Notch on $\phi=50^\circ$ Plane. Flank Angle, $\alpha = 1^\circ$, a = 0.01. 170

4.43 Shear Stress $\sigma_{\rho\phi}$ Ahead of a Crack-Like-Notch on $\phi = 70^\circ$ Plane. Flank Angle, $\alpha = 1^\circ$, a = 0.01. 171

4.44 Shear Stress $\sigma_{\rho\phi}$ Ahead of a Crack-Like-Notch on $\phi = 80^\circ$ Plane. Flank Angle, $\alpha = 1^\circ$, a = 0.01. 172

4.45 Shear Stress $\sigma_{\rho\phi}$ Ahead of a Crack-Like-Notch on $\phi = 80^\circ$ Plane. Flank Angle, $\alpha = 1^\circ$, a = 0.01. 173

4.46 Shear Stress $\sigma_{\rho\phi}$ Ahead of a Crack-Like-Notch on $\phi = 80^\circ$ Plane. Flank Angle, $\alpha = 1^\circ$, a = 0.01. 174

4.47 For a Crack Like Notch the Tangential Stress $\sigma_{\phi\phi}$ / T on Radiused Rim $\alpha = 1^\circ$, a = 0.01. 175

Figure No. Page

4.48 Different Stress Field Separation Boundaries Ahead of a Crack-Like-Notch Showing Tensile, Compressive, Pure Distortion and Mixed Stress Regions. $\alpha = 1^{\circ}$, a = 0.01. A-Tensile Stresses, B-Compressive Radial Stress But Tensile Tangential Stress, C- Compressive Tangential Stress But Tensile Radial Stress, D - Compressive Stresses, E-Core Region 176

4.49(a) Mismatch Radial Normal Stress Ahead of a Crack-Like Notch on $\phi = 0^{\circ}$ Plane Plotted Against Flank Angle, α 177

4.49(b) Mismatch Shear Stress Ahead of a Crack-Like Notch on $\phi = 70^{\circ}$ Plane Plotted Against Flank Angle, α 177

4.50 For an Incompressible Elastic Solid the Total Decrease in Misfit Energy of the Body Ahead of a Crack-Like-Notch Shown Against Notch Flank Opening Angle, α . 178

5.1 An Illustration of Eqn. C.1, Concerning the Multipole Charge Distributions [188] 179

5.2 Shear Strain Localization on Ligament Line PQ in $X_3 = 0$ Plane Between Two Prolate Spheroidal Holes Under Uniaxial Tension. 180

5.3 Shear Strain Localization on Ligament Line PQ in $X_3 = 0$ Plane Between Two Prolate Spheroidal Holes Under Uniaxial Tension. 181

5.4 Shear Strain Localization on Ligament Line PQ in $X_3=0$ Plane Between Two Prolate Spheroidal Holes Under Uniaxial Tension. 182

5.5 Shear Strain Localization on Ligament Line PQ in $X_3 = 0$ Plane Between Two Prolate Spheroidal Holes Under Uniaxial Tension 183

5.6 Shear Strain Localization on Ligament Line PQ in $X_3 = 0$ Plane Between Two Prolate Spheroidal Holes Under Uniaxial Tension. 184

5.7 Shear Strain Localization on Ligament Line PQ in $X_3 = 0$ Plane Between Two Prolate Spheroidal Holes Under Uniaxial Tension 185

Figure No. Page

5.8 Shear Strain Localization on Ligament Line PQ in $X_3 = 0$ Plane Between Two Prolate Spheroidal Holes Under Uniaxial Tension 186

5.9 Shear Strain Localization on Ligament Line PQ in $X_3 = 0$ Plane Between Two Prolate Spheroidal Holes Under Uniaxial Tension 187

5.10 Shear Strain Localization on Ligament Line PQ in $X_3 = 0$ Plane Between Two Prolate Spheroidal Holes Under Uniaxial Tension 188

5.11 Interaction Normal Tensile Strain $(e_{11})_{Int.}$ At P Per Unit Remotely Applied Tensile Strain Plotted Against Void Position Angle θ in Degrees. 189

5.12 Interaction Normal Tensile Strain $(e_{11})_{Int.}$ At P Per Unit Remotely Applied Tensile Strain Plotted Against Void Position Angle θ in Degrees 190

5.13 Interaction Normal Tensile Strain $(e_{11})_{Int.}$ At P Per Unit Remotely Applied Tensile Strain Plotted Against Void Position Angle θ in Degrees 191

5.14 Interaction Normal Tensile Strain $(e_{11})_{Int.}$ At P Per Unit Remotely Applied Tensile Strain Plotted Against Void Position Angle θ in Degrees 192

5.15 Interaction Normal Tensile Strain $(e_{11})_{Int}$ At P Per Unit Remotely Applied Tensile Strain Plotted Against Void Position Angle θ in Degrees 193

5.16 Interaction Normal Tensile Strain $(e_{11})_{Int.}$ At P Per Unit Remotely Applied Tensile Strain Plotted Against Void Position Angle θ in Degrees 194

6.1 Plane Strain Plastically Yielded Boundary Ahead of a Crack-Like-Notch for an Ideally Plastic Von-Mises Material For Different Yield Strengths. $\alpha = 1^\circ$, $a = 0.01$. 195

Figure No. Page

6.2 Slip Line Field for 1° Crack Like Notch with Compressive Stresses at Elastic-Plastic Interface 196

6.3 Elastic-Plastic Stress Distribution Below the Root of a Crack-Like-Notch on 0° Plane for a Von Mises Yielding Ideally Plastic Material. 197

6.4 Elastic-Plastic Stress Distribution Ahead of a Crack Like Notch on 45° Plane for a Von Mises Yielding Ideally Plastic Material. 198

6.5 Overlapping Slip Lines for two Elliptic Holes at 60° with Applied Tension for $a/b = 1.6$ 199

6.6 Stress on $X_3 = 0$ Plane Along Line PQ Between Two Prolate Spheroidal Holes in an Ideally Von Mises Yielding Plastic Material. 200.

SYNOPSIS

HERAMBA KUMAR DEY SARKER
Ph. D. THESIS
INDIAN INSTITUTE OF TECHNOLOGY KANPUR

STRESSES AT THE ROOTS OF CRACKS, NOTCHES AND CAVITIES, AND MECHANISMS OF BRITTLE AND DUCTILE FRACTURE OF METALS

The present work mainly considers certain mechanistic aspects of brittle and ductile fracture of materials in the presence of cracks, notches and cavities.

Firstly, a method of finite integral transform is developed to resolve the boundary conditions for a wedge type plate with radiused notch at the vertex. The stress intensity factor for a crack, radially emanating from the root of a semi-circular edge notched plate in tension, is calculated by this method. These SIF results are then verified by the transmission photoelasticity experiments on model specimens.

Secondly, the elastic stresses at the root of a crack-like-notch are found by applying this finite integral transform method. The geometry of this external notch is

chosen in such a manner that the notch is deep enough to satisfy the Griffith's condition, but at the same time the applied stress at the tip may be raised to a high value in the order of fracture strength of the material. The operable mechanism of fracture at the root of such a crack-like-notch has been studied for elastic as well as elastic-plastic materials.

Thirdly, for an incompressible elastic solid under uniaxial tension with small strain, the exterior interaction strain fields between two adjacent prolate spheroidal holes are determined from the multipole expansion of the displacement potentials. The shear strain localization in the ligament is obtained for a number of prolateness ratios and relative angular positions. At a certain orientation, a shear buckling type of folding instability is seen to occur at a particular point in the ligament. In this critical position of voids, not only the shear strain at that folding point in the ligament becomes infinitely large, but also the stress at a particular point in equatorial plane on the void surface increases indefinitely.

Finally, these results for elastic solution on spheroidal holes and crack-like-notches, are utilised to understand the mechanisms of brittle and ductile fracture of metals.

The present analysis shows, when a constant pressure opening loading is applied on the flat faces of a crack-like charpy type notch, a mismatch radial stress on 0°-plane as well as a mismatch shear stress on 70°-plane will be produced. For a brittle elastic solid, this mismatch radial pulling force causes the notch tip to expand. For an elastic-plastic material, the mismatch could produce a generalised Somigliana dislocation on the crack extension plane. The decrease in misfit energy of the body has maxima first at 0.2° and then again at 0.6° notch opening angles, irrespective of the tip blunting. Experimental observations on short edge-cracked beams in different metals confirm this, showing two distinctly different instabilities for elastic-plastic materials. There are five distinct types of stress fields at the root of a crack-like-notch : a small core region very close to the tip followed by a crack-like stress distribution and then, three compressive stress regions at a far field due to the bending action. For a generalised plane stress situation, the radial stress becomes compressive on $47\frac{1}{2}^{\circ}$ plane whereas the tangential component of the stress continues to be tensile ; then around 70° plane both the components become compressive, leaving a pure shear field over a small portion on this plane.

When this model is extended to an elastic-ideally-plastic Von-Mises material, under plane strain condition, a large shear localization is seen to occur on 45° plane, and a high plastic constraint is developed below the notch root on 0° plane. For this material, in the absence of any work-hardening, the maximum plastic constraint factor could easily be as high as five or six. The role of elastic mismatch stresses is discussed in relation to the crack extension on 0° and 45° planes, depending on whether the local instability occurs in a region of high dilatation or pure distorsion with hydrostatic tension. Due to the abrupt release of misfit energy the first local instability can take place in these stagnant flow regions, nucleating micro-cracks or micro-voids close to the last vestige of elastic cores. The criterion for discontinuous ductile dimple fracture ahead of a crack-like-notch largely depends on the stability of growing voids and their coalescence due to high shear strain localization in the ligament between adjacent spheroidal holes. For a Von-Mises ideally plastic material, based on slip-line theory, a simplified analysis on the stress strain fields between two spheroidal holes reveals that there is a thin layer of material in the ligament which does not require any further deformation. As there is a sharp shear strain gradient in this region, this would be favourable for local plastic necking, causing ductile fracture.

These theoretical results agree favourably with the experimental observations.

CHAPTER 1

INTRODUCTION

Strength and toughness are usually regarded as the two most important mechanical properties to select a material for an engineering design. These properties of a material are not determined by an average behaviour of regular atoms, but mainly by their gross disorder in the aggregate. Energy required to create a new surface during the fracture of a truely brittle solid is obtained from the area under the force-displacement relation between the pairs of atoms representing the cohesion of the solid. For these materials, the distance between the two cracks surfaces at the tip is in the order of an interatomic spacing at the onset of a brittle fracture, giving a stress level as high as the cohesive strength of the material. On the contrary, it is observed that the maximum attainable stress at the root of a machined notch is well below the material cohesive strength. Thus, there is a need for a careful study of a crack like notch problem from the mechanics of elastic continuum.

Fig. 1.1 shows the geometry for such a crack like notch. The flank angle and tip-root radius are small, but, always finite. This geometry is very similar to a charpy type notch near the root region, but it is deep enough to satisfy the Griffith's condition [1, 2] at the onset of fracture.

1.1 Griffith Criterion for Brittle Fracture of Elastic Solids

Griffith first made a systematic study on the problem of brittle fracture of solids in the presence of a crack. The Griffith-equation [1, 2] is based on an energy balance criterion. So, Griffith considered the First Law of thermodynamics at the onset of crack instability leading to catastrophic fracture. Fig. 1.2 shows the geometry considered by Griffith. According to Griffith [1, 2], the crack will propagate under a constant applied stress if an incremental increase in crack length produces no change in the total energy of the system. This means, the increased surface energy is compensated by a decrease in elastic strain energy at the onset of crack instability. Thus, a crack will propagate when the decrease in elastic strain energy is at least equal to the energy required to create the new surface. Fig. 1.2 shows a centrally through-cracked plate having crack length 2C which is loaded by a remotely applied stress σ_o. For this geometry, the Griffith's condition at the onset of fracture, gives, $\sigma_o = \sigma_f$ where

$$\sigma_f = \sqrt{[\frac{2E\gamma}{\pi C}]} \quad \text{for plane stress} \tag{1.1}$$

$$= \sqrt{[\frac{2\,E\gamma}{\pi C(1 - \nu^2)}]} \quad \text{for plane strain} \tag{1.2}$$

where γ is the surface energy per unit area, E and ν are Young's modulus and Poisson's ratio of the material respectively.

Griffith's equation is a necessary condition for fracture, but not always sufficient for the growth of a crack [3] . The additional condition to be met is that, there must be an operable mechanism of fracture at the tip of a crack. In our crack-like-notch problem, the geometry has been chosen in such a manner that the notch is deep enough to satisfy the Griffith's condition, but at the same time due to the tip blunting, the applied stress at the tip may be raised to the fracture strength of the material.

The problem of wedge opening of a crack which is explained in Fig. 1.3 has been studied by several investigators [3 - 8] If a crack is sprung open by a fixed wedge inserted between its faces, the equilibrium is stable, because the wedge applies a load on the crack face in a direction normal to the wedge, and hence, as the wedge is moved in, the wedge load point does not suffer any relative displacement in the direction of the load. The crack grows to a fixed length governed by the thickness of the insert. There would be a misfit energy created by the fixed insert of given thickness on the plane of crack extension which must be compensated by the generation of new surfaces at the crack-tip. Measurement of stable crack length by this wedge opening method provides a means for determining the surface energy of brittle materials.

1.2 Barenblatt's Hypothesis at the Tip of an Equilibrium Crack in a Brittle Solid

The equilibrium and finiteness of stresses at the tip of a crack were introduced by Barenblatt [9]. According to Barenblatt, the tensile stress at the contour of an equilibrium crack is finite, and the opposite faces of a crack close smoothly at the end where forces of attraction (or cohesive forces), are present in small zones (Fig. 1.4 (a)). These cohesive forces pull the crack faces together and form a smoothly joined cusp of two crack faces. Griffith was aware of this, and mentioned about the "molecular attractions" across such a crack very close to the tip. The width of this cohesive edge region of a crack is very small compared to the size of the whole crack. The form of the normal section of the crack surface in this cohesive edge region does not depend on the acting loads, and is always the same for a given material under given conditions.

The forces of cohesion that act at the surface of a crack, compensate the applied extensional loads and secure finiteness of stresses with the smooth closing of the crack faces. With an increase in extensional loads, forces of cohesion grow, thus adjusting themselves to the increase in tensile stresses. The crack starts expanding only upon reaching the highest possible forces of cohesion at the edge. The successive expansions of the crack edge under increasing loads are schematically shown in Fig. 1.4 (b). It will be shown later, that if a crack-like-notch does not expand, and the plane section remains plane near the tip, then a generalised Somigliana dislocation will be produced on the crack extension plane.

1.3 Elastic Stresses at the Roots of Cracks and Notches

Fig. 1.5 shows a schematic representation of the stresses on zero degree plane for a notch as well as a crack for comparison purpose. The infinite stress at the tip of a crack has arisen due to the assumption that the crack tip is very sharp, and the tip root radius is exactly zero. The inverse square root singularity of stresses would be valid near the tip region [20 - 27]. But, actually the tip edge boundary is always traction free. Hence, there is a need to study the problem of a crack-like edge notch where the crack is infinitely deep with some finite small flank angle and tip-root radius blunting.

Elasticity equations consist of the equilibrium equations, compatibility condition and the boundary conditions. The very basic fundamental assumption for deriving the equilibrium equation is that, the stresses and strains must remain finite everywhere. Thus, the existence of a strong discontinuity in the formulation of the equilibrium equation is ruled out. However, in the theory of linear homogeneous isotropic Hookean elastic solid, a weak discontinuity in the form of a "generalised Somigliana dislocation" is well recognised in the frame work of infinitesimal strain theory [10 - 13]. Displacement gradient jumps like kinks, foldings etc. are well known in the theory of elasticity. Furthermore, excluding the possibility of generating discontinuity in the form of shock waves or dislocations, it is an impossibility to have a stationary discontinuity in an elastic solid. The second question arises whether a weak stationary discontinuity is possible on the crack extensional plane in an elastic solid if the gradient of stress goes to infinity at a point with continuous finite stresses everywhere. Thomas [12] and Hill [13] have shown that such local abrupt strain jumps are necessarily propagated.

1.4 Brittle Fracture at the Root of a Crack-Like-Notch in an Elastic Solid

Obreimov's [6] cracked body wedge opening problem is of great practical importance in fracture mechanics [29]. Cottrell [3] equated the misfit energy created by a fixed insert of thickness b_o during wedge opening of a crack, with surface energy for stable crack growth. The length of the stable crack growth can be calculated as follows :

$$\text{Misfit energy} = G\, b_o^2 / 4\pi(1 - \nu)$$

$$\text{Surface energy} = 2\,\gamma\, C$$

Hence, the stable crack size is given by,

$$C = G b_o^2 / 8\pi(1 - \nu)\gamma \tag{1.3}$$

where C = equilibrium length of the stable crack extension

γ = the energy required to create a new surface

ν = Poisson's ratio of the material

G = the shear modulus of the material.

b_o = length of stable crack growth

The essential features of equilibrium stable crack growth during wedging are incorporated while formulating our crack-like-notch problem. The present work considers only a finite radiused-tip notch with small flank angle. The author considers this as a more realistic geometrical configuration for a crack. This problem is analogous to hydraulic fracture of rocks and oil-bearing stratum [30].

Thus, there must be two distinctly different conditions for fracture of a crack like notch [31]. Firstly, the mechanistic equilibrium condition satisfying the finiteness and continuity of stresses, strains and strain-derivatives everywhere, and secondly, thermodynamic condition for an energy balance at the crack-tip during the onset of fracture. In many problems the Griffith condition may be sufficient. However, for a crack-like-notch, if one satisfies all the conditions of stresses and strains, the mechanistic condition causes either a radial expansion of the notch tip (or produces a Somigliana dislocation on the crack extension plane due to a mismatch radial stress). If this expansion is taken as a small crack, emanating from the radiused notch tip, like Bowie's problem [32], a brittle fracture criterion for a crack-like-notch can be proposed. Alternatively, one could think of a force of attraction on this dislocation due to its image [33].

1.5 Bowie's Problem and Stress Intensity Factor for Cracks Emanating from an Edge Notch

In an actual service situation, small cracks are generally seen ahead of stress concentrations like notch-roots, key-ways etc. Failures are very often seen to occur due to the initiation of a small crack emanating from these machined notch-groove stress raisers. As soon as a very small crack in the order of few grains starts from a notch root surface, stress field pattern in the root region alters drastically. Bowie [32] considered the fracture behaviour of cracks emanating radially from the diameter of the circular hole in a tension plate as shown in Fig. 1.7. It is very important to understand the effect of notch geometry on the stress-intensity factor for such cracks. The participation of notch taking an equivalent crack length should be known for such geometries [34 - 37].

Fig. 1.8 shows the geometries and the loading patterns of the problems considered. The S.I.F. of such cracks has been calculated by using a finite Mellin transform method [14 - 18], and then reducing the problem to a Weiner-Hopf integral equation, which is finally solved by factorization principle [38]. These results can easily be verified by transmission photoelasticity experiments. In a brittle material, at the onset of fracture, the notch tip starts expanding for a crack like notch, and the fracture load can be calculated by S.I.F. methods used in Bowie's problem. These calculations are found to be very useful to predict the fracture load for a crack in a notched body.

1.6 Elastic-Plastic Stresses Ahead of Cracks and Notches Under A Plane Strain Condition

In metals, plasticity-spread at the root of a crack is well established [39 - 44]. For high strength materials, or materials with small scale yielding property, the plastically yielded zone is normally small, and could be neglected. From Irwin [45] and Orowan's [46] observations, it is known that in Griffith's equation the constant ($= \sigma_f \sqrt{a}$) is a function of the plastic energy dissipation rate and the energy required to create a new surface at the onset of fracture. However, in metals, energy required to create a new surface can be ignored and the Griffith's constant which is a material property can be taken as entirely due to the plastic energy dissipation rate. When the plastic zone is very small compared to the crack size, then either a simple LEFM approach, or Irwin-McClintock's plasticity correction [42] on crack length, may be sufficient to predict the fracture load. Some tip blunting, flank angle opening and plasticity-spread below the root are always noticed in a metal, before the crack becomes unstable in static fracture. So, in an elastic-plastic material it would be more appropriate to treat the geometry of a crack-tip as a blunted notch, rather than always a sharp tip. A brittle fracture of mild steel plate can take place under a plane strain situation, and the local tensile stress of a metal ahead of a crack tip can be several times the yield strength of the material [31, 47 - 50]. During fracture tests of a short cracked beam , it is found that, it would be better to treat the geometry as a crack-like-notch [51]. Recent experiments further confirm the notch-like behaviour of a short crack during the fracture of elastic-plastic materials [51 - 53]. Fig. 1.9 shows a typical load-COD diagram and crack geometry observed at the tip together with the plasticity spread during the fracture tests of a short cracked steel plate. In metals, during the plane strain fracture of a cracked beam, the plastic constraint and shear localization inside the plastic zone normally play the most important roles [54, 55]. One must also distinguish between the yield stress for general yielding and that for local yielding in a region of concentrated stress. Experiments [56, 58] on mild steel notched bars at low temperature have shown a brittle cleavage fracture which is preceded by deformation twinning, and a deformation twinning is further preceded by a slip in the grains ahead of the notch.

For an ideally plastic material, under plane strain deformation, the maximum stress elevation below a notch root depends on [59 - 64] : the yield strength of the material, notch flank angle, and the tip root radius. The

FEM approach adopted by the previous investigators to find the elastic-plastic stress fields ahead of a notch (Figs. 1.10 and 1.11) is far from complete. The major difficulty in applying FEM analysis for such a crack like notch geometry arises due to the matching of the elastic far field with the bifurcations of plane strain plasticity equations. A pure distortional stress in an elliptic field could arise, demanding a bifurcation of hyperbolic differential equation of plane strain plasticity inside the yielded zone [50]. It is known that, during elastic-plastic torsion of a prismatical bar, there could be an elastic core inside the plastically yielded material [50, 65 - 67]. Hence, in strict formulation, the problem is extremely complex, and possibly, the characteristics method would only give an accurate elastic-plastic stress field. Under plane strain deformation, a pure shear field with hydrostatic tension on 45° plane could exist, for a large scale yielding ideally plastic Mises material [28, 123].

1.7 Mechanism of Elastic-Plastic Fracture at the Root of a Crack-Like-Notch

The purpose of measuring the fracture toughness of a material is to determine a single parameter characterising its resistance to fast fracture [68]. The crack toughness is regarded as the critical value of the strain energy release rate for that material at the onset of fracture. Thus, the toughness is also a measure of the resistance to crack extension. The load at which a crack extends needs to be determined with reasonable accuracy.

Irwin-McClintock's plasticity correction method, ASTM recommended secant shift procedure on LEFM and Rice's [69] path independent J-integral in terms of pseudo-potential energy have been partially successful for small scale yielding materials only.

Thus, it is necessary to understand the nature of elastic as well as elastic-plastic stresses ahead of a crack-like-notch. So, in an elastic-plastic solid, the plasticity spread is neither all that small, nor the effect of tip blunting can be ignored. When the fracture stress approaches the yield strength of the material, the effects of tip blunting, plasticity spread and notch toughness rather determine the fracture behaviour. Brittle fracture in steel has, however, been observed at stresses well below the yield strength of the material.

Experiments conducted on charpy type edge notched beams give an idea about the overall deformation produced by localized slip. Using Griffiths-Owen [59] results on charpy notch, Knott [70] and Smith, Cook and Rau [71] have explained the nature of cleavage fracture at the root of a crack. Bilby, Cottrell and Swinden [43] calculated the plastic strain ahead of a sharp notch from dislocation theories. Experimental observation ahead of yielded notch shows, micro-cracks, micro-voids, flow localization, glide band decohesion and other types of localized deformations in the regions of high dilatation and pure distortion. Under plane strain situation, in some materials micro-cracks are produced near the elastic-plastic interface on 0° plane, whereas in other materials micro-voids and their coalescence are seen to occur first on 45° plane inside the plastic zone [72 - 73]. Metal intrusions and extrusions are also visible on the free surface at the onset of crack growth.

It will be shown later, that the nature of mismatch stresses observed at the root of a crack-like-notch is in the form of strain derivative jump. This type of weak discontinuity can travel freely like waves and has a tendency to produce a displacement jump and velocity discontinuity at the elastic-plastic interface [12]. This mismatch can cause asymmetry of the loading as well. As there are two stagnant flow separation regions in a fully developed plastic flow pattern ahead of a crack-like notch, velocity discontinuities in plastic flow [50, 66] can occur in these regions where there are sharp changes in the boundary from elastic to plastic [74 - 75]. The discontinuity in shear strain-derivatives can also occur in these regions [12, 13, 74].

The discontinuous plastic yielding of steel produces a sudden large avalanche of dislocations, so that the local stress can build up very rapidly which might create cleavage micro-cracks ahead of the notch [76 - 78]. There must be a driving force to nucleate a micro-crack in the high dilatational region ahead of the notch, and then this micro-crack needs some applied stress for its growth. Thus, under plane strain condition, in an elastic-plastic material, the crack extension can take place either on 0^{o}plane due to the maximum normal stress in a hyperbolic-parabolic field, or on 45^{o} plane due to the shear stress component elevation in a parabolic-elliptic field.

Fig. 1.12 shows the nature of the formation of micro-cracks and micro-voids inside the plastic zone ahead of a crack-like notch.

1.8 Interaction Strain Field Between Spheroidal Cavities And Mechanisms of Ductile Rupture Due to Shear Localization

In ductile metals, fracture normally occurs by the growth and coalescence of holes. During tensile test of a round mild steel bar, small three dimensional holes are commonly seen to occur in the necked region before final fracture. Orowan [79] first pointed out that at the centre of a round specimen, there would be a large quadrilateral shape prolate spheroidal void in the middle portion of the necked region. This can be explained as follows : from tensor algebra, a uniaxial tension can be resolved into a hydrostatic tension plus two 45° shears [80]. Thus, the hydrostatic tension at the centre of a necked tensile specimen helps to create void around second phase particle, and the rotationally symmetric 45° pure shear stress deforms the void into a spheroid. At the onset of void instability, the prolate-spheroid becomes a quadrilateral shape [81]. In recent years, considerable attention has been focused on the stability of a single growing void and the ligament-fracture-instability of an array of voids in plastically yielded material [135]. The growth and stability of a three dimensional spheroidal hole will be different from the plane growth of cylindrical holes. A cylindrical hole in a plane strain situation, can grow very rapidly beyond a certain nominal strain giving a quadrilateral shape [81]. A single prolate spheroidal hole in an incompressible elastic solid can also become completely unstable violating the energy balance criterion, especially when the prolateness ratio reaches a particular value [82].

McClintock [83] and Berg [84] studied the plastic flow and shear localization between two cylindrical holes considering the traction-displacement boundary conditions for plastic fracture [85]. The plastic flow localization at a point would occur when a non-deforming surface through that point, and some field of relative motion across a thin layer parallel to that surface, does not require any further deformation in the material on either side of the layer (Fig. 1.13).

As elastic stresses in an incompressible solid give a prior history to the elastic-plastic fields at the incipience of yielding, it might be worthwhile to study the exterior interaction strain field between two adjacent prolate spheroidal holes in tension. Fig. 1.14 describes the geometry and tension-loading for a pair of prolate holes in space inside an incompressible solid.

1.9 Objective of the Present Work

The purpose of undertaking this work is, firstly, to study the brittle as well as elastic-plastic fracture behaviour for a crack-like-notch geometry, and secondly, to understand the mechanism of ductile fracture due to the shear localization between two adjacent holes. So, in the present thesis an attempt has been made to investigate the mechanisms of brittle, quasi-brittle and ductile fractures purely from continuum mechanics. However, there are limitations in applying continuum mechanics on such problems [88]. Thus, this work is merely an attempt to explain the brittle fracture postulates of Griffith-Barenblatt, the elastic-plastic fracture concepts of Irwin-Orowan-Bilby-Cottrell, and the ductile fracture theories proposed by Berg-McClintock.

Firstly, the advantage of using finite Mellin transform is demonstrated, mainly to resolve the boundary conditions for a notched plate more easily. Then a general formulation of elastic stress field at the root of an external deep crack like notch is presented. The effect of notch angle on mismatch stresses and misfit energy is emphasized.

Secondly, the stress intensity factors for a crack emanating from a semi-circular edge notch are given.

Analytical S.I.F. result obtained are verified by transmission photoelasticity experiments. This method is then used to find the load carrying capacity of a crack-like-notched plate.

Thirdly, for a Von-Mises ideally plastic material, the elastic-plastic stress field at the root of a crack-like-notch is presented, showing the regions of high dilatation and pure distortion. The roles of mismatch stresses are explained. The nature of velocity discontinuity and local plastic instability in relation to the crack extension is also discussed.

Finally, the theory of ductile fracture is studied considering the ligament instability of two adjacent voids. A highly simplified model is proposed for the shear localization between two prolate spheroidal holes. The entire analysis is based on the exterior interaction strain field in an incompressible elastic medium. This model is then extended to explain the velocity discontinuity and local plastic instability. Void surface critical normal strain is also examined for a number of prolateness ratios.

The above theoretical results on crack-like-notch and spheroidal cavity interactions are compared with experimental observations of others.

CHAPTER II

LITERATURE REVIEW

2.1 Theories of Brittle Fracture

A brittle fracture is normally characterised by a catastrophic failure associated with fast propagation of cracks. The plastic deformation at the tips of cracks or notches is either negligibly small or practically zero. Normally, in high strength materials such types of fracture are commonly seen. Griffith [1, 2] first considered the energy balance at the onset of fracture. Griffith was fully aware that this is a necessary condition, but not sufficient, because at crack-tip the equilibrium condition should also be satisfied. To satisfy the equilibrium condition, Griffith made an attempt to improve the description of the crack-tip, and according to his own estimate the magnitude of the radius of curvature with a finite radiused tip, at the end of the crack is in the order of intermolecular distance.

Mott [4] gave an excellent discussion on the real atomic structure of a crack-tip. Barenblatt [9] first investigated the equilibrium condition and on crack-tip shape systematically from both continuum and atomistic points of view. Barenblatt [9] pointed out, if the equilibrium equations of elasticity were to be satisfied at the crack-tip maintaining the finiteness of stresses, strains and displacements, then the tip of the crack must expand (Fig. 1.4(b)). Fig. 1.4(a) shows the shape of Barenblatt's equilibrium-crack which is different from Griffith's elliptic crack of finite tip root radius. The opposite faces of the crack must close smoothly and the tensile stress at the tip of a crack is always finite. The rounded tip must expand and form a cusp at the tip to satisfy the equilibrium conditions together with the finiteness of stresses, strains and displacements. Obreimov [6], Mott [49], Bailey [5] and Benbow and Roesler [7] considered the stable crack growth by inserting a finite thickness wedge which provided a means of determining the surface energy of brittle materials such as mica. Cottrell [3] emphasized that in this method, the misfit energy created by the fixed insert was expended in generating a new surface for stable crack growth. Barenblatt [9] and Frenkel [29] suggested that the mismatch energy on the crack extension plane would be responsible, either for the expansion of the crack-tip, or for generation of the elastic mismatch displacement. Recently, Cherepanov [89], Cook, Rau and Smith [90] studied the elastic mismatch ahead of a crack-tip as well as on the interface of two-phase materials. Cottrell [31], Bilby, Cottrell and Swinden [43], and Bilby and Eshelby [11] represented the crack-tip deformation by an array of dislocations. Again, it is known from Eshelby's [10] analysis on mismatch in an elastic medium that a generalised Somigliana dislocation has a displacement discontinuity with continuous stresses and strains. This means that the stresses and strains are finite and continuous everywhere, the strain-derivative may be discontinuous at a point. Hill [13], Bilby [91], Thomas [12] and Cherepanov [89] gave considerable emphasis on such folding type of displacement jump in the theory of fracture instability of solids.

Our analysis on the elastic stress field of a crack-like external deep notch shows that such a generalised Somigliana dislocation can be generated on the plane of crack extension. This means, there will be a misfit radial stress developed on the crack extension plane pulling the crack-tip outward for its expansion. This misfit is obtained entirely due to the geometry of a crack-like-notch upon loading. As the notch flank angle is increased, this mismatch on the crack-extension plane decreases rapidly. It will be shown later that the creation of this type of mismatch stress due to loading has to be the operable mechanism, in addition to satisfying the Griffith's energy balance criterion at the onset of fracture.

2.2 Stress Intensity Factor for Cracks Emanating from Machined Notches

Machined notches, grooves and under-cuts are practically unavoidable in designing machine members. Such type of abrupt change in the geometrical configuration always produces stress concentration. The majority of service failures due to fatigue-cracks normally originates from some form of notches or stress concentration regions. The extent of the notch stress field influencing the crack growth behaviour is of great practical importance. As the basic parameter in linear elastic fracture mechanics is the stress intensity factor for a crack, one must evaluate the influence of notch stress field on S.I.F. for such cracked bodies. The initiation of this type of fatigue-crack can be considered in two stages. Firstly, a definite number of cycles is required to fatigue-harden the notch root, and secondly, a small visible crack is initiated from the machined boundary of the notch. Finally, this minutely small crack propagates under the application of the notch stress field, until it becomes so large that the effect of notch geometry on S.I.F. can be neglected completely.

Winnie and Wundt [92] emphasised the practical importance of this problem in the case of failure for turbine hubs. The failure analysis of Hinkly-Point [93] turbine revealed a short fatigue crack propagated from the root of a key-way notch of a turbine hub. Bowie [32] analytically obtained the stress intensity factor of cracks emanating from a hole along the transverse diameter in a tension plate. Newman [34] examined the nature of S.I.F. variation for cracks emanating from various holes and cut-outs. Isida and Nisitani [94], and Yokobori, Kamei and Konosu [95] considered the geometry of cracks emanating from elliptic holes and determined the stress intensity factors in Mode-I and Mode-III respectively. In a recent compendium, Rooke and Cartwright [96] reported many such results for the S.I.F. of cracks emanating from various types of cut-outs and holes. Smith, Jerram and Miller [37] determined the S.I.F. of cracks radially emanating from the root of edge-grooved machined notch in a pin-loaded tension specimen. The participation of notch geometry with fatigue crack length had been investigated by Miller [35] considering an equivalent crack length. According to Smith and Miller [97] at the instant of initiation of a crack from a notch root, the participation of notch depth to crack length could be zero. However, when the crack grows some distance into the bulk material, the equivalent crack length will involve both notch geometry and crack size. Broek [99] studied the propagation of fatigue crack emanating from a semi-circular edge notch in finite plates. His results agree favourably with our calculations. Bowie and Neal [100] and Kutter [101] also considered the stresses at the roots of radiused tip edge slots and cracks emanating from various grooves and cut-outs. In all these results, as expected, at a certain value of C/R ratio the effect of notch geometry on S.I.F. vanishes, the S.I.F. (K_I) is then simply calculated as follows:

For centrally slit cracks $K_I = \sigma_o \sqrt{\pi l/2}$, which is obtained from Griffith's result [1, 2], whereas, for an edge crack $K_I = 1.1215 \ \sigma_o \sqrt{\pi l}$, as derived by Wigglesworth [24], Koiter [25], Sneddon [17] and Sih and Liebowitz [26].

The influence of notch geometry on the size of plastic zone at the tip of a crack symmetrically emanating from a circular hole, was considered by Sumpter and Turner [102]. Mubeen and Bandyopadhyay [52] experimentally observed the effects of notch root radius and crack size on the shape of plastic zone for a crack emanating from a charpy type edge notch.

Therefore, to predict the fracture behaviour of a beam containing a short crack emanating from an edge notch, it is highly important to determine the S.I.F. accurately. Fig. 1.8 shows the details of the geometries considered. In the first problem there is a semi-circular edge-notch in a semi-infinite plate with a crack radially emanating from the notch root but perpendicular to the straight edge, whereas the geometry of the second problem being a very short crack emanating from the radiused tip root of an external deep crack-like-notch.

2.3 Photoelastic Determination of S.I.F. for a Crack

One of the easiest ways of direct observation of the stress field near a crack-tip is by transmission photoelasticity experiments. Photoelastic technique is a powerful experimental tool to study the crack-tip stress-strain fields and for the determination of stress intensity factors for cracks. Wells and Post [103] and Pratt and Stock [104] studied the dynamic stress distribution surrounding a running crack. Wells and Post found that the stress fields around stationary and dynamic cracks were identical. Kobayashi, Harris and Engstrom [105] determined transient displacements and strain distributions in the vicinity of running crack-tips in centrally notched magnesium plates by moire-fringe technique. Dixon and Visser [106] used photoelastic coating technique to determine the plastic zone size around crack-tip in a centrally cracked tension specimen. Their results agreed favourably with those of Dugdale [39] under similar situations. Gerberich [107] measured the thickness variation within the plastic zone in a centrally cracked thin tensile plate specimen. He was, thus, able to determine the third directional principal strain from the condition of incompressibility and hence, he was able to separate all the three principal strains in the plastic enclave surrounding the crack-tip. Kobayashi [108], Theocaris [109], Theocaris and Gdouts [110] and Vitvitskii et al [111] calculated the S.I.F. and also studied the elastic-plastic stress distributions surrounding a crack-tip.

Fig. 2.1 shows the coordinate system adopted by Williams [22] for which the stresses at the root of a crack-tip are given by,

$$\sigma_{xx} = \frac{K_I}{\sqrt{2\pi r}} \left[1 - \operatorname{Sin}\frac{\theta}{2}\operatorname{Sin}\frac{3\theta}{2}\right] \operatorname{Cos}\frac{\theta}{2} + \ldots.$$

$$\sigma_{yy} = \frac{K_I}{\sqrt{2\pi r}} \left[1 + \text{Sin}\ \frac{\theta}{2}\ \text{Sin}\ \frac{3\theta}{2} \right] \text{Cos}\ \frac{\theta}{2} + \ldots$$

$$\tau_{xy} = \frac{K_I}{\sqrt{2\pi r}} \left[\text{Sin}\ \frac{\theta}{2}\ \text{Cos}\ \frac{\theta}{2}\ \text{Cos}\ \frac{3\theta}{2} \right] + \ldots$$

Hence, $$\tau_{max} = \left[\left(\frac{\sigma_{yy} - \sigma_{xx}}{2} \right)^2 + \tau_{xy}^2 \right]^{1/2} = \frac{K_I}{2\sqrt{2\pi r}} . \text{Sin}\ \theta + \ldots \qquad (2.1)$$

Irwin [112] found an excellent agreement between the above theoretical results and those of the photoelastic experiments conducted by Wells and Post [103]. Irwin modified the above equations by adding one more constant term to the R.H.S. of the expression for σ_{xx}. Raju [113] used Irwin's modified equations to calculate the stable crack growth in an elastic-plastic solid.

From the stress-optic law in a photoelastic material [114] the isochromatic fringe order N is related to the difference of principal stresses ($\sigma_{11} - \sigma_{22}$) = 2 τ_{max} , where τ_{max} is the maximum inplane shear stress, and therefore,

$$2\ \tau_{max} = \left[(\sigma_{yy} - \sigma_{xx})^2 + 4\ \tau_{xy}^2 \right]^{1/2} = \frac{Nf_\sigma}{t} \qquad (2.2)$$

where f_σ is the well-known stress-optic constant and t is the thickness of the plate.

Hence, from equation (2.1) and (2.2),

$$K_I = \frac{Nf_\sigma}{t} \cdot \frac{\sqrt{2\pi r}}{\sin\theta} \tag{2.3}$$

When a plastic coating sheet is cemented on the surface of a cracked specimen and loaded, the surface strain would be the same as in the plastic sheet. Hence, for photoelastic coating technique,

$$K_I = \frac{N\ f\ E\sqrt{2\pi r}}{2(1+\nu)\ \sin\theta} \tag{2.4}$$

where the fringe value of the coating sheet f is related to f_ε, the fringe constant of the plastic in terms of strains by the expression, $f = f_\varepsilon / t_c$, ν is the Poisson's ratio and E is the Young's modulus of the metal prototype. Eqns. (2.3) and (2.4) suggest a method of determining the stress intensity factor (K_I) for a crack by making observations of isochromatic fringe orders at different values of r and θ in the close vicinity of the crack-tip.

The accuracy of the photoelastic technique depends on the sharpness of the crack-tip and how closely one could measure the fringe orders at the vicinity of the crack-tip. Knott [63] gave the percentage error involved in the S.I.F. calculations against the distance from the crack-tip. Gerberich [107] used the modified form of Eqn.(2.1) by substituting $K_I = \sigma_o \sqrt{\pi a}$ where σ_c is the applied gross stress, and he obtained the following results:

$$\frac{N}{\sigma_c} = \underline{\sigma_{11} - \sigma_{22}} = \frac{2(1 + \nu)}{f\ E} \sqrt{a/2r} \ . \ \mathrm{Sin}\ \theta \qquad (2.5)$$

Photoelastic techniques have been applied in the present work to study the influences of notch geometry and crack length on the stress intensity factor of a crack radially emanating from the notch-root. These experimental results are then used to verify the theoretical solutions.

2.4 Elastic-Plastic Fracture at the Roots of Cracks and Notches

In metals, plasticity spread ahead of cracks and notches is well-known. For a small scale yielding material, this yielded zone is normally small compared to a crack length and the load-COD diagram is almost linear under plane strain situation. However, in an actual metal, the plastic zone size ahead of the tip of a crack need not always be too small. Simplified LEFM approach may not predict an exact elastic-plastic stress-strain field in such a situation. On the other hand, the results of 45° charpy notch cannot be used either. So, it is as much important to know the elastic-plastic stress field as the cleavage and fibrous micro-mechanisms of fracture at the root of a notch [56 - 59]. This information may provide some basis for evaluating the fracture toughness of a metal [54].

The geometry of the crack-tip is very crucial and the details of the notch tip shape is somewhat controversial [99]. McClintock [115] assumed a V-notch shape at the tip to investigate the shear localization inside the plastic zone on 45^{0} plane. Fig. 2.2 shows Berg-McClintock model [83 - 85] on micro-voids formation on 0^{0} and 45^{0} planes. Fracture can take place entirely due to the nucleation, growth and coalescence of such voids in a highly ductile material. To understand the nature of elastic-plastic stress field, overall deformation produced by the localized slip, and to distinguish between the yield stress for general yielding and that for local yielding, it might be more appropriate to assume the crack-tip as semi-circular.

FEM calculations of Griffiths and Owen [59] showed that the maximum stress elevation would occur very close to the elastic-plastic boundary, but inside the plastic zone. Fig. 1.11 shows these FEM results for a 45^{0} flank angle charpy notch. Rice and Johnson [62], Rice and Rosengren [116] Rice and Hutchinson [117] and Rice and Mcmeeking [61] obtained elastic-plastic stress fields ahead of a blunt crack based on a similar FEM calculations. Fig. 1.10 shows these results at the tip of a blunt crack. According to these authors, the strain hardening has a pronounced effect on the plastic constraint factor. Koning [118] and Andersson [117] reported, the flank-angle opening of the notch must also be incorporated in the geometry along with the tip blunting. In the present work, the author makes an attempt to solve the crack-like-notch problem (Fig. 1.1). Green and Hundy [40], Ewing and Griffiths [120], Richards and Ewing [121] and Rice and Johnson [62] observed that Hill's [50] logarithmic spiral slip-lines near the root of a radiused notch would become straight line giving an uniform stress field at some distance from the blunt notch-tip (Fig.1.10). Thus, the characteristics of the partial differential equations governing the plane strain ideal plasticity, would alter from hyperbolic to parabolic. Furthermore, McClintock's slip-line field analysis at the root of a crack shows the tendency for a pure shear field at 45° plane under a plane strain situation.

Our analysis on a crack-like-notch shows that a pure shear field would be produced at an angle with respect to the plane of symmetry. When this model is extended to an elastic-plastic material under a plane strain situation, a pure shear field would lie on 45° plane at some distance inside the plastically yielded zone.

calculations. Fig. 1.10 shows these results at the tip of a blunt crack. According to these authors, the strain hardening has a pronounced effect on the plastic constraint factor. Koning [118] and Andersson [117] reported, the flank-angle opening of the notch must also be incorporated in the geometry along with the tip blunting. In the present work, the author makes an attempt to solve the crack-like-notch problem (Fig. 1.1). Green and Hundy [40], Ewing and Griffiths [120], Richards and Ewing [121] and Rice and Johnson [62] observed that Hill's [50] logarithmic spiral slip-lines near the root of a radiused notch would become straight line giving an uniform stress field at some distance from the blunt notch-tip (Fig.1.10). Thus, the characteristics of the partial differential equations governing the plane strain ideal plasticity, would alter from hyperbolic to parabolic. Furthermore, McClintock's slip-line field analysis at the root of a crack shows the tendency for a pure shear field at 45° plane under a plane strain situation.

Our analysis on a crack-like-notch shows that a pure shear field would be produced at an angle with respect to the plane of symmetry. When this model is extended to an elastic-plastic material under a plane strain situation, a pure shear field would lie on 45° plane at some distance inside the plastically yielded zone.

Sokolovsky [65], Prager and Hodge [66], Nadai [67] and Hill [50] established that there would be an elastic core inside the plastic region, as a last vestige, during the elastic-plastic torsion of a prismatical bar. Hence, for a plane strain situation, there would be a tendency to form a hinge-point under bending action, inside the plastic zone on 45° plane. Thus the characteristic root [122] of the plane-strain (ideal) plasticity equations are changing inside the plastic region from hyperbolic to parabolic on 0° plane and hyperbolic to parabolic and then elliptic on 45° plane, to match the elastic stresses on the yielded boundary. Therefore, a simple FEM analysis would be inadequate to solve such crack-like-notch problems. It would be more appropriate to formulate the problem analytically, taking into account the bifurcation, velocity discontinuity and local plastic instability. Thomason [123] presented characteristics solutions for hyperbolic-parabolic stress fields at the root of a crack under plane stress situation.

Fig. 2.3 shows Singh's [178] observations on crack-tip deformations and plasticity spread at the root of a short edge-cracked beam. Recent experimental observation shows, in a ductile material under plane strain situation, a crack can extend either on 0°-plane or on 45°-plane (Begley and Landes [72], Rice and Sorensen [73]). Our analysis proves, under a plane strain situation, not only the plastic constraint factor could be in the order of five for a non-strain hardening Von-Mises yielding material, but also only two possible manners in which crack extension can take place. If the material has a small scale yielding property and is more susceptible to form micro-cracks and micro-voids at high dilatational region, then the crack would naturally extend along 0^o-plane. On the contrary, if the material is ductile and more prone to nucleate micro-voids under the action of hydrostatic tension with a pure distortional stress, then the crack can extend along 45^o-plane under plane strain loading. In a ductile metal, if the crack extension does not take place along 45^o plane, then a rapid increase of plastic zone size on 0^oplane on the surface would be visible first, before showing any noticeable slow stable crack growth [53].

Kfouri and Miller [124], Cook, Rau and Smith [90] and Knott [63] proposed a local Griffith-like critical separation energy concept as a criterion for continuing fracture for a stable crack growth. In a ductile material, it may be inappropriate to employ such energy fracture criteria, especially, when the plastic strain dominates fracture mechanisms near tip region, such as nucleation, growth and coalescence of micro-voids or large shear strain localizations. Bilby [91] and McClintock [55] pointed out, the fracture in an elastic-plastic material would depend not only on the high stresses, but also on the strain-localizations. Green and Knott [125], Rice and Sorensen [73], and, Rice and Tracey [126] emphasised that the critical crack opening displacement, δ_{tip} would control the fracture at the onset of stable crack growth. Cherepanov [89] also presented a similar analysis for the crack-tip in the case of an elastically incompressible material. Furthermore, at the onset of ductile fracture, the tip opening displacement attains a size which could be comparable to the localized slip and fracture process zone (Hahn, Rosenfield and Kanninen [127]). In addition to critical δ_{tip} COD method and well-known J-integral criteria, Paris, Tada, Zahoor and Ernst [128] proposed a dimensionless crack growth resistance parameter $T \equiv E(dJ/dl)/\sigma_o^2$ in fully plastic specimens. Paris et al suggested from experiments on long edge-cracked bend specimens that a T-stability criterion would be consistent with the observations of stable and also unstable crack growths. For stable crack growth situation in a ductile metal, R-curve method has also been found to be very useful [129].

In the present work, it will be shown that the mismatch radial stress on 0° plane and mismatch shear stress on 45^{o} plane must play an important role for nucleation of micro-cracks and micro-voids in high dilatational and pure distortional regions. In a ductile metal, if no such micro-defects are produced, then a large shear flow would occur first on the 0^{o}-plane at the end of the plastic zone before any slow stable crack growth. Experiments on elastic-plastic materials show, during a crack extension, that the crack always propagates from the free notch surface to these high strained regions. Hence, the fracture of metals is a problem of surface instability [130] due to the metal intrusions and extrusions which are normally visible [131] on the notch-root free-surface before the onset of stable crack growth.

2.5 Ductile Fracture Due to Three-Dimensional Hole Growth Inside a Plastically Yielded Material

The general behaviour of ductile fracture usually involves the formation of voids (around inclusions or second-phase particles) [133], and the subsequent growth of these voids to coalesce in an unstable manner [134] . Fig. 2.4 shows the discontinuous modes of deformation ahead of a notch root produced by growth and coalescence of holes. McClintock [55, 83, 134], Berg [84], Cottrell [132] and Brown and Embury [86] studied the growth of cylindrical holes and the strain required to coalesce these holes in plastically yielded materials. These models on ductile fracture are based on two dimensional deformation of cylindrical holes. On the contrary, during ductile fracture, three dimensional spheroidal cavities are commonly seen inside a metal, particularly, in a plane strain situation. The criterion of ductile fracture largely depends on the stability of a growing void as well as the shear localization and ligament instability between spheroidal cavities. At present, no such three dimensional analysis is available on plastic unstable hole growth mechanisms, which give a local instability of spheroidal surfaces. Rice and Tracey [135], Brown [136] and Nix and Goods [137] considered the growth of spherical holes in a plastic material. During a plane strain deformation state the holes do not remain spherical and would always have a tendency to grow in spheroidal shape [134], particularly under uniaxial tension.

To understand this three dimensional spheroidal hole growth problem, Singh and Bandyopadhyay [82] studied the shape dependent instability of a single prolate spheroidal hole in a linear elastic incompressible solid in pure shear and in uniaxial tension loading. In a simple shear field, the shear buckling strength is given by the shear modulus times a shape factor [80] . In the presence of a source of disturbance, a single prolate spheroidal hole surface can become unstable under uniaxial tensile field. The source of disturbance could arise in many ways e.g. a dislocation or an inclusion nearby, or a slight imperfection of the shape of the spheroid. As soon as the applied tensile load reaches a critical value the prolate hole will try to rotate at this load to increase its rotational shearing resistance, but it cannot, due to the alignment of its major axis in the direction of the applied tension. Therefore, the prolate hole becomes unstable in Biot's [130] internal shear buckling mode of deformation. In this situation the principal axis of strain can only rotate [138] . When the applied tension exceeds Biot's slide modulus of the surrounding materials in the presence of the void, the Saint-Venant type of torque vanishes and the local torsional stiffness is entirely due to the applied initial stress. Eshelby [139] and McClintock [140] pointed out that such three dimensional analysis in an incompressible rubber-like elastic solid may help to understand the trend of void growth mechanism.

In a plastically yielded material, the three dimensional hole growth mechanism is fairly complex. Pending such an exact solution, in the present work the interaction strain field between two identical prolate holes is considered inside an incompressible elastic solid under uniaxial tension field.

Ductile fracture of metals at high temperature involves other mechanisms, mainly due to the diffusion and gas formation inside the cavities. Incorporating these complexities along with the three dimensional surface deformation together with interaction stress field inside a plastically yielded material, would be a formidable task. One has to rely on, or compare with, the experimental (and simplified theoretical) results obtained by McClintock [134] , Brown and Embury [86], Raj and Ashby [141], Tait and Taplin [142] and El-Sudani and Knott [143]. Orowan's [79] observations at the centre of a necked tensile specimen as well as Perra and Finnie's [81] experimental investigation on plane strain hole growth, explain the shear dominant instability of voids. Bilby, Eshelby, Kundu and Kolbuzweski's [144] work on three dimensional ellipsoidal surface deformation of a liquid embedded in another liquid, is highly valuable for the future work on unstable void growth. Therefore, it is clear that the contribution arising out of the unstable void growth and shear localization between cavities leading to ligament ductile fracture should be established. Recent work reveals that the shear localization in a narrow shear band causes concentrated flow localization leading to ductile rupture through profuse micro-void formation and growth within the band [28].

The application of continuum theory of plasticity to such homogeneous and inhomogeneous flow localization problems is a major subject of interest (Rudnicki and Rice [145], Asaro and Rice [146] and Yamamoto [147]). Experimental work on localized plastic deformation was considered by Green and Knott [125], El-Sudani and Knott [143], Argon [148], Backofen [149], Blackburn and Williams [150], Cottrell and Stokes [151], Beevers and Honeycombe [152] and Price and Kelly [153]. A theoretical model on flow concentration in two-phase materials has been proposed by Cook, Rau and Smith [90]. According to Orowan, the quadrilateral void formation at the centre of a tensile specimen during necking state of large plastic deformation is due to high shear localization at 45° planes. The necking mode of plastic instability [154] and the instability due to abrupt void growth at the centre of a tensile specimen are normally considered as two independent modes leading to fracture [153]. Sih [155], Thomason [156], Hancock and Mackenzie [157] and Hill and Hutchinson [122] considered the details of the mechanism involved in these two fracture modes.

Nevertheless, the basic points put forward by Price and Kelly remained that the void formation at the centre of the specimen observed by Orowan, was mainly due to high shear localization on 45° plane. Fig. 2.5 shows the nature of shear localizations in the tension-compression fieldfor the necked region of a tensile bar [158, 159]. Figs. 2.6 and 2.7 show some examples of shear localizations [160].

The present work shows, if two prolate spheroidal cavity-holes are present in an uniaxial tension field inside an incompressible elastic solid, then there will be one or at the most two high shear strain localization regions. There is a particular angular orientation between the two holes at which large scale plastic yielding on the void surface will be visible together with a high shear localization in the ligament. This model is then extended to a plastically yielded material. Our analysis on plastic stress field satisfies all the necessary and sufficient conditions for velocity discontinuity and plastic instability, put forward by Hill, Kachanov and Berg-McClintock. An approximate analysis based on Hencky-Prandtl slip-line field construction reveals that there exists a small region between the two holes, in which there is a steep shear strain gradient. During an incompressible slow plastic flow, such large shear strain localizations and velocity discontinuity in a narrow band are favourable for local plastic instability, and possibly tantamount to fracture.

CHAPTER III

STRESS INTENSITY FACTOR FOR A CRACK EMANATING FROM A SEMI-CIRCULAR EDGE NOTCH

The problem of determining the stress distribution in a semi-infinite plate which contains straight radial cracks originating from the boundary of a semi-circular cut-out machined notch, and which is subjected to a prescribed loading, is one of great practical importance. Solution of such problems may provide some theoretical justification for the stress relief used in engineering practice. During dynamic service loading, small fatigue cracks are normally seen to emanate from the root of machined stress concentration regions. Cracks ahead of welded joints, key-ways, fillets, under-cuts, roots of turbine blades and gear teeth are a few such examples. Many catastrophic failures in actual service situations occur due to the presence of such short cracks emanating from the root of radiused machined notches. Mubeen and Bandyopadhyay [52, 176, 177] experimentally studied the fracture behaviour of such geometrical bodies in different materials. The most general and complete discussion of the subject would appear to be those due to Bowie [32], Wiggelsworth [24], Newman [34], Nisitani [36], Smith, Jerram and Miller [37] and Rooke and Cartwright [96]. Only a few analytical solutions are available in the literature so far on this type of problems. The present work, firstly, demonstrates the application of finite Mellin transform to such type of problems, and then obtains an asymptotic analytical expression for S.I.F. of crack, after solving a Weiner-Hopf integral equation [38].

3.1 Finite Mellin Transforms of Stresses and Displacements in a Notched Plate

In terms of polar coordinates (ρ, ϕ), as shown in Fig. 3.1(a), an Airy stress function $\chi(\rho, \phi)$ satisfies the well-known biharmonic equation [179]:

$$\left(\frac{\partial^2}{\partial\rho^2} + \frac{1}{\rho}\frac{\partial}{\partial\rho} + \frac{1}{\rho^2}\frac{\partial^2}{\partial\phi^2}\right)\left(\frac{\partial^2\chi}{\partial\rho^2} + \frac{1}{\rho}\frac{\partial\chi}{\partial\rho} + \frac{1}{\rho^2}\frac{\partial^2\chi}{\partial\phi^2}\right) = 0 \quad \dots (3.1)$$

Our unknown $\chi(\rho,\phi)$ has certain properties on the cut-out rim $\rho = a$, which are explained in Appendix A. Following Green and Zerna [164] and Love [180], the stresses and displacements may be expressed in terms of the Airy stress function $\chi(\rho,\phi)$ as follows:

Tangential stress, $\sigma_{\phi\phi} = \dfrac{\partial^2 \chi}{\partial \rho^2}$ (3.2)

Radial stress, $\sigma_{\rho\rho} = \dfrac{1}{\rho^2} \dfrac{\partial^2 \chi}{\partial \phi^2} + \dfrac{1}{\rho} \dfrac{\partial \chi}{\partial \rho}$ (3.3)

Shear stress, $\sigma_{\rho\phi} = \dfrac{1}{\rho^2} \dfrac{\partial \chi}{\partial \phi} - \dfrac{1}{\rho} \dfrac{\partial^2 \chi}{\partial \rho\, \partial \phi}$ (3.4)

In the case of generalised plane stress, radial displacement, u_ρ and tangential displacement, u_ϕ are related to Airy stress function as :

$$E \left(\frac{1}{\rho} \frac{\partial u_\phi}{\partial \phi} + \frac{u_\rho}{\rho} \right) = \left[\frac{\partial^2 \chi}{\partial \rho^2} - \nu \left(\frac{1}{\rho^2} \frac{\partial^2 \chi}{\partial \phi^2} + \frac{1}{\rho} \frac{\partial \chi}{\partial \rho} \right) \right] \qquad \ldots (3.5)$$

$$E \frac{\partial u_\rho}{\partial \rho} = \left[\frac{1}{\rho^2} \frac{\partial^2 \chi}{\partial \phi^2} + \frac{1}{\rho} \frac{\partial \chi}{\partial \rho} - \nu \frac{\partial^2 \chi}{\partial \rho^2} \right] \qquad \ldots (3.6)$$

$$E \left(\frac{1}{\rho} \frac{\partial u_\rho}{\partial \phi} + \frac{\partial u_\phi}{\partial \rho} - \frac{u_\phi}{\rho} \right) = 2(1 + \nu) \left[\frac{1}{\rho^2} \frac{\partial \chi}{\partial \phi} - \frac{1}{\rho} \frac{\partial^2 \chi}{\partial \rho \partial \phi} \right] \qquad \ldots (3.7)$$

E denotes Young's modulus and ν is the Poisson's ratio .

Now, if we transform radial distance ρ to a new variable w through a finite Mellin transform, then the integrated values of transformed stresses, displacements and Airy stress function in the finite range are defined from Appendix A, as,

$$\int_a^{\infty} \chi(\rho, \phi)\, \rho^{2w-2}\, d\rho \text{ , for } \rho \geq a$$

$$= \int_0^{\infty} \chi(\rho, \phi)\, \rho^{2w-2}\, d\rho \quad \text{for } \rho > a \;=\; \bar{\chi}(w,\phi) \qquad (3.8)$$

$$\int_a^{\infty} \sigma_{\phi\phi}(\rho,\phi)\, \rho^{2w}\, d\rho \text{ , for } \rho \geq a$$

$$= \int_0^{a} (\sigma_{\phi\phi})\, \rho^{2w}\, d\rho + \int_0^{\infty} \sigma_{\phi\phi}(\rho,\phi)\, \rho^{2w}\, d\rho \quad \text{for } \rho > a$$

$$= \frac{(\sigma_{\phi\phi})_a\; a^{2w+1}}{2w + 1} + \bar{\sigma}_{\phi\phi}\,(w, \phi) \qquad (3.9)$$

$$\int_a^{\infty} \sigma_{\rho\rho}(\rho,\phi)\, \rho^{2w}\, d\rho \text{ , for } \rho \geq a$$

$$= \int_0^{\infty} \sigma_{\rho\rho}(\rho,\phi)\, \rho^{2w}\, d\rho \text{ , } \quad \text{for } \rho > a \;=\; \bar{\sigma}_{\rho\rho}(w,\phi) \qquad (3.10)$$

$$\int_a^{\infty} \sigma_{\rho\phi}(\rho,\phi)\, \rho^{2w}\, d\rho \text{ , for } \rho \geq a$$

$$= \int_0^{\infty} \sigma_{\rho\phi}\,(\rho,\phi)\, \rho^{2w}\, d\rho \text{ , for } \rho > a \;=\; \bar{\sigma}_{\rho\phi}\,(w,\phi) \qquad (3.11)$$

$$\int_a^{\infty} u_\rho\,(\rho,\phi)\rho^{2w}\, d\rho \text{ , } \quad \text{for } \rho \geq a$$

$$= \frac{(u_\rho\,)_a\; a^{2w}}{2w} + \int^{\infty} u_\rho\,(\rho,\phi)\, \rho^{2w}\, d\rho \text{ , for } \rho > a$$

$$\sigma_{\phi\phi}\Big|_{\phi=\pi/2} = T\left[1 + 4\sum_{k=1,2,3,4,\ldots} (-1)^k \{-(k-1)B_{2k}(a/\rho)^{2k} + k\,C_{2k+1}(a/\rho)^{2k+1}\}\right]$$

for $\rho \geq a$

$$= T\left[1 + \sum_{n=3,4,5,6,\ldots} R_n(a/\rho)^n\right] \qquad (3.14)$$

The coefficients R_n are calculated from Bowie's result [184] who has actually computed the values of B_{2k} and C_{2k+1} and tabulated them. Table 3.1 gives the numerical values of the coefficients, R_n. Now, let us transform the boundary conditions and get the following relations:

On $\phi = 0$ plane, the normal and shear stresses are zero on the flat edge,

$$\bar{x} = d\bar{x}/d\phi = 0, \qquad (3.15)$$

and on $\phi = \pi/2$ plane, the shear stress is zero. This gives,

$$d\bar{x}/d\phi = 0 \qquad (3.16)$$

The tangential normal stress on plane $\phi = \pi/2$ can be written as the sum of the stress from $\rho = a$ to 1 and $\rho = 1$ to infinity. Thus, transforming the tangential normal stresses on $\phi = \pi/2$ plane one gets,

$$2w\,(2w-1)\,\bar{\chi}\,(w,\,\pi/2) = F^{+}(w) + G^{-}(w) \qquad (3.17)$$

where, $F^{+}(w) = \int_{0}^{a} (\sigma_{\phi\phi})_{\pi/2}\,\rho^{2w}\,d\rho + \int_{a}^{1} \sigma_{\phi\phi}(\rho,\pi/2)\,\rho^{2w}\,d\rho$

$$= T\left[\frac{1}{2w+1} + \frac{R_3 a^3}{2w-2} + \frac{R_4 a^4}{2w-3} + \frac{R_5 a^5}{2w-4} + \dots \right.$$
$$\left. \dots + \frac{R_n\,a^n}{2w-(n-1)} + \dots\right] \qquad (3.18)$$

and $G^{-}(w) = \int_{1}^{\infty} \sigma_{\phi\phi}(\rho,\,\pi/2)\,\rho^{2w}\,d\rho\,,\quad \rho > 1 \qquad (3.19)$

On plane $\pi/2$, at $\rho = a$, the radial displacement is zero, so $(u_\rho)_{\rho=a} = 0$ and if we measure u_ϕ with reference to $(u_\phi)_{\rho=a}$, then, the transformed relative displacement at the notch root is,

$$U^{+}(w) = \int_{a}^{1} \phi(\rho,\,\pi/2)\,\rho^{2w-1}\,d\rho\,,\quad \rho > a \qquad (3.20)$$

Thus, following Doran and Buchwald [27], Weiner-Hopf type of integral equation can be constructed satisfying all these boundary conditions. Appendix A describes the nature of the solution of the differential equation for transformed Airy stress function.

From Appendix A,

$$\bar{\chi}(w,\phi) = A\cos(2w-1)\phi + B\sin(2w-1)\phi + C\cos(2w+1)\phi$$
$$+ D\sin(2w+1)\phi + \chi_c(w,\phi) \qquad (3.21)$$

The four unknown constants A, B, C and D are determined from Eqns. (3.15), (3.16) and (3.17), and then, substituting for transformed displacement $\bar{u}_\phi$ to Eqn. (3.20), one obtains,

$$G^-(w) + F^+(w) + 2E\ U^+(w) . \frac{H^+(w)}{H^-(w)} = 0 \qquad (3.22)$$

where,

$$\frac{H^+(w)}{H^-(w)} = \frac{w}{\sin 2\pi w} (\sin^2 \pi w - 4w^2)$$

Thus, following Doran and Buchwald [27], it is possible to separate the function H (w) in two regions S^+ and S^-. The function is analytic in S^+ when superscript (+) sign is written on top of a function, and similarly (-) sign is for analytic function on S^-.

Eqn. (3.22) can also be written in the following form :

$$2E.\ U^+(w)\ H^+(w) + C^+(w) = - G^-(w)\ H^-(w) - C^-(w)$$

$$= - [G^-(w) + C^-(w)] = K(w) \qquad \ldots (3.23)$$

where, $\quad F^+(w)\ H^-(w) \equiv C^+(w) + C^-(w)$

$$C^{-}(w) = T \Big[\frac{1}{2w+1} \{H^{-}(w) - H^{-}(-\tfrac{1}{2})\} + \frac{R_3 a^3}{2w-2} \{H^{-}(w) - H^{-}(1)\} + \frac{R_4 a^4}{2w-3} \{H^{-}(w) - H^{-}(\tfrac{3}{2})\} + \ldots \Big]$$

and

$$C^{+}(w) = T \Big[\frac{H^{-}(-1/2)}{2w+1} + \frac{R_3 a^3}{2w-2} H^{-}(1) + \frac{R_4 a^4}{2w-3} H^{-}(\tfrac{3}{2}) + \ldots \Big]$$

$H^{-}(w)$ can be calculated from Titchmarsh [38] and Noble's [193] formula :

$$H^{-}(w) = e^{-\frac{1}{2\pi i} \int_{\gamma - i\infty}^{\gamma + i\infty} \frac{\ln [H(z)]}{z - w} dz}$$

for $\gamma > \mathrm{Re}(w)$

This integral can be evaluated either numerically or by applying residue theorem in complex plane, considering poles and zeroes of H(z) function.

The stress intensity factor can be obtained from [27] :

$$K_I = \sqrt{\pi}\,\sqrt{1-a}\;C^{+}(0) \qquad (3.24)$$

where, $C^{+}(0) = T \Big[H^{-}(-\tfrac{1}{2}) - \{ \frac{R_3}{2} a^3 H^{-}(1) + \frac{R_4 a^4}{3} H^{-}(\tfrac{3}{2}) + \frac{R_5 a^5}{4} H^{-}(2) + \ldots$

NPUR
NTRAL BRARY

$$H^{-}\left(-\frac{1}{2}\right) = \frac{1}{4H^{+}\left(\frac{1}{2}\right)} = 1.1215\sqrt{\pi/2}$$

$H^{-}(1)$, $H^{-}(3/2)$, $H^{-}(2)$ etc. have been calculated from the properties of generalised factorial function [185]. In terms of Gaussian product $\prod$,

$$H^{-}(w) = \frac{1}{\sqrt{\frac{\pi}{2}\left(1-\frac{2}{\pi^{2}}\right)}} \; \frac{\prod\limits_{m/2>w}\left[\left(1-\frac{w}{m/2}\right)e^{w/\frac{m}{2}}\right]}{\prod\limits_{R_e(\alpha_n)>w}\left[\left(1-\frac{w}{\alpha_n}\right)\left(1-\frac{w}{\alpha_n}\right)e^{w/n}\right]\prod\limits_{R_e(\beta_n)>w}\left[\left(1-\frac{w}{\beta_n}\right)\cdot\left(1-\frac{w}{\beta_n}\right)e^{w/n}\right]} \qquad (3.25)$$

where, α_n are the roots of $\sin\pi w + 2w = 0$ and β_n being the roots of $\sin\pi w - 2w = 0$ equations. These roots have been calculated by Doran and Buchwald [27 , 185]. Taking logarithm on both sides, the asymptotic summation series converges very slowly, but still the series is absolutely convergent (Whittaker and Watson [186]). Table 3.1 gives the computed values of $H^{-}\left(\frac{n-1}{2}\right)$ for $n = 3,4,5,\ldots$. Finally, the stress intensity factor for a crack emanating from a semi-circular edge notch is given by,

$$\frac{K_I}{K_o} = \sqrt{1-a}\ \left[1 - \sum_{n=3,4,5,..} \bar{B}_n\, a^n\right] \qquad (3.26)$$

where, $K_o = 1.1215\ T\sqrt{\pi}\sqrt{l}$ and $\bar{B}_n$ for $n = 3,4,5,....$ are calculated and shown in Table 3.1.

Fig. 3.2 shows the non-dimensional stress intensity factor for a crack radially emanating from the root of a semi-circular edge notch against the ratio of crack size to notch radius. These computed results agree favourably with photoelastic experimental observations. Hence, the three components of stresses, very close to the crack-tip, can be determined from Eqn. 2.1.

TABLE 3.1 Numerical Values of the Coefficients in Eqns. (3.14), (3.25) and (3.26)

n	R_n	$\bar{H}(\frac{n-1}{2})$	$\bar{B}_n$
3	2.65132	0.7314	0.68981
4	-2.60824	0.3164	-0.19571
5	2.71264	0.3149	0.15193
6	-0.35248	0.2839	-0.01424
7	-0.69060	0.3932	-0.03220
8	0.27900	0.1635	0.00464
9	0.28240	0.2616	0.00657
10	-0.21728	0.1544	-0.00265
11	-0.12320	0.2950	-0.00259
12	0.17000	0.1062	0.00117
13	0.04776	0.2262	0.00064
14	0.13464	0.1021	0.00075
15	-0.00896	0.2456	-0.00011
16	0.10780	0.0774	0.00040
17	-0.01216	0.2025	-0.00011
18	-0.08704	0.0750	-0.00027
19	0.02376	0.2162	0.00020
20	0.07128	0.0604	0.00016
21	-0.02960	0.1859	-0.00020
22	-0.05880	0.0586	-0.00012
23	0.03256	0.1955	0.00021
24	0.04840	0.0486	0.00007
25	-0.03360	0.1725	-0.00017
26	-0.04032	0.0480	-0.00006
27	0.03380	0.1820	0.00017
28	0.03380	0.0411	0.00004
29	-0.03304	0.1645	-0.00014
30	-0.02856	0.0407	-0.00003
31	0.03180	0.1721	0.00013
32	0.02400	0.0357	0.00002
33	-0.03008	0.1580	-0.00011
34	-0.02048	0.0354	-0.00002
35	0.02856	0.1647	0.00010
36	0.01700	0.0316	0.00001
37	-0.02736	0.1533	-0.00008
38	-0.01440	0.0315	-0.00001
39	0.02584	0.1596	0.00008
40	0.01216	0.0288	0.00001

CHAPTER IV

ELASTIC STRESSES AHEAD OF A CRACK-LIKE-NOTCH

It is of major interest in fracture mechanics to correlate the local fracture parameters with the fracture toughness of a material. Short cracked beams in metals normally fail at a fracture stress comparable to the yield strength of the material and at the onset of fracture the geometry is very similar to a notch. Analysis on a crack-like-notch may give some valuable insight. Combined effects of bending and tension on crack-tip may produce local strain derivative jumps inside the material ahead of a crack-like-notch. Thus, it is highly important to know the elastic as well as elastic-plastic stresses ahead of a crack-like-notch.

4.1 Elastic Stress Field Ahead of a Crack-Like-Notch

The present section describes a method of determining the elastic stresses at the root of a crack like notch.

Let us consider the geometry shown in Fig. 4.1. An infinitely deep external charpy type notch with a small flank angle, α is loaded by a constant pressure over an unit length on its flat faces. The tip of the notch is rounded by radius 'a'. The rounded portion having included angle, $\pi - \alpha$ at the centre, is traction-free. Thus, our problem is very similar to Obreimov's wedging problem, but with a finite tip-root radius. This problem is also analogous to the bending problem of a 45° charpy-notch studied by Griffiths and Owen [59] or a hyperbolic external deep notch studied by Neuber [19].

We propose to solve this problem by a simple set of imaginary cutting and welding operations [161]. Let us make two straight through cuts on the body, one along ODA and the other along OEC. Thus, we are left out with two identical 90° wedges, symmetrically resting on a single $\pi - \alpha$ semi-circular edge-notched wedge plate. In order to restore these regions to their original form, let us introduce σ and τ as surface-traction distributions applied on the plane DA (and similarly on EC). σ is the normal stress distribution and τ being the shear stress distribution on these 90° - sectors acting on the faces DA and EC. Equal and opposite forces will act on the straight boundaries of the semi-circular notched plate. Fig. 4.1(b) explains the cutting and welding operations. Now, if we rejoin all the three bodies together by welding along lines DA and EC, and leave it as original body, then some displacement mismatch may be generated along these straight lines. Now, if we do not allow any such displacement discontinuities to happen on these planes, by satisfying the continuity of displacements and their derivatives along welded lines DA and EC, then we are left out with the original problem, but with an unknown layer of body force artificially produced on the $\pi - \alpha$ notched sector. The purpose of formulating this problem in such an unconventional manner is to prove later that, when the notch flank angle is in the order of $\frac{1}{2}^{\circ}$ or 1° or even less, there will be a mismatch radial outward pulling force generated on crack extension plane giving an account of Irwin-Barenblatt crack extension force for Obreimov-Mott-Cottrell problem.

For 90°- wedge sector plate, we select D as the origin, with polar co-ordinate (r, θ), as shown in Fig.4.1. The stresses and displacements of this region can easily be calculated by applying a standard Mellin transform method in the zero to infinity range, as suggested by Tranter [16, 163], Koiter and Sternberg [23].

Let $\chi_s(r,\theta)$ be the Airy stress function for this 90°-wedge with σ and τ acting on 0°-plane over the face DA and a pressure loading on the face DM, with-T over $0 \leq r \leq 1$, on 90° plane. Then we have

$$\chi_s(r, \theta) = \frac{1}{2\pi i} \int_{\gamma - i\infty}^{\gamma + i\infty} \bar{\chi}_s(p,\theta)\, r^{-2p+1}\, d(2p)$$

$$= \frac{1}{2\pi i} \int_{\gamma - i\infty}^{\gamma + i\infty} \Big[A(p) \cos \overline{(2p-1)\theta} + B(p) \sin \overline{(2p-1)\theta} + C(p) \cos \overline{(2p+1)\theta} + D(p) \sin \overline{(2p+1)\theta} \Big] . \, r^{-2p+1} \, d(2p) \qquad (4.1)$$

where, r^{2p-1} is the usual Mellin transform multiplying factor with $2p-1$ as transformation parameter on Airy stress function, as explained by Tranter [16], Sneddon [14] and Oberhettinger [18].

Constants A,B,C,D are obtained from the knowledge of stresses on $\theta = 0^\circ$ and 90° planes. After solving four equations $2p(2p-1)\ \bar{x}_s(p,0^\circ) = F(p)$, $2p(2p-1)\ \bar{x}_s(p,\pi/2) = \frac{T}{2p+1}$, $2p\ \bar{x}_s{}'(p,0^\circ) = S(p)$, and $2p\ \bar{x}_s{}'(p,\pi/2) = 0$ ...(4.2)

the constants are

$$A = \frac{F(2p+1)(2p-\sin^2 \pi p) + \frac{1}{2} S(2p-1) \sin 2\pi p - (2p-1)\, T \sin \pi p}{4p(2p-1)\ (4p^2 - \sin^2 \pi p)}$$

$$B = \frac{S(2p-1)(2p+\sin^2 \pi p) + \frac{1}{2} F(2p+1) \sin 2\pi p + 2pT \cos \pi p}{4p(2p-1)\ (4p^2 - \sin^2 \pi p)}$$

$$C = \frac{T \sin \pi p + F(2p + \sin^2 \pi p) - \frac{1}{2} S \sin 2\pi p}{4p(4p^2 - \sin^2 \pi p)}$$

$$D = \frac{S(2p+1)(2p-\sin^2 \pi p) - \frac{1}{2} F(2p+1) \sin 2\pi p - 2Tp \cos \pi p}{4p(2p+1)\ (4p^2 - \sin^2 \pi p)}$$

...(4.3)

Then, the transformed stresses and displacements, may be written in terms of transformed Airy stress function as,

$$\bar{\sigma}_{rr} = \int_0^\infty \sigma_{rr}(r,\theta)\, r^{2p}\, dr = \bar{\sigma}_{rr}(p,\theta) = \frac{d^2 \bar{X}_s}{d\theta^2} - (2p-1)\, \bar{X}_s$$

$$\bar{\sigma}_{\theta\theta} = \int_0^\infty \sigma_{\theta\theta}(r,\theta) r^{2p} dr = \bar{\sigma}_{\theta\theta}(p,\theta) = 2p(2p-1)\, \bar{X}_s$$

$$\bar{\sigma}_{r\theta} = \int_0^\infty \sigma_{r\theta}(r,\theta)\, r^{2p}\, dr = \bar{\sigma}_{r\theta}(p,\theta) = 2p\, \frac{d\, \bar{X}_s}{d\theta}$$

and for a generalized plane stress situation,

$$\bar{u}_r = \int_0^\infty u_r(r,\theta)\, r^{2p-1}\, dr = -\frac{1}{2pE}\left[\frac{d^2 \bar{X}_s}{d\theta^2} - (2p-1)(1+2p\nu)\, \bar{X}_s\right]$$

$$\bar{u}_\theta = \int_0^\infty u_\theta(r,\theta)\, r^{2p-1}\, dr = -\frac{1}{2p(2p+1)E}\left[\frac{d^3 \bar{X}_s}{d\theta^3} + \{1 - 2p(1-\nu) + 4(2+\nu)p^2\}\, \frac{d\, \bar{X}_s}{d\theta}\right] \qquad (4.4)$$

By using standard inversion formula for Mellin transform, one can evaluate the stresses and displacements, provided F and S are known. Based on the Mellin transform, let us keep F(p) and S(p) as unknown quantities, defined on

$\theta = 0$ i.e. $\phi = \pi/2 - \alpha/2$ plane, σ and τ are transformed as,

$$F(p) = \int_0^\infty \sigma_{\theta\theta}(r,0^\circ)\, r^{2p}\, dr \quad \text{and} \quad S(p) = \int_0^\infty \sigma_{r\theta}(r,0^\circ)\, r^{2p} dr \qquad \ldots(4.5)$$

Thus, in terms of two unknown quantities, F and S, we have been able to determine all the stresses and displacements.

Let us now take the finite Mellin transform for the notched $\pi - \alpha$ wedge, with a radiused cut-out machined hole at the vertex. From the knowledge of finite Mellin transform mentioned in section 3.1 and Appendix A , the Airy stress function is given by

$$\chi(\rho,\phi) = \chi_{\text{field}}(\rho,\phi) + \chi_{\text{core}}(\rho,\phi) \qquad \ldots(4.6)$$

where,

$$\chi_{\text{core}}(\rho,\phi) = \frac{1}{4} a^2 \left(\frac{\rho^2}{a^2} - 1\right) \cdot \sum_{m=0,1,2,3,\ldots} (-1)^m \frac{(\ln \rho/a)^{2m+1}}{(2m+1)!} \cdot \frac{d^{2m} \sigma_{\phi\phi a}}{d\phi^{2m}} \qquad \ldots(4.7)$$

$$\chi_{\text{field}}(\rho,\phi) = \frac{1}{2\pi i} \int_{\gamma - i\infty}^{\gamma + i\infty} \left[\bar{A}(w,\phi).\ \cos \overline{(2w-1)\phi} + \bar{C}(w,\phi) \cos \overline{(2w+1)\phi} \right] \rho^{-2w+1}\, d(2w) \qquad (4.8)$$

The constants are determined from the stresses given on $\phi = \pi/2 - \alpha/2$ plane, and vanishing shear stress on $\phi = 0$ plane. Therefore;

$$\bar{A}(w,\phi) = \frac{\left(F(w) + \frac{T\beta a^{2w+1}}{2w+1}\right) \sin(2w+1)(\pi/2 - \alpha/2) + S(w)(2w-1)\cos(2w+1)(\pi/2 - \alpha/2)}{2w\,(2w-1)\left[\sin 2w\,(\pi-\alpha) + 2w\sin(\pi-\alpha)\right]}$$

$$\bar{C}(w,\phi) = -\frac{\left(F(w) + \frac{T\beta a^{2w+1}}{2w+1}\right) \sin\,(2w-1)(\pi/2-\alpha/2) + S(w)\cos(2w-1)(\pi/2-\alpha/2)}{2w\left[\sin 2w\,(\pi-\alpha) + 2w\sin(\pi-\alpha)\right]}$$

...(4.9)

$2w$ is the usual Mellin transform parameter for the notched wedge portion, with ρ being measured from the centre of the hole, and angle ϕ is measured from the symmetric plane. On cutting plane DA, the transformed variables p and w are basically the same parameter provided one separates out the notch-stress

$\sigma_{\phi\phi}(a, \overline{\pi/2 - \alpha/2}) = \sigma_{\theta\theta}(0, 0^{\circ}) = \beta\, T$ from the integral transformed function, defined in Appendix A and section 3.1. Hence, if F and S are known, then it is a matter of simple algebra to determine the stresses and displacements for the $\pi-\alpha$ notched wedge portion, using the properties of inversion Mellin transform.

Equating the normal and tangential displacements on plane DA , for both 90° sector and $\pi-\alpha$ notched wedge, one gets,

$$u_r(r,0^{\circ}),\ \text{for } 0 \leq r \leq \infty \ = \ u_\rho\left(\rho, \overline{\pi/2 - \alpha/2}\right), \quad \text{for } a \leq \rho \leq \infty$$

and

$$u_\theta(r,\ 0^{\circ}),\ \text{for } 0 \leq r \leq \infty \ = \ u_\phi\left(\rho,\ \overline{\pi/2 - \alpha/2}\right), \quad \text{for } a \leq \rho \leq \infty \qquad (4.10)$$

Solving these two equations, F and S are determined explicitly, and by using inversion formula one can at once determine σ and τ on plane DA or plane EC for that matter. If F and S are found by this method, then one can obtain the stresses and displacement fields at the root of a notch. For a given flank angle and tip-root radius, this general method would give the stresses and displacements in an external deep notch.

Fracture mechanics people only accept the stress field near the root of a crack, as independent of Poisson's ratio of the material [20 - 27] . During the fracture of a high strength material, the notch opening angle and the tip blunting are normally very small. So, we are merely interested in incorporating the blunting effect together with a small flank angle opening to the present knowledge of crack stress field. Therefore, the requirement of fracture mechanics demands for the understanding of the stress near the tip of a crack-like- external deep notch, particularly when α is very small and the tip root radius 'a' is also sufficiently low.

If we rule out the possibility of any displacement discontinuity mismatch or jump on the plane of cutting after rewelding, then from the continuity of stresses, the transformed displacement equations in terms of a common transform variable $p = w$, would give as,

$$\left[\frac{d^2 \bar{\chi}_s}{d\theta^2}\right]_{\theta = 0 \text{ plane}} \text{for } 0 \leq r \leq \infty \quad = \quad \left[\frac{d^2 \bar{\chi}_s}{d\phi^2}\right]_{\phi = \pi/2-\alpha/2 \text{ plane}} \text{for } a \leq \rho \leq \infty \qquad \ldots(4.11)$$

and

$$\left[\frac{d^3 \bar{\chi}_s}{d\theta^3}\right]_{\theta = 0 \text{ plane}} = \left[\frac{d^3 \bar{\chi}_s}{d\phi^3}\right]_{\phi = \pi/2-\alpha/2 \text{ plane}}$$

$$\text{for } 0 \leq r \leq \infty \qquad\qquad \text{for } a \leq \rho \leq \infty \qquad \ldots(4.12)$$

Thus, from these two equations, F and S can be solved, for a crack-like-notch geometry. Once F and S are known, σ and τ stresses can be found from the inversion theorem of Mellin transform. For the equilibrium of 90° sector, all resultant forces and moments acting on the body are equated to zero, and thereby β is determined numerically for a given value of a and α. $(\sigma_{\phi\phi})_{\rho=a}$ is determined from the traction-free boundary condition $\chi(a, \phi) = 0$ on the rim, following Green and Zerna [164] given in Appendix A. Finally, tangential normal stress $\sigma_{\phi\phi}$, radial normal stress $\sigma_{\rho\rho}$ and the shear stress $\sigma_{\rho\phi}$ are evaluated from the inversion theorem of Mellin transform. The evaluation of stresses, involve the application of residue theorem, considering the poles of the denominator functions in the complex plane, and these are described in Appendix B.

4.2 Computed Results :

The radial, tangential and shear stresses are evaluated by applying the residue theorem in complex plane, provided the roots of the two equations are known before hand. The first few roots of $\sin 2z(\pi-\alpha) + 2z \sin\alpha = 0$ equation are given in Table B.2 for notch flank angle $\alpha = 1^{\circ}$. Whereas, the roots of $\phi(z) = 0$ equation for 1° flank angle are reported in Table B.1. The discussion is confined to $\alpha = 1^{\circ}$ notch flank angle, unless otherwise stated. Only the misfit stresses are calculated at different notch angles. The contours of the integral in all cases were closed over a semi-circular path, for which the contribution vanishes. The path of integration was chosen in the range of $1/2 < z < 1/2 + \lambda$, where λ is a fixed value for a given notch angle α. In this strip, the functions remain analytic. Hence, by summing up all the residues, the stresses are calculated. Fig. 4.2 shows the radial and tangential normal stresses on 0°-plane very close to the rim in the range of $a \leq \rho \leq 10\,a$. Equation (B.8) given in Appendix B was used to calculate the stresses in the range of $a \leq \rho \leq 2a$. Airy stress function χ_{core} is mainly dominant in this region. The stresses are finite and behave like an external deep hyperbolic notch [19]. Figs. 4.3 to 4.16 show the variation of tangential normal stress $\sigma_{\phi\phi}$ against ρ/a on different planes in certain ranges. As the stresses are varying from very small to fairly large values, this type of plot was found to be the most convenient. The stresses are plotted at an interval of 10° starting from 0° to 80°. Stresses on other planes are also calculated but not presented here. Figs. 4.3 to 4.5 show the plot for $\sigma_{\phi\phi}$ on 0° and 45° planes in three different ranges. Similarly, Figs. 4.6 to 4.8 show $\sigma_{\phi\phi}$ on 20° and 50° planes, and so on.

Figs. 4.17 to 4.31 show radial stresses $\sigma_{\rho\rho}$ on different planes. Fig. 4.17 and 4.18 show the variation of $\sigma_{\rho\rho}$ on 0°, 30° and 60° planes for different ranges of ρ/a. Figs. 4.19, 4.20 and 4.21 describe the mismatch $[\sigma_{\rho\rho}]_M$ radial stress near $\rho/a = 100$ on these planes. The radial stresses are calculated from Eqn. (B.12) based on residue theorem. Figs. 4.22 to 4.25 show the nature of $\sigma_{\rho\rho}$ against distance ρ/a on 20° and 80° planes. Similarly, the radial stresses on 45° and 50° planes are also shown in Figs. 4.26 to 4.31. All these stresses are drawn for 1° notch flank angle. The jump radial stress on 0° plane at $\rho = 100\ a$ is calculated with a high degree of accuracy. There was no mismatch (or jump) in $\sigma_{\phi\phi}$ component of stresses anywhere, on the contrary for $\sigma_{\rho\rho}$ component the jump is seen to be maximum on 0° plane. So, there is a mismatch between the far and near field regions for the radial stress.

The shear stresses $\sigma_{\rho\phi}$ are obtained from Eqn. (B.13) again calculating the residues. Figs. 4.32 to 4.35 show the plot for the shear stress on 20° and 30° planes. Figs. 4.36 to 4.39 describe the nature of $\sigma_{\rho\phi}$ on 45° and 60° planes. Similarly, $\sigma_{\rho\phi}$ on 50° and 70° planes are given in Figs. 4.40 to 4.43, and so on. The maximum jump in shear stress is seen to occur on 70° plane. The tangential stress on the rim $\rho = a$ is calculated from Eqn. (B.10) by evaluating the integral. This line integral is first reduced to a real integral in the range of 0 to $+\infty$, and then by applying Simpson's rule the numerical values are obtained at different angles. Fig. 4.47 shows the nature of rim stress on $\rho = a$ for the range of $-89.5 \leq \phi \leq +89.5$. This agrees favourably with the results of others [181 - 184]. Fig. 4.48 shows the different regions of stress fields summarising all the results. There are five regions of different stress fields ahead of 1° flank angle crack like notch. The stresses beyond $\phi > 89.5°$ i.e. on the 90° - plate, are also calculated from Eqn. (4.1) for a few limited cases. First few typical roots of equation $\phi(z) = 0$ are shown in Table B.1 for $\alpha = 0.2°$ and 0.6° notch flank angles. The values of the maximum jump stresses are calculated at 0.1°, 0.2°, 0.3°, 0.4°, 0.5°, 0.6°, 0.8°, 0.9°, 1° etc.to study the variation of mismatch. Fig. 4.49 shows these jump radial stress (on 0° plane) as well as the jump shear stress (on 70° plane). The misfit energy for the entire body is shown in Fig. 4.50. It is interesting to note that the decrease in misfit energy for a crack like notch has maxima first at 0.2° and then again at 0.6° notch flank angle.

CHAPTER V

DUCTILE FRACTURE DUE TO INTERACTION OF PROLATE SPHEROIDAL VOIDS

Normally, in a ductile material, a large plastic zone size is developed below a notch root. By plastic constraint there will be some increase in local tensile stress ahead of the notch, but the constraint effect may not be so high as to nucleate or to propagate micro-cleavage-cracks, rather it could initiate micro-voids more easily. The unstable growth of voids and the stability of the ligament region between two adjacent holes usually determine the criteria for void coalescence at large strains.

The process of ductile fracture involves, firstly, the mechanics of deformation due to surface interactions, secondly, shear-localizations in the ligament between two holes, and lastly, high local normal-strain-concentration on the void surface [55, 132] . The interaction effects between two growing spheroidal holes in space are studied in relation to the stability of deformation in the ligament region.

5.1 Shear Localization and Ligament Instability Between Two Prolate Spheroidal Holes in an Incompressible Elastic Solid Under Uniaxial Tension

From the previous discussion it is clear that the shear strain localization between two three dimensional holes could cause a local instability inside the material. Therefore, it is of great practical importance to determine the maximum shear strain concentration between two spheroidal holes. An attempt has been made in this chapter to calculate the exterior strain field at different points between two spheroidal regions. The method used here is fairly general and would be applicable to two ellipsoidal regions. Cracks, cylinders and spheroids are merely special cases which can be derived from the general formulation. The numerical computations are confined to a pair of prolate spheroidal holes in space inside an incompressible elastic solid which is shown in Fig. 1.14. McClintock [134] emphasised the importance of this particular geometry in relation to the shear localization between two voids leading to ductile rupture.

In an infinite elastic medium, the displacement u_i at an exterior point for an ellipsoidal region is given by [162] :

$$u_i^c = \frac{1}{16\pi G(1-\nu)} p^T_{jk} \psi_{,ijk} - \frac{1}{4\pi G} p^T_{ik} \phi_{,k} \qquad (5.1)$$

where, $\phi = \int_V dv / |\mathbf{r} - \mathbf{r}_o|$ is the harmonic Newtonian potential, and ψ is the biharmonic potential of attracting matter of unit density filling the ellipsoidal volume. Therefore, $\psi = \int_V |\mathbf{r} - \mathbf{r}_o| dv$, the integrals being taken over the volume V. p_{ij} denote stresses in usual tensor notation. A repeated suffix is always summed over the values 1,2,3 co-ordinates and suffixes preceded by a coma denote differentiation notation. The superscript T on u_i^T , e_{ij}^T , p_{ij}^T denotes the transformed displacements, strains and stresses after loading, whereas the superscript c on u_i^c , e_{ij}^c, p_{ij}^c denotes the constrained displacements, strains and stresses respectively. G is the shear modulus and ν being the Poisson's ratio of the material. The definitions of constrained and transformed strains are explained by Eshelby [161, 187].

The biharmonic potential ψ can again be expressed in terms of harmonic potentials of solids bounded by the ellipsoidal surface having variable densities as,

$$\psi = r^2\phi - 2x_i \int_V \frac{x_i' dv}{|\mathbf{r} - \mathbf{r}_o|} + \int_V \frac{r'^2 dv}{|\mathbf{r} - \mathbf{r}_o|} \qquad (5.2)$$

In other words, $\psi = (x_1^2 + x_2^2 + x_3^2)\,\phi_1 - 2(x_1\phi_{x_o} + x_2\phi_{y_o}$

$$+ x_3\phi_{z_o}) + (\phi_{x_o^2} + \phi_{y_o^2} + \phi_{z_o^2}) \qquad (5.3)$$

Thus, the displacements are,

$$u_i^c = \frac{1}{16\,\pi G(1-\nu)}\, p_{jk}^T \,\frac{\partial^3}{\partial x_i \partial x_j \partial x_k}\Big[(x_1^2 + x_2^2 + x_3^2)\phi_1 + (\phi_{x_o^2} + \phi_{y_o^2} + \phi_{z_o^2}) - 2(x_1\phi_{x_o} + x_2\phi_{y_o} + x_3\phi_{z_o}) \Big] - \frac{1}{4\pi G}\, p_{ik}^T \,\frac{\partial \phi_1}{\partial x_k} \qquad (5.4)$$

where,

$$\phi_1 = \int_V dv/\,|\mathbf{r}-\mathbf{r}_0|\ , \quad \phi_{x_o} = \int_V x_1 dv/|\mathbf{r}-\mathbf{r}_0|\ ,$$

$$\phi_{y_o} = \int_V x_2 dv\,/\,|\mathbf{r}-\mathbf{r}_0|\ , \quad \phi_{z_o} = \int_V x_3 dv/\,|\mathbf{r}-\mathbf{r}_0|\ ,$$

$$\phi_{x_o^2} = \int_V x_1^2\, dv/\,|\mathbf{r}-\mathbf{r}_0|\ , \quad \phi_{y_o^2} = \int_V x_2^2 dv/\,|\mathbf{r}-\mathbf{r}_0|$$

and $\phi_{z_o^2} = \int_V x_3^2\, dv\,/\,|\mathbf{r}-\mathbf{r}_0|$

The volume integral is taken within the ellipsoidal region i.e.

$$\frac{x_1^2}{a^2} + \frac{x_2^2}{b^2} + \frac{x_3^2}{c^2} = 1 \quad \text{with origin 0 at } x_1 = 0,$$

$x_2 = 0$, $x_3 = 0$.

The subscript notation on ϕ has the following meaning, e.g. ϕ_p gives a harmonic potential outside an ellipsoidal region having density distribution inside the body varying as p_{th} law, (as commonly used in gravitational field calculations). Thus, ϕ_1(or ϕ) represents the exterior potential at a point having unit density of the ellipsoid, ϕ_{x_0} stands for exterior potential with ellipsoid density linearly varying with x_1 along axis -1. Similarly, $\phi_{x_0}{}^2$ represents exterior potential having ellipsoid density increasing with $x_1{}^2$ law inside the body along axis - 1, and so on.

Applying Hooke's law on Eqn. (5.4) and then simplifying in terms of strain components, the displacements are expressed as :

$$
\begin{aligned}
u_i^c = \frac{1}{8\pi(1-\nu)} \Big[& e^T_{11}\,\psi_{,i11} + e^T_{12}\,\psi_{,i12} + e^T_{13}\,\psi_{,i13} \\
& + e^T_{21}\,\psi_{,i21} + e^T_{22}\,\psi_{,i22} + e^T_{23}\,\psi_{,i23} + e^T_{31}\,\psi_{,i31} \\
& + e^T_{32}\,\psi_{,i32} + e^T_{33}\,\psi_{,i33} \Big] - \frac{1}{2\pi} \Big[e^T_{i1}\phi_{,1} + e^T_{i2}\,\phi_{,2} \\
& + e^T_{i3}\,\phi_{,3} \Big] - \frac{\nu}{4\pi(1-\nu)} \left(e^T_{11} + e^T_{22} + e^T_{33} \right) \phi_{,i}
\end{aligned}
\qquad \ldots(5.5)
$$

So far our discussion was confined to potential at a point due to a single ellipsoidal region. Now, let us consider two ellipsoidal regions in space, with axes 1,2,3 of the first ellipsoid being parallel to axes 1', 2', 3' of the second ellipsoid. The potential at a point P in the ligament between two such regions will be the sum of the potentials due to the first body and the second body, provided the inside density distributions of both the ellipsoids along their parallel axes are identical.

Hence, at an exterior point P, the displacements u_i can be calculated from the sum total of two potentials. If all the strains and potentials are calculated with respect to origin 0 of the first body, then the same Eqn.(5.5) may be used with ϕ as equivalent to

$$\bar{\phi} = \phi_{\text{1st body}} + \phi_{\text{second body w.r.t. origin } 0}$$

Similarly, ψ should be replaced by, $\bar{\psi} = (x_1^2 + x_2^2 + x_3^2)\bar{\phi} - 2(x_1 \bar{\phi}_{x_0} + x_2 \bar{\phi}_{y_0} + x_3 \bar{\phi}_{z_0}) + (\bar{\phi}_{x_0^2} + \bar{\phi}_{y_0^2} + \bar{\phi}_{z_0^2})$

where, $\bar{\phi}_{x_0} = \phi_{x_0 \text{ 1st body}} + \phi_{x_0 \text{ second body w.r.t. origin } 0}$

$$\bar{\phi}_{x_0^2} = \phi_{x_0^2 \text{ 1st body}} + \phi_{x_0^2 \text{ second body w.r.t. origin } 0}$$

and so on.

The concept of additive potentials of identical objects is well known in the gravitational and potential field theories [188]. The application of multipole potential expansion theorem in two body problems is explained in Appendix C.

Let us now determine the strains at an exterior point P, due to the interaction of two identical prolate spheroidal cavities in an infinite medium with geometrical configuration as shown in Fig. 5.1. The tension loading field is remotely applied and parallel to the major axes 1 and 1'. Thus, the applied strains are e^A_{11} along axis - 1, $-\nu e^A_{11}$ along axis - 2 and $-\nu e^A_{11}$ along axis - 3. For a cavity, Eshelby's ellipsoidal inhomogeneity eigen-strain transformation problem simplifies to [161, 187] :

$$e^T_{ij} - e^C_{ij} = e^A_{ij} \tag{5.6}$$

If we confine our calculations only on $x_3 = 0$ plane, Eqn. (5.6), after substituting the additive potentials, reduces to the following form :

$$\begin{aligned}\bar{e}^T_{11} - 1 = \frac{1}{4\pi}\Big[&\bar{e}^T_{11}(\bar{\psi}_{,1111} - 3\bar{\phi}_{,11}) + \bar{e}^T_{22}(\bar{\psi}_{,1221} - \bar{\phi}_{,11}) \\ &+ \bar{e}^T_{12}(\bar{\psi}_{,1121} + \bar{\psi}_{,1211} - 2\bar{\phi}_{,21}) - \bar{e}^T_{33}\bar{\phi}_{,11}\Big]\end{aligned} \qquad \ldots(5.7)$$

$$\begin{aligned}\bar{e}^T_{22} + \frac{1}{2} = \frac{1}{4\pi}\Big[&\bar{e}^T_{11}(\bar{\psi}_{,2112} - \bar{\phi}_{,22}) + \bar{e}^T_{22}(\bar{\psi}_{,2222} - 3\bar{\phi}_{,22}) \\ &+ \bar{e}^T_{12}(\bar{\psi}_{,2122} + \bar{\psi}_{,2212} - 2\bar{\phi}_{,12}) - \bar{e}^T_{33}\bar{\phi}_{,22}\Big]\end{aligned} \qquad \ldots(5.8)$$

$$\begin{aligned}\bar{e}^T_{12} = \frac{1}{8\pi}\Big[&\bar{e}^T_{11}\{(\bar{\psi}_{,1112} - 3\bar{\phi}_{,12}) + (\bar{\psi}_{,2111} - \bar{\phi}_{,21})\} \\ &+ \bar{e}^T_{22}\{(\bar{\psi}_{,1222} - \bar{\phi}_{,12}) + (\bar{\psi}_{,2221} - 3\bar{\phi}_{,21})\} \\ &- \bar{e}^T_{33}(\bar{\phi}_{,12} + \bar{\phi}_{,21}) + \bar{e}^T_{12}\{(\bar{\psi}_{,1122} + \bar{\psi}_{,1212} - 2\bar{\phi}_{,22})\end{aligned}$$

$\bar{e}^T_{33} = -\frac{1}{2}$, $\bar{e}^T_{13} = 0$, $\bar{e}^T_{23} = 0$

where, $e^T_{ij} / e^A_{ij} = \bar{e}^T_{ij}$ Poisson's ratio ν was taken as $\frac{1}{2}$ for an incompressible elastic medium.

Solving Eqns. (5.7), (5.8) and (5.9), the three unknown strain transformation ratios e^T_{11} / e^A_{11}, e^T_{22} / e^A_{11} and e^T_{12} / e^A_{11} can be calculated. From Kellog's [189] result, the expressions for the exterior potentials of the first prolate spheroid and that of the second prolate spheroid with respect to the origin of the first, are given in Appendix C. The potentials with different variable densities are calculated for the first spheroid and also the second spheroid with respect to the origin of the first spheroid. From the knowledge of multipole-potential-expansion [167, 188], the expressions for the asymptotic expansion of the additive exterior potentials $\bar{\phi}$, $\bar{\phi}_{x_o}$, $\bar{\phi}_{y_o}$, $\bar{\phi}_{z_o}$, $\bar{\phi}_{x_o^2}$, $\bar{\phi}_{y_o^2}$ and $\bar{\phi}_{z_o^2}$ are given in Appendix C.

5.2 Computed Results :

Firstly, the expressions for $\bar{e}_{11}^{T}$, $\bar{e}_{22}^{T}$ and $\bar{e}_{12}^{T}$ are obtained by solving three Eqns. (5.7), (5.8) and (5.9). Secondly, the shear strains $\bar{e}_{12}^{T}$ are calculated for $\nu = \frac{1}{2}$ and different a/b ratios with known values of α and β. Ψ_{ijkl} are given in Eqn. (5.3), whereas Φ_0 , Φ_{x_0}, Φ_{y_0} etc are mentioned in Appendix C. Thirdly, the numerical differentiations are carried out for the functions Φ and Ψ in a high speed computer. Once these numerical differentiations are completedby central difference formula, it would be possible to calculate the ligament strains at any point on $X_3 = 0$ plane. These shear strains are computed, and then finally plotted in Figs. 5.2 to 5.10. The strains are to be measured, from the line PQ by drawing a vertical line parallel to the major axes of the holes. Fig. 5.2 shows the shear strain build-up on the line PQ between two prolate holes with OO' = 1.00, b = 1/40 and prolateness ratio a/b = 1.20, for a position of $\theta = \tan^{-1}(\beta/\alpha) = 35^\circ$. The vertical scale is drawn non-dimensionally for a unit remote applied normal strain. Similarly, the shear strain jumps are also calculated for 45°, 60° and 80° for this prolateness ratio a/b = 1.20. For a prolateness ratio of a/b = 1.60, the shear strains are again calculated for

$\theta = 45^\circ$, 50°, 60°, 70° and 80°. The angular position, at which the shear-strain becomes maximum, is also presented in Table 5.1. As our calculations are confined to a rubber like material ($\nu = 1/2$) only, the strain-derivative jumps are discussed in the next chapter.

The normal strain $\bar{e}_{11}^T$ on the hole surface at the equatorial plane is also calculated from Equations (5.7), (5.8) and (5.9). At the same critical angle, the void surface normal strain at point P rapidly rises. This rise in the void surface (at P) normal strain on $X_3 = 0$ plane is shown in Figs. 5.11 to 5.16 for a number of cases. As the material is assumed to be a rubber like incompressible elastic solid, there will be a sharp notch like expansion from the void surface on $X_3 = 0$, at point P, producing an abrupt displacement jump with a very high local strain (or stress). The strain on the void surface can be calculated from these plots by adding the ordinary eigen-strain on the void surface, which is also given in Table 5.1. Table 5.1 describes the details of these critical angles θ_c for various prolateness ratios. At this critical configuration, there will be a shear-folding on the ligament at point X producing flow-localization.

TABLE 5.1 Critical Orientation Angle, θ_c for Various Prolateness Ratios (Ref. Fig. 1.14) For an Incompressible Solid

Prolateness Ratio	Centre distance of two adjacent holes is taken as unity						
	b = 0.025			b = 0.050			
	Angles at which strain concentration reaches a minimum		Critical angle	Angles at which strain concentration reaches a minimum		Critical angle	Maximum normal strain concentration on the void surface for an isolated single hole in tension
a/b	θ_a (Degrees)	θ_b (Degrees)	θ_c (Degrees)	θ_a (Degrees)	θ_b (Degrees)	θ_c (Degrees)	
1.05	27.8	76.7	46.5	26.9	77.5	45.9	1.65059
1.10	27.7	76.2	48.3	27.7	76.7	46.8	1.63426
1.15	27.9	76.0	49.9	27.9	76.4	47.7	1.61785
1.20	28.0	75.9	51.5	28.0	76.2	48.5	1.60153
1.25	28.0	75.9	53.0	28.1	76.1	49.3	1.58539
1.30	28.0	75.8	54.5	28.2	76.0	50.0	1.56953
1.35	28.0	75.8	56.0	28.2	75.9	50.7	1.55401
1.39	28.1	75.8	57.2	28.2	75.8	51.3	1.54186
1.40	28.1	75.7	57.5	28.2	75.8	51.4	1.53886
1.50	28.1	75.7	60.7	28.3	75.7	52.7	1.50984
1.60	28.1	75.7	64.4	28.3	75.6	53.9	1.48259
1.70	28.1	-	-	28.3	75.6	55.2	1.45713
1.80	28.1	-	-	28.2	75.5	56.4	1.43342
2.00	28.1	-	-	28.2	75.3	58.8	1.39089
2.50	28.1	-	-	28.0	74.9	66.0	1.30815

CHAPTER VI

DISCUSSION

The basic conception of fracture involves three stages atomic, microscopic and macroscopic. The relative importance of each stage obviously depends on the type of material and also the nature of the problem. For a truely brittle elastic solid, the tip of a very fine crack like notch expands to satisfy the equilibrium conditions before breaking atomic bonds in a small cohesive zone [9]. Whereas, in the case of a high strength elastic-plastic small scale yielding material, the notch tip may not expand, but an avalanche of dislocations movement is seen to occur first very close to the elastic-plastic interface inside the plastically yielded small zone on 0°-plane, before an abrupt notch surface fracture instability [3, 48, 49, 56 57]. However, for a ductile material, one gets a large global plastic strain by accomodating local discontinuous fracture with the nucleation, growth and coalescence of voids. The characteristic feature of ductile fracture is fibrous, with a series of concave depressions as dimples [55, 83, 86, 149].

In the present work, firstly, the advantage of using finite Mellin transform has been demonstrated, which is found to be suitable to resolve the boundary conditions more easily for crack and notch problems. An example is also given evaluating the stress intensity factor for a crack radially emanating from the surface of a semi-circular edge notch in a tension plate. Secondly, this method of integral transform is applied to satisfy all the boundary conditions for an infinitely deep external crack like notch, opened under a constant pressure applied on flat faces. Elastic stresses, mismatch jump-stresses, misfit energy are calculated for small flank angle openings. The review of previous literature on an yielding material suggests, micro-cracks and micro-voids formation ahead of such geometries before fracture. So, finally, the interaction strain field between two prolate spheroidal cavities in space has been studied under uniaxial tension field inside an incompressible material, to find the conditions for a shear-localization in the ligament and an abrupt increase in normal strain on the void surface.

6.1 S.I.F. of a Crack Radially Emanating from semi-circular edge notch in a Tension Plate.

When a sharp tip crack emanates from the surface of a machined hole or cut-out, the notch stress field due to the geometry of a hole appears to be essentially governing the propagation of the crack [32, 37]. This means, the stress intensity factor for such a crack is strongly dependent on the local notch stress field. The participation of notch vanishes when the crack becomes somewhat large compared to the notch radius size. Fig. 3.2 shows that, when the crack is about seven times the edge notch radius, there is no appreciable effect of the cut-out on the stress field close to the tip region. The non-dimensional stress intensity factor always remained less than unity, and increases less rapidly compared to Bowie's problem [32]. Figs. 3.3, 3.4, and 3.5 show the isochromatic fringe patterns observed near the root of a fine razor blade slit-cut emanating from a semi-circular edge notch surface. Fig 3.3 confirmsthe predominant effect of the notch stress field on isochromatic fringes, especially when the slit length is small. This is clearly demonstrated showing a change in the shape of isochromatic fringes. On the contrary, our stress field pattern is almost identical to that of a long crack observed by Wells and Post [103]. Stresses at the root of the slit was measured with sufficient accuracy by observing high order fringes very close to the tip. S.I.F.s calculated theoretically agree favourably with the photoelastic experimental measurements.

6.2 Elastic Stresses Ahead of a Crack Like Notch

The determination of elastic as well as elastic-plastic stress field near the root of a crack-like-notch is very important not only to understand the mechanics of local deformations, but also to obtain global specimen fracture criteria in the presence of crack tip blunting and opening. Layers of elastic body forces are being generated below the roots of a crack like notch by imaginary cutting and welding operations [161, 179]. No weak discontinuity in the form of strain derivative jump has been allowed on the plane of cutting after welding. Furthermore, near the unloaded radiused rim, no weak or strong discontinuity has been permitted, and thereby plane section will remain plane near the notch root.

The present analysis is valid for generalised plane stress case, but can certainly be used for plane strain elastic situation. The influence of outward radial mismatch stress on 0^o-plane and the mismatch shear stress produced on 70^o plane is examined carefully from the mechanics of fracture.

The combined actions of bending and tension have produced compressive stresses and a pure shear field region at some distance from the notch tip. On the radiused rim

T sin $(\alpha/2)$ component of the load gives a bending action in the presence of tension opening load T cos $(\alpha/2)$.

The stresses very close to the rim surface (i.e. in the core region) have been calculated from Airy stress function χ_C (ρ, ϕ) and a logarithmic nature of stress field occurs in the range $a \leq \rho \leq 2a$. The value of the rim stress $(\sigma_{\phi\phi})_a$ together with its higher derivatives must be computed in order to determine the stresses in this region. The nature of logarithmic stresses and the stress distribution patterns agree favourably with the results obtained by others [25, 73]. There was no difficulty in applying the residue theorem in the range beyond $\rho > 6a$ to find the tangential, radial and shear stress components, because the first few real roots were found to be sufficient enough for an accurate result. The calculations for 1° flank angle notch with 1% tip root radius blunting are only presented. Similar calculations based on this procedure can easily be carried out on other small notch angles. For higher notch angles, the complex roots of equations $\phi(z) = 0$ and $\sin 2z(\pi - \alpha) + 2z \sin\alpha = 0$ should be considered to find an accurate stress field. The accurate determination of the components of stresses in the range of $a < \rho < 6a$ involves the residue contributions arising out due to the complex conjugate roots of the above

This has been explained in Fig. 4.48 which shows that there are five distinctly different stress field regions ahead of a crack like notch. These are :

(i) A core region, in which the stresses behave like an external deep hyperbolic notch (Figs. 1.5, 4.2 and Neuber [19]). Logarithmic nature of stresses are seen to occur in this region.

(ii) Then over a fairly large portion, a crack like stress field exists. A rapidly decaying nature of stresses is noticed in this region.

(iii) The radial stress changes its sign and becomes compressive between planes $47\frac{1}{2}^\circ \leq \phi \leq 70^\circ$ and beyond $\rho > 100$ a, **but the** tangential stress still continues to be tensile in nature.

(iv) Beyond $\phi > 70^\circ$ plane and $\rho < 100a$, at a far field, the signs of these stresses will be reversed. This means, in this region, the tangential normal stress becomes compressive, whereas the radial component of the stress will be tensile.

(v) For $\phi > 70^\circ$ plane and beyond $\rho > 100$ a, both the tangential and radial normal components of stresses become compressive due to the bending action, leaving a pure shear field region over a small portion.

The nature of $(\sigma_{\phi\phi})_a$ on the radiused rim surface is calculated by evaluating the integral and presented in Fig. 4.47.

6.3 Mismatch Stresses and Misfit Energy for a Crack Like Notch

To understand the stability of the geometrical configuration for a crack like notch upon loading, it is necessary not only to satisfy the equilibrium equations, boundary conditions, compatibility conditions, finiteness of stresses and strains, but also it is highly important to study the finiteness of strain-derivatives on the body everywhere. When the flank opening angle for a crack like notch is very small, it is seen that on the crack extension plane all the above conditions are not fulfilled. For a brittle elastic solid it is difficult to generate a generalised Somigliana dislocation on the parent body in the form of a strain-derivative jump. So, the mismatch outward extra pulling radial stress will expand the notch tip. For such materials, the misfit energy released will be required to create the new surface as proposed by Obreimov [6], Frenkel [29] and Cottrell [3].

Calculations for mismatch stresses were done at an interval of 0.1° notch angle. The roots of the necessary equations are calculated first, and then from residue theorem, the mismatch stresses are determined for each notch angle. Fig. 4.49 (a) shows the variation of radial mismatch stress on 0°plane against notch flank angle openings, whereas the nature of mismatch shear stress on 70° plane is shown in Fig. 4.49(b). The total misfit energy of the entire body is shown in Fig. 4.50. The mismatch in a crack like notch rapidly decreases as the notch angle is increased beyond 2°. The decrease in misfit energy becomes maximum first at 0.2° and then again at 0.6° angle. These are favourable for instability.

If c is the new crack length emanating from the notch tip being generated by abruptly releasing the misfit energy on 0° plane due to mismatch outward radial stress, then, the new crack length c is given by

$$2 \gamma c = \frac{1}{2E} \left[(\sigma_{\rho\rho})_M \right]^2 \qquad (6.1)$$

C is the crack length per unit loading distance

where, $(\sigma_{\rho\rho})_M$ is the misfit radial outward pulling stress, E is the Young's modulus and γ being the energy required to create a new surface per unit area, per unit specimen thickness.

This additional displacement for the notch tip on 0° plane can also be approximately calculated as,

$$U = 100\ a\ \frac{(\sigma_{\rho\rho})_M}{E} \qquad (6.2)$$

where a is the notch tip radius .

As U/a is normally small, Bowie type expression for the stress intensity factor can be used to calculate the fracture load of a crack like notch,

$$K_I = 1.1215\ Ts \sqrt{\pi} \sqrt{U} \qquad (6.3)$$

where, s is the geometrical factor, as explained in Chap.III, considering the stress concentration and the stress distribution near the rim on 0^o plane.

Hence, it is clear from Eqns. 6.1, 6.2, and 6.3 that, when the mismatch radial stress on 0^o plane reaches a critical value, the fracture of a crack like notch could occur. For an elastic material this is also equivalent to, when the misfit energy reaches a critical value, crack extension occurs from the root of a crack like notch. On the contrary, for an elastic-plastic material, it is easy to produce a strain-derivative jump and generalised Somigliana dislocations on the crack extension plane, and the mismatch stresses can be responsible for the initiation of fracture ahead of a notch.

6.4 Plane Strain Elastic-Plastic Stresses and Mechanism of Crack Extension at the Root of Yielded tip Crack Like Notch

The elastic stresses for generalised plane stress can be extended to determine the plane strain elastic-plastic stresses below the root of a crack like notch. The elastic mismatch between the far and near fields remains inside the elastic portion and will not be affected due to some plastic yielding near the tip root region. Thus, the shape and size of the yielded elastic-plastic boundary can be obtained from the elastic stress field. For a Von Mises ideally plastic material, the yielded boundary is shown in Fig. 6.1. These boundaries ahead of a crack like notch are obtained from the relation,

$$\tau_{max} = \frac{\sigma_y}{\sqrt{3}} = \sqrt{\left[\left(\frac{\sigma_{\phi\phi} - \sigma_{\rho\rho}}{2} \right)^2 + \sigma_{\rho\phi}^2 \right]} \qquad (6.4)$$

The way this yielded boundary has been formed can only be examined from the velocity of plastic flow field. The maximum spread is seen to be on 45° plane for a plane strain situation. The problem has been assumed to be statically determinate. At the yielded elastic-plastic interface all the three components of stresses and their derivatives are continuous. Two possible cases can arise, either pure shear field region is not within the plastic zone but inside the elastic portion, or pure shear region is within the plastic zone producing a hinge due to bending inside the yielded material. The first case is well known [13, 48, 59], as the maximum normal stress elevation occurs on 0° plane, in this situation, the crack is likely to extend on 0° plane only, with small shear stress on 45° plane. When the misfit elastic radial stress reaches a critical value, the elastic misfit energy is abruptly released ahead of the thin last vestige elastic wedge. Thus, the misfit is expended to generate an avalanche of dislocations, micro-cracks or micro-voids on 0° plane inside the plastic zone causing the onset of local fracture. So, there will be a strain-derivative jump $\partial \sigma_{\rho\rho} / \partial \rho$ at the interface of the yielded boundary. From equilibrium equations, this is also equivalent to a shear-stress derivative jump $\partial \sigma_{\rho\phi} / \partial \phi$ across a thin non-deforming layer producing a velocity discontinuity inside the plastic zone, on the maximum dilatational region. Hence, for a very small scale yielding high strength material, when the misfit radial stress on 0° plane reaches a critical value, fracture could occur. As soon as the misfit is released on 0° plane, the local disturbance thus created ahead of the notch helps to cause the notch surface instability [130, 153, 154]. As the misfit reaches maximum first at 0.2° and then again at 0.6°, there will be two distinctly different instabilities for a crack like notch, provided the notch can open to such a large angle. Then, in this case, the first instability at 0.2° will occur locally inside the material, and the second one at 0.6° should be on the notch surface.

For a large scale yielding situation when the plastic hinge forms within the plastically deformed region, a strain-derivative jump and velocity discontinuity can occur inside the plastic zone. For a plane stress case, elastic mismatch shear stress is on 70° plane, and a large plasticity spread around this plane is commonly noticed. Whereas, for a plane strain situation the formation of plastic hinge due to bending action can alone give a large strain gradient and local velocity discontinuity (Prager and Hodge [66]). Fig. 6.2 shows a fully developed slip line field pattern when a pure shear region lies within plastically yielded zone and compressive stresses in the yielded boundary. This velocity discontinuity line in parabolic - hyperbolic region is taken from Nadai [67], Sokolovsky [65] , Rice and Johnson [62], and Hill [50] . This boundary agrees favourably with the experimental observations of others [41, 121]. The plastically yielded boundary shown in Figs. 6.1 and 6.2 also agree with the experimental observations of Hahn and Rosenfield [41], Dixon and Visser [106], Ewing and Richards [121], Gerberich [107], Bandyopadhyay and Mubeen [52] and Singh, Bandyopadhyay and Murthy [53]. The last vestige of elastic wedge below the notch root on 0^o plane produces a parabolic-elliptic field, which is favourable for a local plastic instability. In the case of a fully developed plastic zone, the presence of compressive stresses on the yielded boundary with a small pure shear field inside the yielded material could give the possibility of existing an elastic core as a last vestige around this pure shear region [50, 65 - 67]. The characteristics lines, (which coincide with the slip lines for a plane strain case), are changing first from logarithmic spiral, (hyperbolic field) to straight lines (parabolic field), and then finally to the boundary of (elliptic field) elastic core. Plastic flow can take place from the two sides of the elastic core like a flow past over an aerofoil blade. If no elastic core is formed in the case of a fully developed plastic zone, bending action alone can produce an abrupt strain derivative jump inside the plastically yielded medium.

Normally, the plane strain plasticity stress field and the velocity equations are hyperbolic [50] but for a fully developed plastic zone in a large scale yielding material, these partial differential equations can have bifurcations giving elliptic equations, especially when

$\sigma_{\phi\phi}\ \sigma_{\rho\rho} \leq \tau^2_{max}$ (Sokolovsky [65]). Thus, the presence of compressive stresses on the yielded boundary can cause bifurcations and local necking plastic instability inside the deformed zone. The second velocity discontinuity line on the last vestige elliptic core is obtained purely through graphical constructions, by matching the characteristics (i.e. slip lines) of three different fields. As the boundary of the elastic core is unknown, the problem is fairly complex and could even be statically indeterminate. Pending such an exact analytical solution for stress and velocity fields, in the present work through simple graphical constructions (magnified to twenty times scale), a first hand idea of this extremely complex problem is given qualitatively. Thus, there are two regions where local plastic instability could arise : (i) one at 0° plane below the notch root, where a high dilatation occurs, and the other (ii) on 45° plane (for a plane strain case), where pure shear with a high hydrostatic tension could exist (Figs. 6.3 and 6.4). Approximate stress fields on 0° and 45° planes shown in Figs. 6.3 and 6.4 are for a material of yield strength $\sigma_y = 0.65$ T. In the absence of work hardening for a Von Mises material, the plastic constraint factor could be in the order of 5 or more below a crack like notch. These stress plots and slip line constructions are not all that accurate, but would certainly give the order and general pattern for an elastic-plastic deformation ahead of a crack like notch in a ductile material. Micro-voids can easily be created in a ductile material in the presence of a high hydrostatic tension combined with shear stresses along 45° planes [79, 82, 152, 153].

The local plastic constraint factor on 0° plane for a crack like notch could be more than 2.71 for an ideal situation. Recent experimental observations on spheroidised steel [64] show the p.c.f. could be as high as 3.5. A high local plastic constraint is also observed by Singh, Bandyopadhyay and Murthy [53] while testing the fracture strength of short edge cracked beams in steels. These experimental observations on 25 mm thick mild steel bars have revealed that when the crack length is in the order of 3 mm, an abrupt plastic shear flow localization begins on 45° plane at some distance from the crack tip, whereas for long cracks of more than 6 mm, the abrupt local plastic flow was mainly confined to 0° plane. This abrupt flow localization at the root of short cracked beams observed through photoelastic coating clearly demonstrates that a crack extension could arise along 45° plane for such highly yielded crack like notch situation [53]. Rice and Sorensen [73] have reported that Begley and Landes [72] also made similar observations.

6.5 Ligament Instability and Shear-Localization between two Prolate Spheroidal Voids inside an Incompressible Medium

A simplified model based on the interaction of strain field between a pair of prolate spheroidal holes is presented in the present work. The major axes and the equatorial planes of the holes are parallel, and the two holes are situated inside an incompressible elastic medium with major axis being parallel to the direction of applied remote tension loading. Abrupt strain and strain derivative jumps are permitted inside this (rubber like) incompressible medium, possibly allowing folding in the ligament and formation of sharp tip notches emanating from the void surfaces. Such theoretical analysis may help to understand the mechanism of unstable hole growth and void coalescence leading to local ductile rupture.

Figs. 5.2 to 5.10 show the nature of shear-strain distributions in the ligament between two such holes inside an incompressible (Poisson's ratio = 1/2) material. The first cavity on the left hand side is trying to rotate clockwise, whereas the second one in anticlockwise direction, as if the two major axes can be aligned along line OO' . The total rotational torque in any (x_3 = constant) plane, is always balanced at all time in the ligament. As the major axes of the prolate holes are aligned to the direction of applied tension, this is energetically the most favourable configuration. So, the holes can never rotate. But, in this situation, the principal axes of strain can rotate at a point in the ligament to increase local shearing resistance [130, 138]. Hence, in our case, there has to be a local shear strain build up in the ligament. Figs. 5.2 to 5.10 confirm that, there exists a critical angle θ, at which the rotational effect on the void reaches maximum for a given prolateness ratio. Thus, when two prolate holes are situated in space in a tension loading field, and if the distances between their two parallel equatorial and meridian planes are known, then there is a particular prolateness ratio at which the shear-strain localisation will be maximum. A local abrupt shear strain derivative jump in the ligament will be noticed at this configuration. As the material has been assumed to be incompressible, at this critical configuration an abrupt local normal strain increase will also be visible on the void surface. There will be a tendency of folding at a point in the ligament localizing a large shear strain, which further causes a normal displacement jump on the void surface with a large local normal strain rise (Figs. 5.11 to 5.16). Table 5.1 describes these critical angles for different prolateness ratios. Hence, for a given prolateness ratio, at this critical geometrical configuration, the ligament between the holes will have a tendency for buckling instability. The decrease in elastic strain energy is also maximum at this orientation. It is also noticed that, there is no shear localization when $\theta < \theta_a$, whereas shear can localize in two small regions for $\theta > \theta_b$.

If the above arguments are qualitatively extended to a Von Mises ideally plastic material, then it may be possible to give a schematic plane strain slip-line field on $x_3 = 0$ plane. Fig. 6.5 shows such a slip line field between two elliptic holes with a/b ratio = 1.6 and $\theta = 60^\circ$ and for centre to centre distance = 40 b. Fig. 6.6 describes the nature of plastic constraint and local shear stress build up in a small region. The slip lines are terminated at X on $x_3 = 0$ plane, shown by dotted lines, assuming that there could be a possibility of existing a non-deforming layer of material. Although magnified to twenty times and drawn graphically, these slip lines and stress plots are approximate only. Inside a plastically yielded material, such a large abrupt local increase in shear strain, with a possibility of a discontinuity in a shear strain derivative, may cause velocity discontinuity as well as local plastic instability [85, 153], which may further increase the void surface strain and lateral growth.

CHAPTER VII

CONCLUSIONS

The following conclusions can be drawn from this work :

1. Applying Mellin type integral transform, the stress intensity factor for a crack radially emanating from the root of a semi-circular edge notch is obtained analytically in a tension plate. These theoretical solutions agree favourably with the experimental observations on model photoelastic specimens.
2. The complete elastic stress field for an infinitely deep external charpy type notch with 1° flank opening angle and 1% tip root radius blunting is presented. It is proved that, there could be five distinctly different stress field regions ahead of a crack like notch. Compressive stresses and pure shear regions are observed due to the combined action of bending and tension. Logarithmic nature of stresses is seen to occur very close to the notch tip.
3. When the flank opening angle of a crack like notch is very small, an outward radial mismatch on 0°-plane as well as a shearing mismatch on 70° plane will be generated ahead of the notch upon loading.

4. For an ideal elastic solid, the mismatch on 0^o will cause the notch tip to expand to satisfy the equilibrium conditions on this plane. The decrease in misfit energy of a crack-like-notched body has maxima first at 0.2^o and then again at 0.6^o notch flank opening angles. The misfit energy on 0^o-plane will be expended to create new surface producing a stable crack extension from the notch root. This occurs when the radial outward mismatch stress reaches a critical value on 0^o-plane.

5. For a small scale yielding elastic-plastic material under plane strain situation, the mismatch on 0^o plane can produce generalised Somigliana dislocation on this crack extension plane. This is equivalent to a shear-strain-derivative-jump across a thin undeformed layer inside the plastically yielded zone at high dilatational region causing a local velocity discontinuity and plastic instability. This misfit energy on 0^o plane will be released abruptly to create an avalanche of dislocations, micro-cracks or micro-voids. Furthermore, it is seen that, the maximum normal stress elevation below the root of an elastic-plastic crack like notch (with $\alpha = 1^o$ and $a = 1\%$ of the loading distance on flat faces), could be more than 2.71, for a non-strain-hardening ideally plastic Von-Mises material.

6. Under plane strain deformation in a large scale yielding ductile material, pure distortional fields could be present on 45° planes within the plastic zone. This could produce either an elastic core, or a thin layer of undeformed material inside the plastic zone on 45° planes. The presence of compressive stresses on the yielded boundary gives bifurcations on plane strain plasticity equations, which could further cause local velocity discontinuity and plastic instability at some region ahead of the notch tip on 45° planes inside the plastic zone. Hydrostatic tension combined with shears on 45° planes may help to create micro-voids on these pure distortional regions.
7. The interaction strain field in the ligament between two prolate spheroidal holes is studied inside an incompressible medium. The stability of growing voids and shear strain localization in the ligament are reported. For a given prolateness ratio of the voids there exists a critical relative angular position at which the ligament is unstable. This means, at this configuration, a large shear strain will be localized at some point in the ligament which helps to build up a high local normal strain concentration at some point on the cavity surface.

Scope for Future Work :

It is necessary to carry out further investigations on the elastic-plastic stress and velocity fields ahead of a crack like notch. Some future experimental work will verify the presence of elastic core inside a fully developed plastic zone. Elastic misfit and strain-derivative jumps inside a metal should be understood through careful experimental observations on different materials. To understand the flow-localizations and unstable void growth mechanisms inside an actual plastically deformed material, more experimental work is needed. Some future work will consider these aspects in more details.

Although more analytical and experimental work should have been carried out on plastic deformations, to propose criteria for ductile fracture, however, in author's opinion, the present theoretical study on a crack like notch and spheroidal hole interfactions will be useful to understand the mechanisms of fracture in metals.

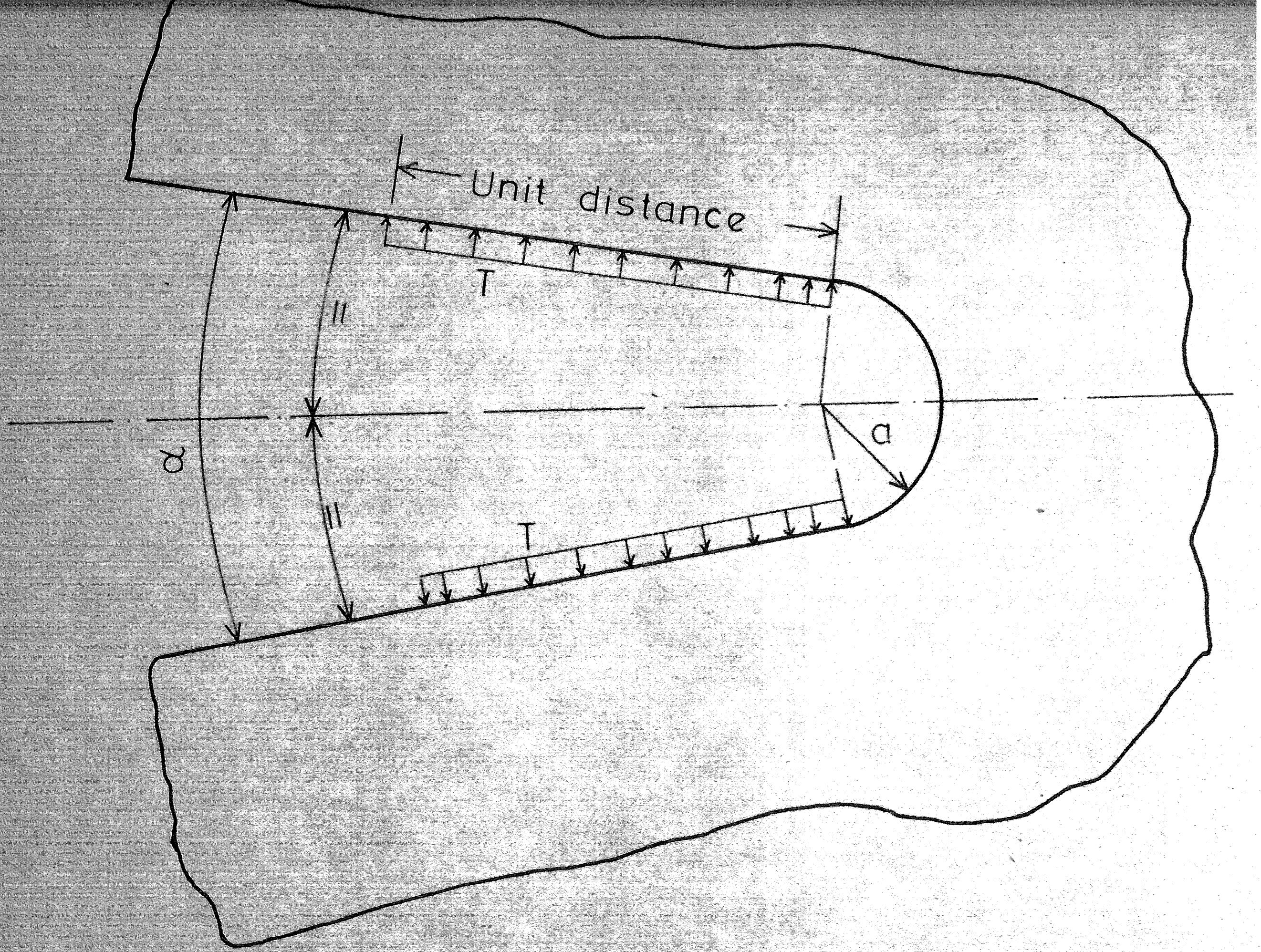
Unit distance
T
T
a
α

FIG.1.1 AN INFINITELY DEEP CRACK-LIKE-NOTCH WITH A FINITE RADIUSED TIP AT THE VERTEX.

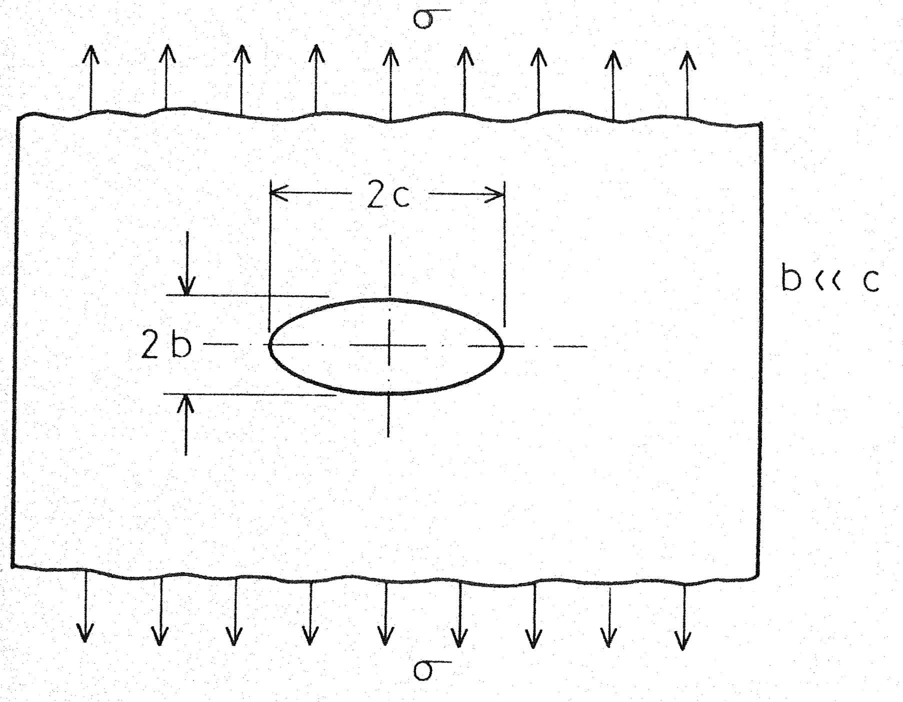

FIG. 1. 2 AN ELLIPTIC THROUGH SLIT IN A TENSION PLATE [1]

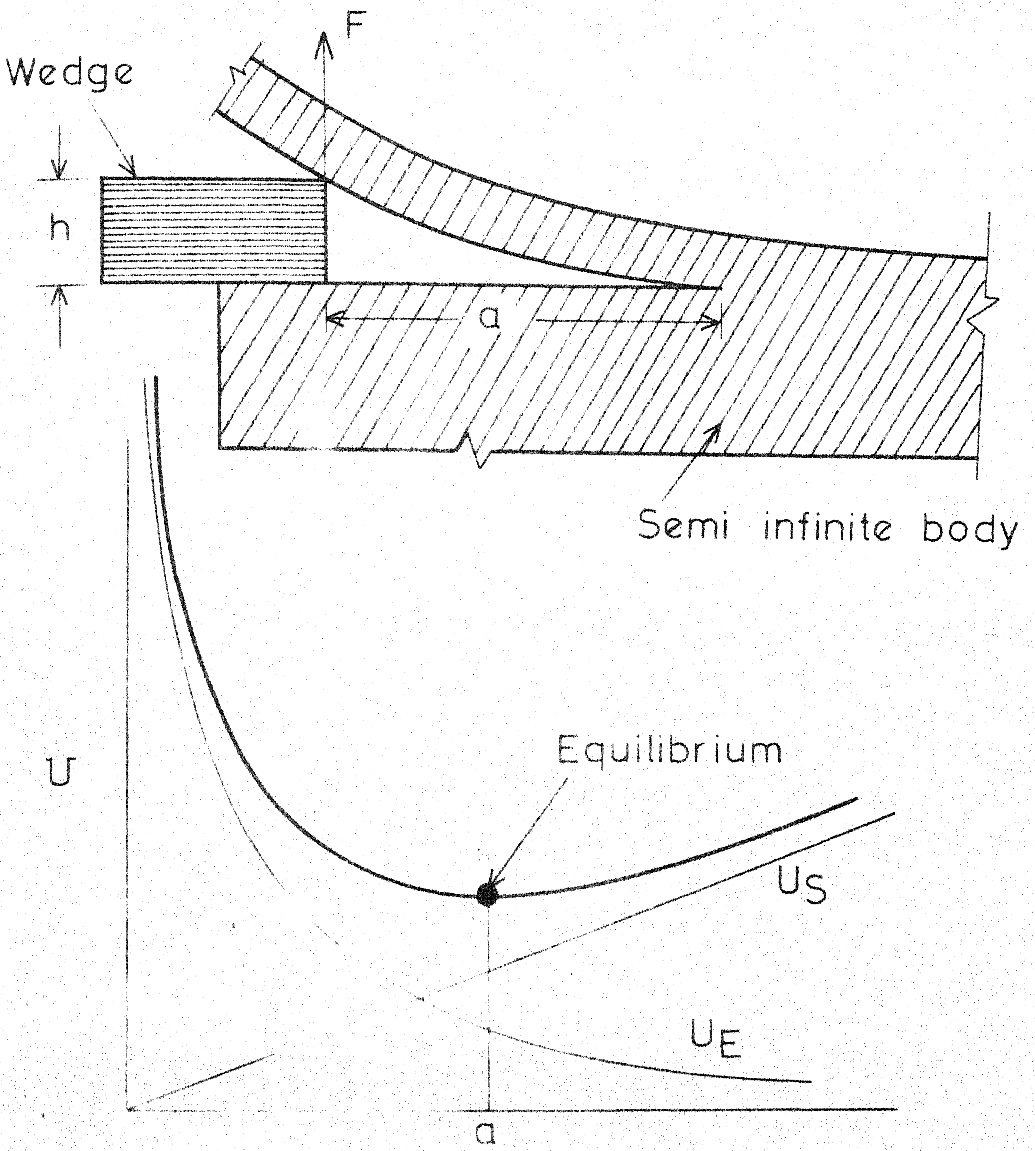
F
Wedge
h
a
Semi infinite body
U
Equilibrium
U_S
U_E
a

IG. 1.3 WEDGE LOADED CRACK — AN EXAMPLE OF A CRACK IN STABLE EQUILIBRIUM [6]. EQUILIBRIUM CRACK LENGTH, $a = \left[3Eb^3\ h^2/16\,\gamma\right]^{1/4}$

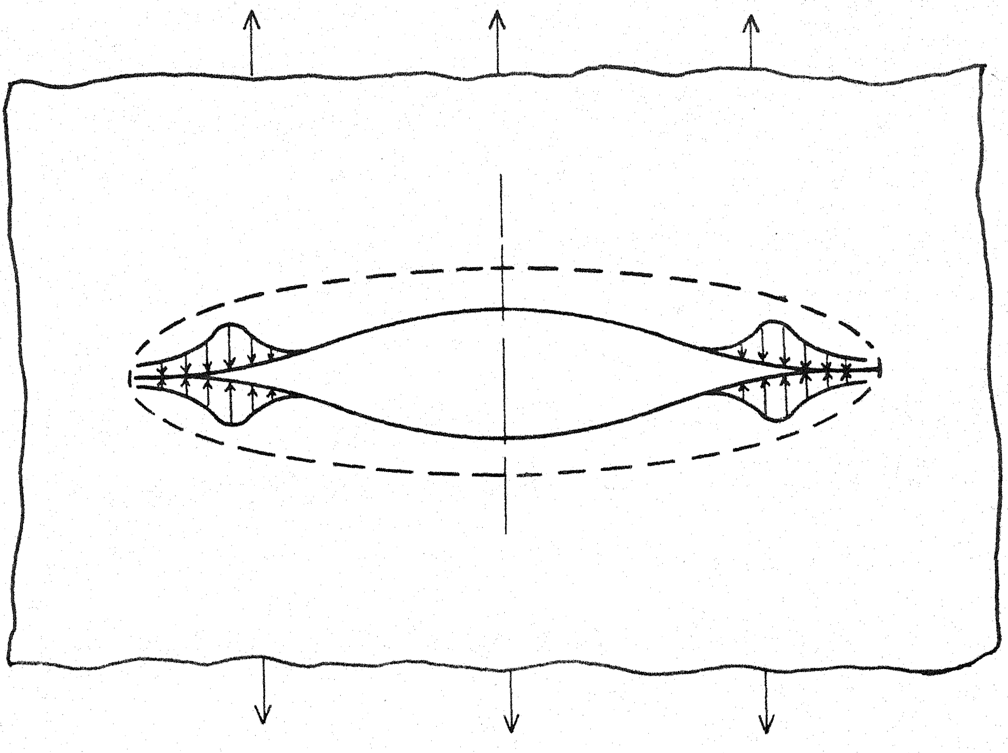

FIG. 1.4(a) SMOOTH JOINING OF FACES AND COHESIVE FORCES AT THE TIP OF BARENBLATT'S EQUILIBRIUM CRACK [

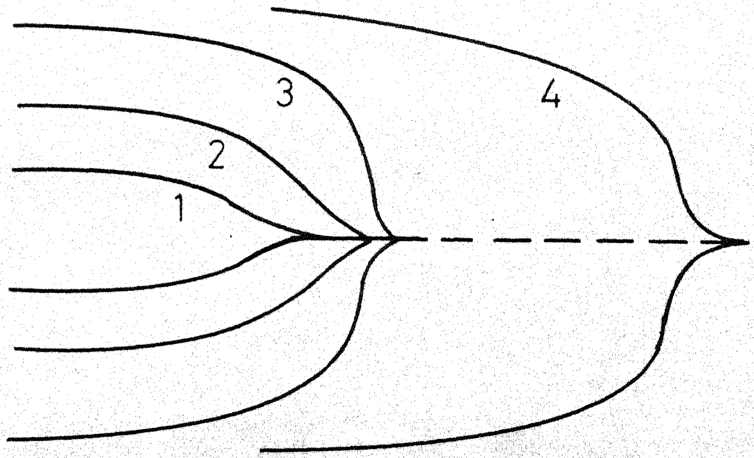

G. 1.4(b) SUCCESSIVE EXPANSION OF THE CRACK EDGE UNDE INCREASING EXTENSIONAL LOAD [9]

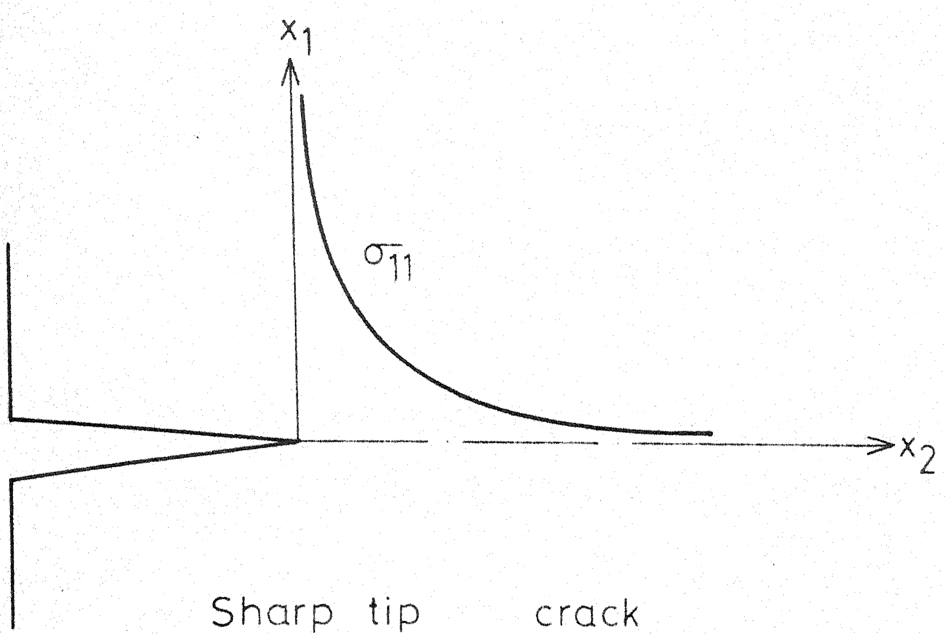
x_1
σ_{11}
x_2

Sharp tip crack

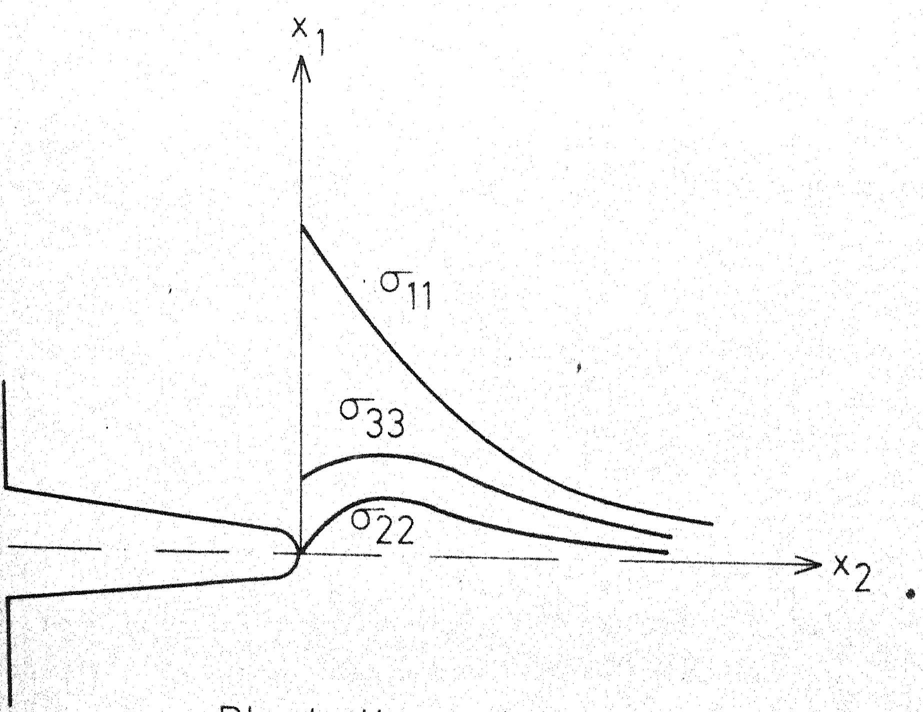
x_1
σ_{11}
σ_{33}
σ_{22}
x_2

Blunt tip notch

FIG. 1.5 SCHEMATIC REPRESENTATION OF STRESSESS AT THE ROOT OF CRACKS AND NOTCHES[19,20,22]

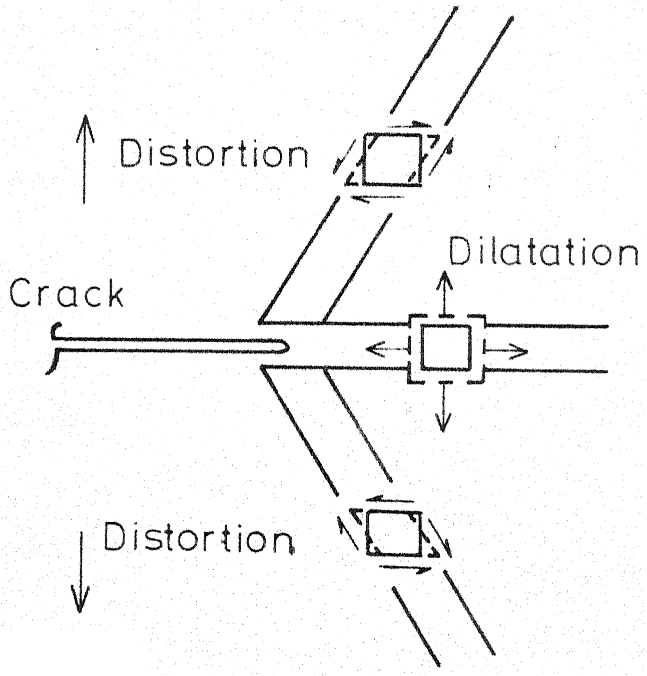
Distortion
Dilatation
Crack
Distortion

FIG. 1.6 ZONES OF PURE DISTORTION AND HIGH DILATATION AHEAD OF A BLUNT CRACK-TIP [28]

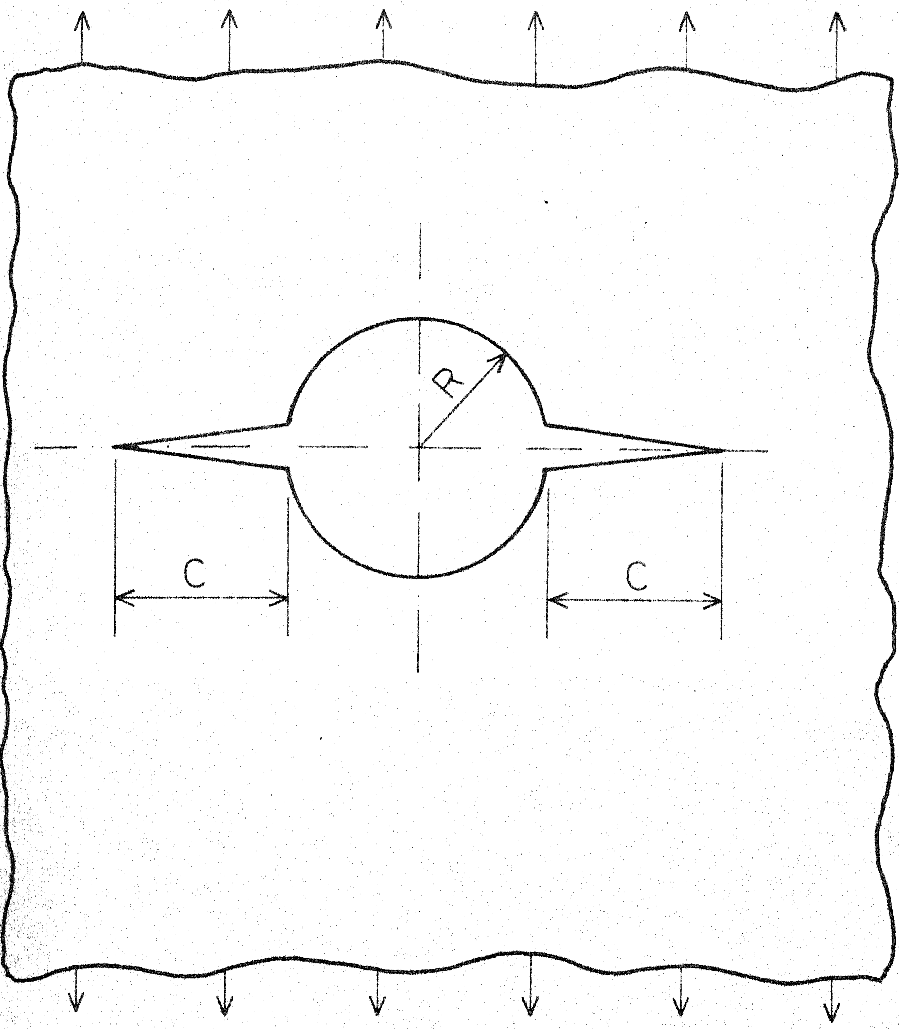

FIG. 1.7 BOWIE PROBLEM FOR CRACKS RADIALLY EMANATING FROM A HOLE IN A TENSION PLATE [32]

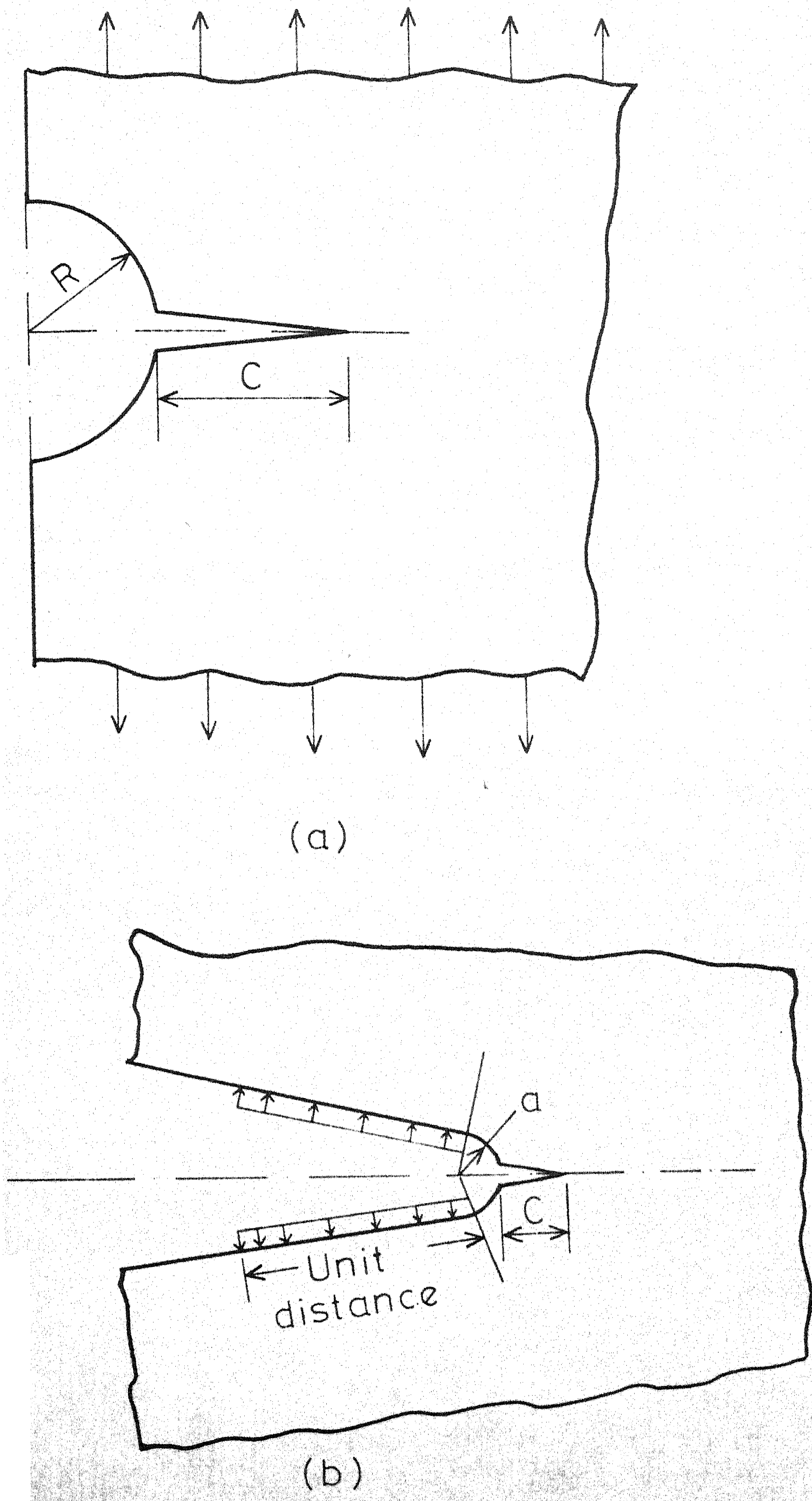
R
C
(a)
a
C
Unit distance
(b)

FIG.1.8 CRACKS EMANATING FROM THE ROOT OF
(i) A SEMI-CIRCULAR EDGE NOTCH AND
(ii) AN INFINITELY DEEP RADIUSED TIP NOTCH

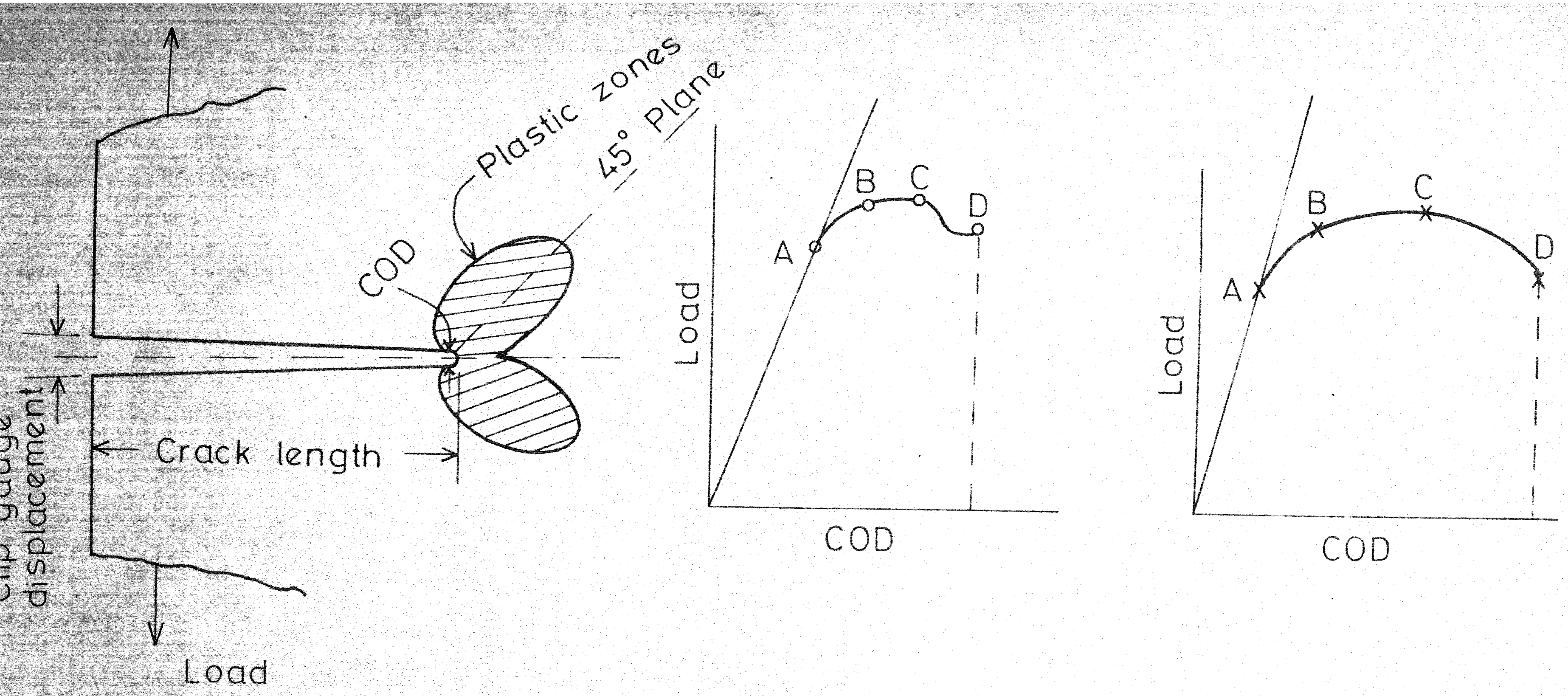
Plastic zones
45° Plane
COD
Crack length
displacement
Load
Load
COD
A
B
C
D
Load
COD
A
B
C
D

FIG. 1.9 TYPICAL OBSERVATIONS ON CRACK OPENING, TIP BLUNTING AND PLASTICITY SPREAD TOGETHER WITH LOAD-COD RECORD FOR A SHORT EDGE-CRACKED FLAT BEAM DURING FRACTURE TEST OF A METAL.

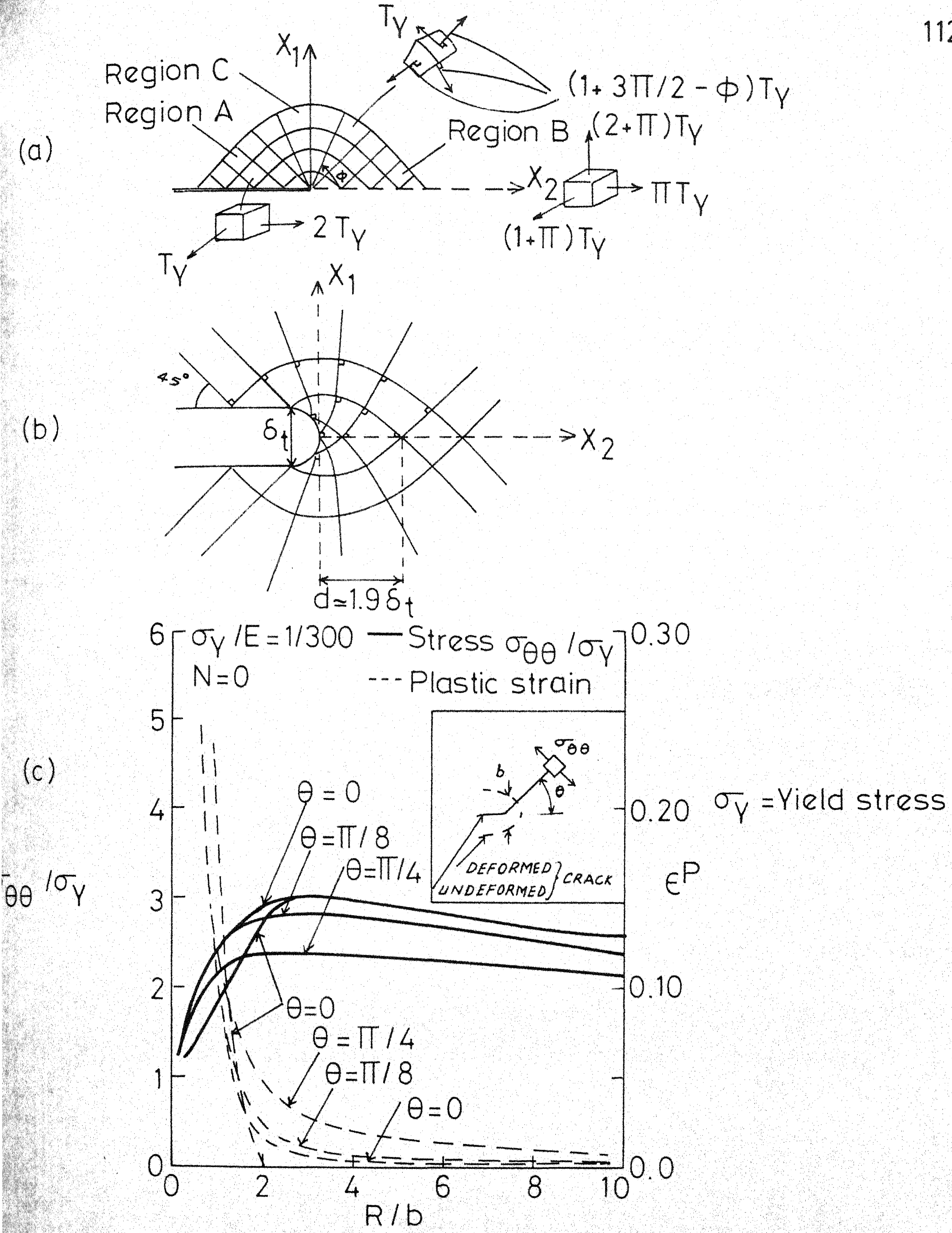
(a)
Region C
Region A
Region B
X_1
X_2
ϕ
T_Y
$(1+3\pi/2-\phi)T_Y$
$(2+\pi)T_Y$
πT_Y
$(1+\pi)T_Y$
$2T_Y$
T_Y
(b)
X_1
X_2
45°
δ_t
$d \simeq 1.9\delta_t$
(c)
$\sigma_Y/E=1/300$
N=0
Stress $\sigma_{\theta\theta}/\sigma_Y$
Plastic strain
$\sigma_{\theta\theta}$
b
θ
DEFORMED
UNDEFORMED
CRACK
$\theta=0$
$\theta=\pi/8$
$\theta=\pi/4$
$\theta=0$
$\theta=\pi/4$
$\theta=\pi/8$
$\theta=0$
$\sigma_{\theta\theta}/\sigma_Y$
ϵ^P
σ_Y =Yield stress
R/b
0
1
2
3
4
5
6
0
2
4
6
8
10
0.0
0.10
0.20
0.30

.10 Local plane strain plastic fields around a crack tip (a)Prandtl field in region of crack tip [63],(b)Modification of slip-line field due to crack-tip blunting [63],(c)Plot of stress $\sigma_{\theta\theta}/\sigma_Y$ and plastic strain around the blunted notch for $\sigma_Y/E=1/300$ and non-strain hardened material[61]

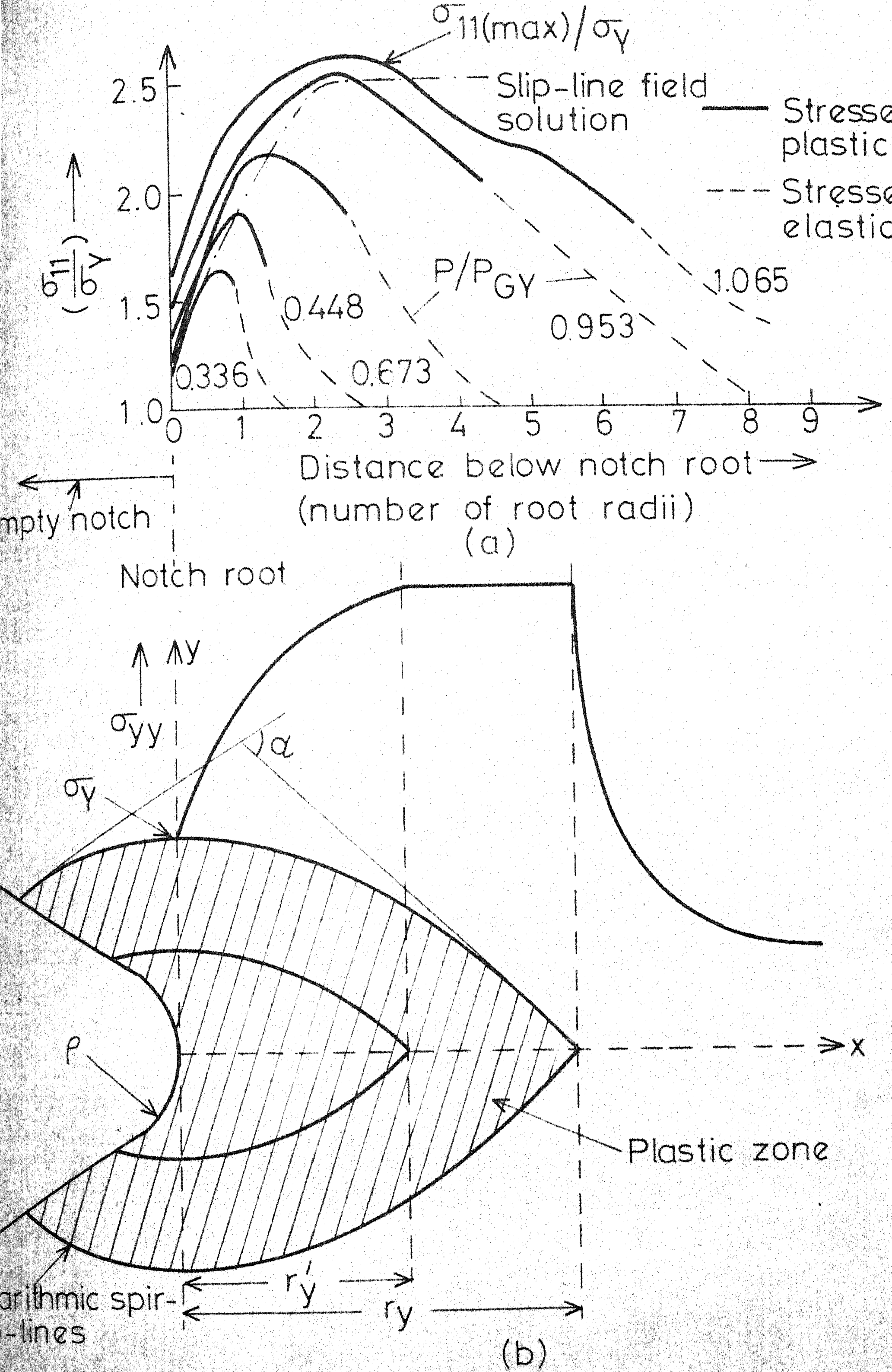

1.11(a) Finite element analysis of stress below a deep charpy notch in pure bending showing the variation of maximum principal stress (σ_{11}) with distance below notch root for various applied loads (P/P$_{GY}$) [59], (b) Schematic longitudinal stress (σ_{yy}) distribution ahead of a rounded notch, radius ρ, at general yield; rigid/plastic slip-line field solution. ($\sigma_Y = 2k$, Tresca criterion, and $= \sqrt{3}k$, Mises criterion.)

$\sigma_Y / E = 1/300$, (σ_Y is the yield strength)

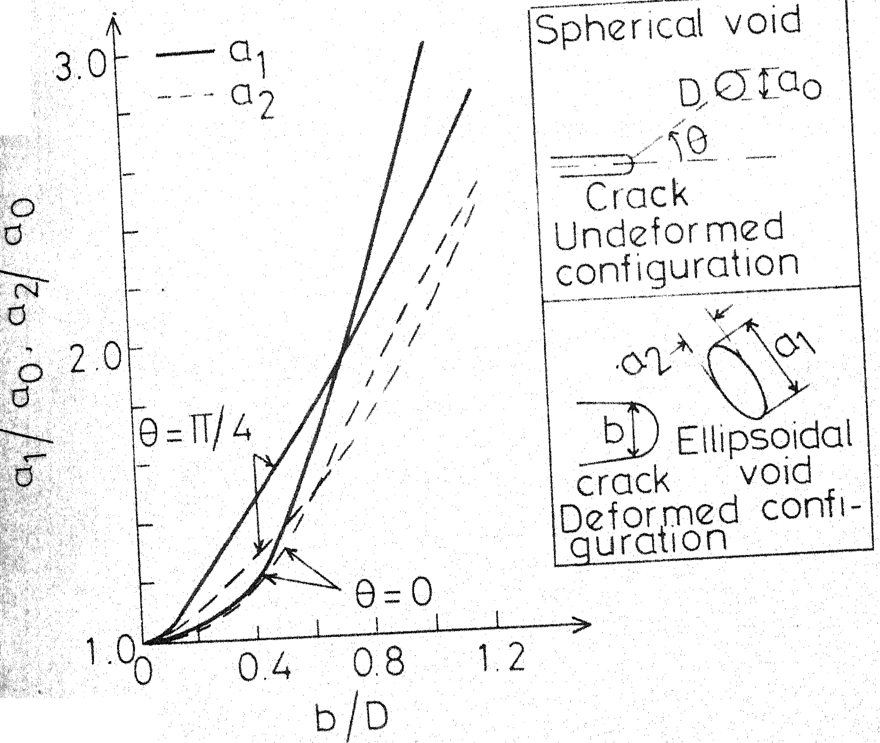

FIG. 1.12 GROWING VOID DIMENSIONS IN THE NEAR-TIP FIELD AGAINST THE NOTCH WIDTH TO VOID DISTANCE RATIO [61]

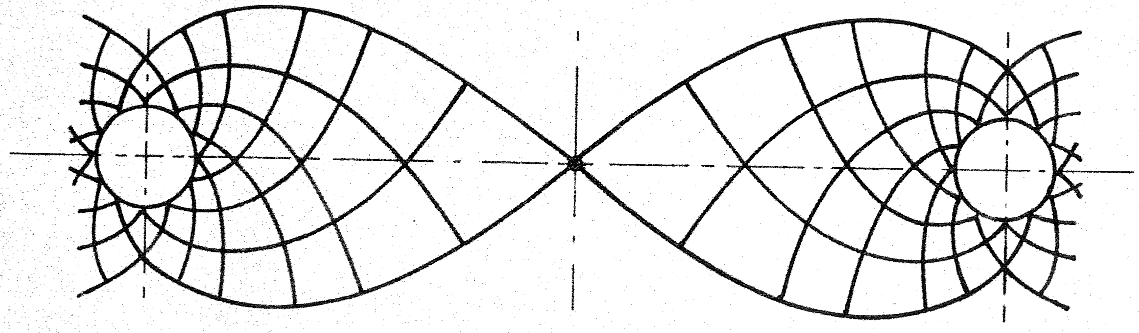

FIG.1.13 OVERLAPPING SLIP-LINE FIELDS IN THE LIGAMENT BETWEEN A PAIR OF CYLINDRICAL HOLES [85]

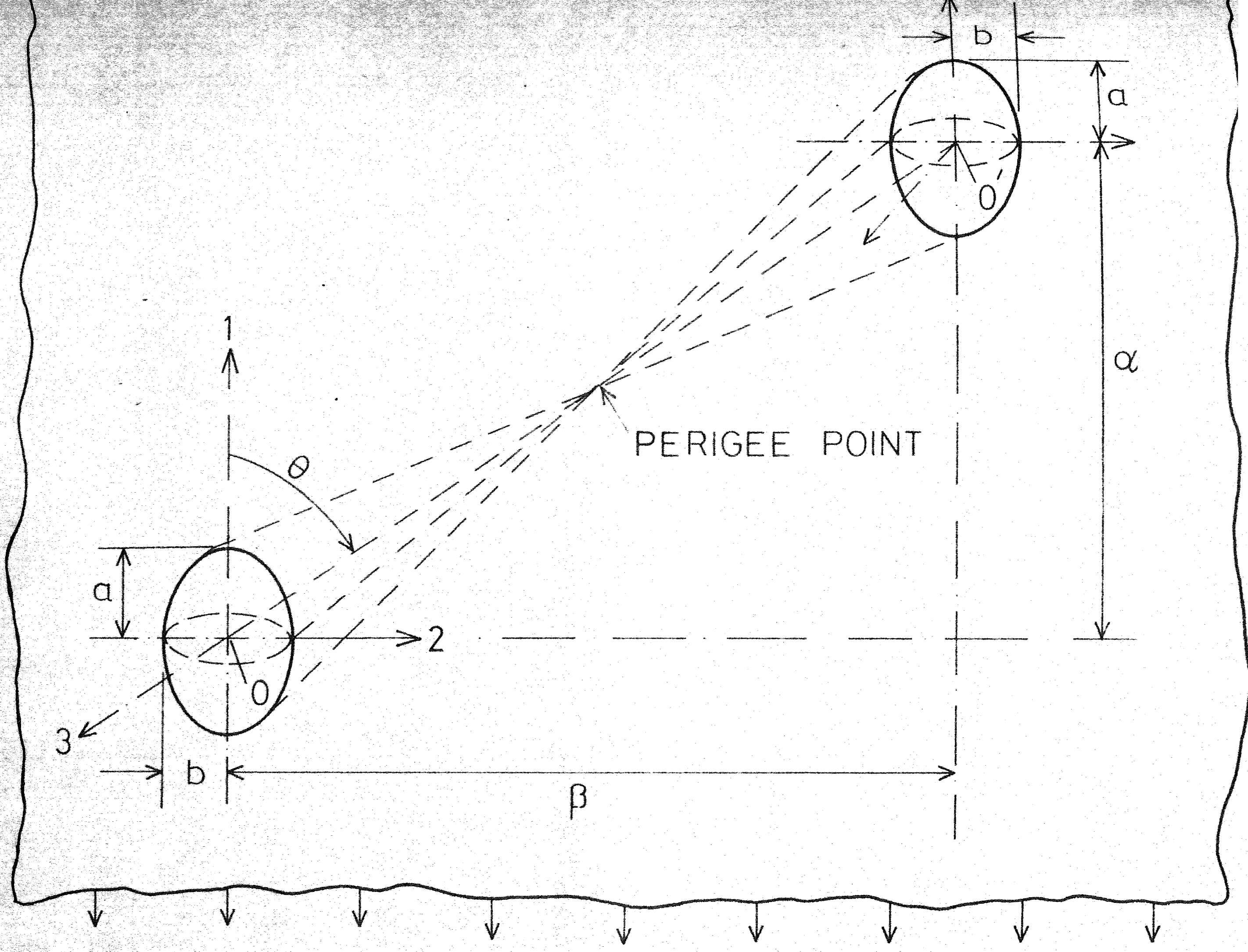
b
a
0
α
PERIGEE POINT
1
θ
a
2
0
3
b
β

FIG. 1.14 GEOMETRICAL CONFIGURATION FOR CALCULATING THE EXTERIOR STRAIN FIELDS OF TWO PROLATE SPHEROIDAL HOLES IN SPACE UNDER TENSION LOADING. $a > b\ (= c)$

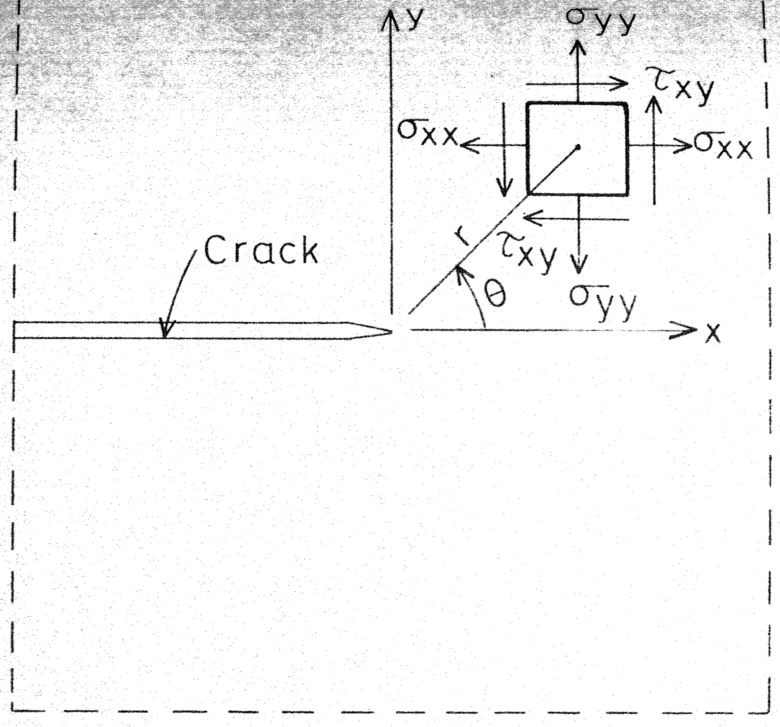
y
σyy
τxy
σxx
σxx
Crack
r
τxy
θ
σyy
x

FIG. 2.1 CO-ORDINATE SYSTEMS NEAR THE TIP OF A CRACK IN AN INFINITE MEDIUM [22]

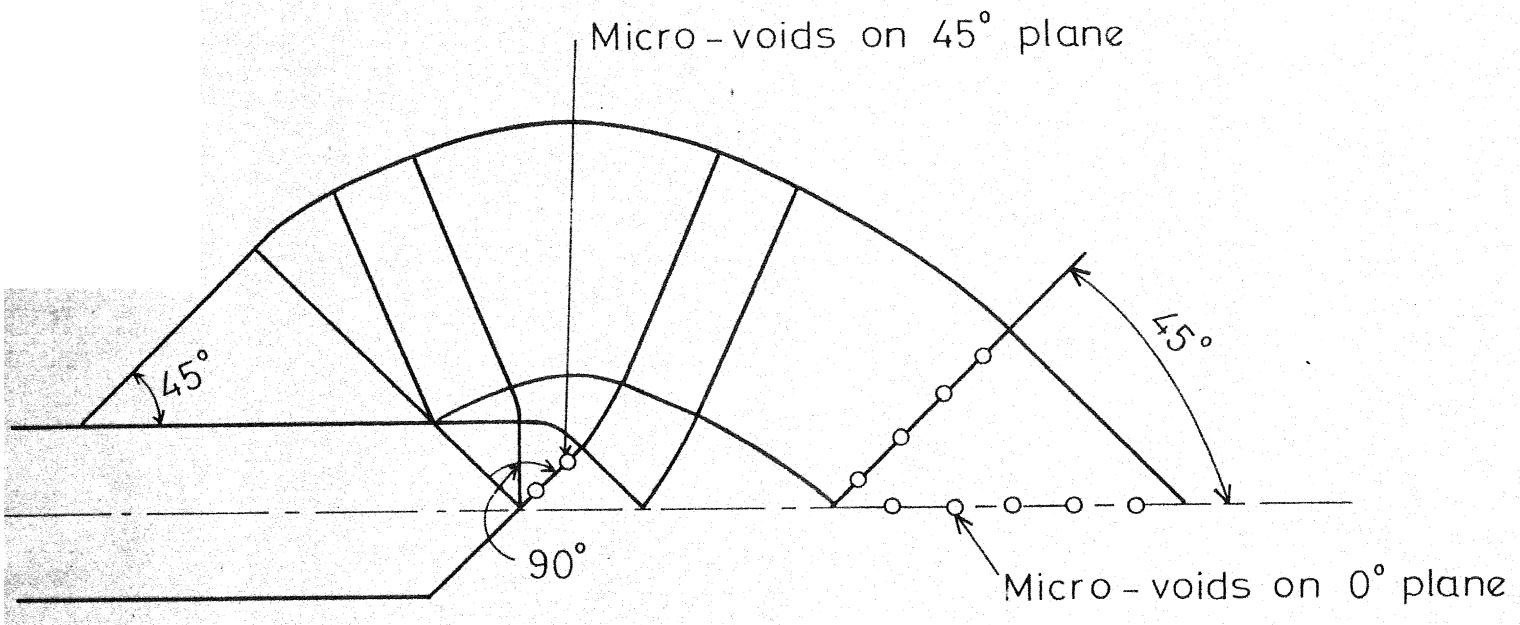
Micro-voids on 45° plane
45°
45°
90°
Micro-voids on 0° plane

FIG. 2.2 POSSIBLE REGIONS OF LOCALIZED FLOW AND SUBSEQUENT VOID FORMATION AHEAD OF A 45° NOTCHED CRACK-TIP [85]

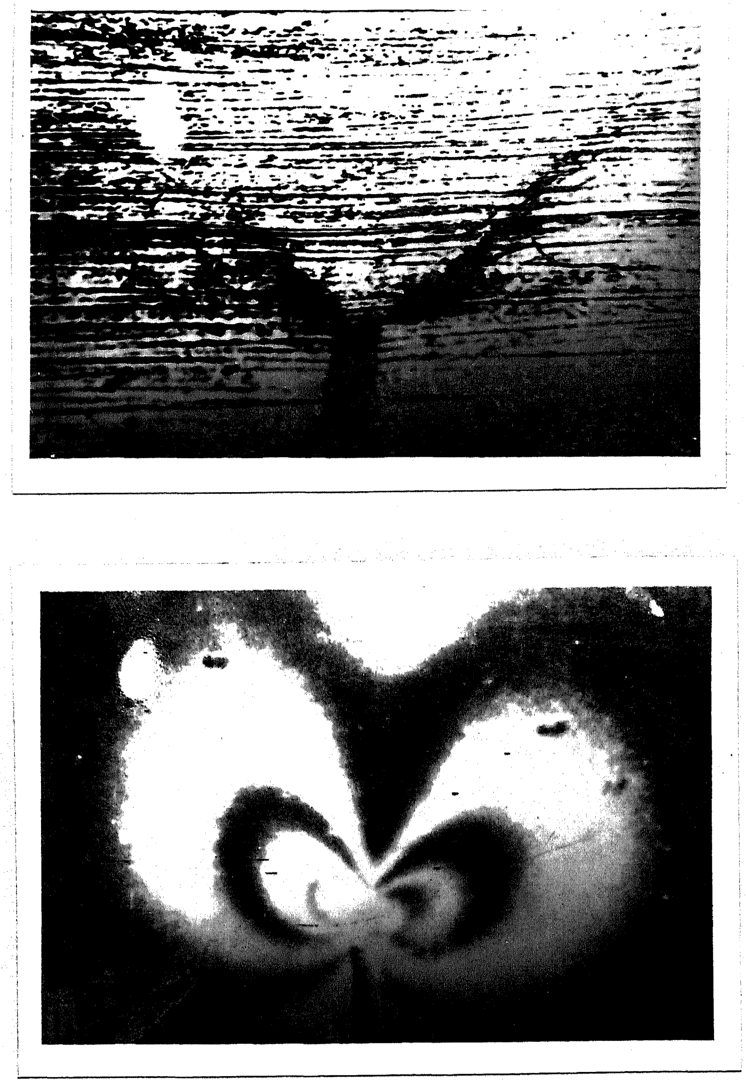

Fig. 2.3 Crack-tip deformation, plasticity spread and isochromatic photoelastic coating observations ahead of a short edge-cracked mild steel beam [178].

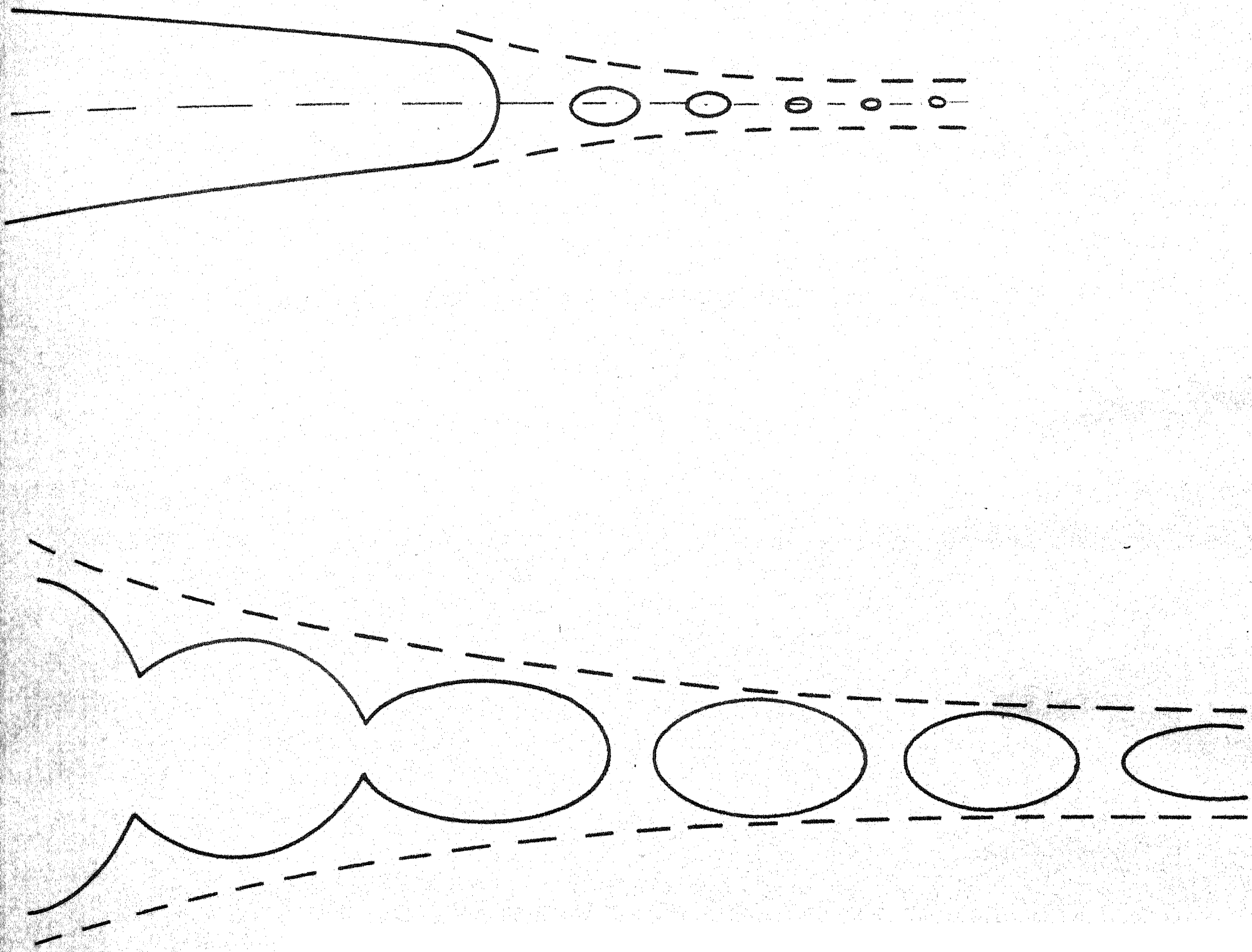

FIG. 2.4 CUMULATIVE DILATATIONAL DUCTILE FRACTURE BY
THE GROWTH AND COALESCENCE OF HOLES ,DISCON
TINUOUS PLASTIC FLOW AHEAD OF A NOTCH [55]

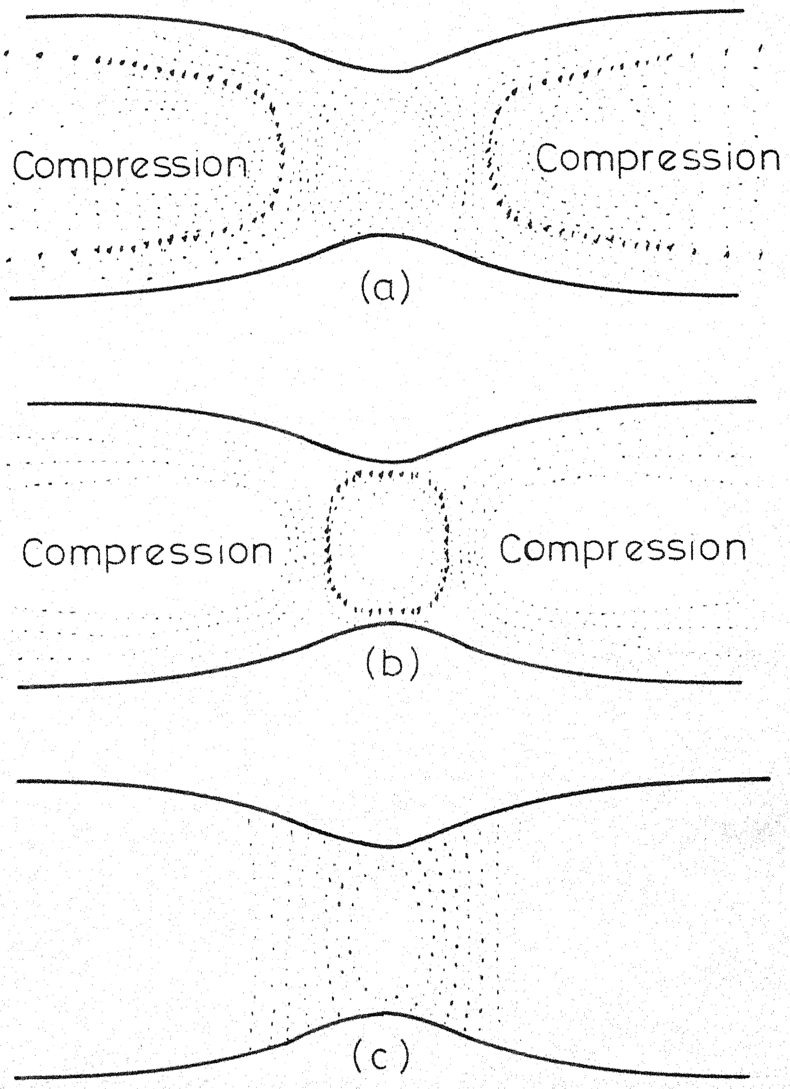
Compression
Compression
(a)
Compression
Compression
(b)
(c)

FIG. 2.5 CONTOURS OF STRESSES AND STRAINS SHOWING TENSION, COMPRESSION AND LOCALIZED SHEAR : COMPUTED CONTOURS OF (a) AXIAL STRESS, (b) MEAN TENSILE STRESS, AND (c) EQUIVALENT PLASTIC STRAIN [159]

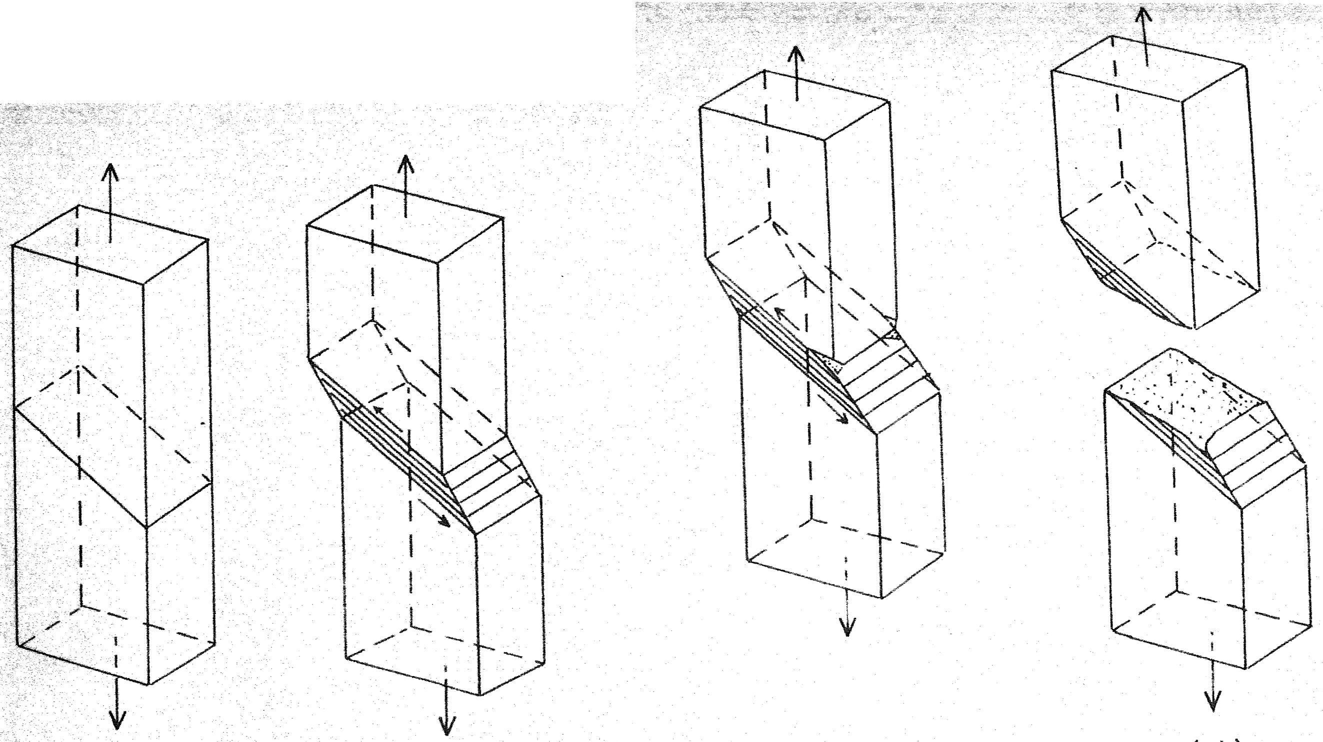

(a) Coarse slip band formation

(b) Localized shear

(c) Crack initiation

(d) Separation

FIG. 2.6 SCHEMATIC DIAGRAM OF THE FRACTURE PROCESS IN ALUMINUM ALLOY SINGLE CRYSTALS AGE HARDENED BY THE FORMATION OF GP ZONES [153]

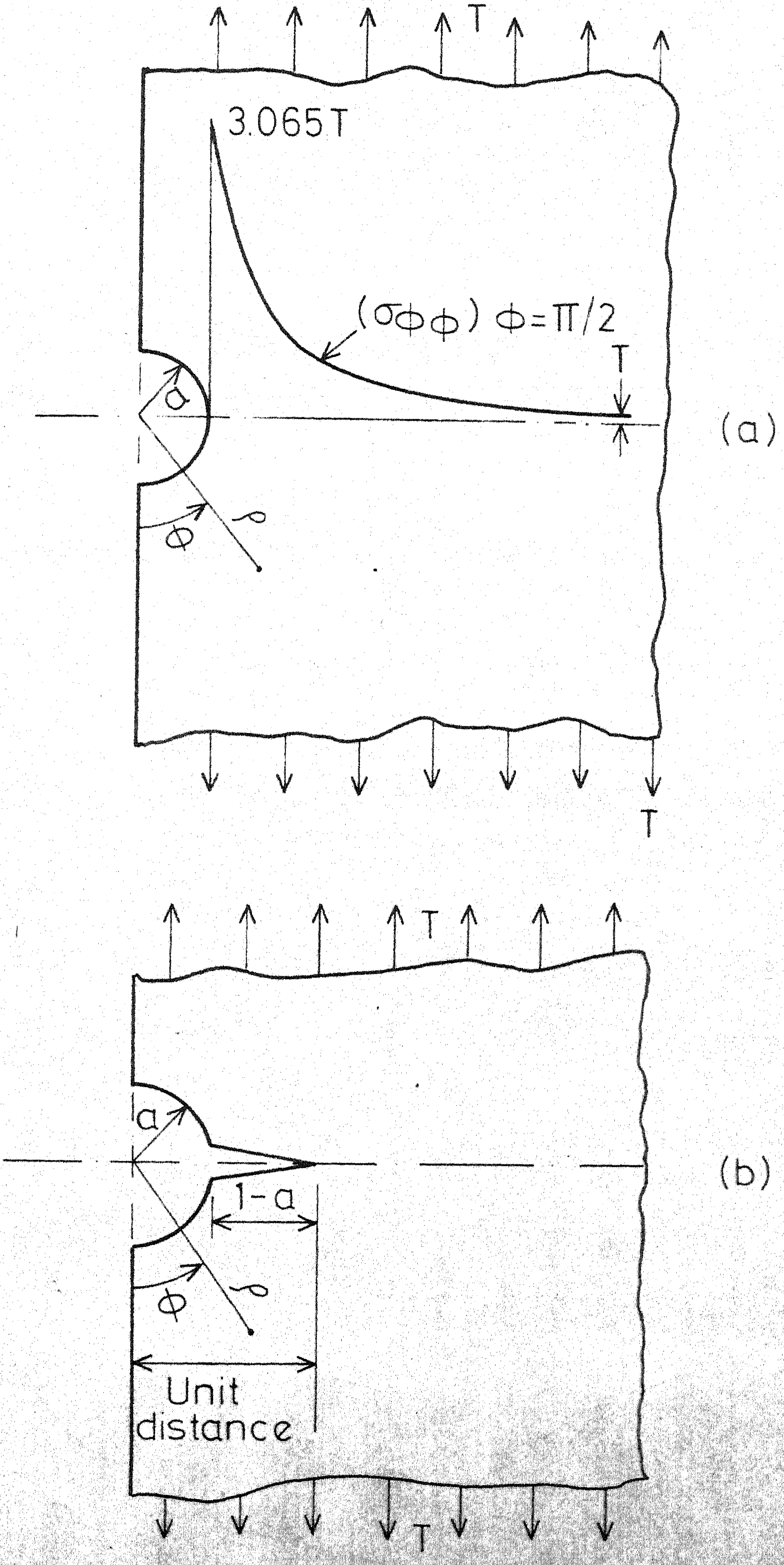
T
3.065T
$(\sigma_{\phi\phi})\ \phi=\pi/2$
T
a
φ
ρ
(a)
T
T
a
1-a
φ
ρ
Unit distance
(b)
T

FIG. 3.1 STRESSES AT THE ROOT OF A SEMI-CIRCULAR EDGE NOTCH AND A CRACK RADIALLY EMANATING FROM ITS

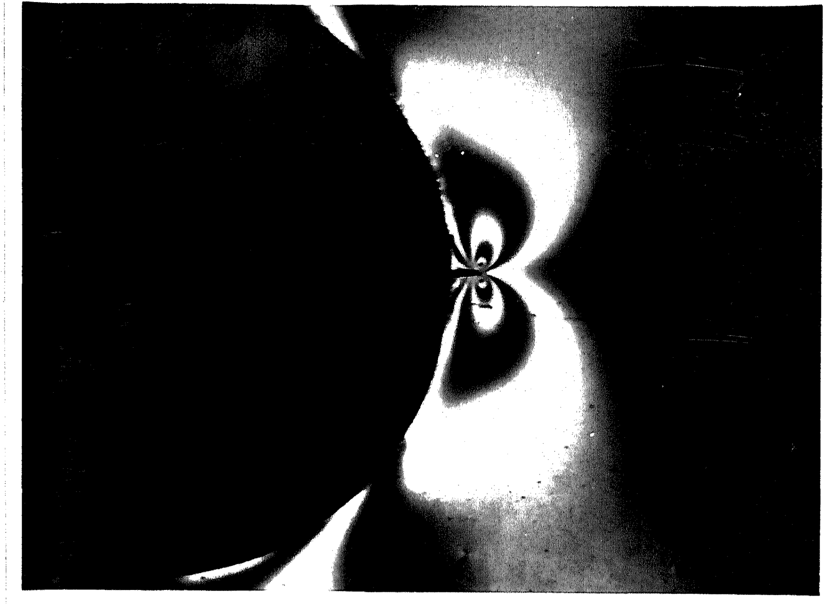

Fig. 3.3 Isochromatic fringe pattern in dark field on plane transmission photoelastic model specimen at the tip of a fine razor blade slit-cut eman from the root of a semi-circular edge notch in tension plate.

Machined notch radius = 10.50 mm

Length of the slit cut = 1.10 mm

Width of the specimen = 75 mm

Thickness of the specimen = 3.66 mm.

Tension load = 71.4 Kg.

Fringe value, f_σ = 10.76 Kg/cm/fringe

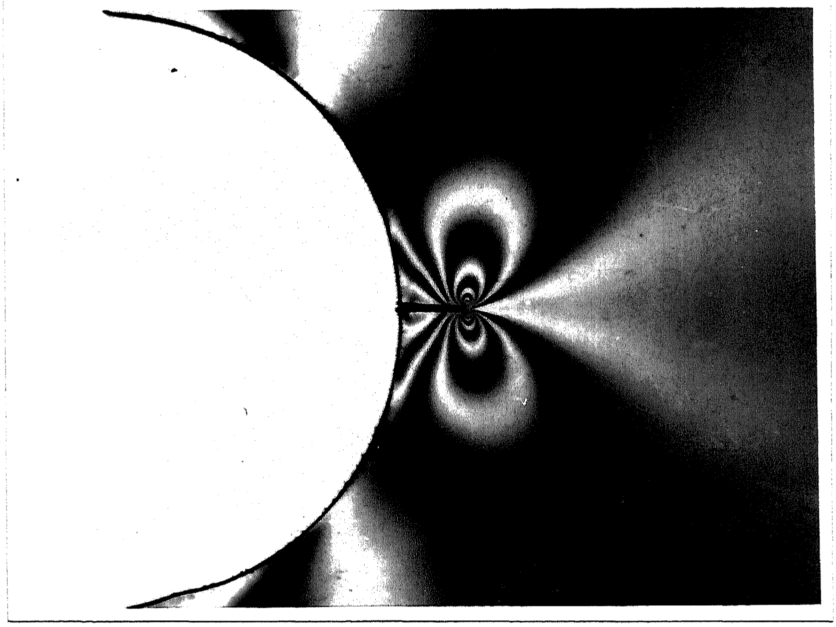

Fig. 3.4 Isochromatic fringe pattern in light field on plane transmission photoelastic model specime at the tip of a fine razor blade slit-cut ema ting from the root of a semi-circular edge-no in a tension plate.

Machined notch radius = 10.50 mm

Length of the slit-cut = 2.79 mm

Width of the specimen = 75 mm

Thickness of the specimen = 3.66 mm

Tension load = 71.4 Kg

Fringe value, f_σ = 10.76 Kg/cm/fringe

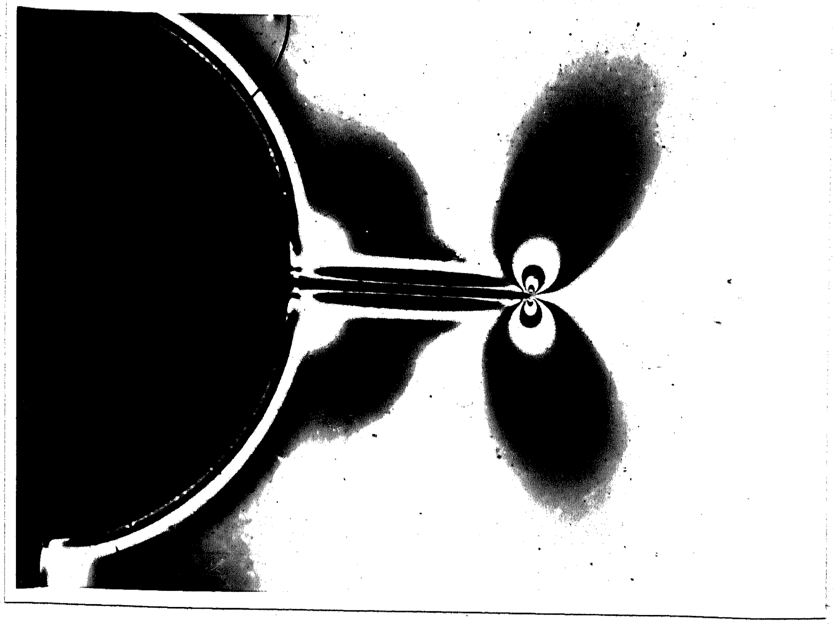

Fig. 3.5 Isochromatic fringe pattern in dark field on plane transmission photoelastic model specimen at the tip of a fine razor blade slit-cut emanating from the root of a semi-circular edge notch in a tension plate.

Machined notch radius = 10.50 mm
Length of the slit = 9.35 mm
Width of the specimen = 75 mm
Thickness of the specimen = 3.66 mm
Tension load = 26.4 Kg
Fringe value f_σ = 10.76 Kg/cm/fringe.

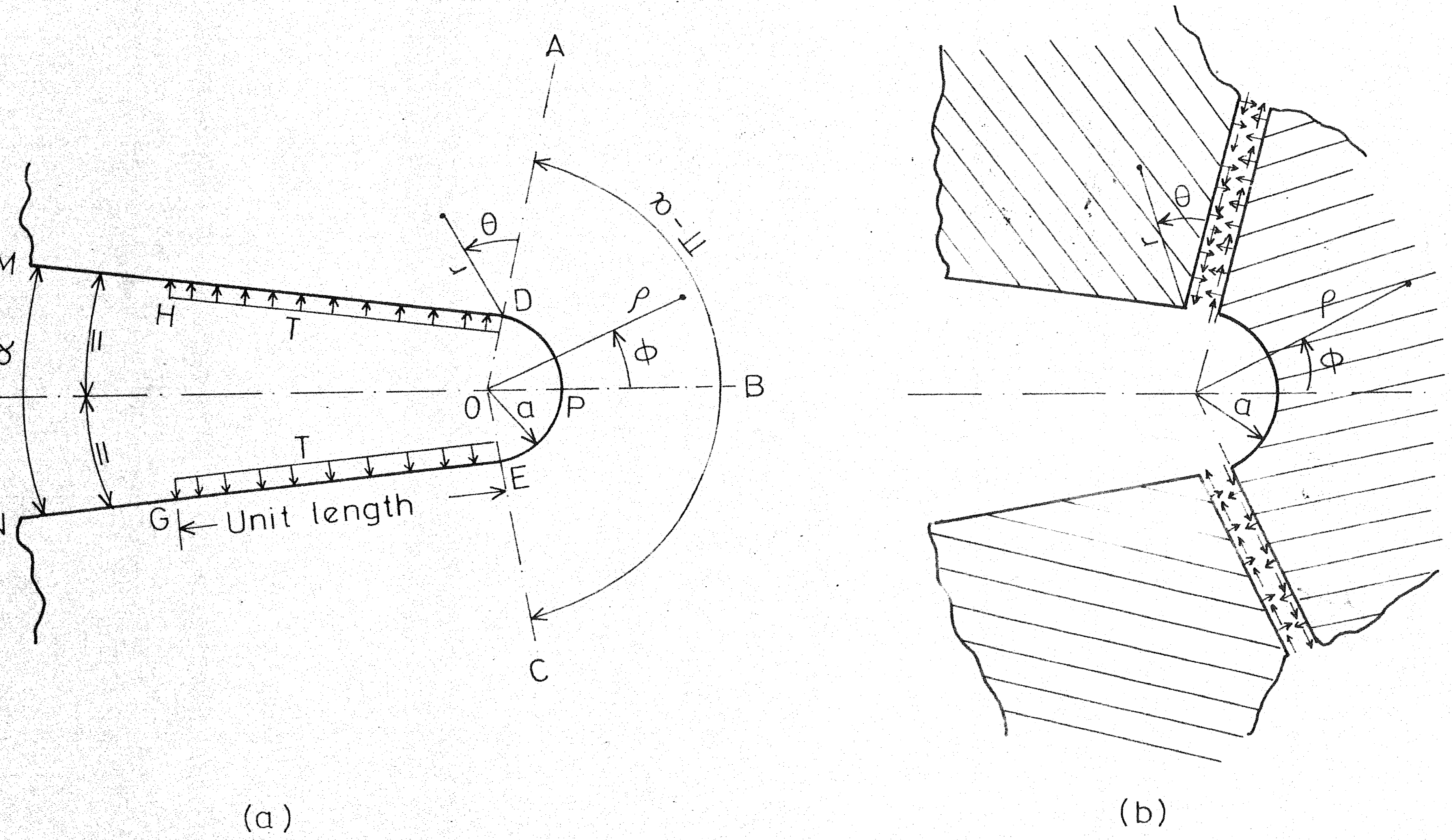
A
B
C
D
E
O
P
a
ρ
φ
θ
r
π-γ
H
G
T
T
M
N
γ
Unit length
(a)
(b)

FIG. 4.1 GEOMETRY OF A CRACK-LIKE-NOTCH AND LOADING ON ITS FLAT FACES.

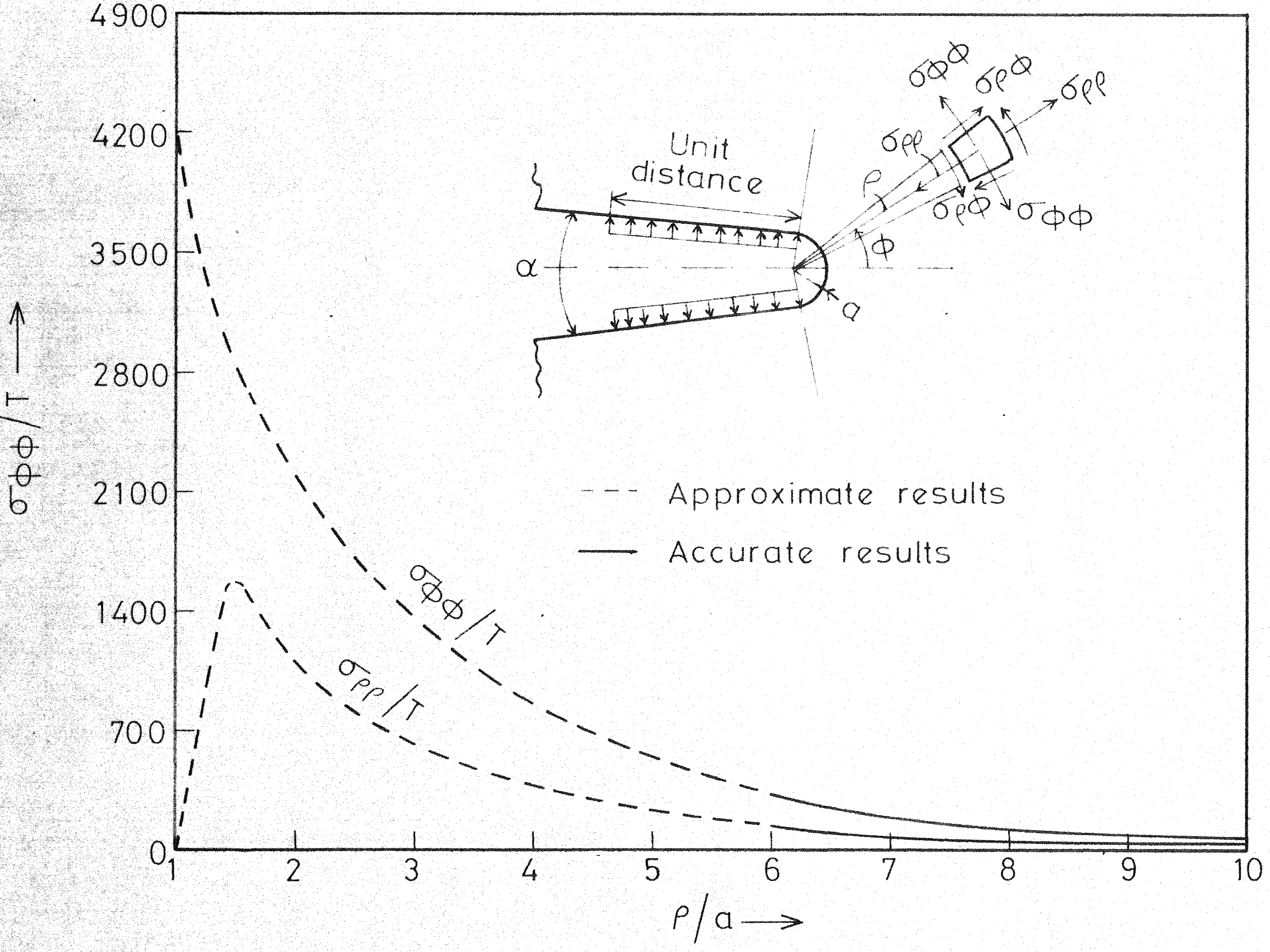

IG. 4.2 TANGENTIAL AND RADIAL NORMAL STRESSES NEAR THE NOTCH ROOT REGION ON 0° PLANE. FLANK ANGLE, $\alpha = 1°$ AND TIP ROOT RADIUS, $a = 1/100$.

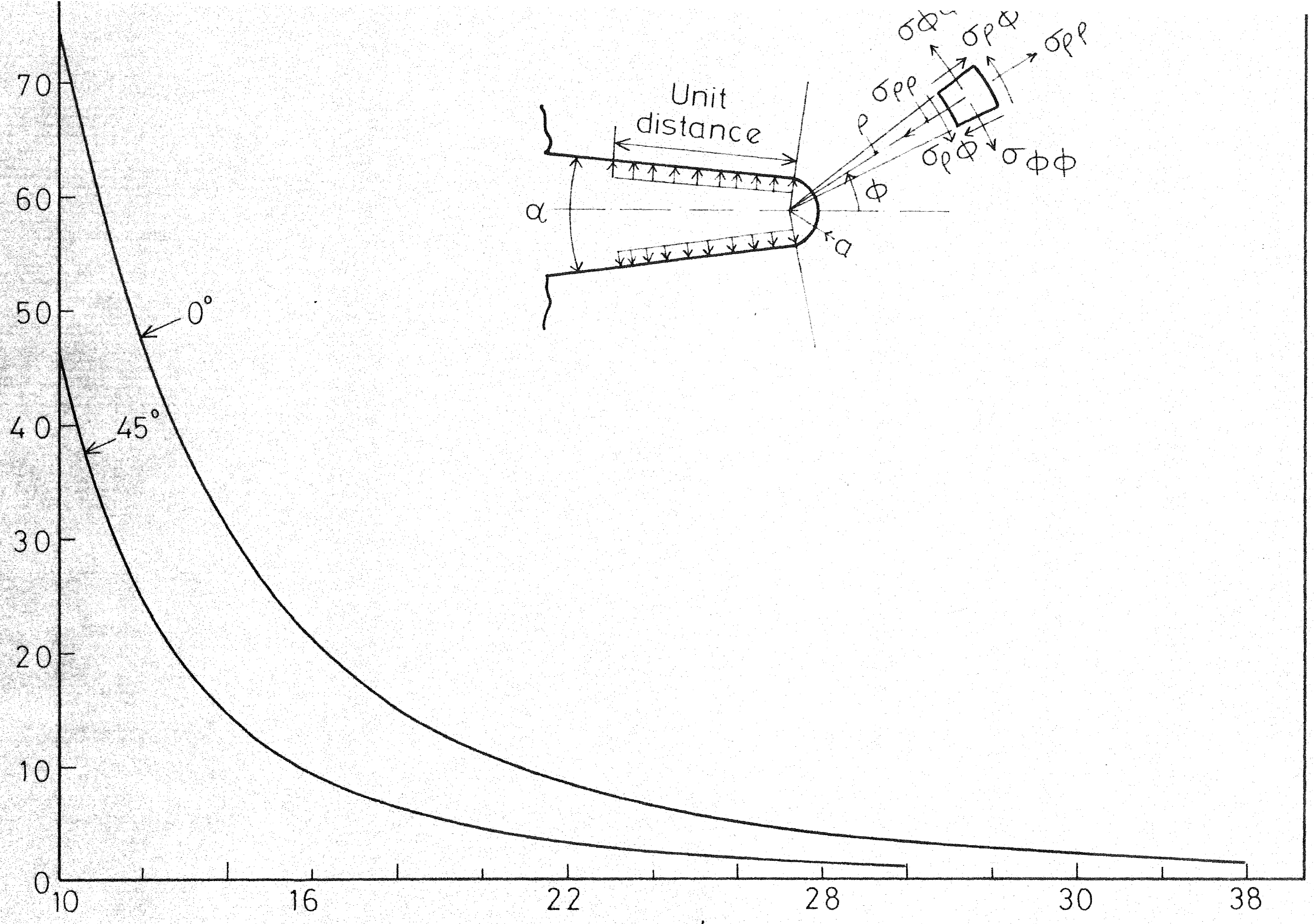

4.3 TANGENTIAL NORMAL STRESS $\sigma_{\phi\phi}$ AHEAD OF A CRACK-LIKE-NOTCH ON $\phi = 0°$ AND 45° PLANES. FLANK ANGLE, $\alpha = 1°$ AND TIP ROOT RADIUS, $a = 1/100$.

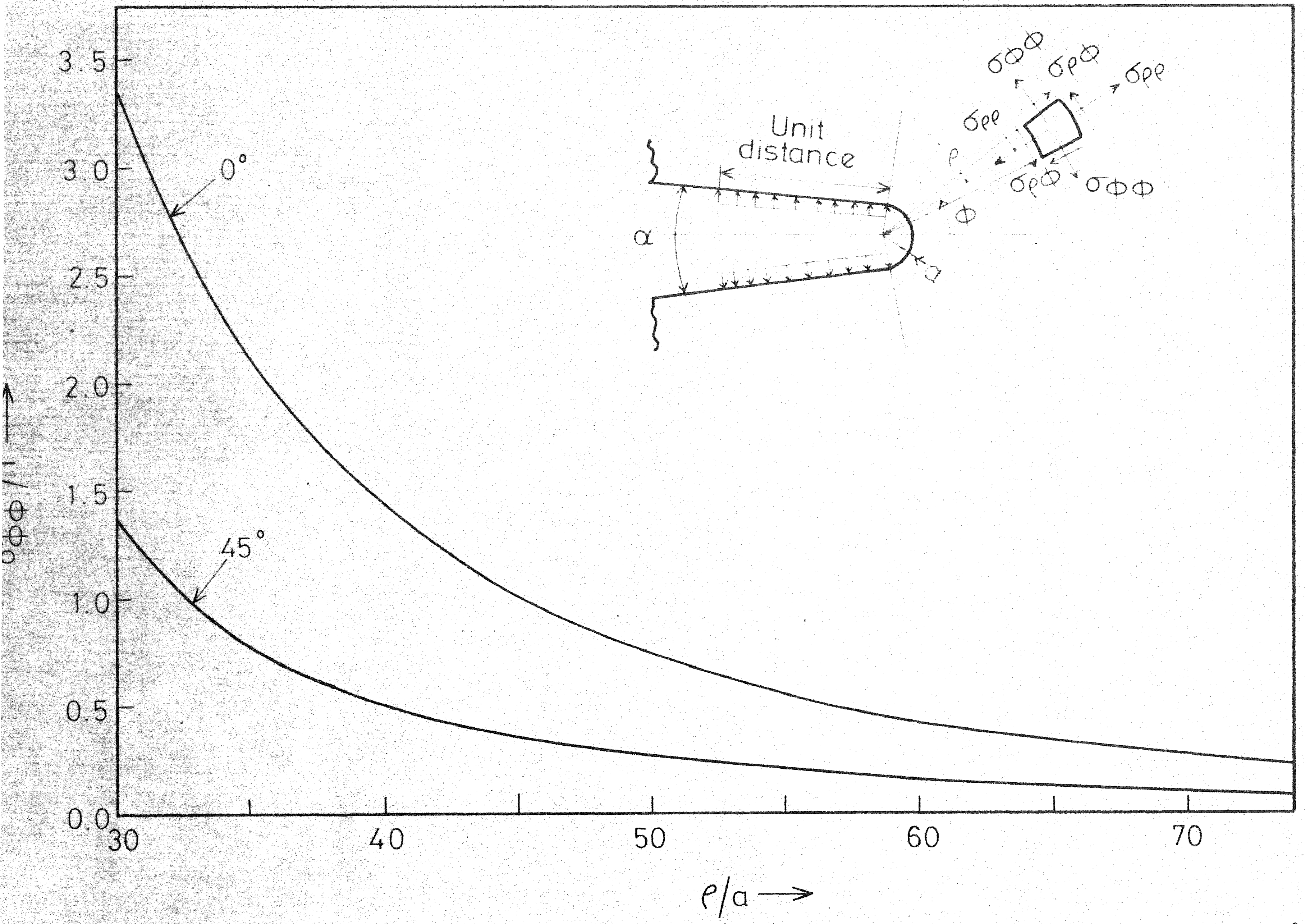

G. 4.4 TANGENTIAL NORMAL STRESS $\sigma_{\Phi\Phi}$ AHEAD OF A CRACK-LIKE-NOTCH ON $\Phi = 0°$

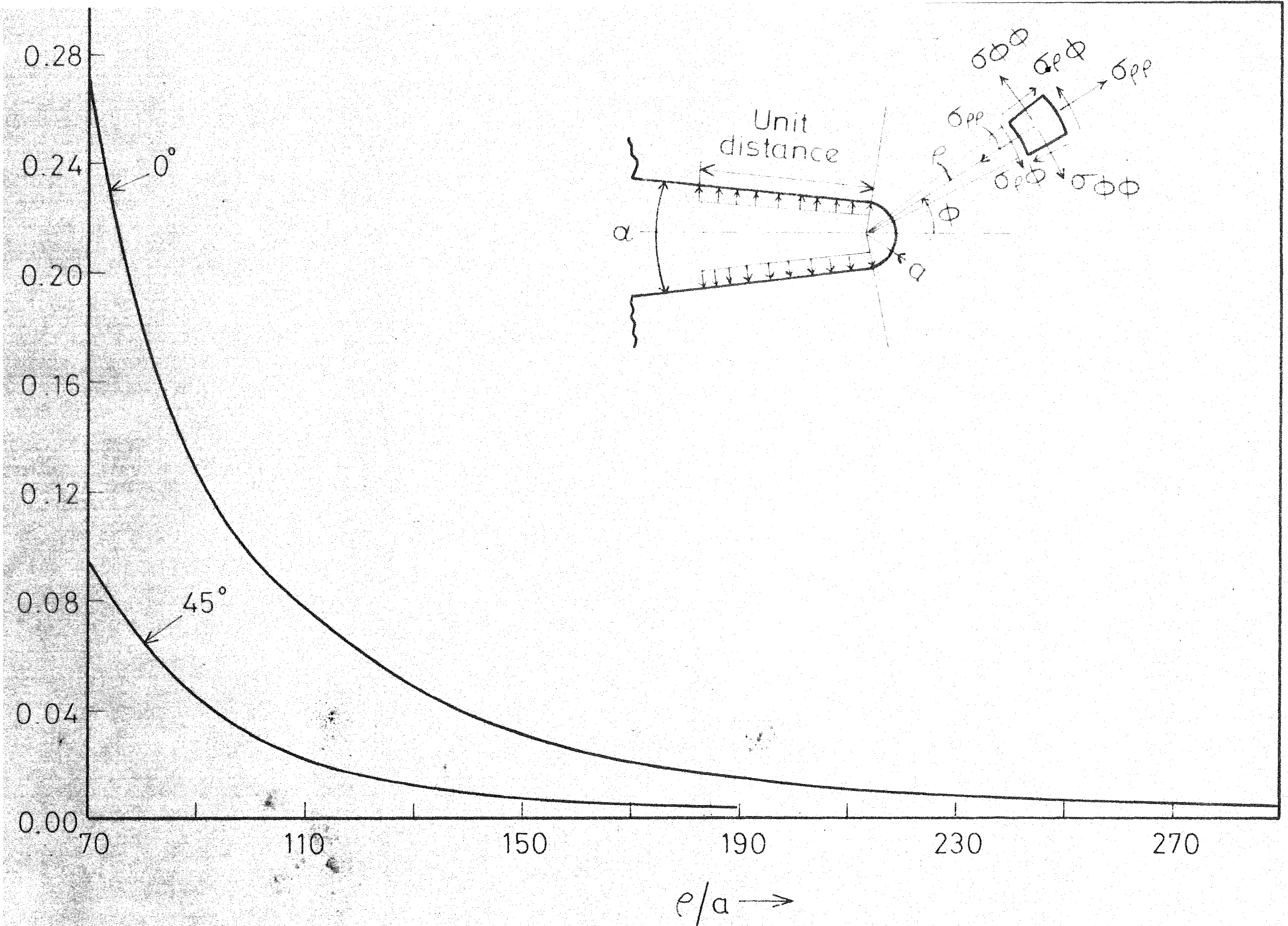

4.5 TANGENTIAL NORMAL STRESS $\sigma_{\Phi\Phi}$ AHEAD OF A CRACK-LIKE-NOTCH ON $\Phi = 0°$ AND 45° PLANES, FLANK ANGLE, $\alpha = 1°$ AND TIP ROOT RADIUS, $a = 1/100$.

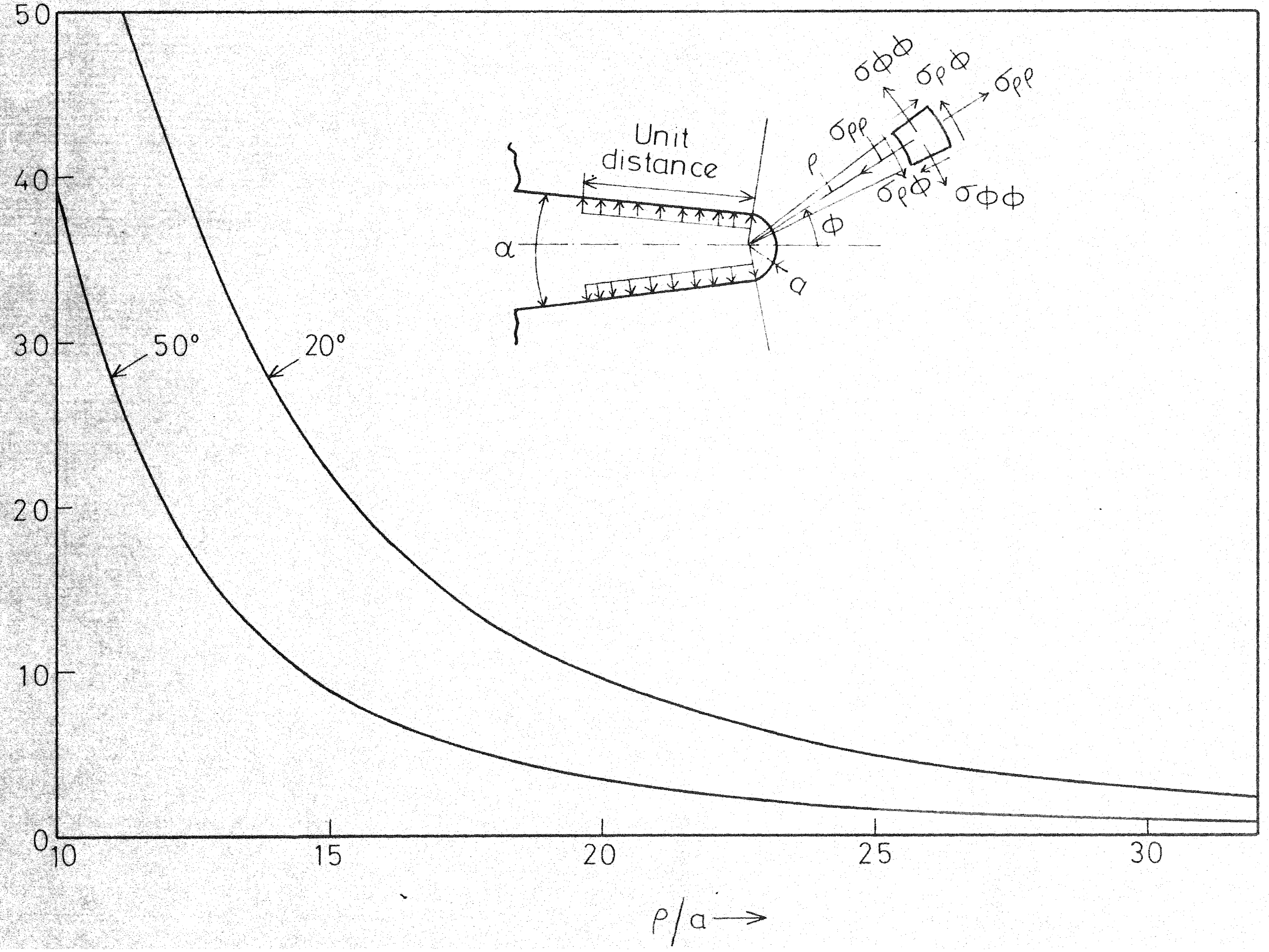
50
40
30
20
10
0
10
15
20
25
30
ρ/a →
50°
20°
Unit distance
α
a
ρ
Φ
σρρ
σΦΦ
σρΦ
σρρ
σρΦ
σΦΦ

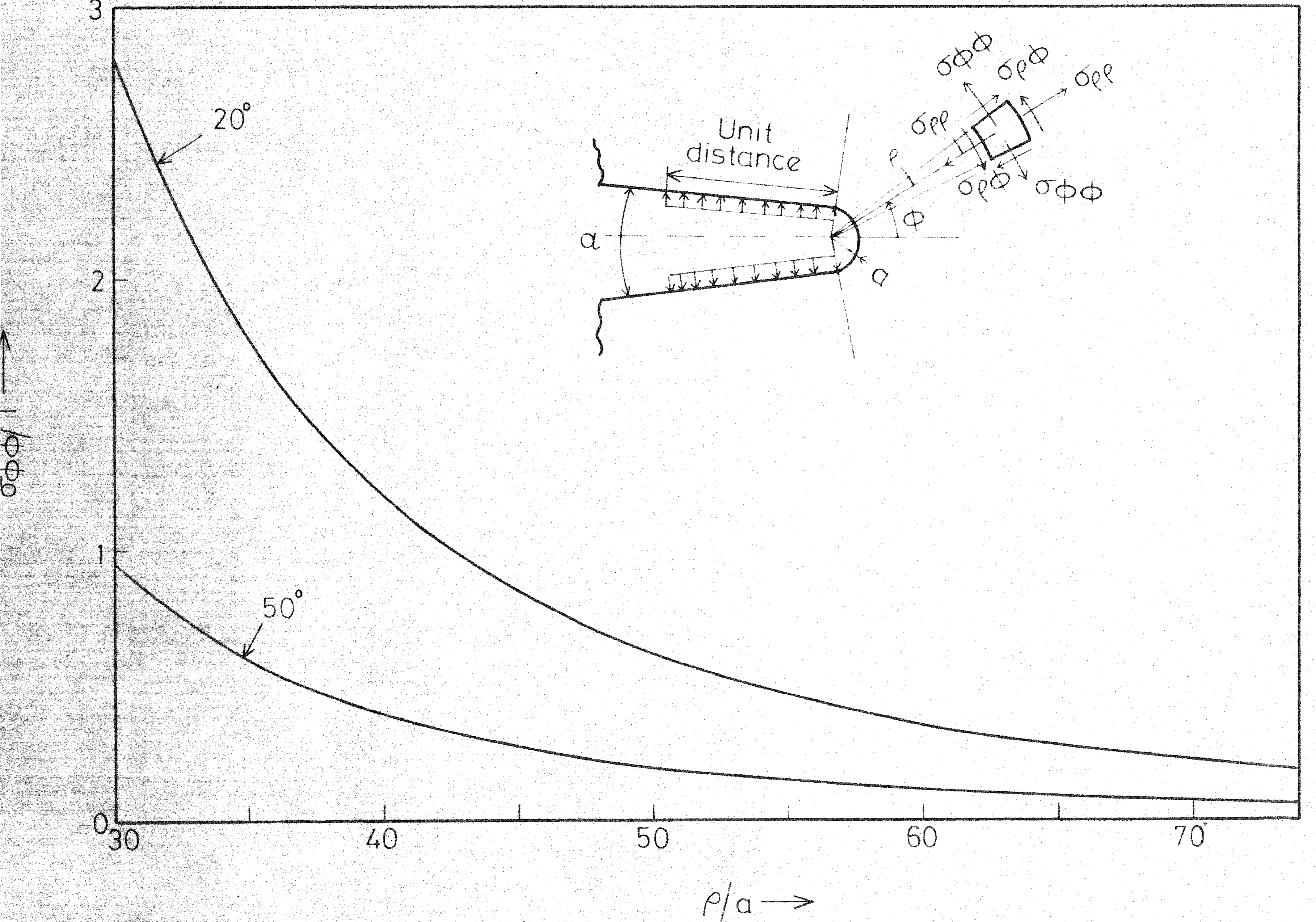

4.7 TANGENTIAL NORMAL STRESS $\sigma_{\phi\phi}$ AHEAD OF A CRACK-LIKE-NOTCH ON $\phi = 20^\circ$

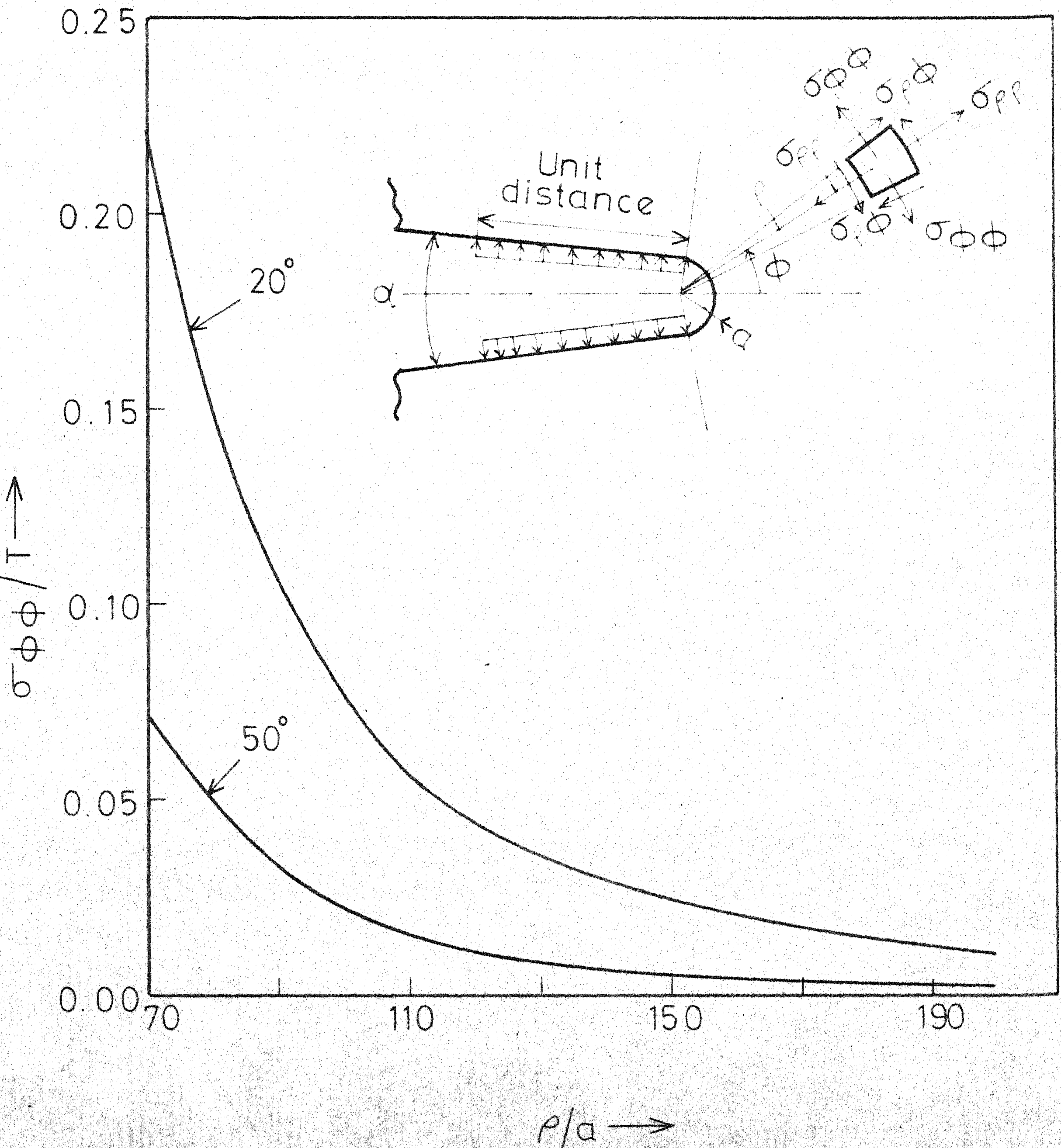

FIG. 4.8 TANGENTIAL NORMAL STRESS $\sigma_{\phi\phi}$ AHEAD OF A CRACK LIKE-NOTCH ON $\phi = 20^\circ$ AND 50° PLANES. FLANK ANGLE, $\alpha = 1^\circ$ AND TIP ROOT RADIUS, $a = 1/100$.

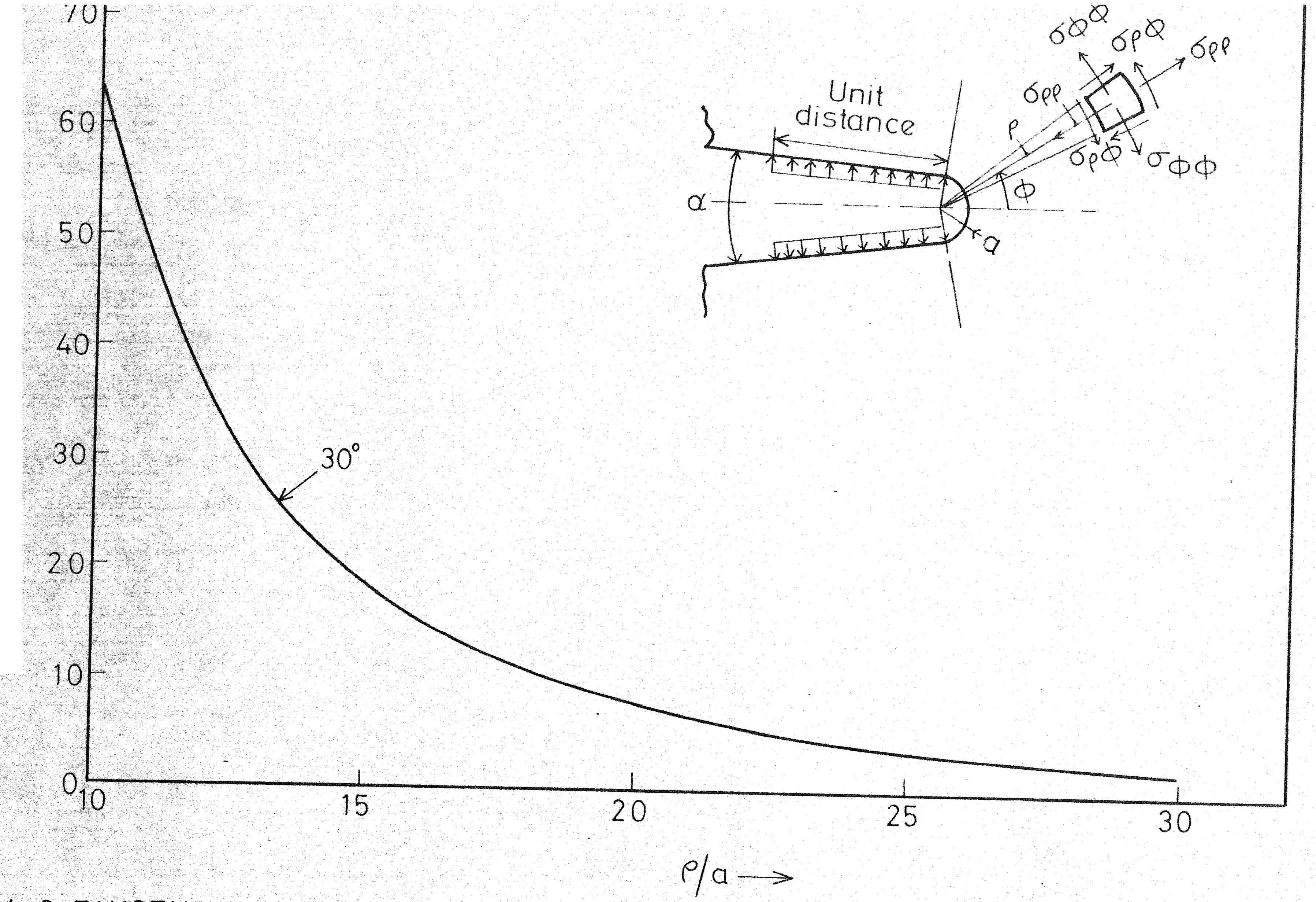

4.9 TANGENTIAL NORMAL STRESS $\sigma_{\phi\phi}$ AHEAD OF A CRACK-LIKE-NOTCH ON $\phi = 30°$ PLANE. FLANK ANGLE, $\alpha = 1°$ AND TIP ROOT RADIUS, $a = 1/100$

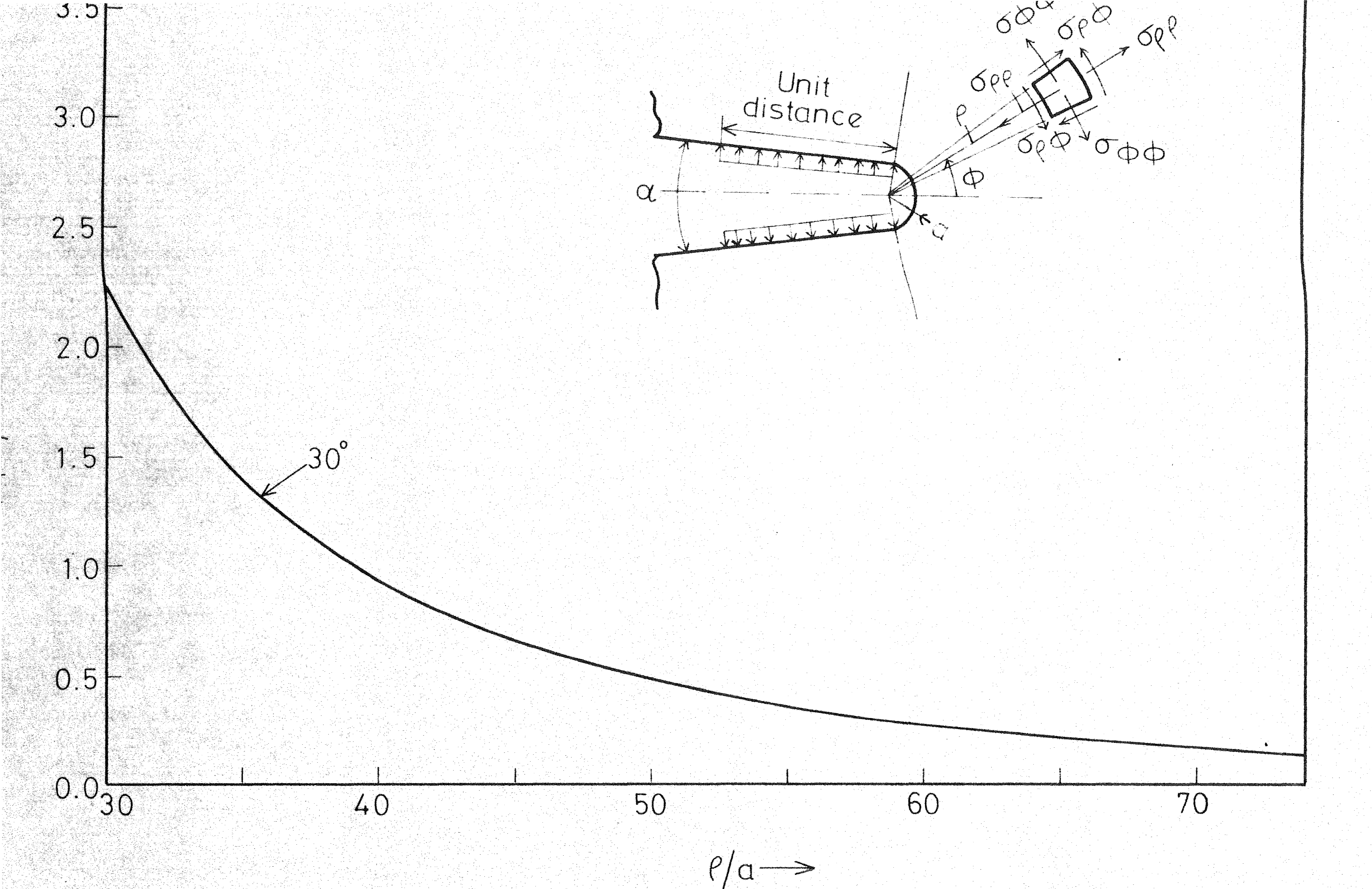

. 4.10 TANGENTIAL NORMAL STRESS $\sigma_{\phi\phi}$ AHEAD OF A CRACK-LIKE-NOTCH ON $\phi = 30°$ PLANE. FLANK ANGLE, $\alpha = 1°$ AND TIP ROOT RADIUS, $a = 1/100$.

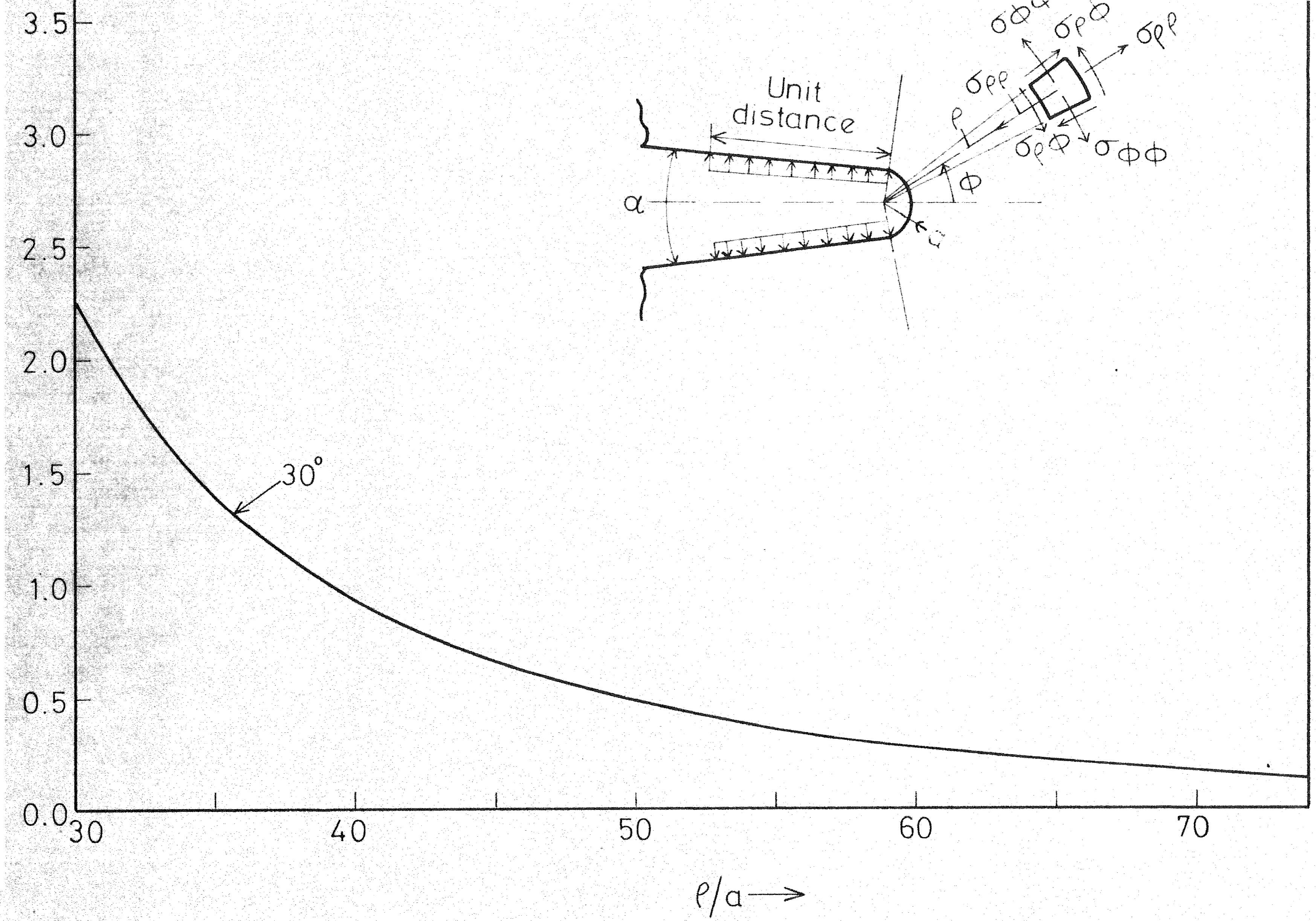

G. 4.10 TANGENTIAL NORMAL STRESS $\sigma_{\Phi\Phi}$ AHEAD OF A CRACK-LIKE-NOTCH ON $\Phi = 30°$ PLANE. FLANK ANGLE, $\alpha = 1°$ AND TIP ROOT RADIUS, $a = 1/100$.

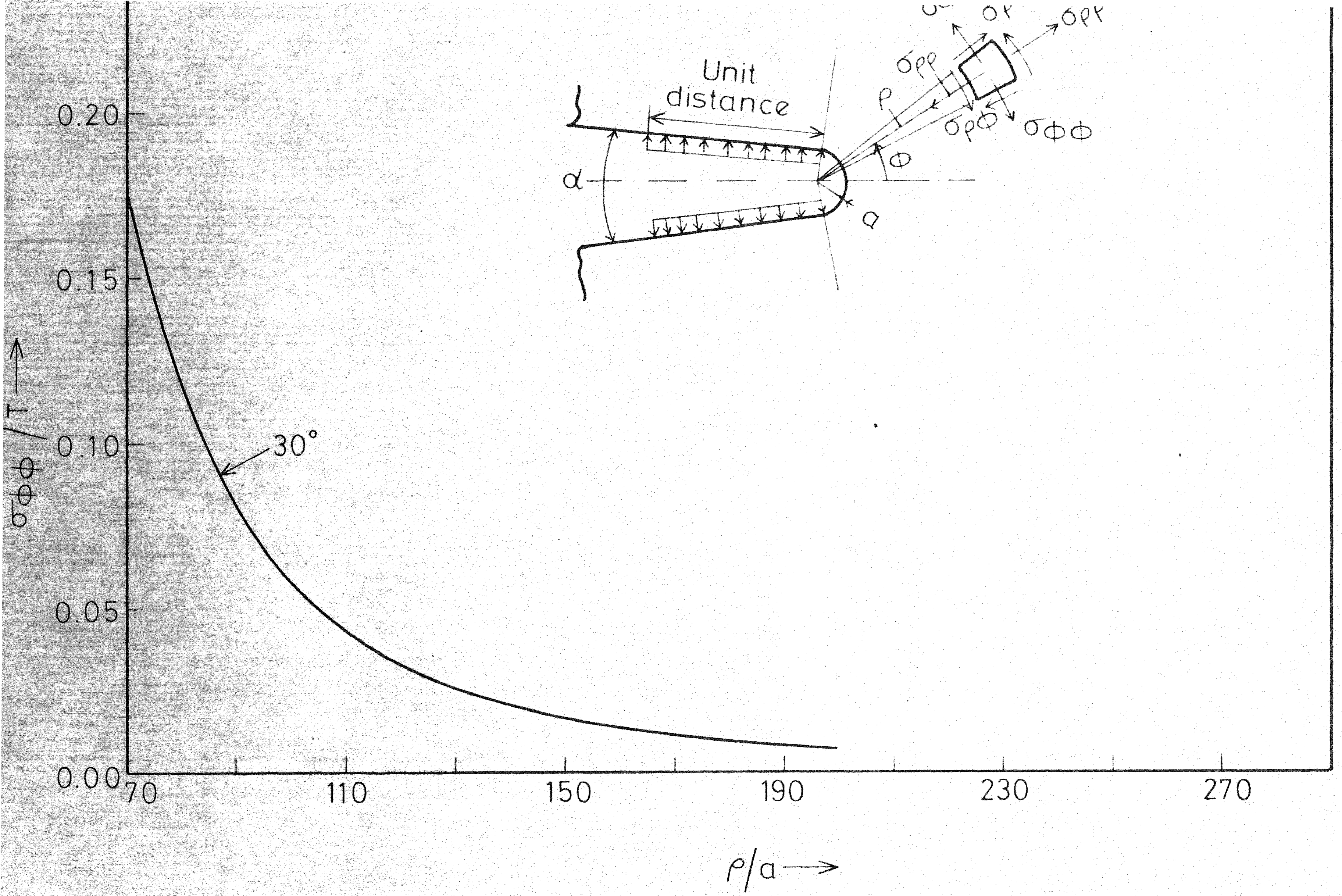

G. 4.11 TANGENTIAL NORMAL STRESS $\sigma_{\phi\phi}$ AHEAD OF A CRACK-LIKE-NOTCH ON $\phi = 30°$ PLANE. FLANK ANGLE, $\alpha = 1°$ AND TIP ROOT RADIUS, $a = 1/100$.

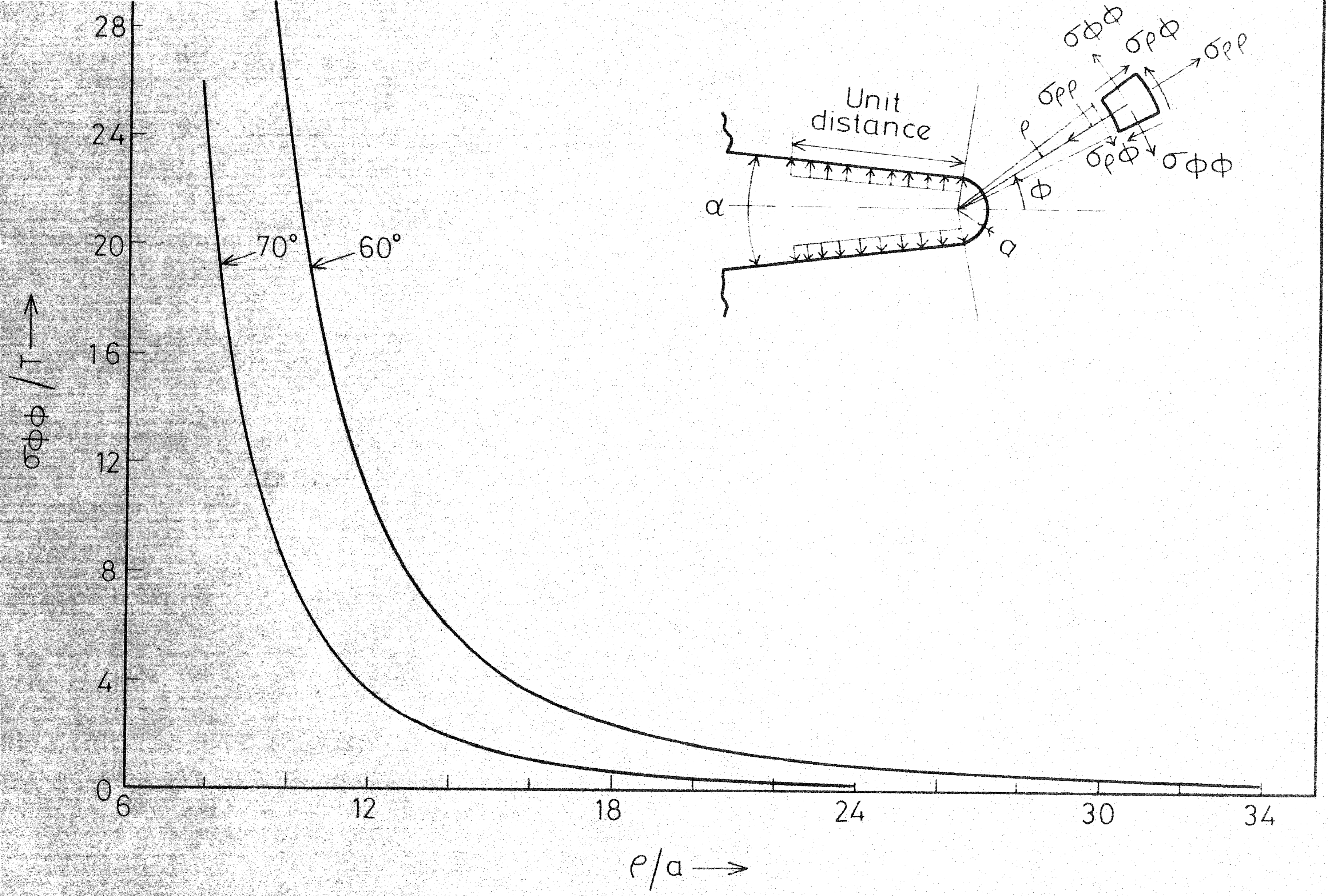

FIG. 4.12 TANGENTIAL NORMAL STRESS $\sigma_{\phi\phi}$ AHEAD OF A CRACK-LIKE-NOTCH ON ϕ = 60° AND 70° PLANES. FLANK ANGLE, $\alpha=1°$ AND TIP ROOT RADIUS, $a=1/100$.

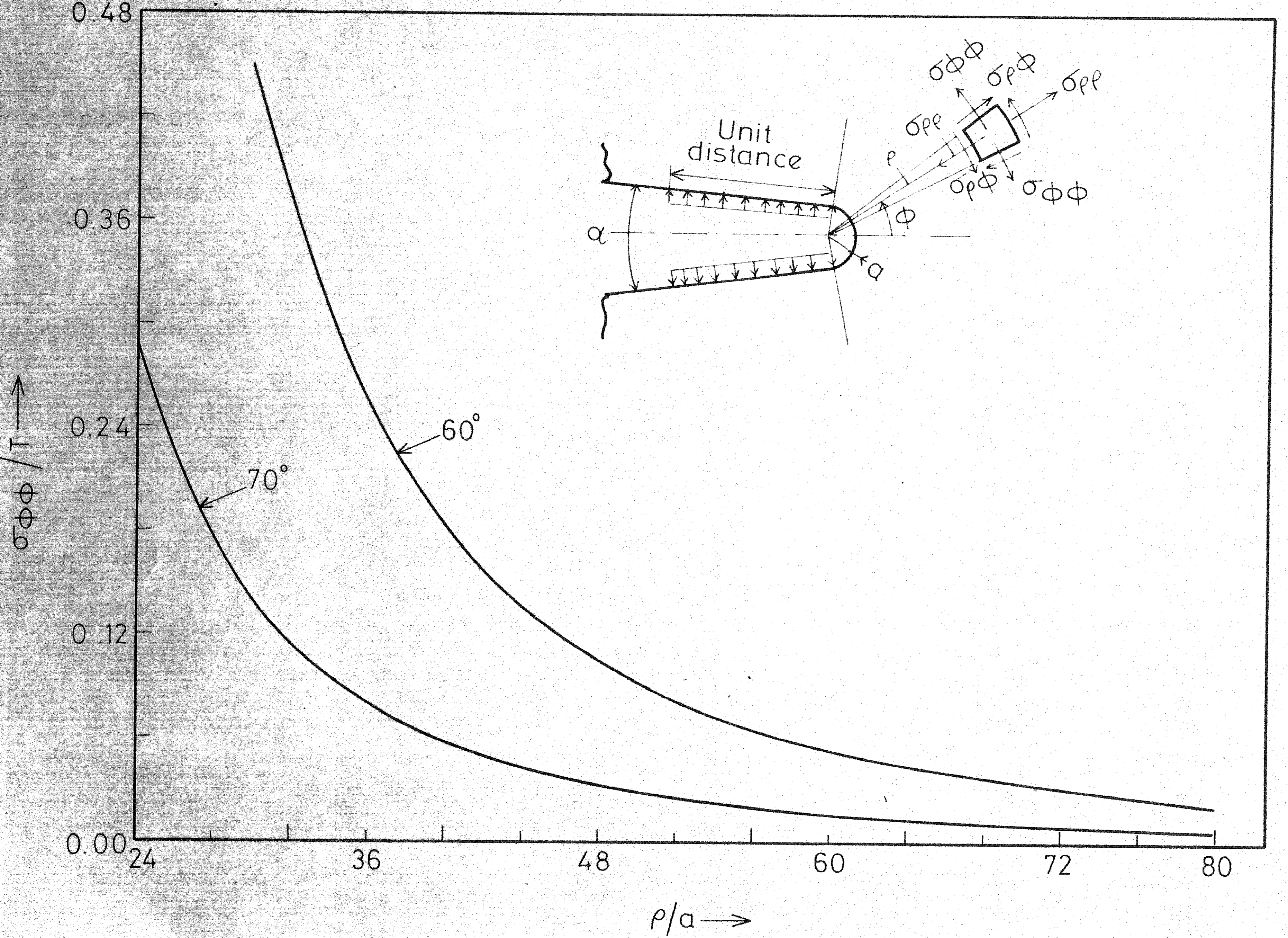

FIG. 4.13 TANGENTIAL NORMAL STRESS $\sigma_{\phi\phi}$ AHEAD OF A CRACK-LIKE-NOTCH ON $\phi = 60°$ AND 70° PLANES. FLANK ANGLE, $\alpha = 1°$ AND TIP ROOT RADIUS, $a = 1/100$

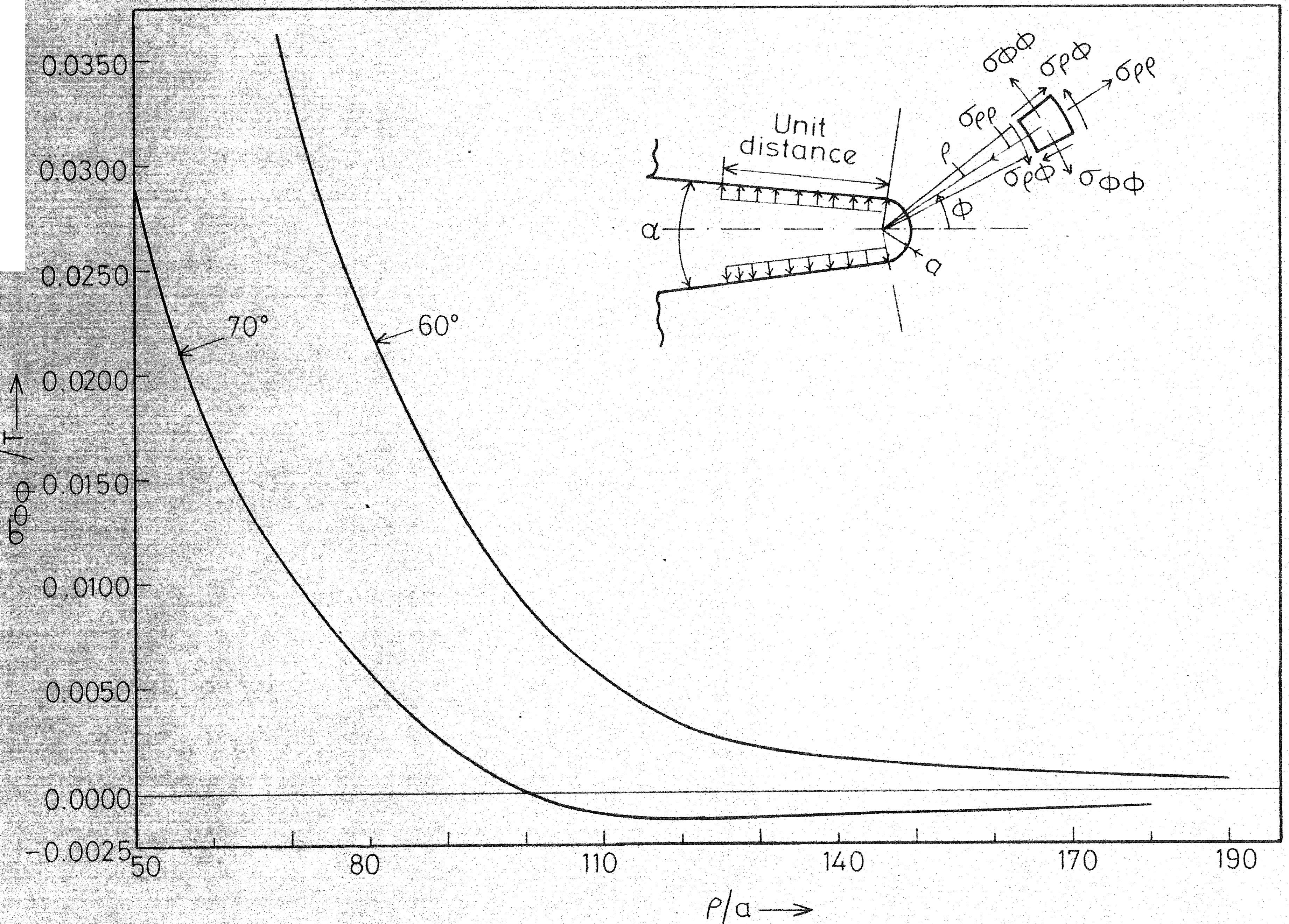

FIG. 4.14 TANGENTIAL NORMAL STRESS $\sigma_{\phi\phi}$ AHEAD OF A CRACK-LIKE-NOTCH ON $\phi = 60°$ AND 70° PLANES. FLANK ANGLE, $\alpha = 1°$ AND TIP ROOT RADIUS, $a = 1/100$.

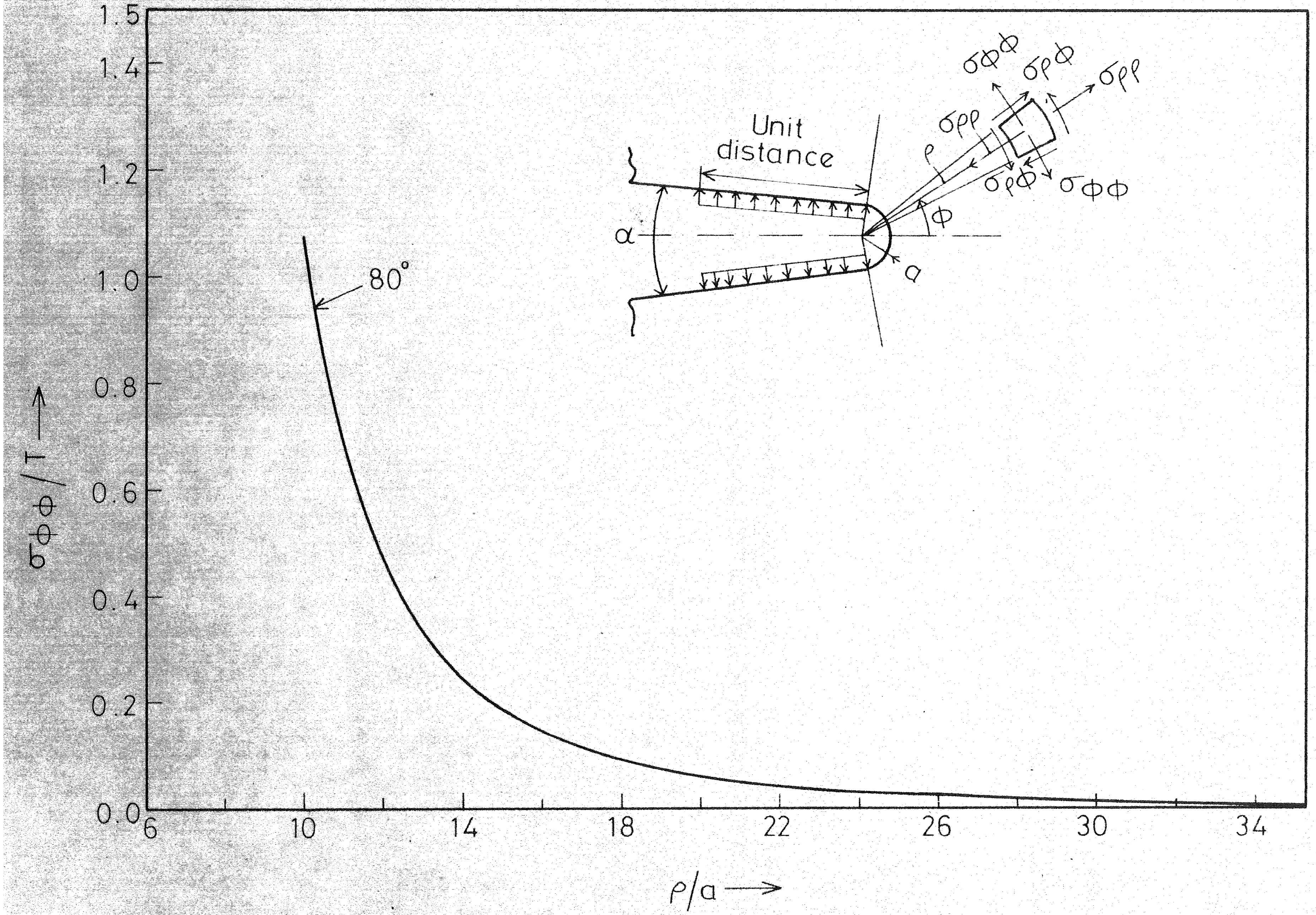

FIG. 4.15 TANGENTIAL NORMAL STRESS $\sigma_{\phi\phi}$ AHEAD OF A CRACK-LIKE-NOTCH ON $\phi = 80°$ PLANE. FLANK ANGLE, $\alpha = 1°$ AND TIP ROOT RADIUS, $a = 1/100$.

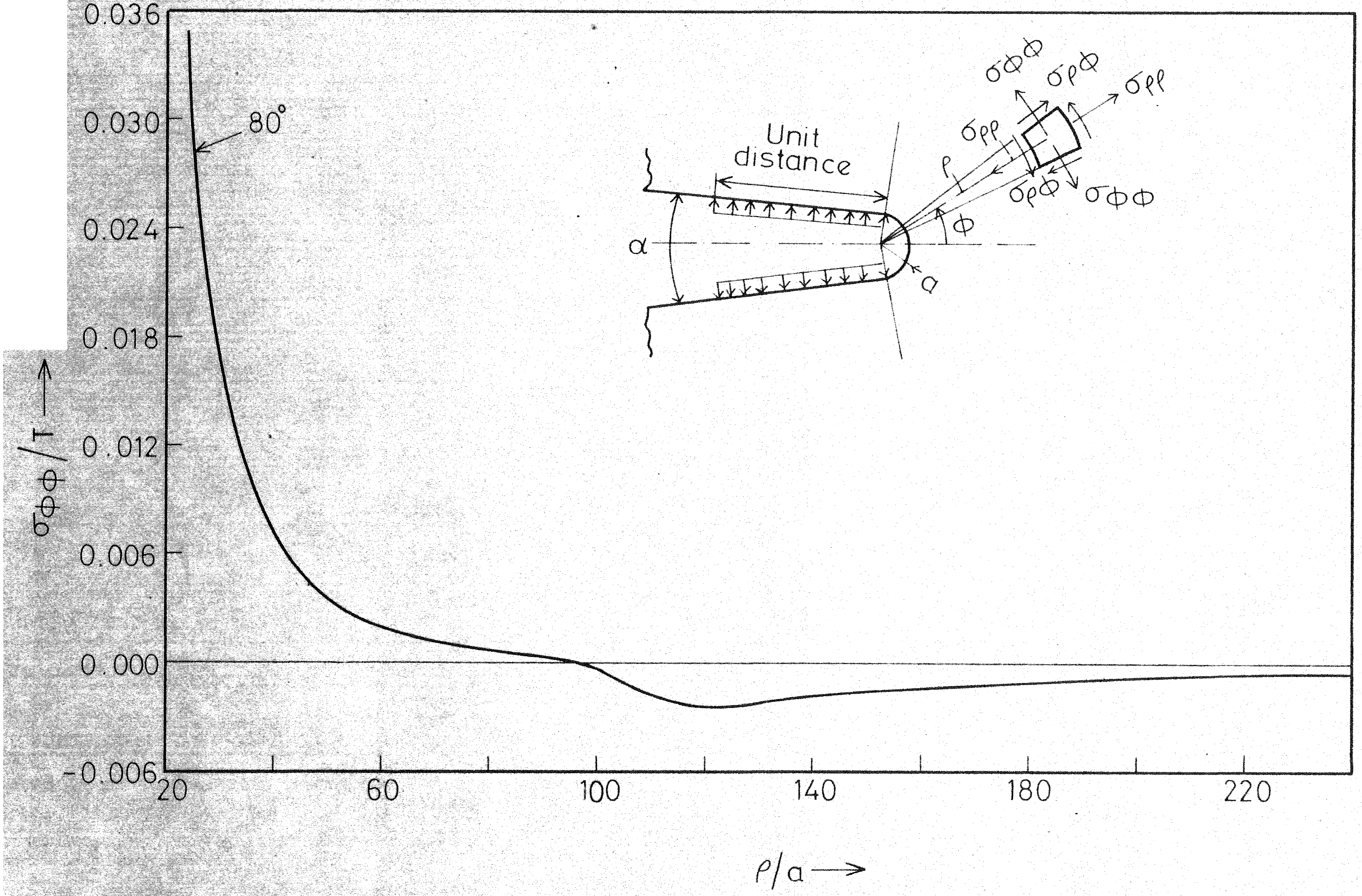

FIG. 4.16 TANGENTIAL NORMAL STRESS $\sigma_{\phi\phi}$ AHEAD OF A CRACK-LIKE-NOTCH ON $\phi = 80°$ PLANE. FLANK ANGLE, $\alpha = 1°$ AND TIP ROOT RADIUS, $a = 1/100$.

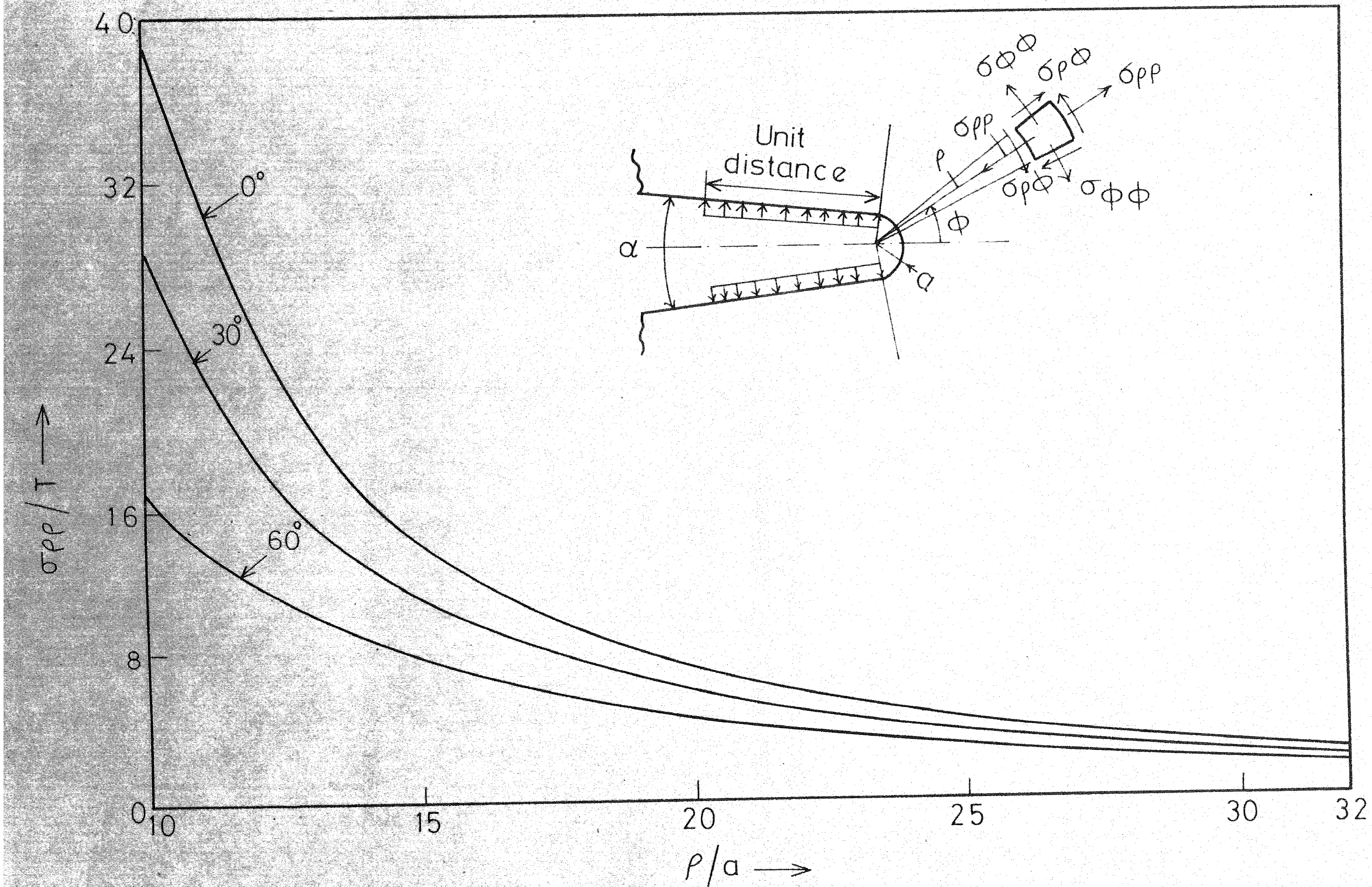

G.4.17 RADIAL NORMAL STRESS $\sigma_{\rho\rho}$ AHEAD OF A CRACK-LIKE-NOTCH ON $\phi = 0°, 30°$ AND $60°$ PLANES. FLANK ANGLE, $\alpha = 1°$ AND TIP ROOT RADIUS, $a = 1/100$

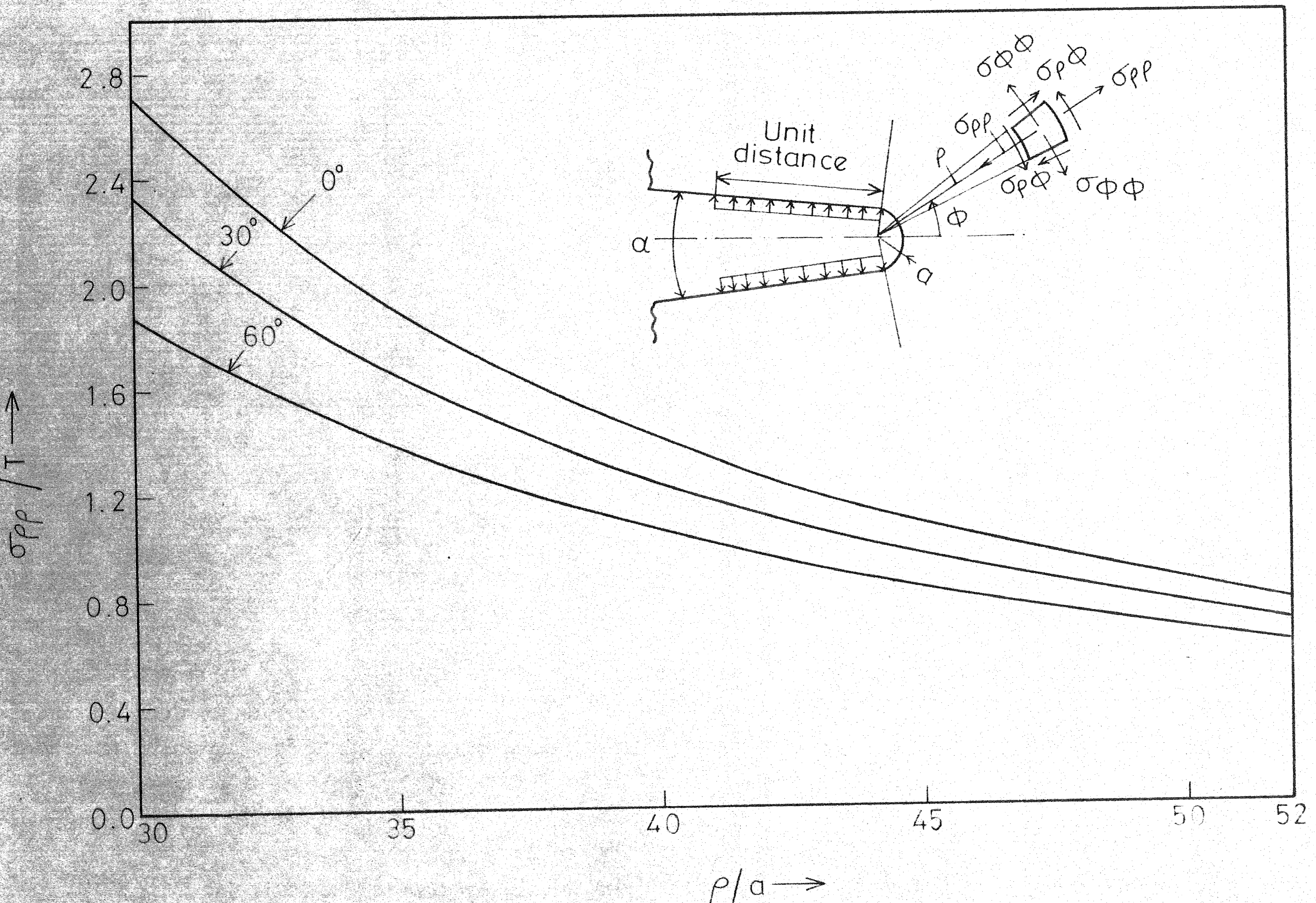

FIG. 4.18 RADIAL NORMAL STRESS $\sigma_{\rho\rho}$ AHEAD OF A CRACK-LIKE-NOTCH ON $\phi = 0°, 30°$ AND FLANK ANGLE, $\alpha = 1°$ AND TIP ROOT RADIUS, $a = 1/100$

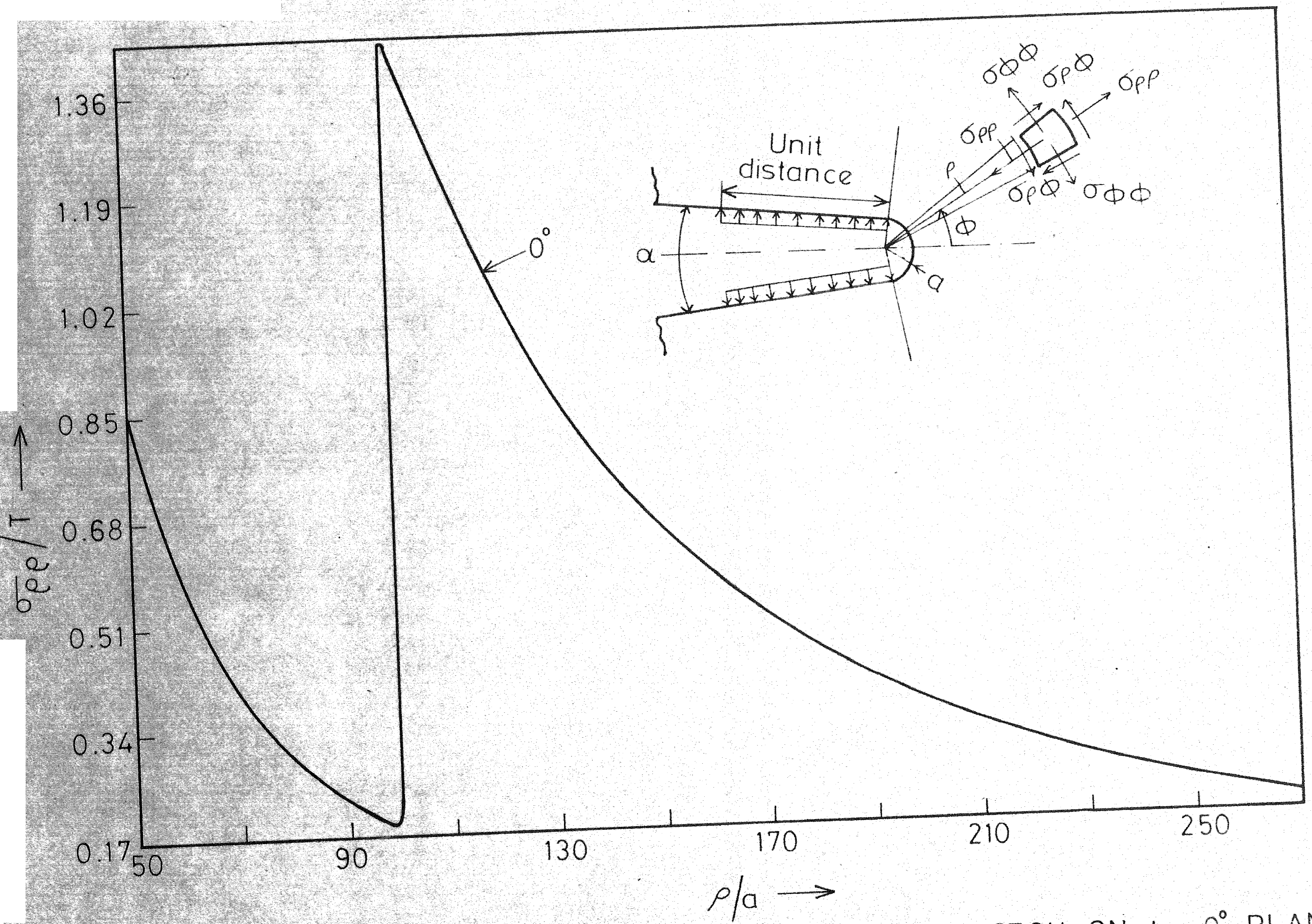

FIG.4.19 RADIAL NORMAL STRESS $\sigma_{\rho\rho}$ AHEAD OF A CRACK-LIKE-NOTCH ON $\phi = 0°$ PLANE FLANK ANGLE, $\alpha = 1°$ AND TIP ROOT RADIUS, $a = 1/100$

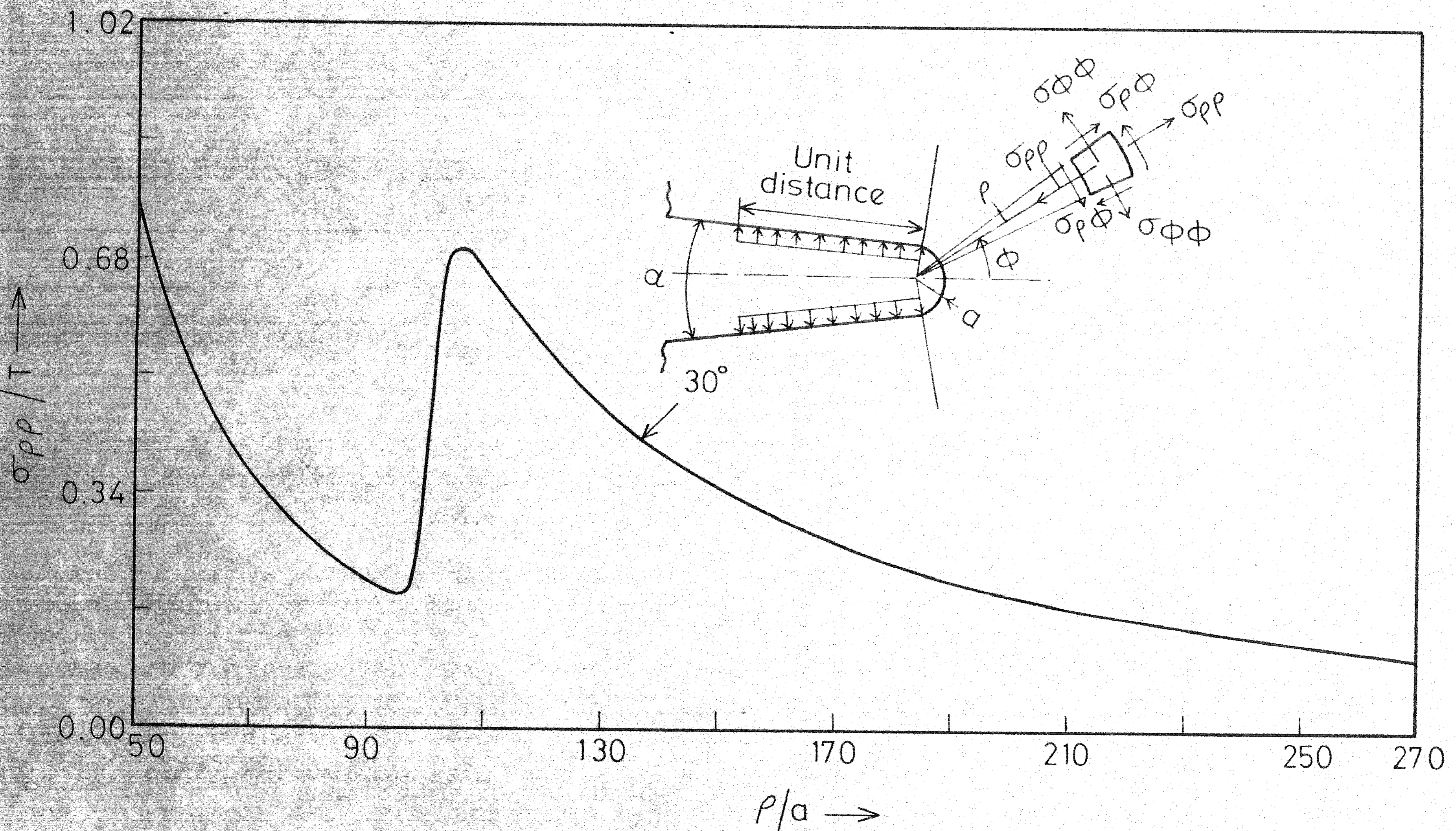

FIG.4.20 RADIAL NORMAL STRESS $\sigma_{\rho\rho}$ AHEAD OF A CRACK-LIKE-NOTCH ON $\phi = 30°$ PLANE. FLANK ANGLE, $\alpha = 1°$ AND TIP ROOT RADIUS, $a = 1/100$.

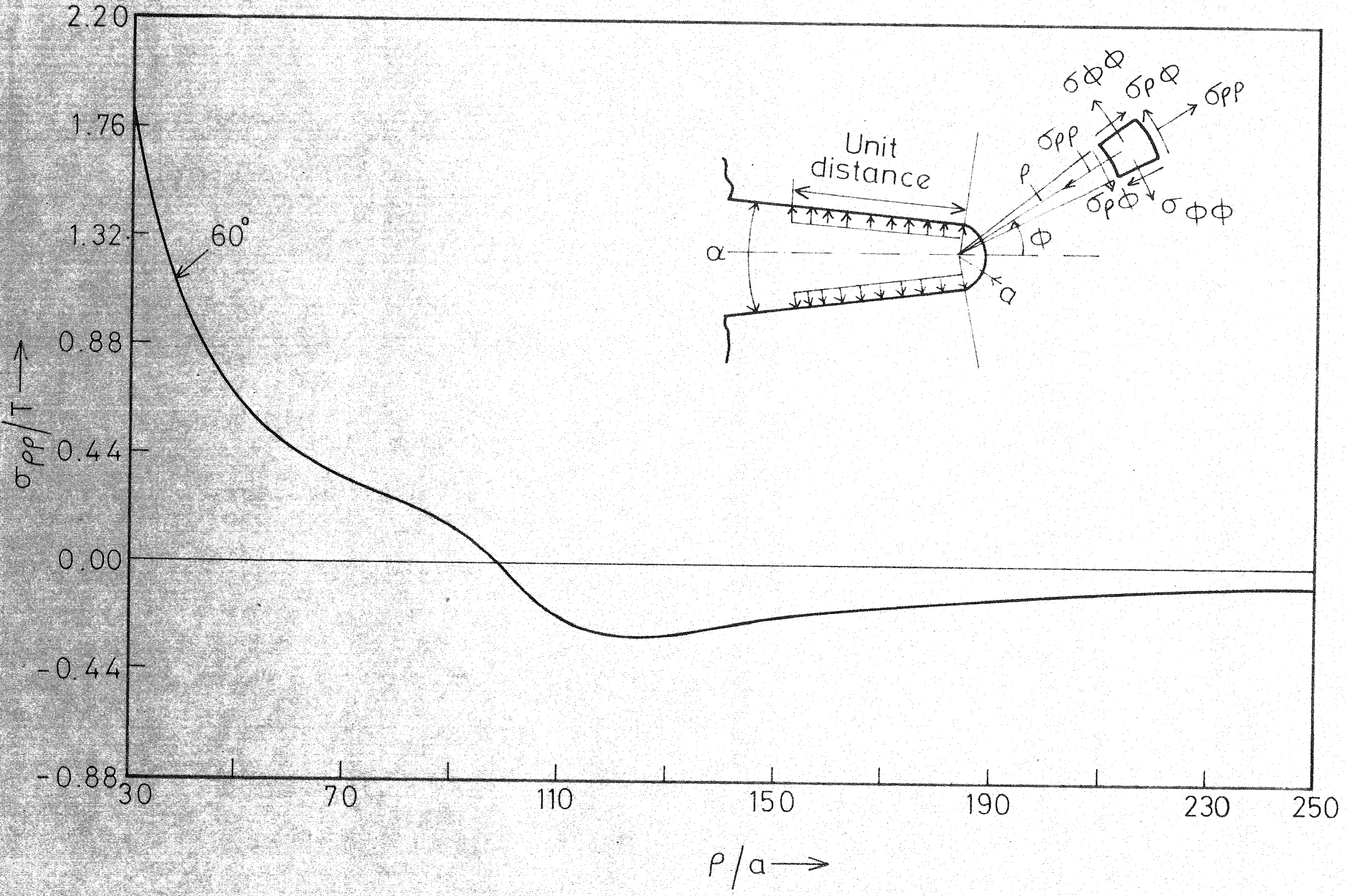

FIG. 4.21 RADIAL NORMAL STRESS $\sigma_{\rho\rho}$ AHEAD OF A CRACK-LIKE-NOTCH ON $\phi = 60°$ PLANE FLANK ANGLE, $\alpha = 1°$ AND TIP ROOT RADIUS, $a = 1/100$

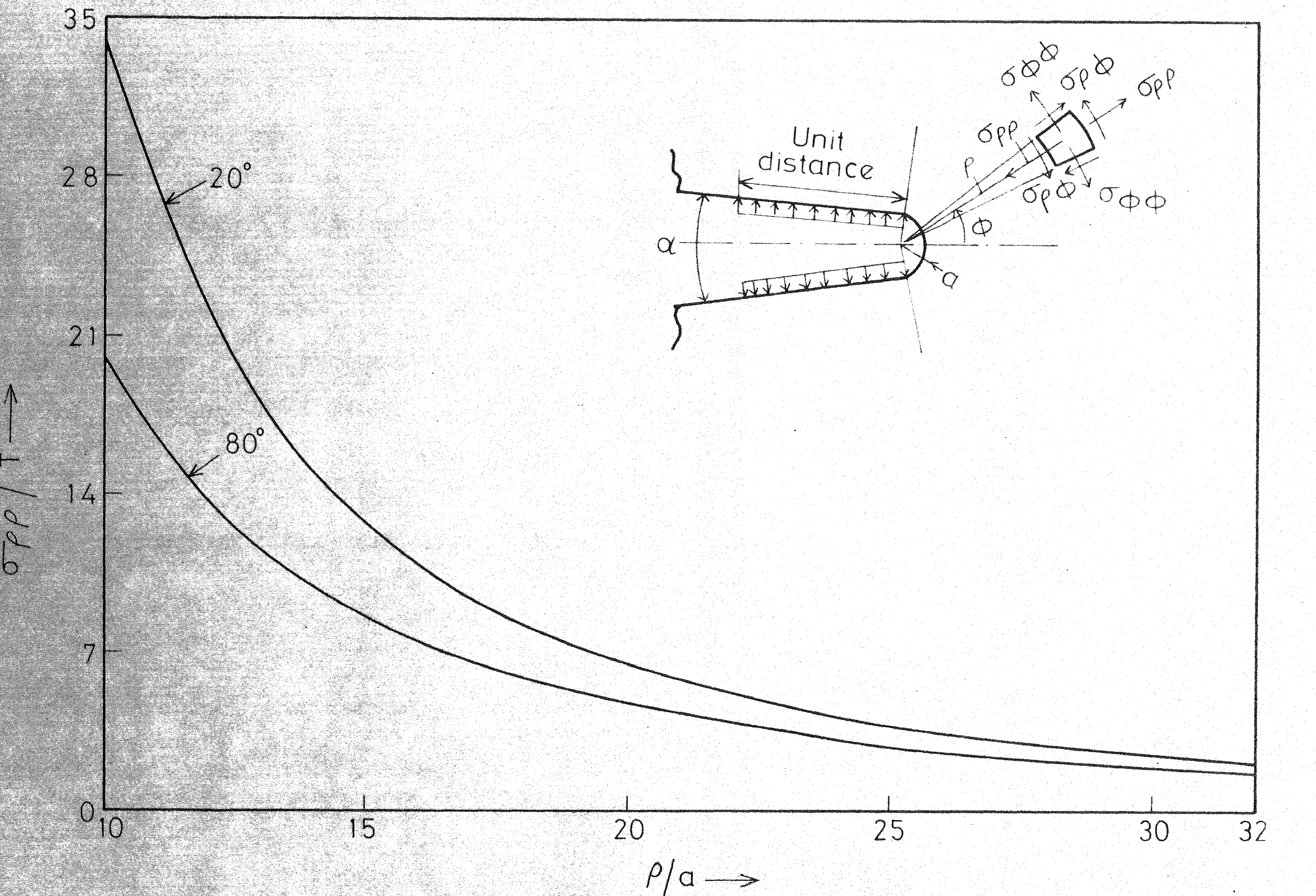

FIG.4.22 RADIAL NORMAL STRESS $\sigma_{\rho\rho}$ AHEAD OF A CRACK-LIKE-NOTCH ON $\phi = 20°$ AND 80° PLANES. FLANK ANGLE, $\alpha = 1°$ AND TIP ROOT RADIUS, $a = 1/100$

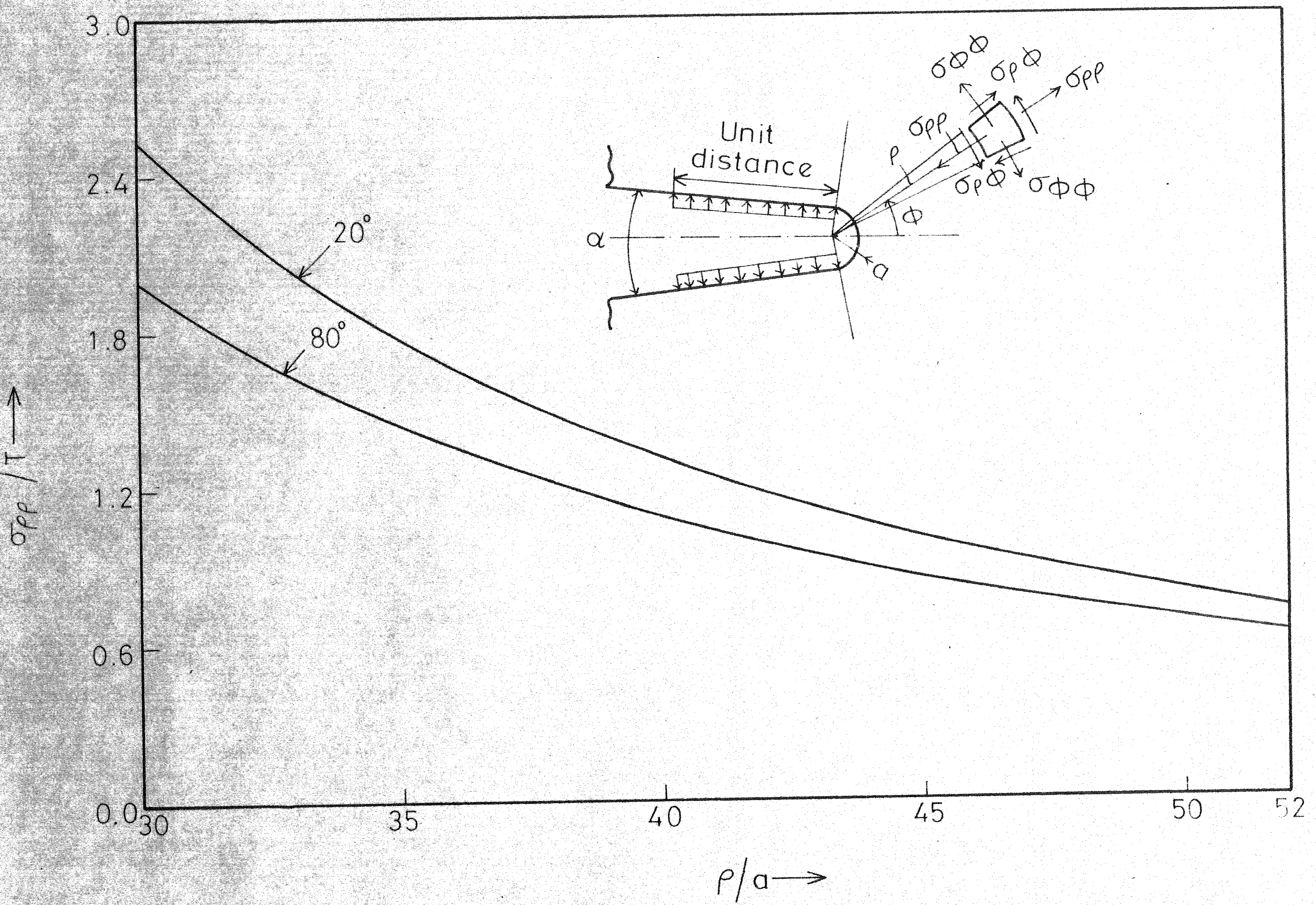

FIG.4.23 RADIAL NORMAL STRESS $\sigma_{\rho\rho}$ AHEAD OF A CRACK-LIKE-NOTCH ON $\phi = 20°$ AND 80° PLANES. FLANK ANGLE, $\alpha = 1°$ AND TIP ROOT RADIUS, $a = 1/100$.

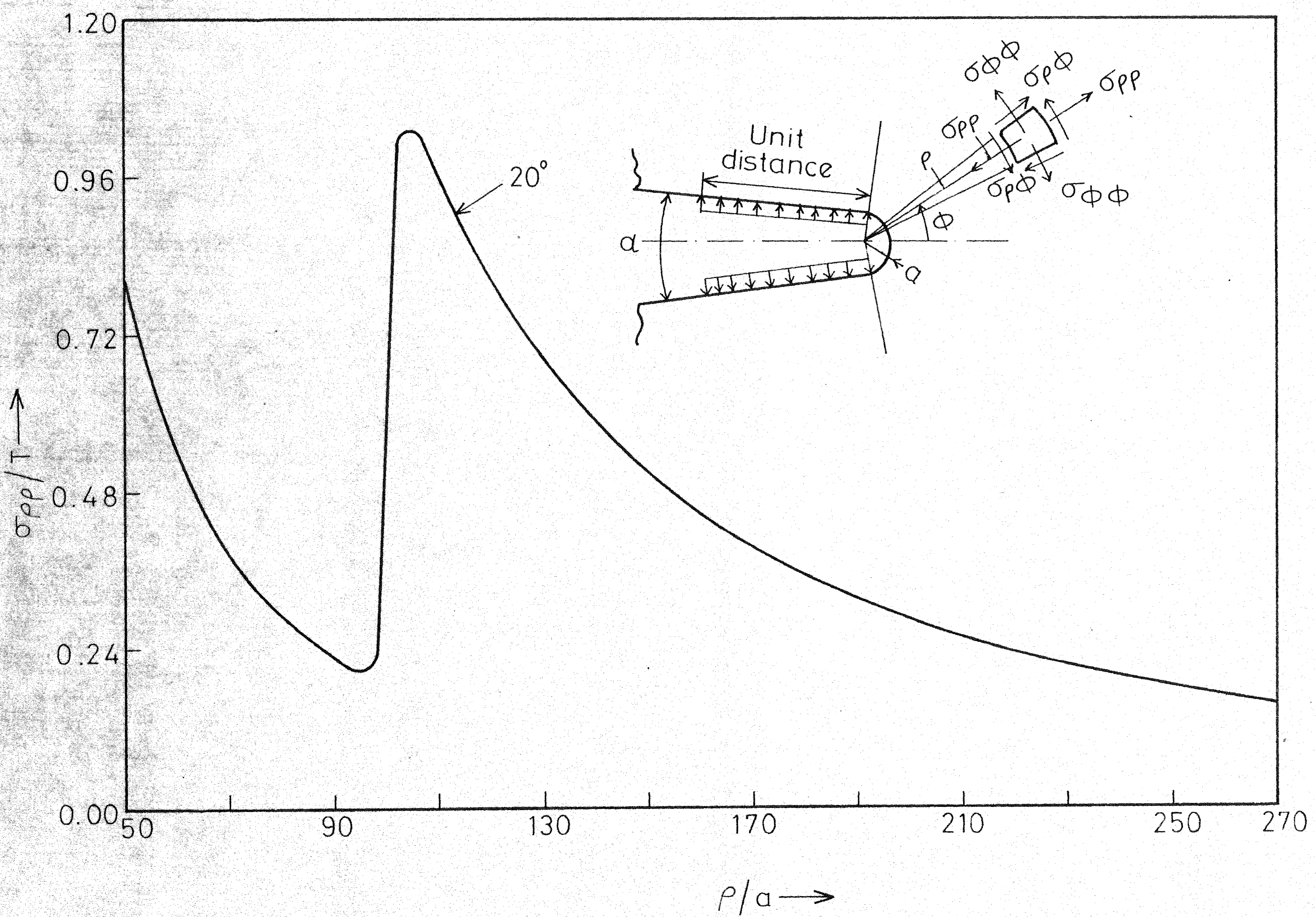

FIG.4.24 RADIAL NORMAL STRESS $\sigma_{\rho\rho}$ AHEAD OF A CRACK-LIKE-NOTCH ON $\phi = 20°$ PLANE. FLANK ANGLE, $\alpha = 1°$ AND TIP ROOT RADIUS, $a = 1/100$

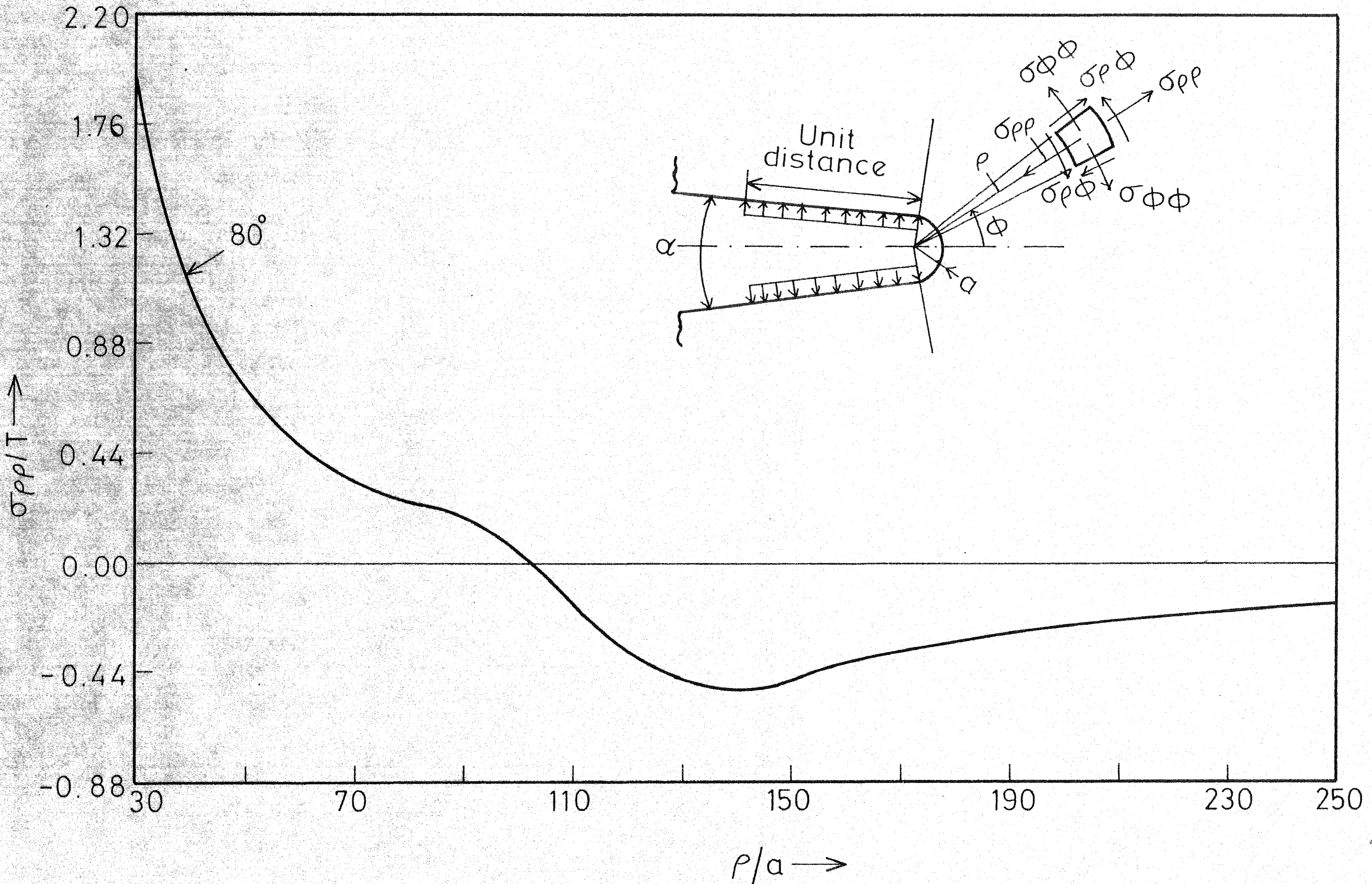

FIG.4.25 RADIAL NORMAL STRESS $\sigma_{\rho\rho}$ AHEAD OF A CRACK-LIKE-NOTCH ON $\phi = 80°$ PLANE . FLANK ANGLE, $\alpha = 1°$ AND TIP ROOT RADIUS, $a = 1/100$.

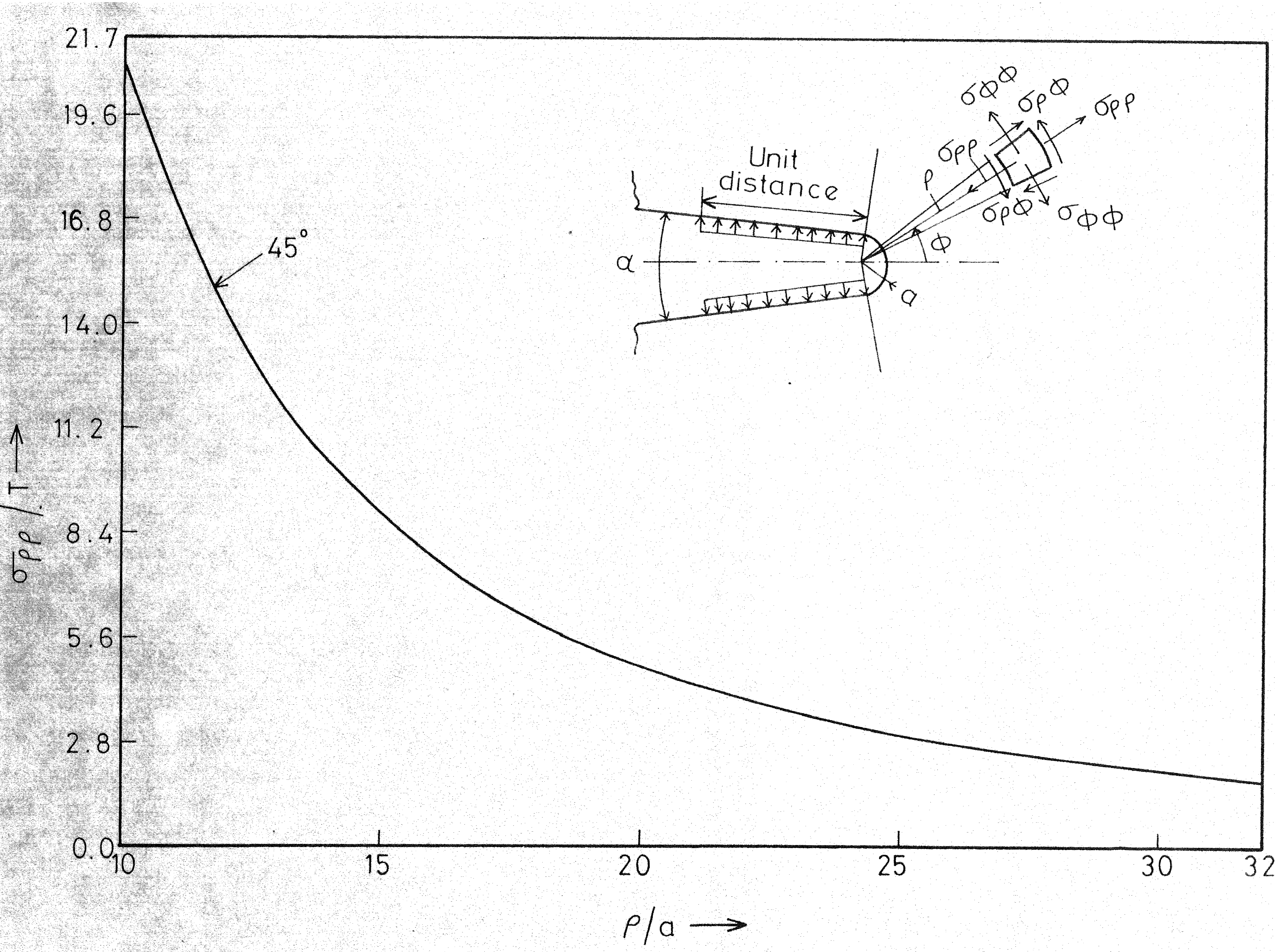

FIG.4.26 RADIAL NORMAL STRESS $\sigma_{\rho\rho}$ AHEAD OF A CRACK-LIKE-NOTCH ON $\phi = 45°$ PLANE. FLANK ANGLE, $\alpha = 1°$ AND TIP ROOT RADIUS, $a = 1/100$.

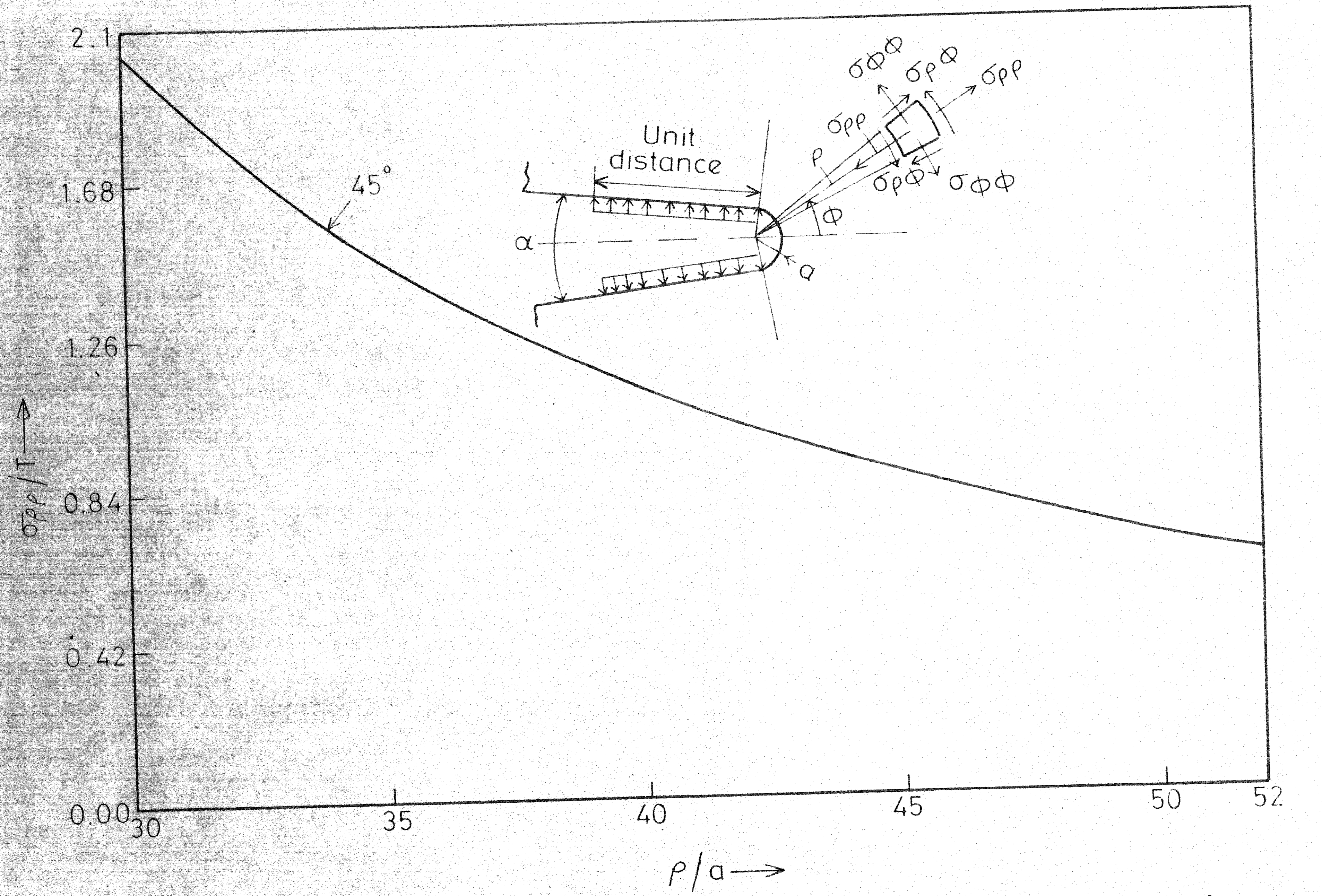

FIG.4.27 RADIAL NORMAL STRESS $\sigma_{\rho\rho}$ AHEAD OF A CRACK-LIKE-NOTCH ON $\phi = 45°$ PLANE FLANK ANGLE, $\alpha = 1°$ AND TIP ROOT RADIUS, $a = 1/100$.

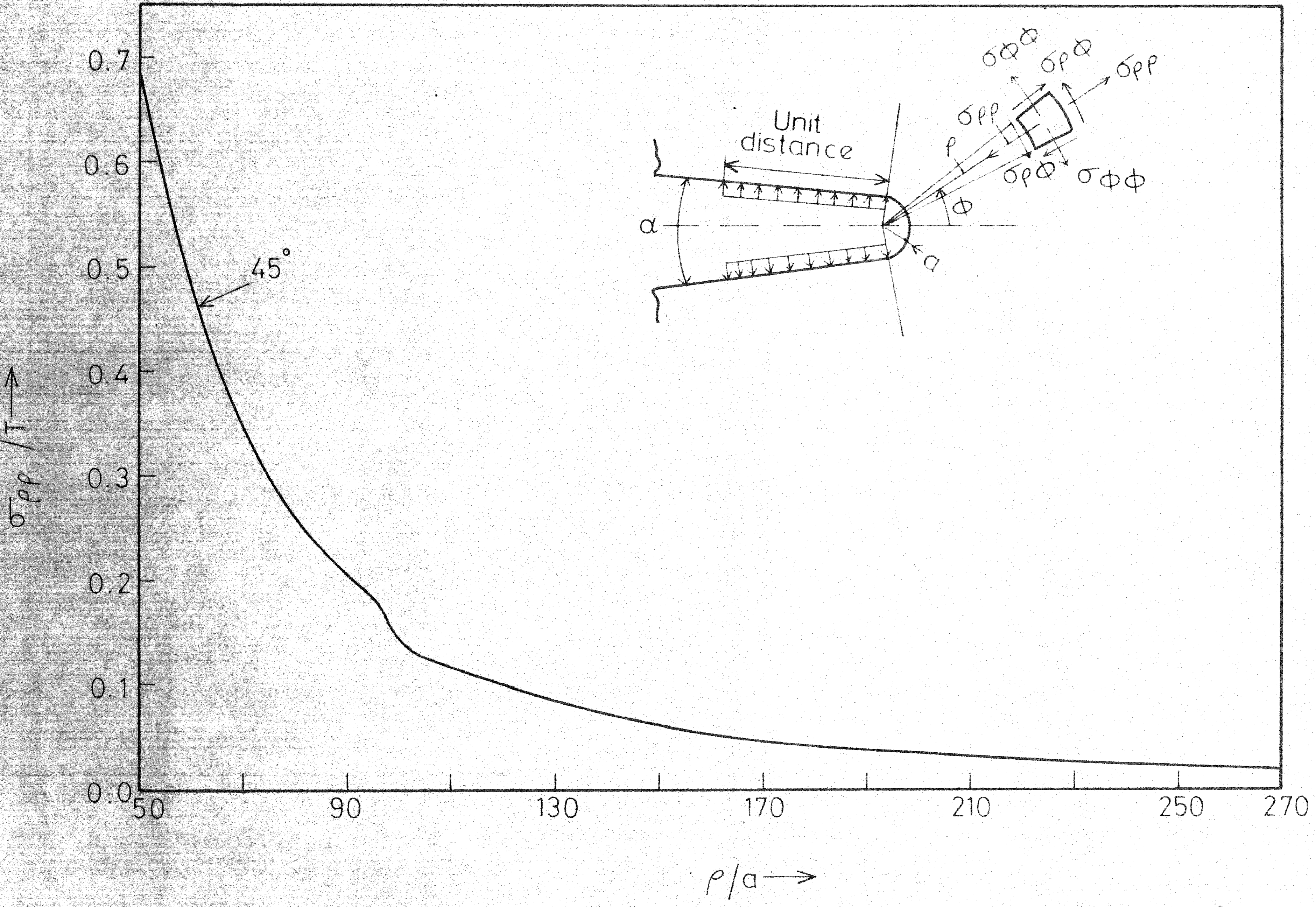

FIG.4.28 RADIAL NORMAL STRESS $\sigma_{\rho\rho}$ AHEAD OF A CRACK-LIKE-NOTCH ON $\phi = 45°$ PLANE FLANK ANGLE, $\alpha = 1°$ AND TIP ROOT RADIUS, $a = 1/100$.

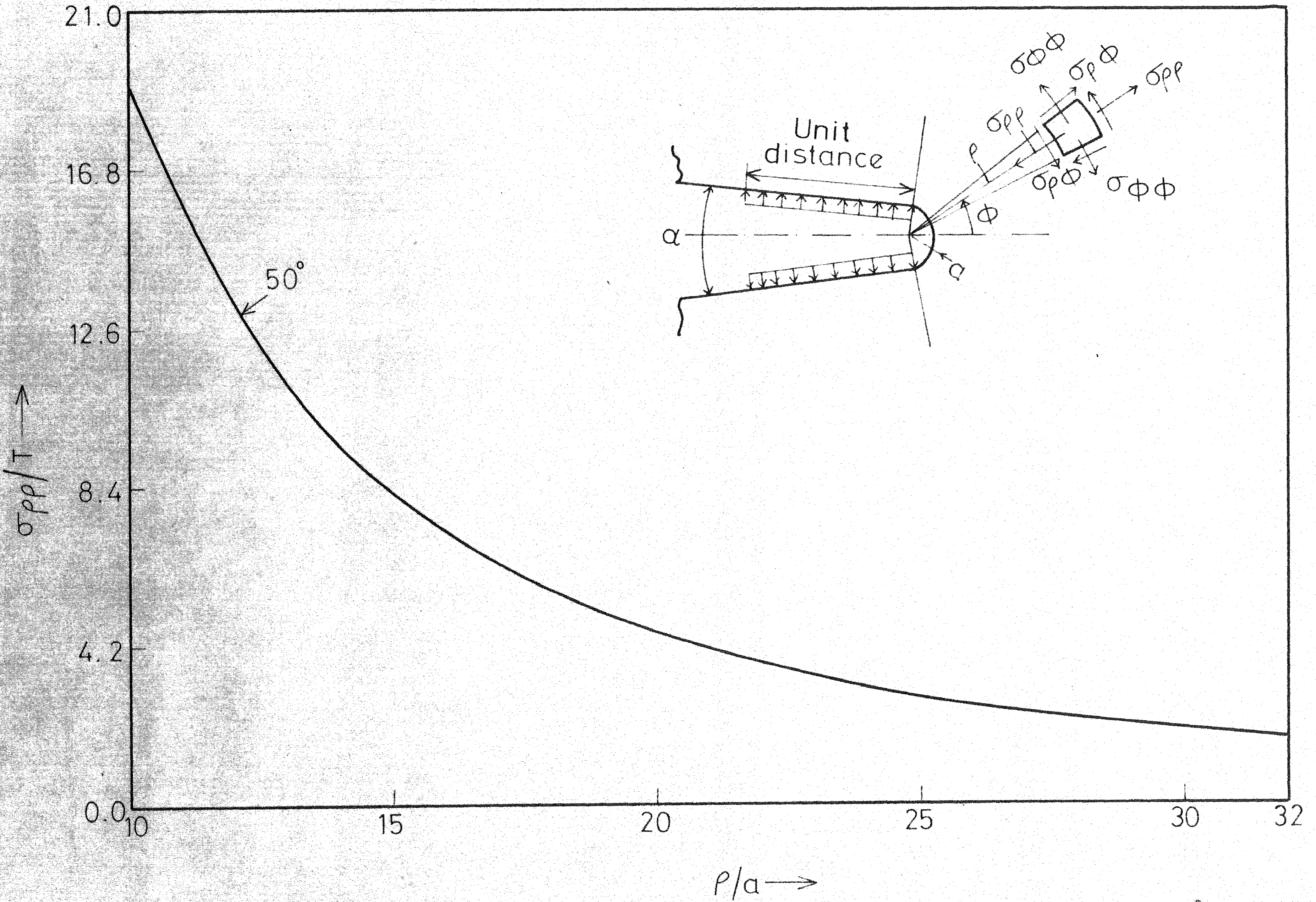

FIG.4.29 RADIAL NORMAL STRESS $\sigma_{\rho\rho}$ AHEAD OF A CRACK - LIKE - NOTCH ON $\phi = 50°$ PLANE FLANK ANGLE , $\alpha = 1°$ AND TIP ROOT RADIUS, $a = 1/100$

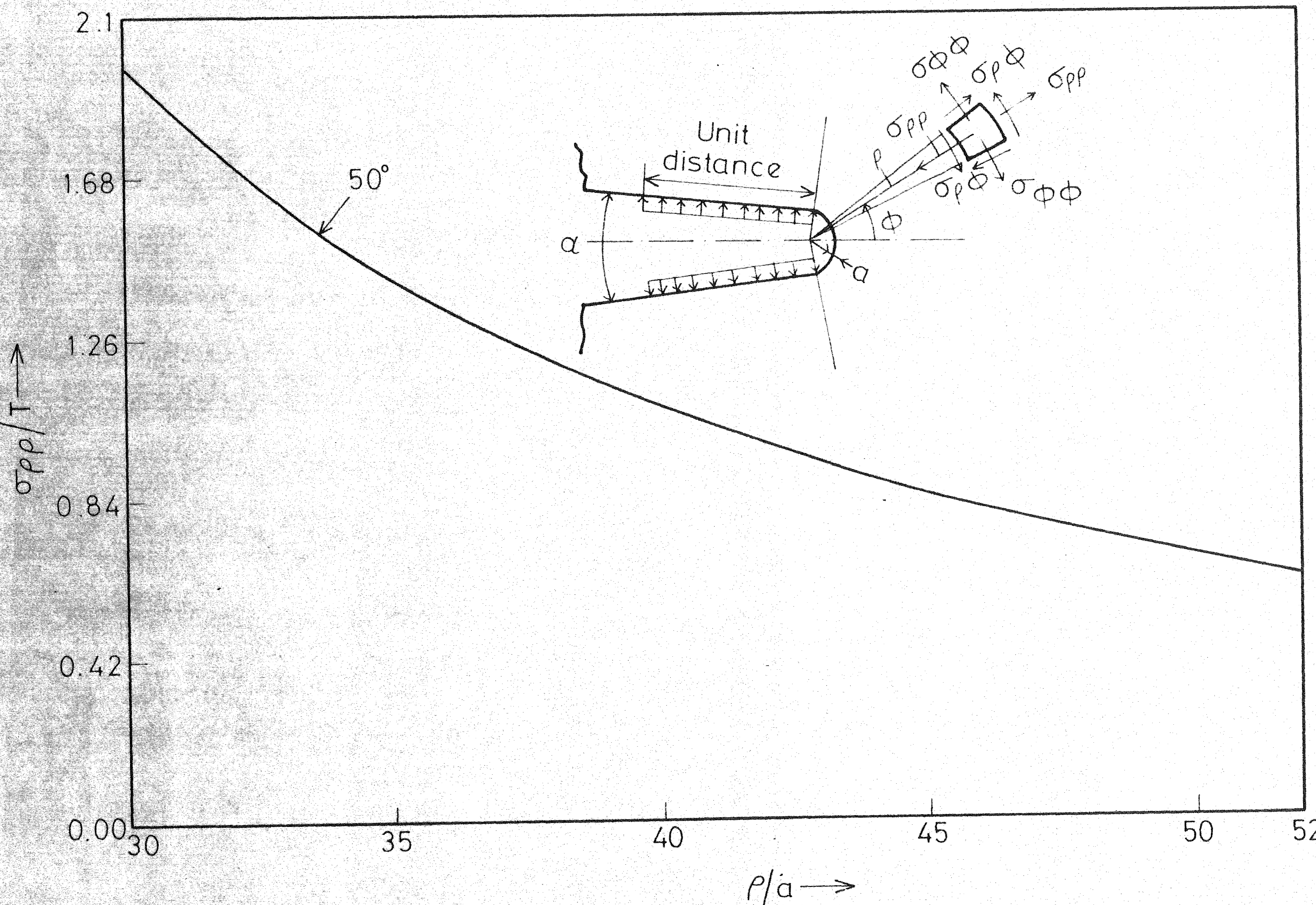

FIG.4.30 RADIAL NORMAL STRESS $\sigma_{\rho\rho}$ AHEAD OF A CRACK-LIKE-NOTCH ON $\phi=50°$ PLANE FLANK ANGLE, $\alpha=1°$ AND TIP ROOT RADIUS, $a=1/100$

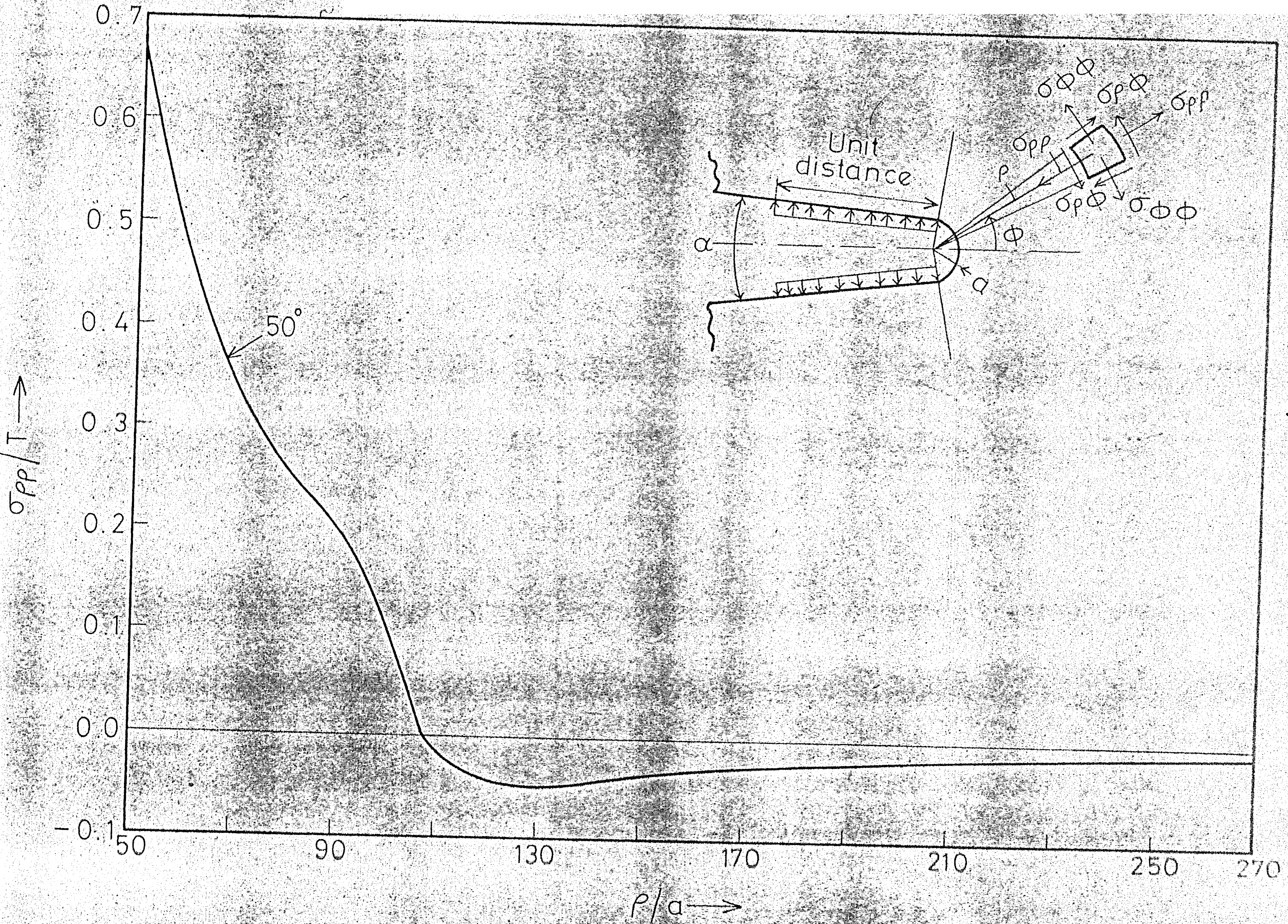

FIG. 4.31 RADIAL NORMAL STRESS $\sigma_{\rho\rho}$ AHEAD OF A CRACK-LIKE-NOTCH ON $\phi=50°$ PLANE. FLANK ANGLE, $\alpha=1°$ AND TIP ROOT RADIUS, $a=1/100$

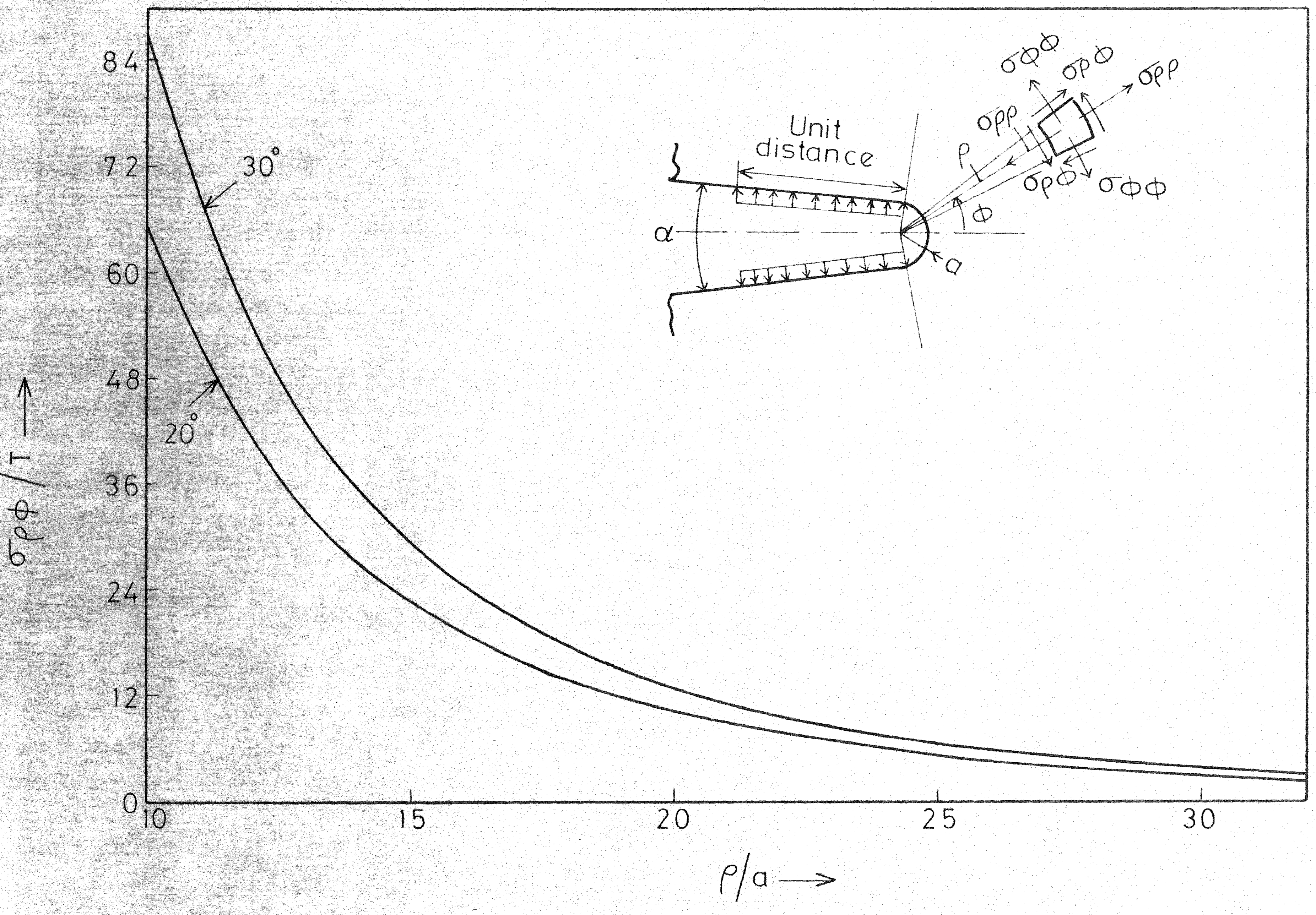

FIG.4.32 SHEAR STRESS $\sigma_{\rho\phi}$ AHEAD OF A CRACK-LIKE-NOTCH ON $\phi = 20°$ AND 30° PLANES. FLANK ANGLE, $\alpha = 1°$, $a = 0.01$

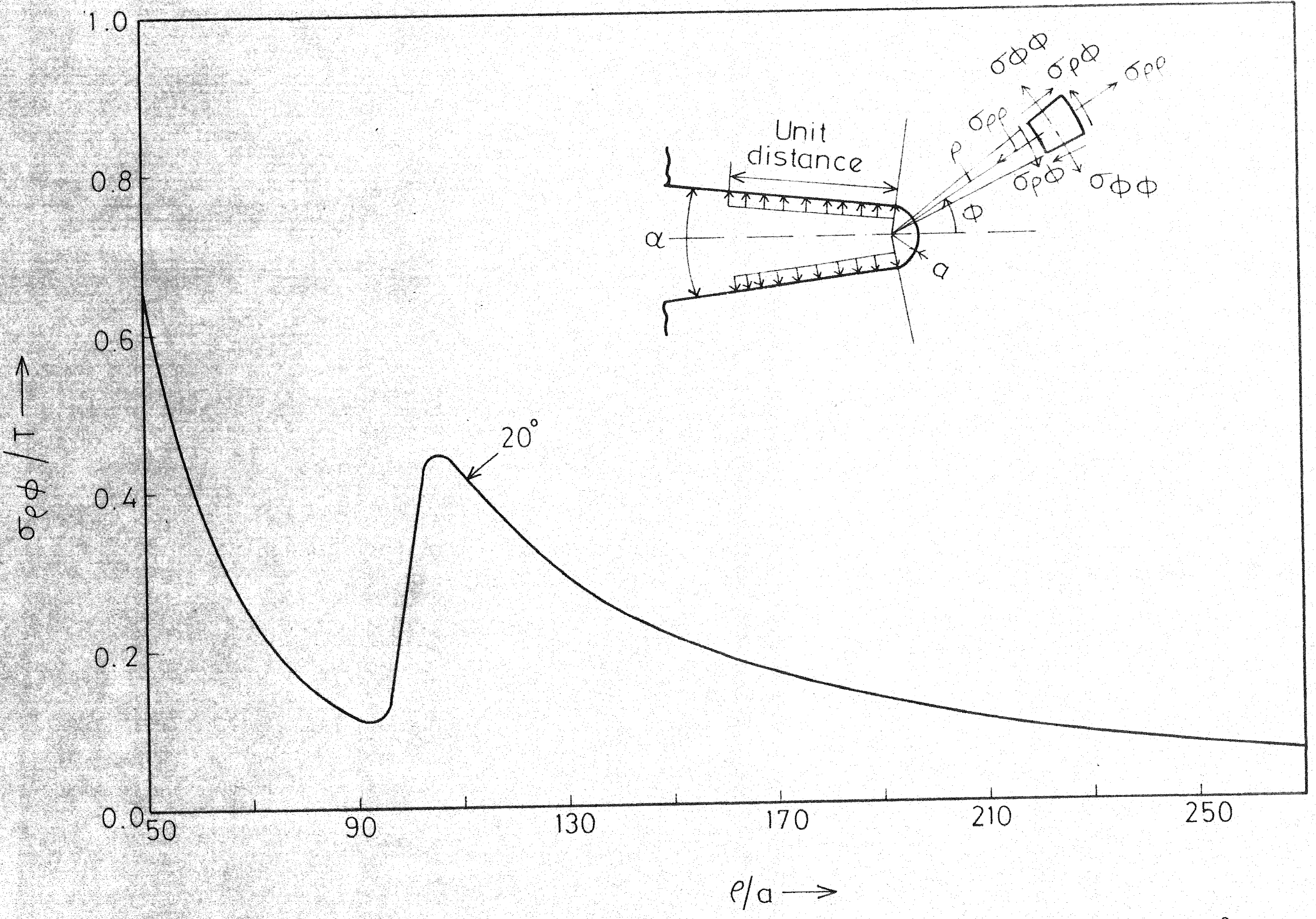

FIG.4.34 SHEAR STRESS $\sigma_{\rho\phi}$ AHEAD OF A CRACK-LIKE-NOTCH ON $\phi = 20°$ PLANE. FLANK ANGLE, $\alpha = 1°$, $a = 1/100$

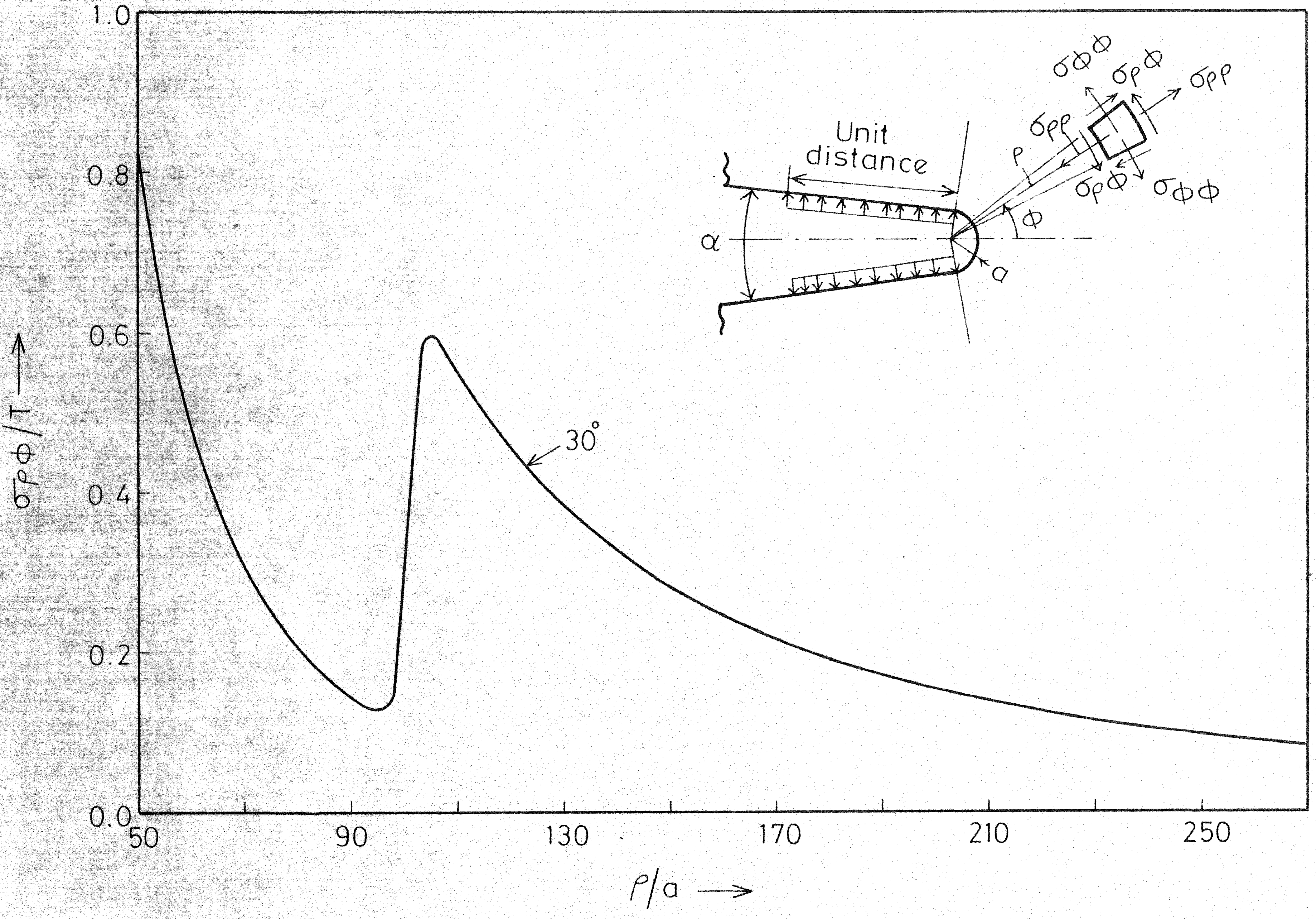

FIG.4.35 SHEAR STRESS $\sigma_{\rho\phi}$ AHEAD OF A CRACK-LIKE-NOTCH ON $\phi = 30°$ PLANE. FLANK ANGLE, $\alpha = 1°$, $a = 1/100$

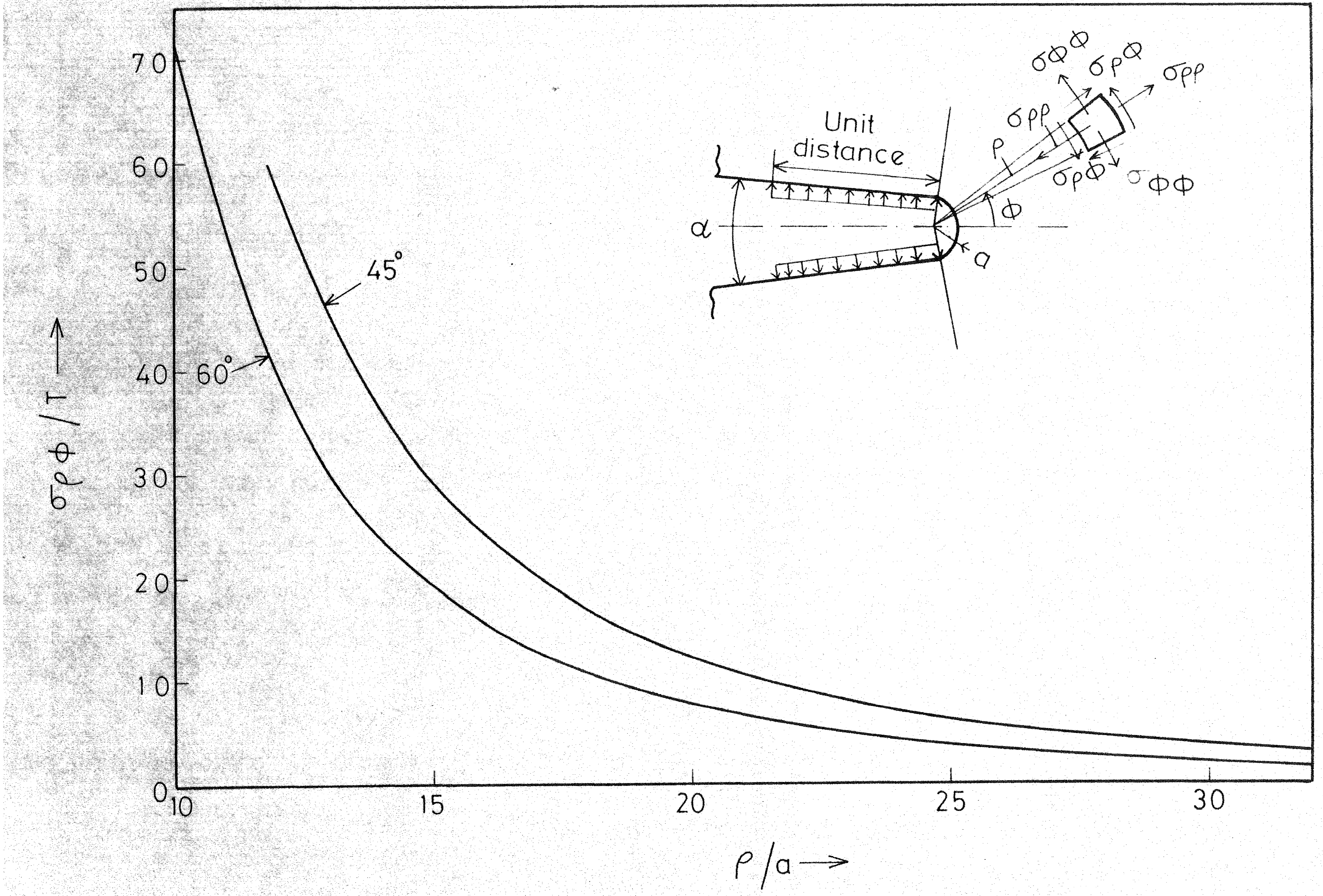

FIG.4.36 SHEAR STRESS $\sigma_{\rho\phi}$ AHEAD OF A CRACK-LIKE-NOTCH ON $\phi = 45°$ AND 60° PLANES. FLANK ANGLE, $\alpha = 1°$, $a = 0.01$

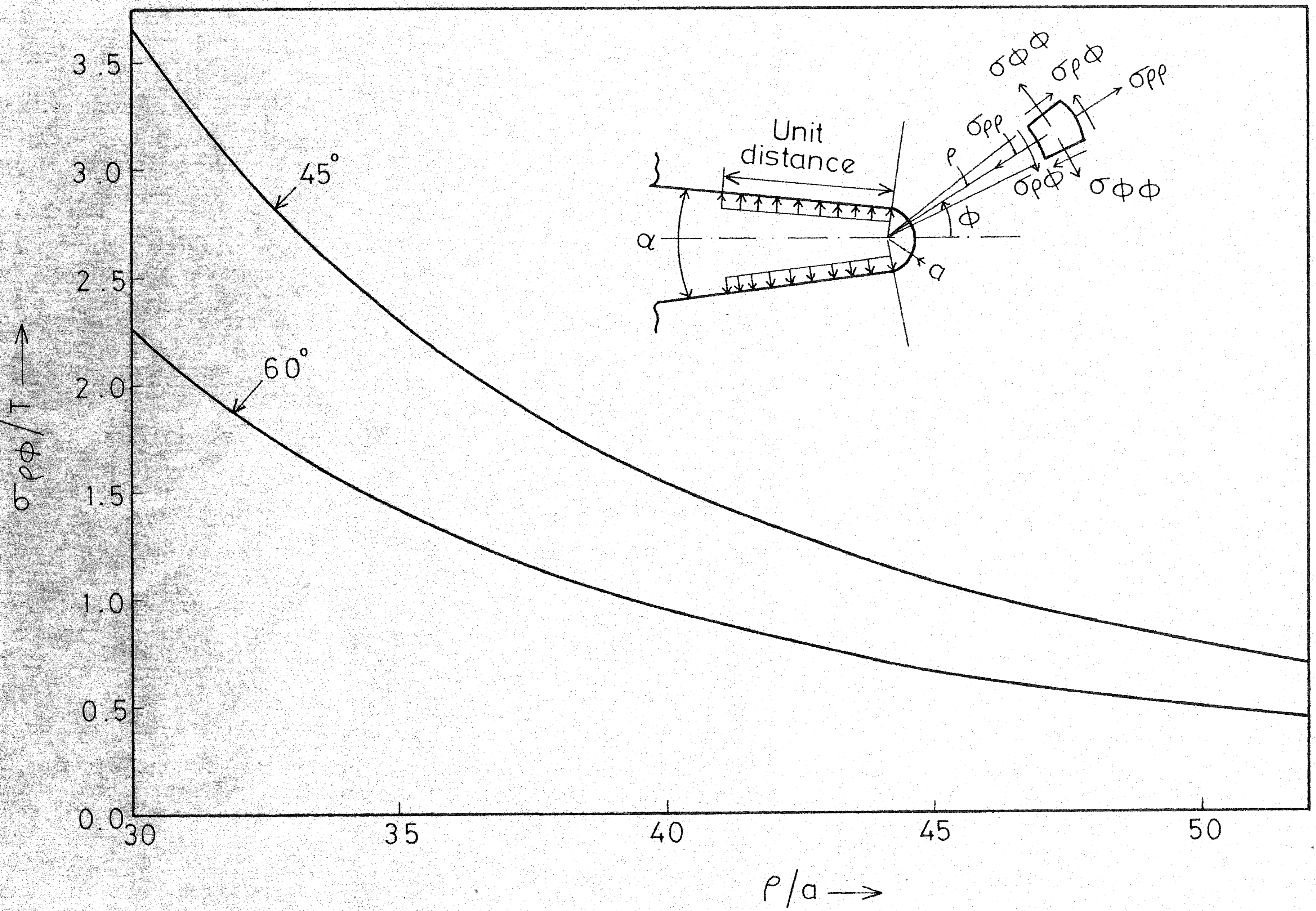

FIG.4.37 SHEAR STRESS $\sigma_{\rho\phi}$ AHEAD OF A CRACK-LIKE-NOTCH ON $\phi = 45°$ AND 60° PLANES. FLANK ANGLE, $\alpha = 1°$, $a = 1/100$

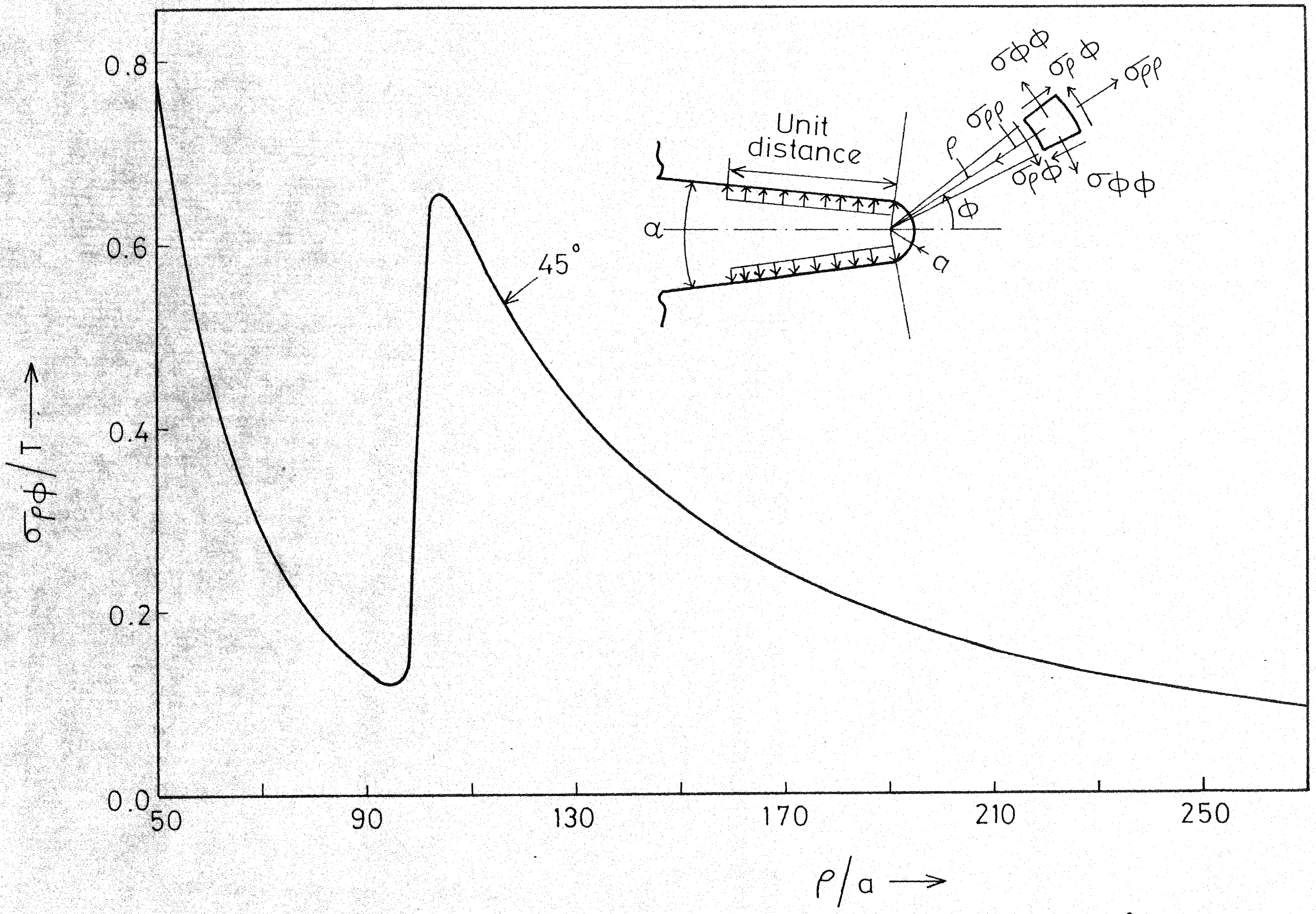

FIG.4.38 SHEAR STRESS $\sigma_{\rho\phi}$ AHEAD OF A CRACK-LIKE-NOTCH ON Φ =45° PLANE. FLANK ANGLE, $\alpha=1°$, $a = 1/100$

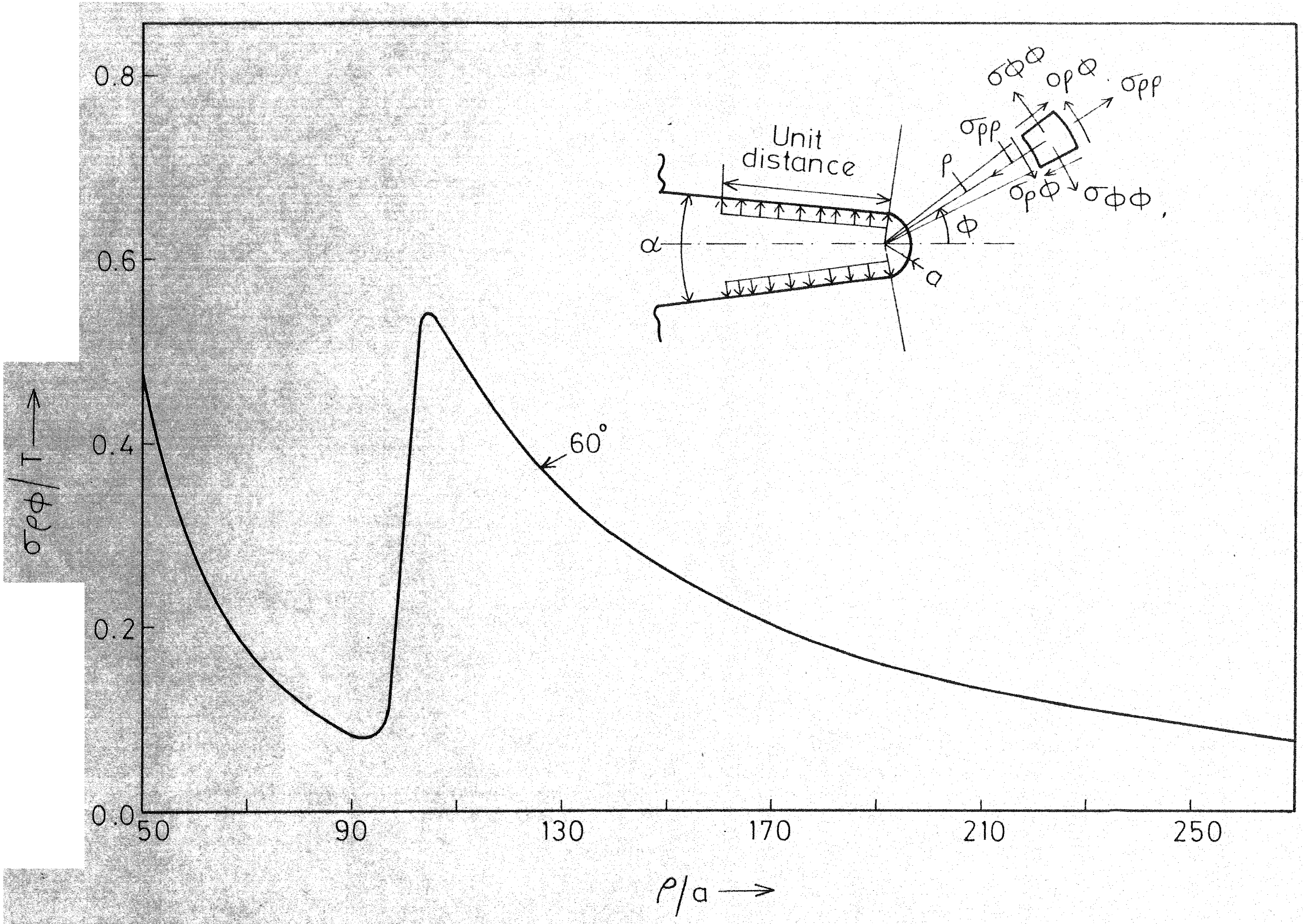

FIG.4.39 SHEAR STRESS $\sigma_{\rho\phi}$ AHEAD OF A CRACK-LIKE-NOTCH ON $\phi = 60°$ PLANE.
FLANK ANGLE, $\alpha = 1°, a = 0.01$

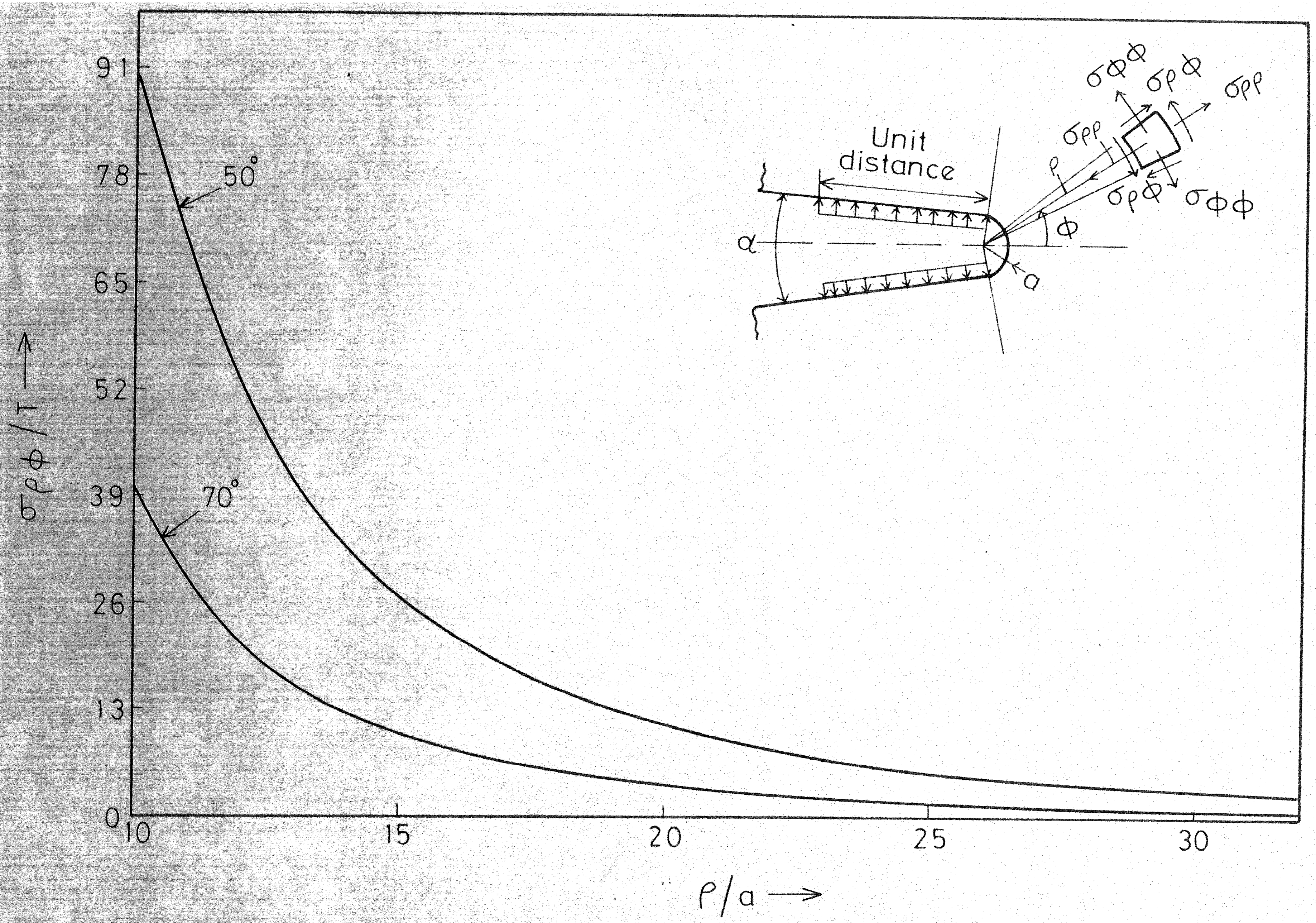

FIG.4.40 SHEAR STRESS $\sigma_{\rho\phi}$ AHEAD OF A CRACK-LIKE-NOTCH ON $\phi = 50°$ AND $70°$ PLANES. FLANK ANGLE, $\alpha = 1°$, $a = 1/100$

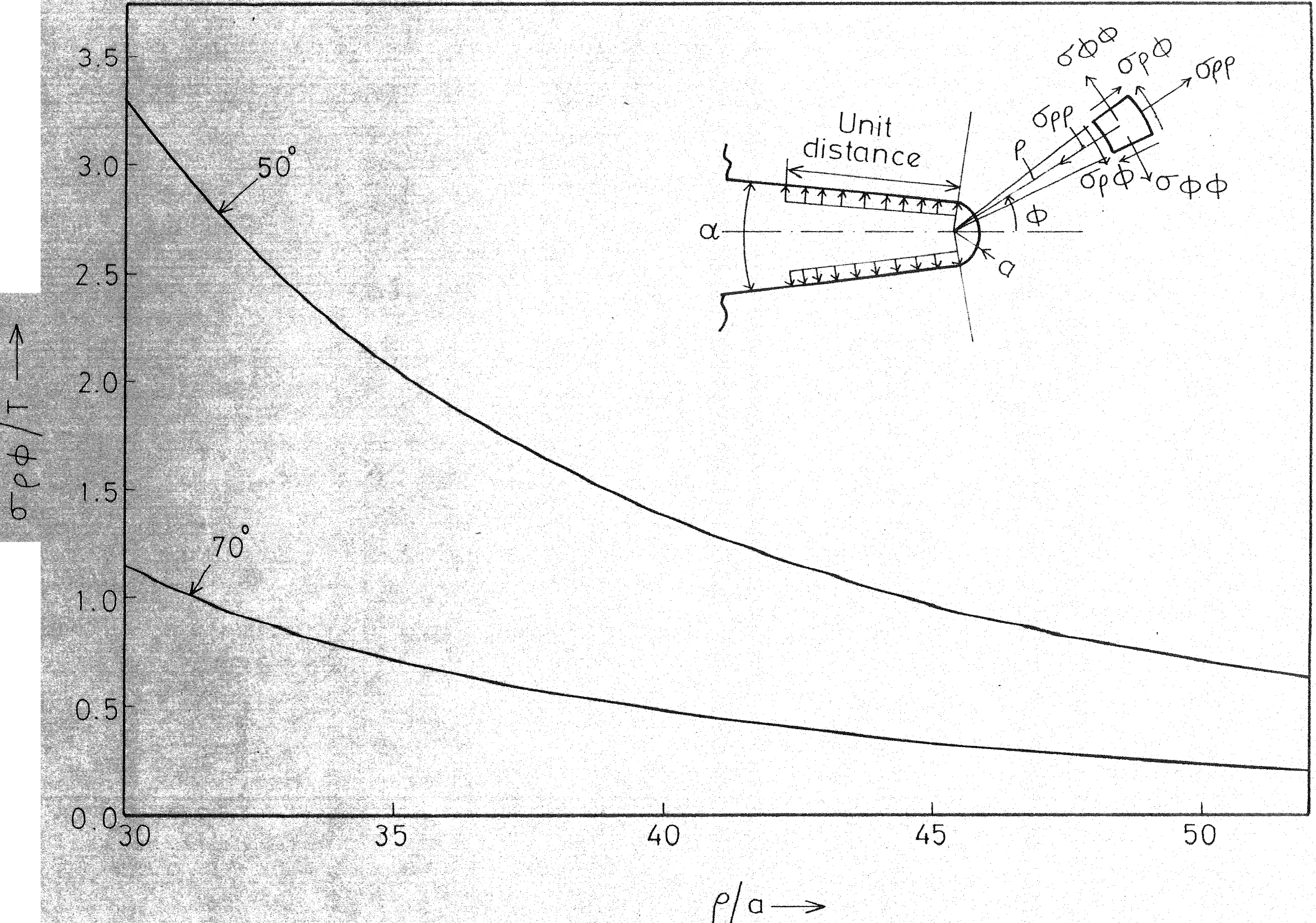

FIG.4.41 SHEAR STRESS $\sigma_{\rho\phi}$ AHEAD OF A CRACK - LIKE - NOTCH ON $\phi = 50°$ AND $70°$ PLANES FLANK ANGLE $\alpha = 1°$, $a = 0.01$

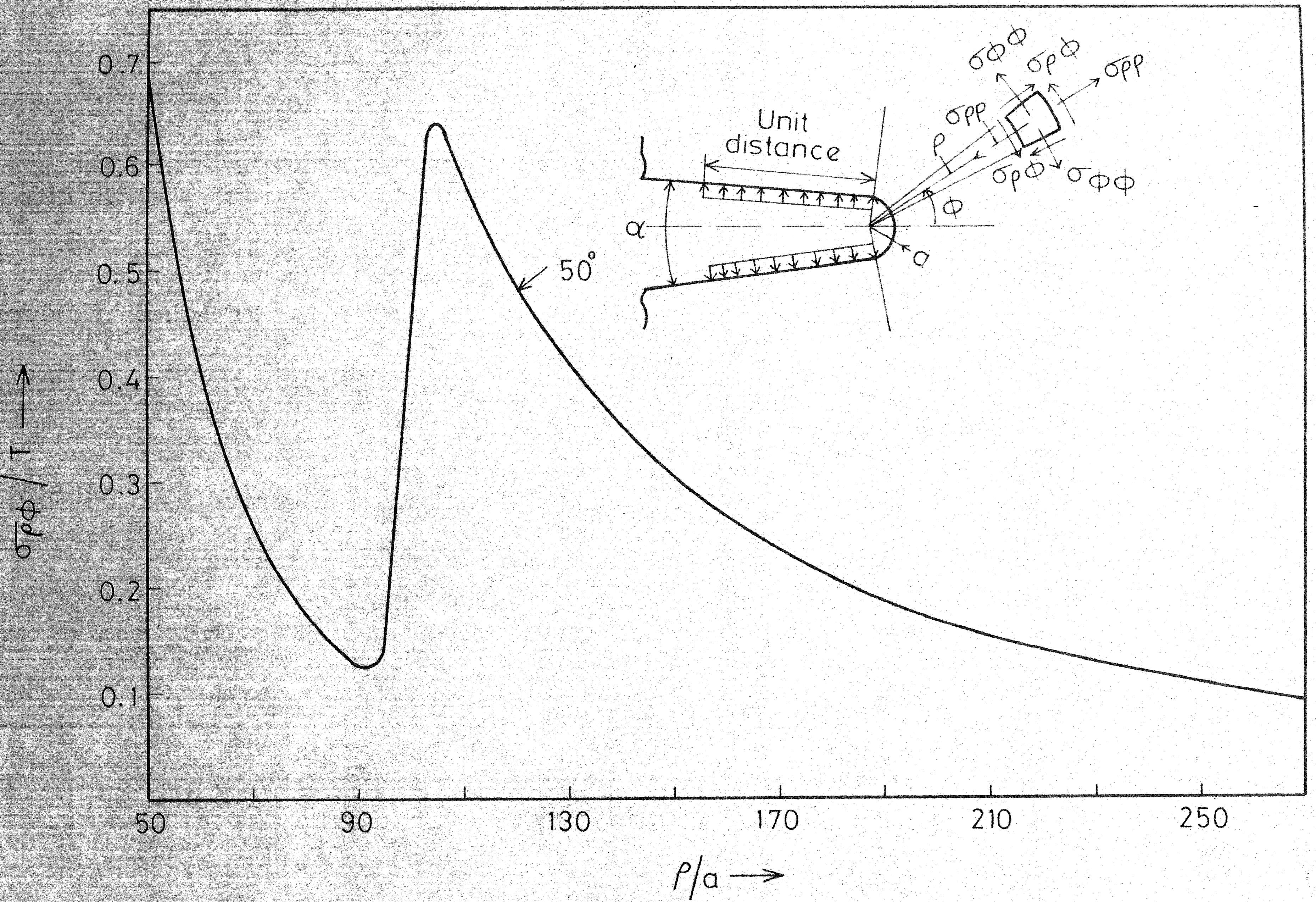

FIG.4.42 SHEAR STRESS $\sigma_{\rho\phi}$ AHEAD OF A CRACK-LIKE-NOTCH ON $\phi = 50°$ PLANE.
FLANK ANGLE, $\alpha = 1°$, $a = 0.01$

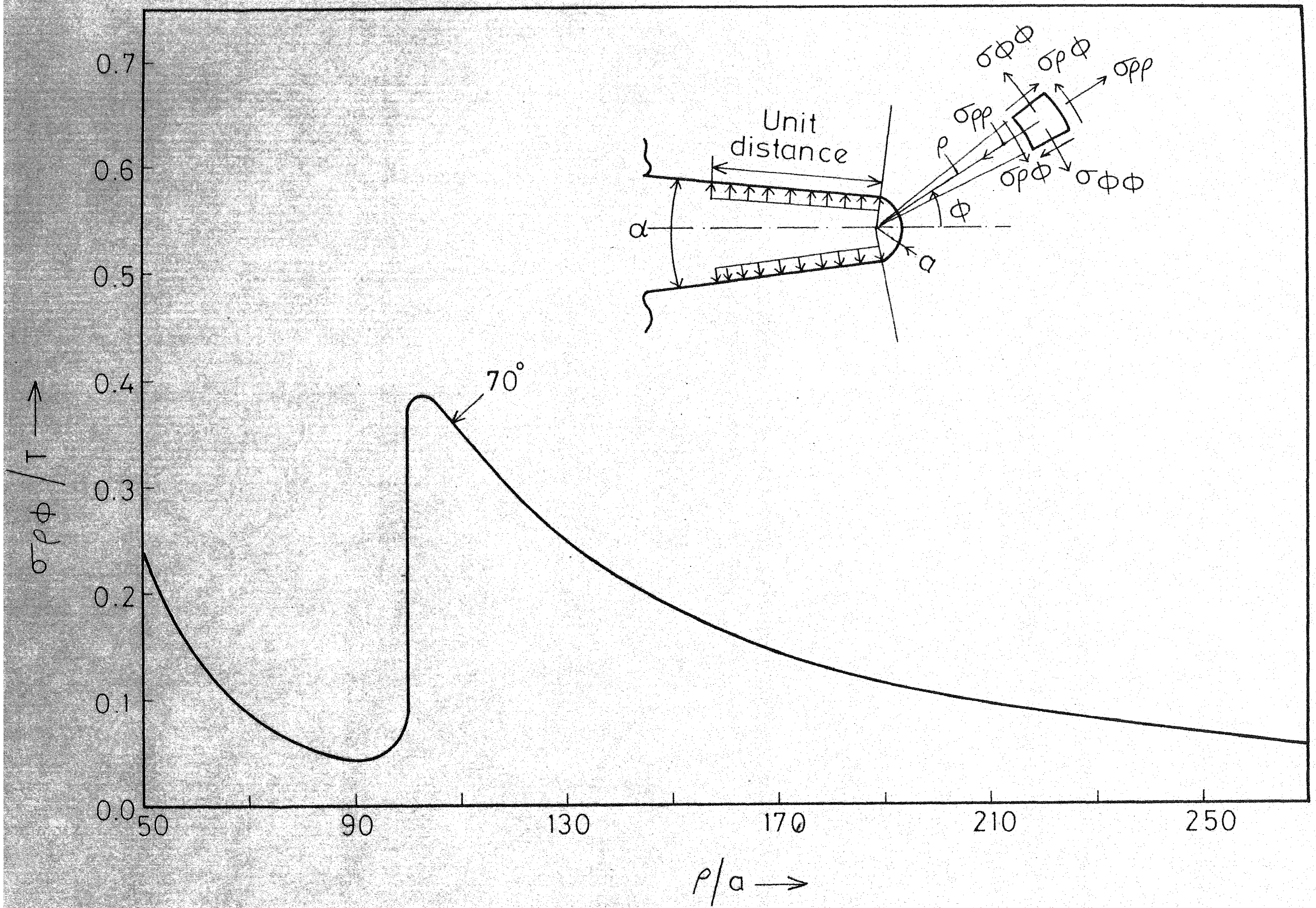

FIG.4.43 SHEAR STRESS $\sigma_{\rho\phi}$ AHEAD OF A CRACK-LIKE-NOTCH ON $\phi = 70°$ PLANE. FLANK ANGLE, $\alpha = 1°$, $a = 0.01$

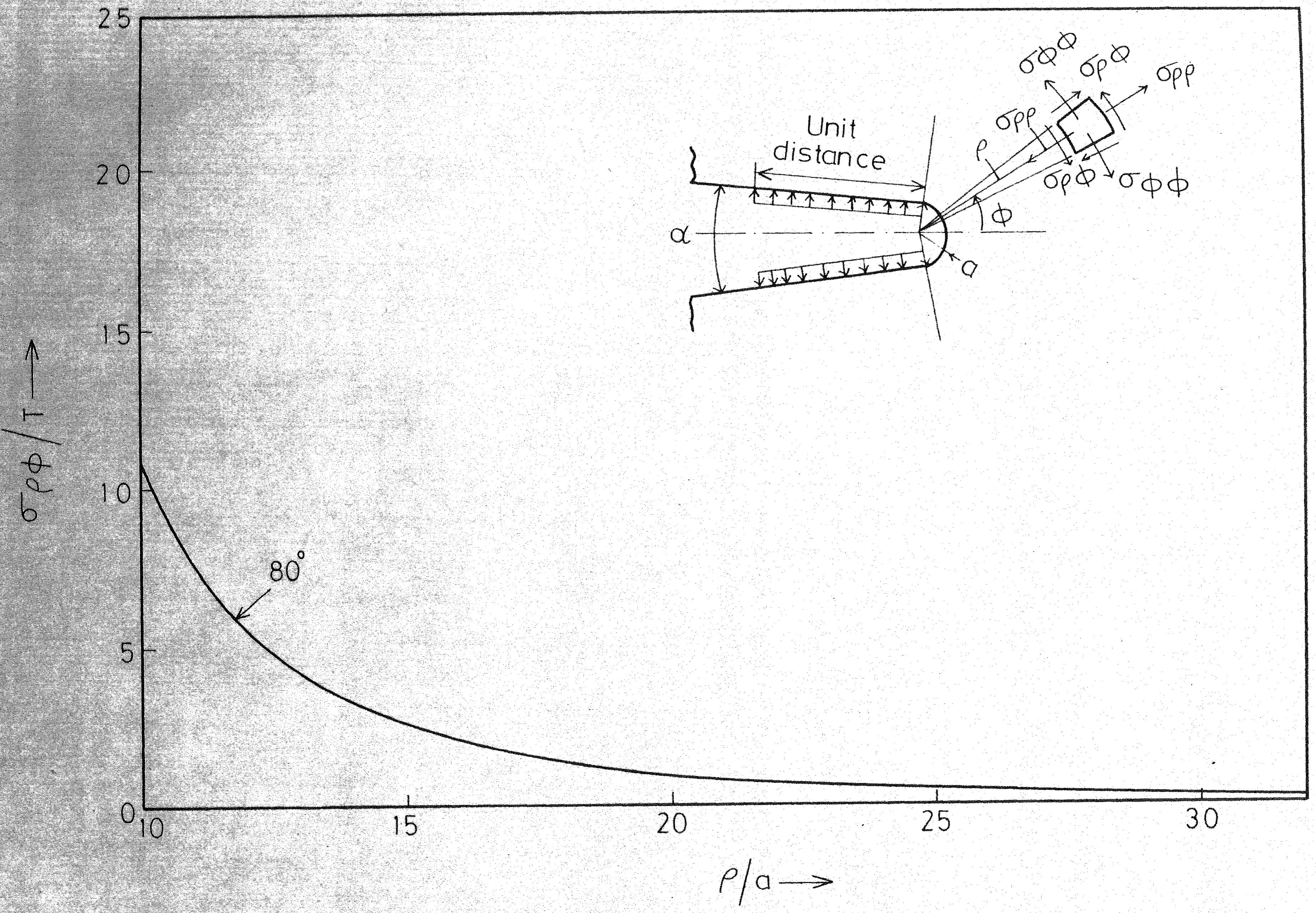

FIG.4.44 SHEAR STRESS $\sigma_{\rho\phi}$ AHEAD OF A CRACK-LIKE-NOTCH ON $\phi = 80°$ PLANE. FLANK ANGLE, $\alpha = 1°$, $a = 0.01$

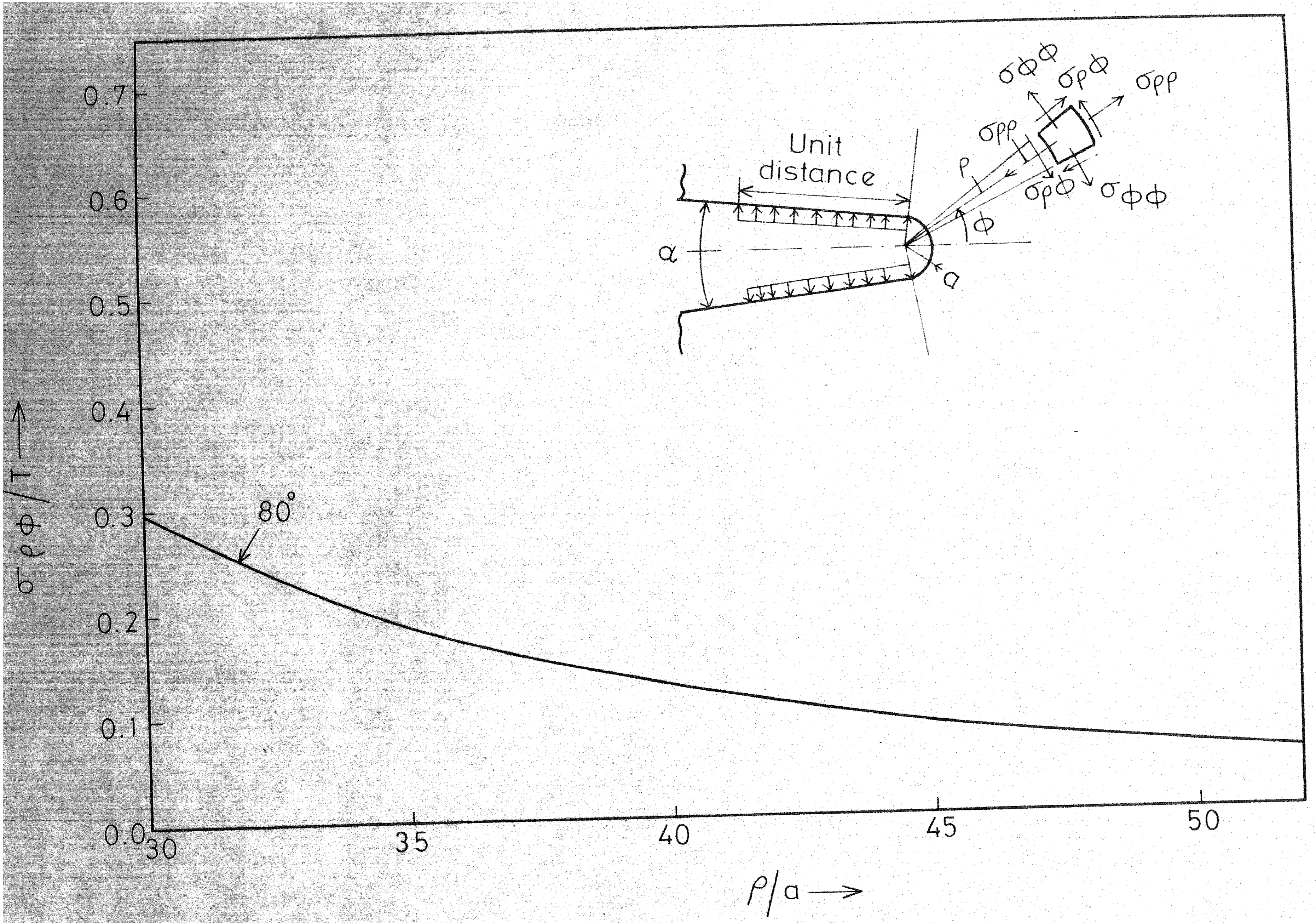

FIG.4.45 SHEAR STRESS $\sigma_{\rho\phi}$ AHEAD OF A CRACK - LIKE - NOTCH ON $\phi = 80°$ PLANE.
FLANK ANGLE, $\alpha = 1°$, $a = 0.01$

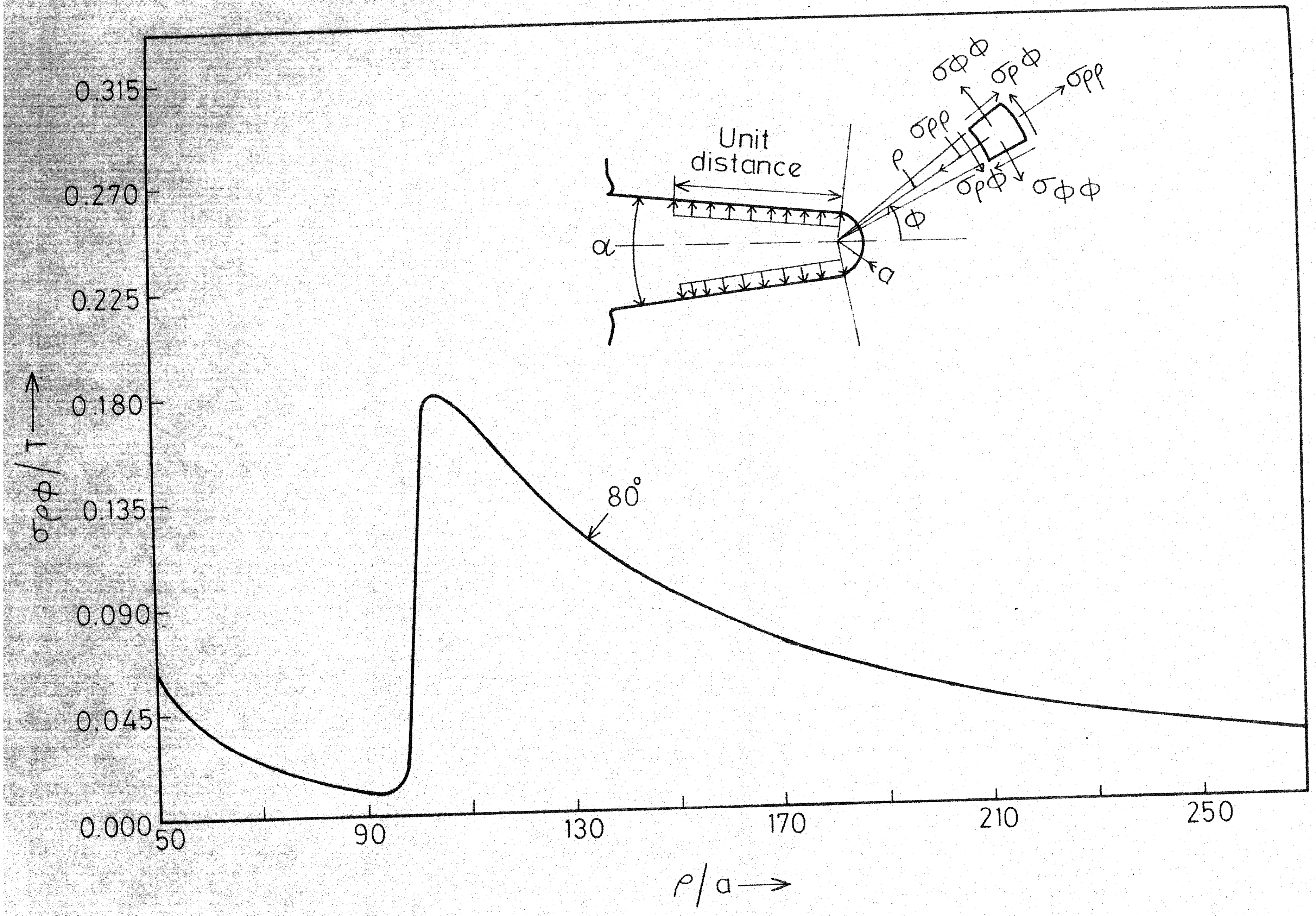

FIG.4.46 SHEAR STRESS $\sigma_{\rho\phi}$ AHEAD OF A CRACK-LIKE-NOTCH ON $\phi = 80°$ PLANE. FLANK ANGLE, $\alpha = 1°$, $a = 0.01$

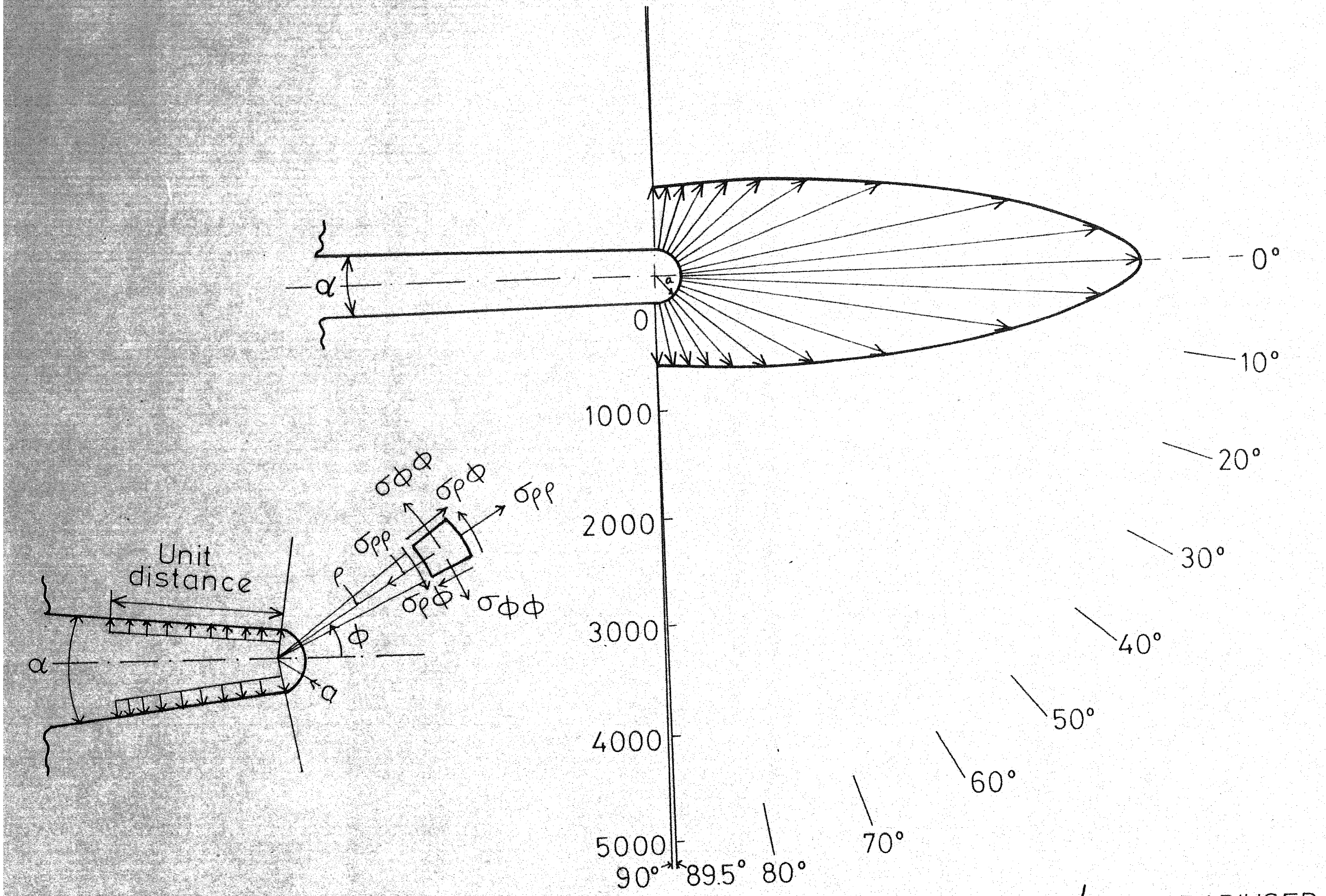

FIG.4.47 FOR A CRACK LIKE NOTCH THE TANGENTIAL STRESS $\sigma_{\Phi\Phi}/T$ ON RADIUSED RIM $\alpha=1°$, $a=0.01$

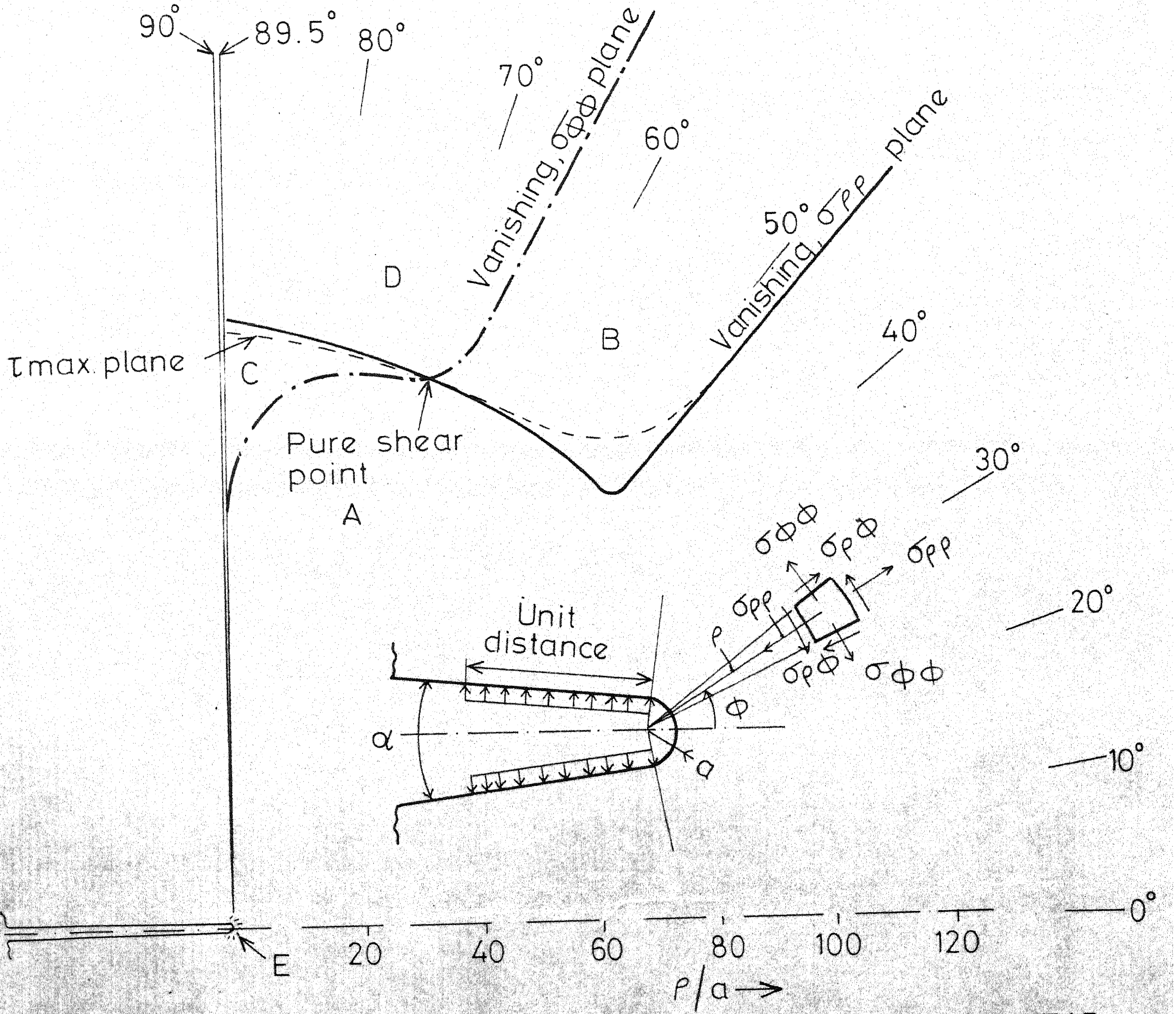
90°
89.5°
80°
70°
Vanishing, $\sigma_{\phi\phi}$ plane
60°
Vanishing, $\sigma_{\rho\rho}$ plane
50°
D
B
40°
τmax plane
C
Pure shear point
A
30°
$\sigma_{\phi\phi}$
$\sigma_{\rho\phi}$
$\sigma_{\rho\rho}$
20°
Unit distance
$\sigma_{\rho\rho}$
ρ
$\sigma_{\rho\phi}$
$\sigma_{\phi\phi}$
ϕ
α
a
10°
0°
E
20
40
60
80
100
120
ρ/a →

FIG.4.48 DIFFERENT STRESS FIELD SEPARATION BOUNDARIES AHEAD OF A CRACK-LIKE-NOTCH SHOWING TENSILE, COMPRESSIVE, PURE DISTORTION AND MIXED STRESS REGIONS. $\alpha = 1°$, $a = 0.01$. A-TENSILE STRESSES, B-COMPRESSIVE RADIAL STRESS BUT TENSILE TANGENTIAL STRESS, C-COMPRESSIVE TANGENTIAL STRESS BUT TENSILE RADIAL STRESS, D-COMPRESSIVE STRESSES, E-CORE REGION

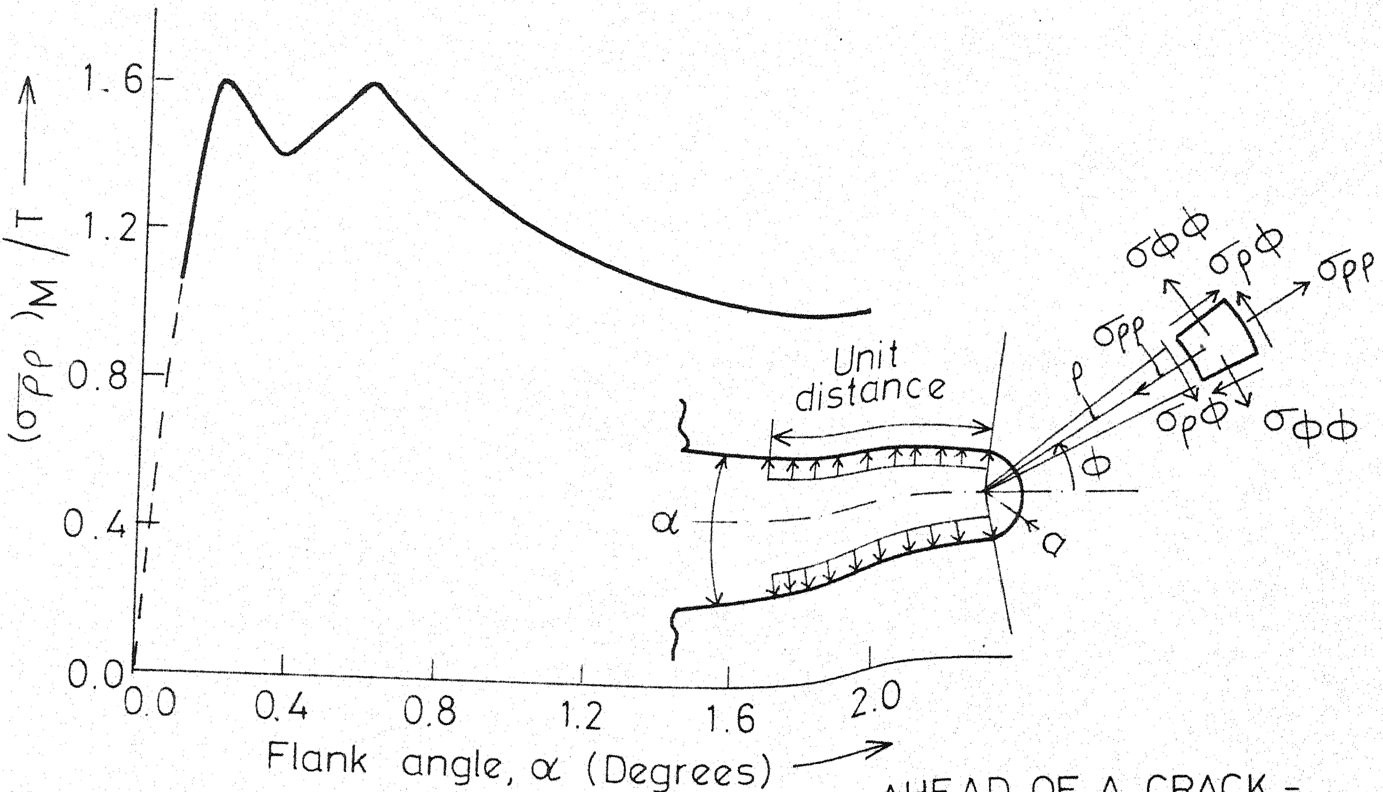

FIG.4.49(a) MISMATCH RADIAL NORMAL STRESS AHEAD OF A CRACK-LIKE NOTCH ON $\phi = 0°$ PLANE PLOTTED AGAINST FLANK ANGLE, α

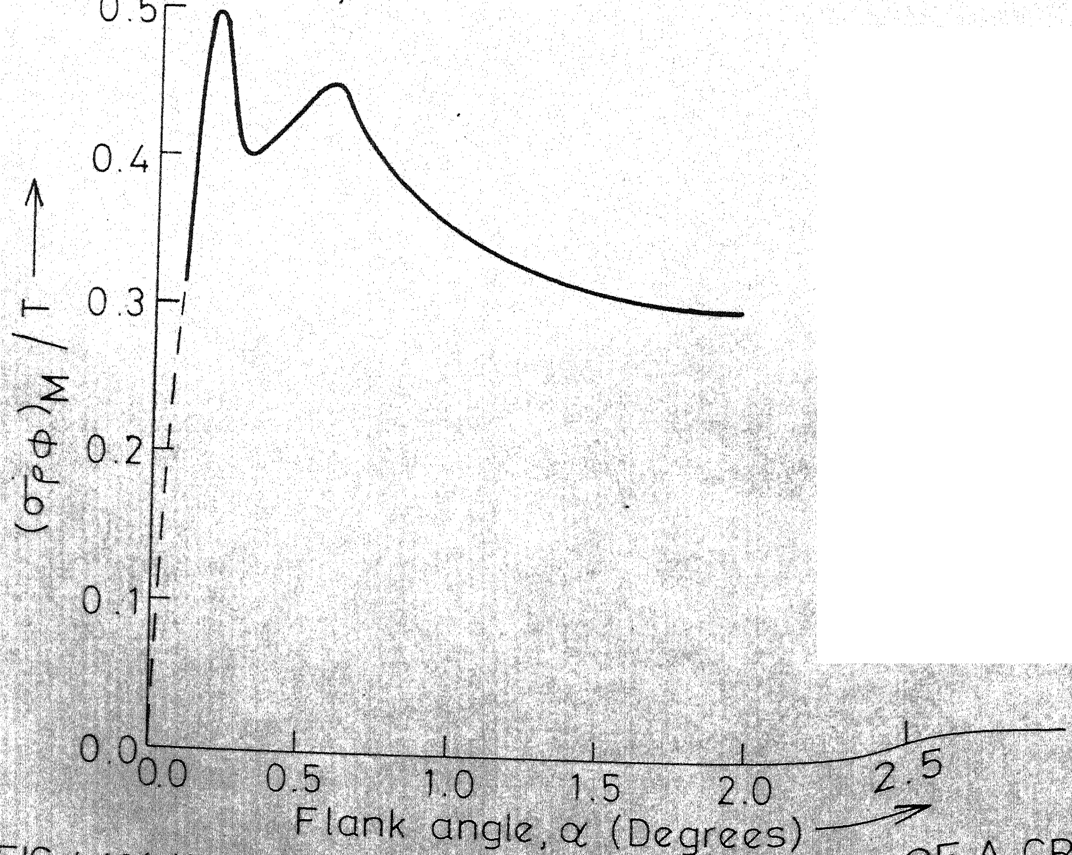

FIG.4.49(b) MISMATCH SHEAR STRESS AHEAD OF A CRACK-LIKE-NOTCH ON $\phi = 70°$ PLANE PLOTTED AGAINST FLANK ANGLE, α

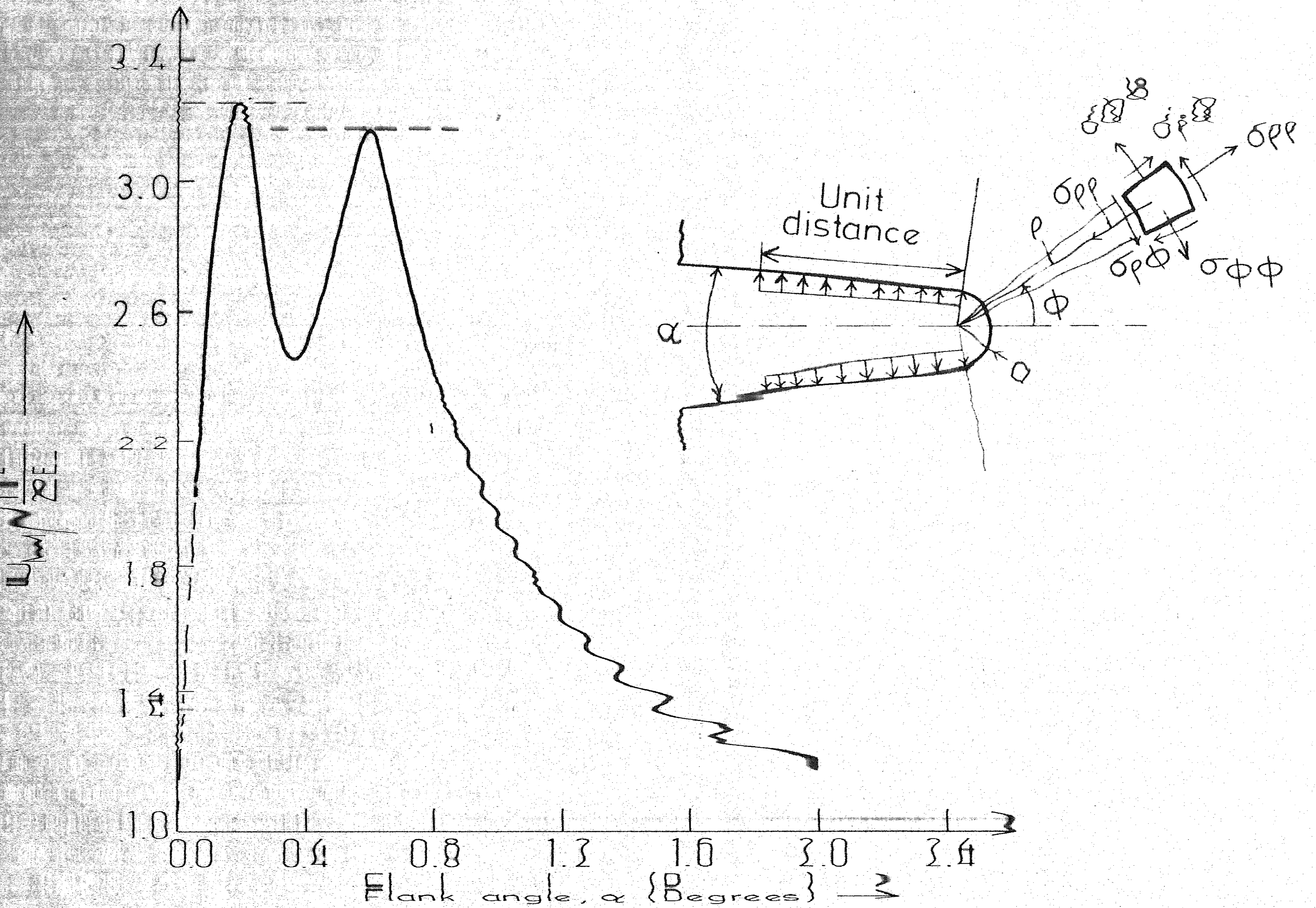

FIG.4.50 FOR AN INCOMPRESSIBLE ELASTIC SOLID THE TOTAL DECREASE IN MISFIT ENERGY OF THE BODY AHEAD OF A CRACK-LIKE NOTCH SHOWN AGAINST NOTCH FLANK OPENING ANGLE, α

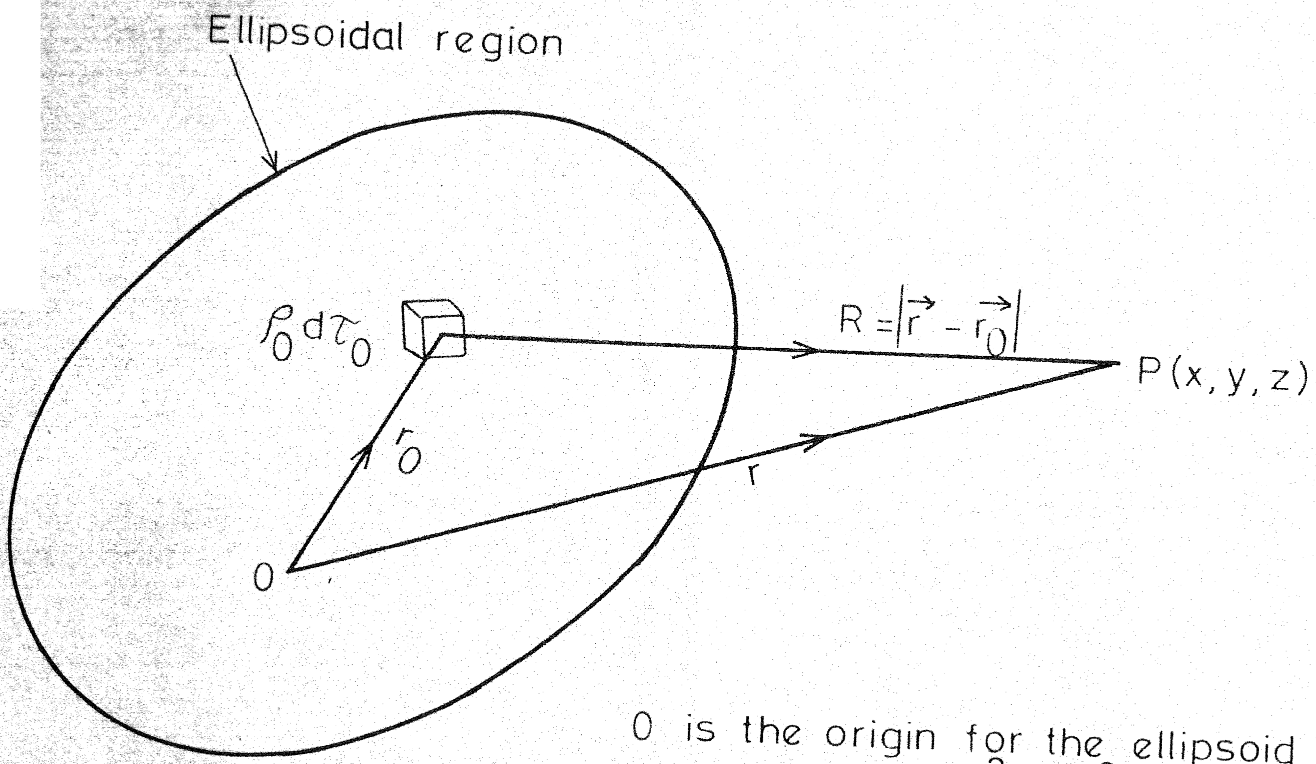
Ellipsoidal region
$\rho_0 d\tau_0$
$R = |\vec{r} - \vec{r_0}|$
P(x, y, z)
r_0
r
0

0 is the origin for the ellipsoid and its eqn. is $\frac{x_0^2}{a^2} + \frac{y_0^2}{b^2} + \frac{z_0^2}{c^2} = 1$

FIG.5.1 AN ILLUSTRATION OF EQN. C.1, CONCERNING THE MULTIPOLE CHARGE DISTRIBUTIONS [188]

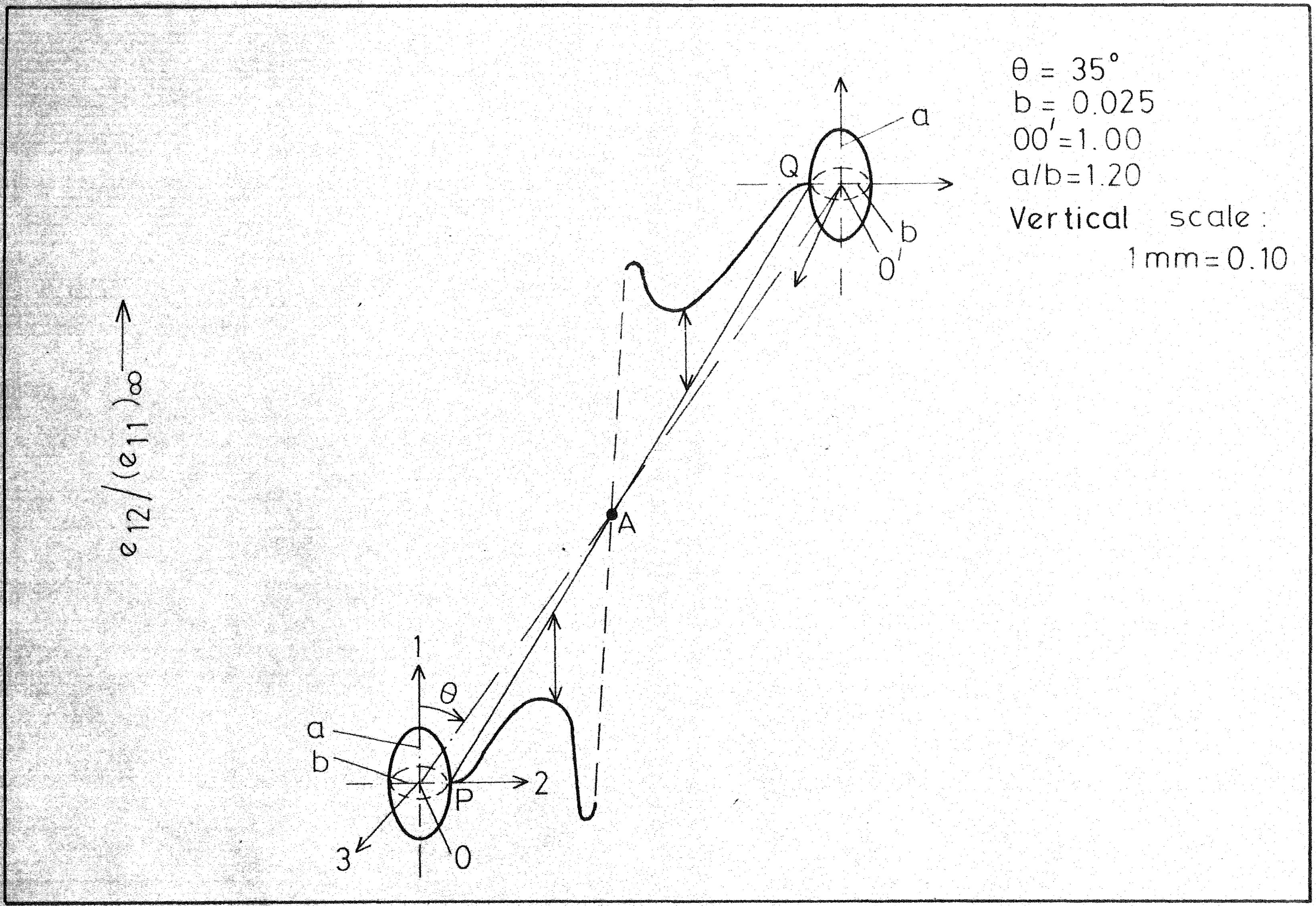

FIG.5.2 SHEAR STRAIN LOCALIZATION ON LIGAMENT LINE PQ IN $X_3 = 0$ PLANE BETWEEN TWO PROLATE SPHEROIDAL HOLES UNDER UNIAXIAL TENSION.

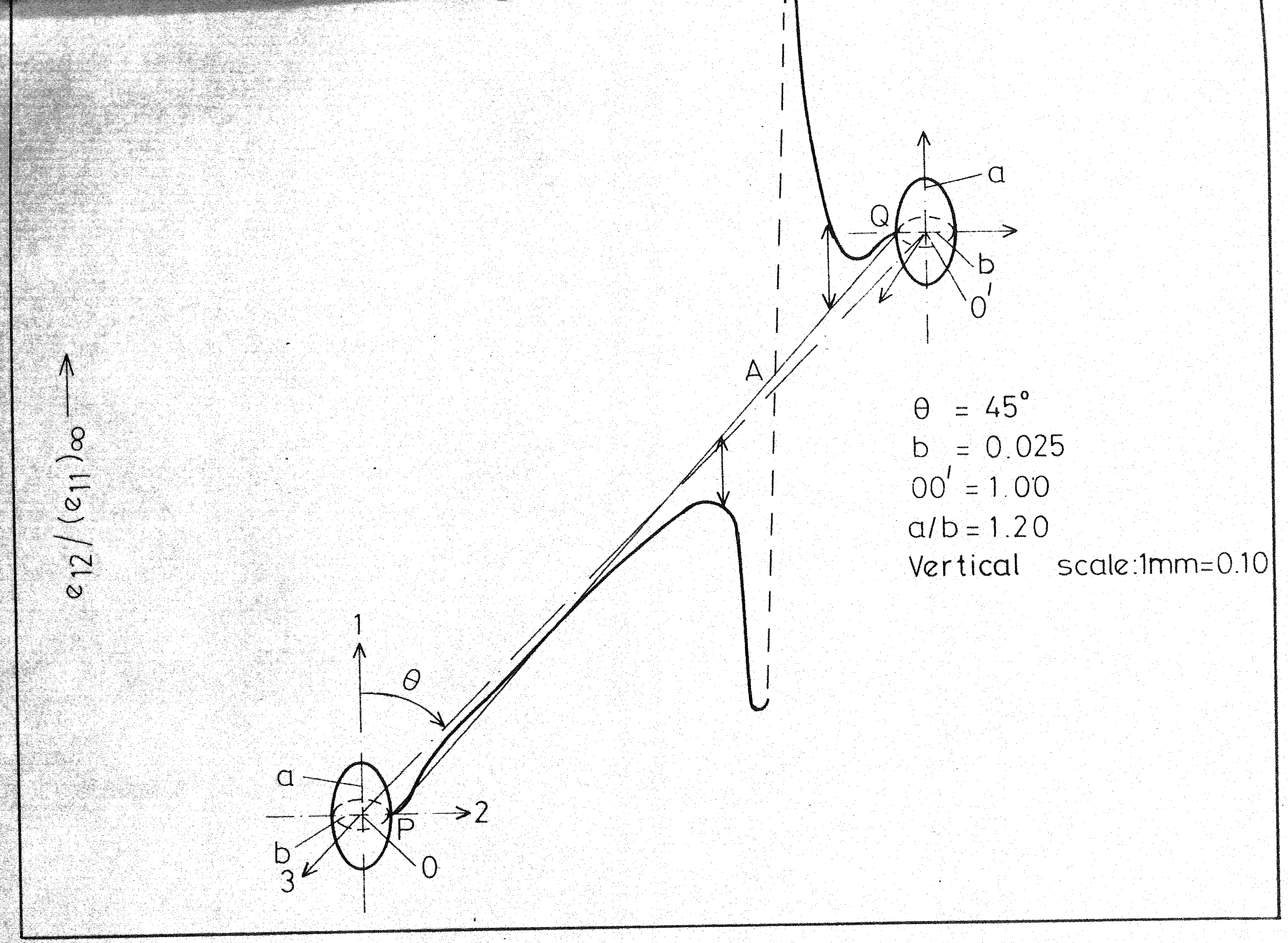

FIG. 5.3 SHEAR STRAIN LOCALIZATION ON LIGAMENT LINE PQ IN $X_3 = 0$ PLANE BETWEEN TWO PROLATE SPHEROIDAL HOLES UNDER UNIAXIAL TENSION.

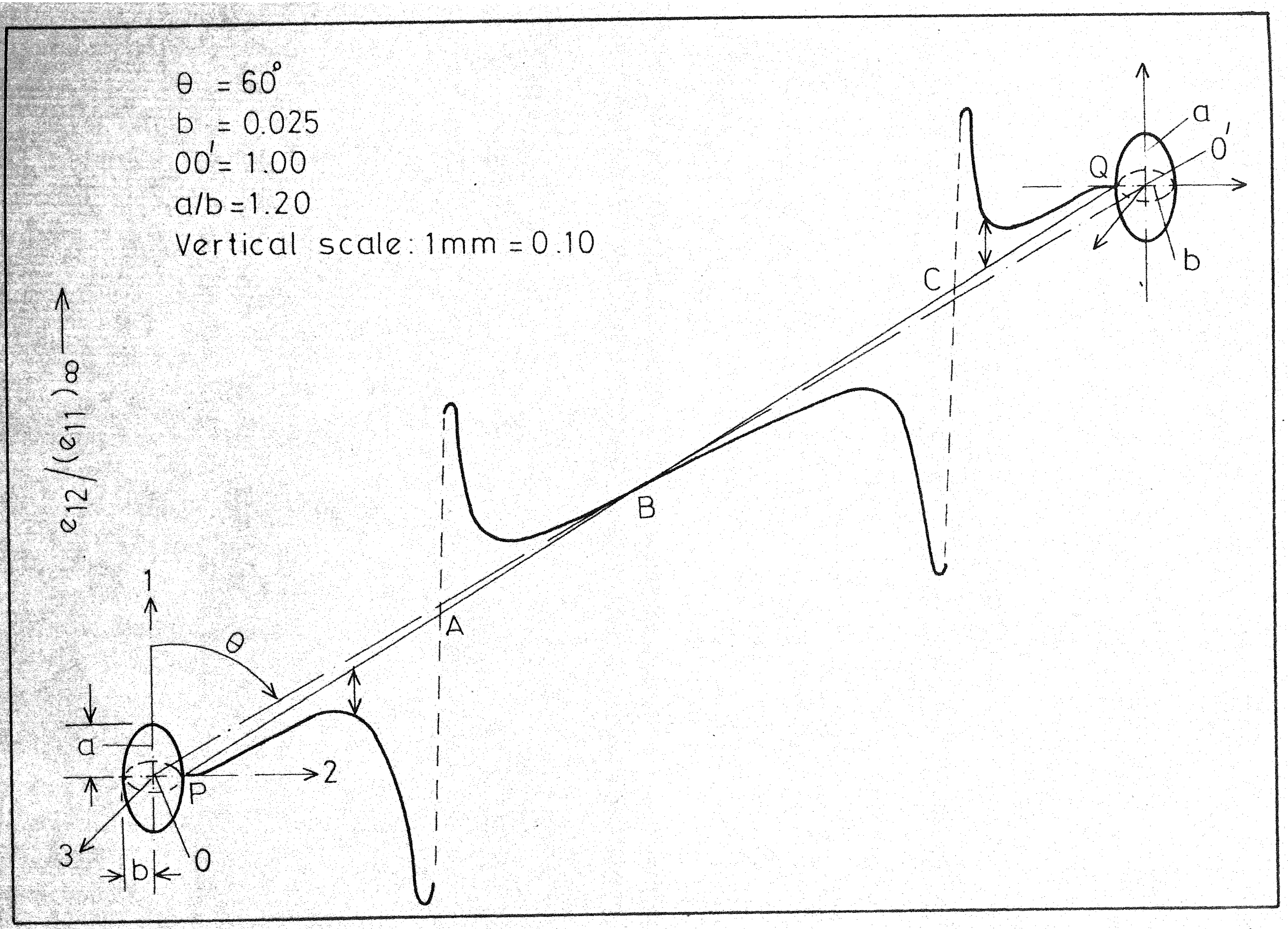

FIG. 5.4 SHEAR STRAIN LOCALIZATION ON LIGAMENT LINE PQ IN $X_3=0$ PLANE BETWEEN TWO PROLATE SPHEROIDAL HOLES UNDER UNIAXIAL TENSION.

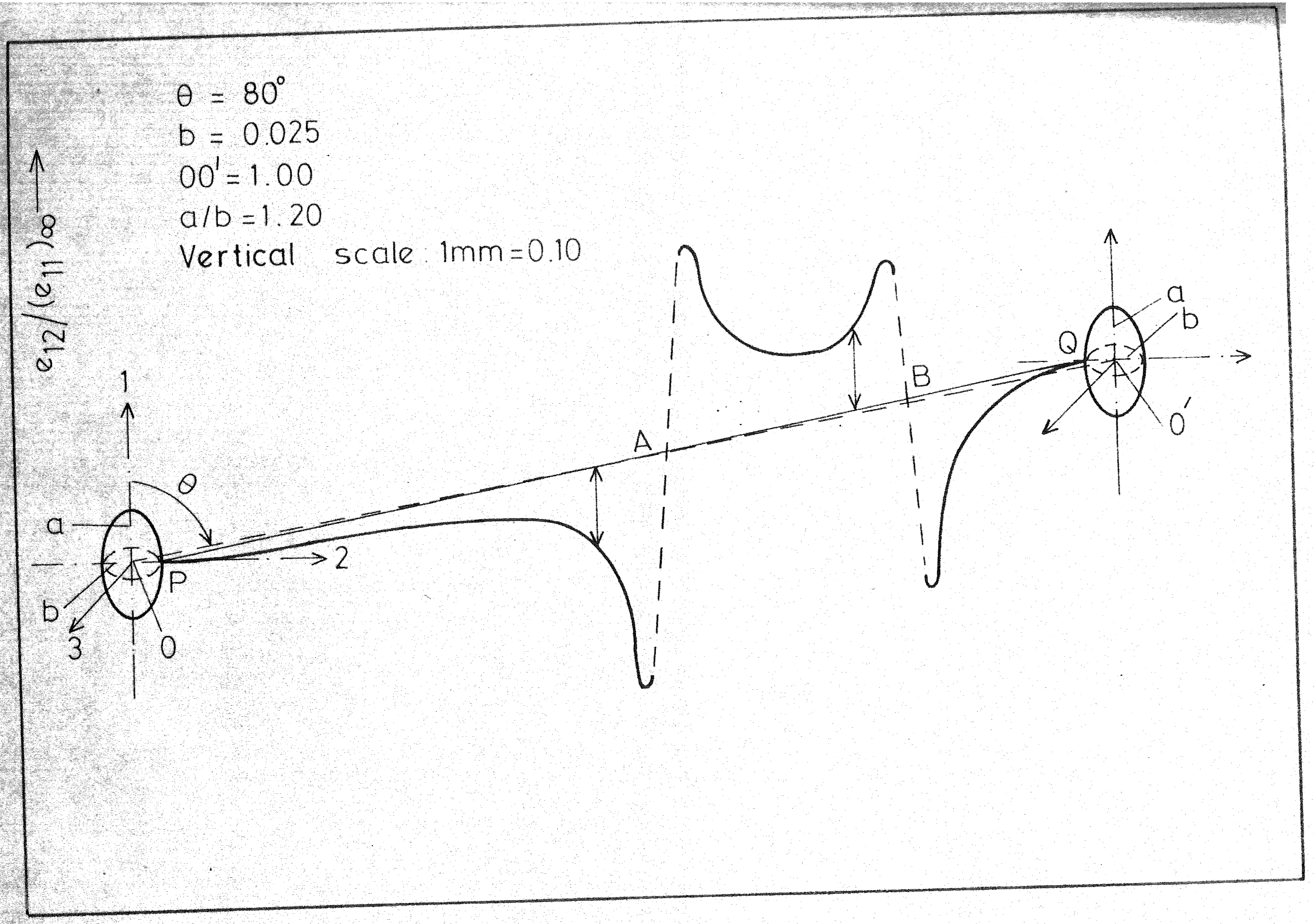

FIG. 5.5 SHEAR STRAIN LOCALIZATION ON LIGAMENT LINE PQ IN $X_3 = 0$ PLANE BETWEEN TWO PROLATE SPHEROIDAL HOLES UNDER UNIAXIAL TENSION.

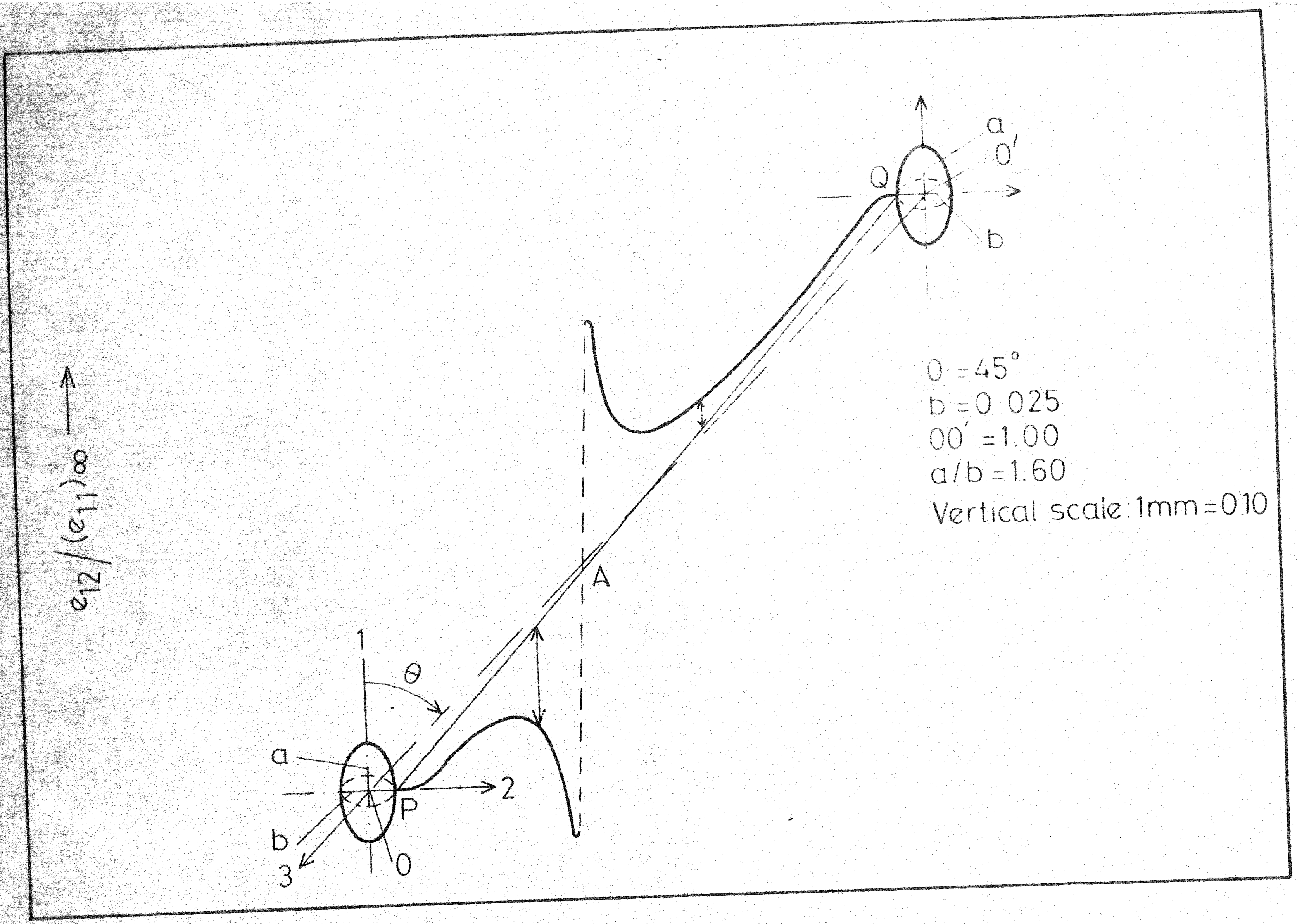
$e_{12}/(e_{11})_\infty$
Q
a
0′
b
0 =45°
b =0 025
00′ =1.00
a/b =1.60
Vertical scale: 1mm =0.10
A
1
θ
a
P
2
b
3
0

FIG. 5.6 SHEAR STRAIN LOCALIZATION ON LIGAMENT LINE PQ IN $X_3 = 0$ PLANE BETWEEN TWO PROLATE SPHEROIDAL HOLES UNDER UNIAXIAL TENSION.

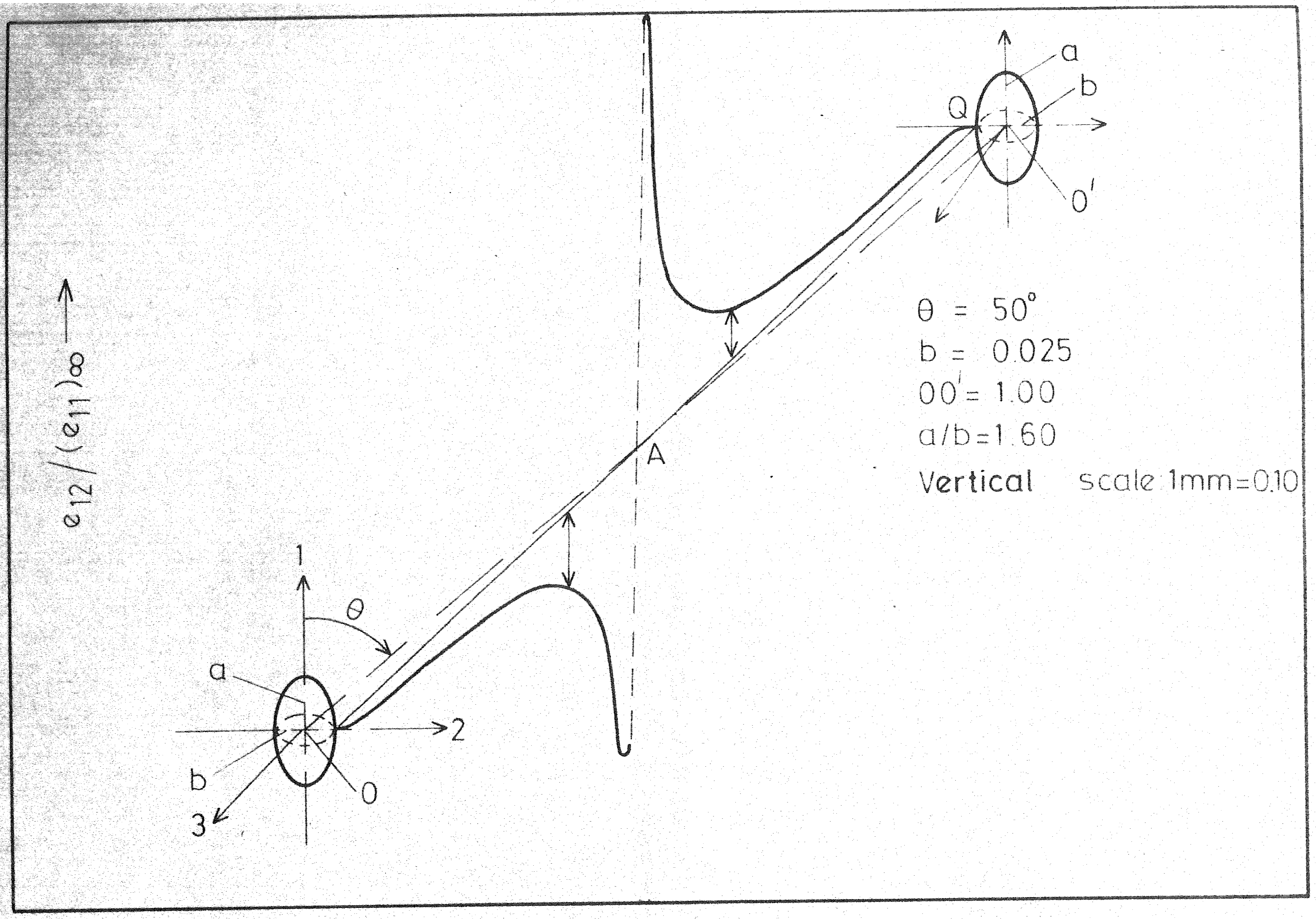

FIG. 5.7 SHEAR STRAIN LOCALIZATION ON LIGAMENT LINE PQ IN $X_3 = 0$ PLANE BETWEEN TWO PROLATE SPHEROIDAL HOLES UNDER UNIAXIAL TENSION.

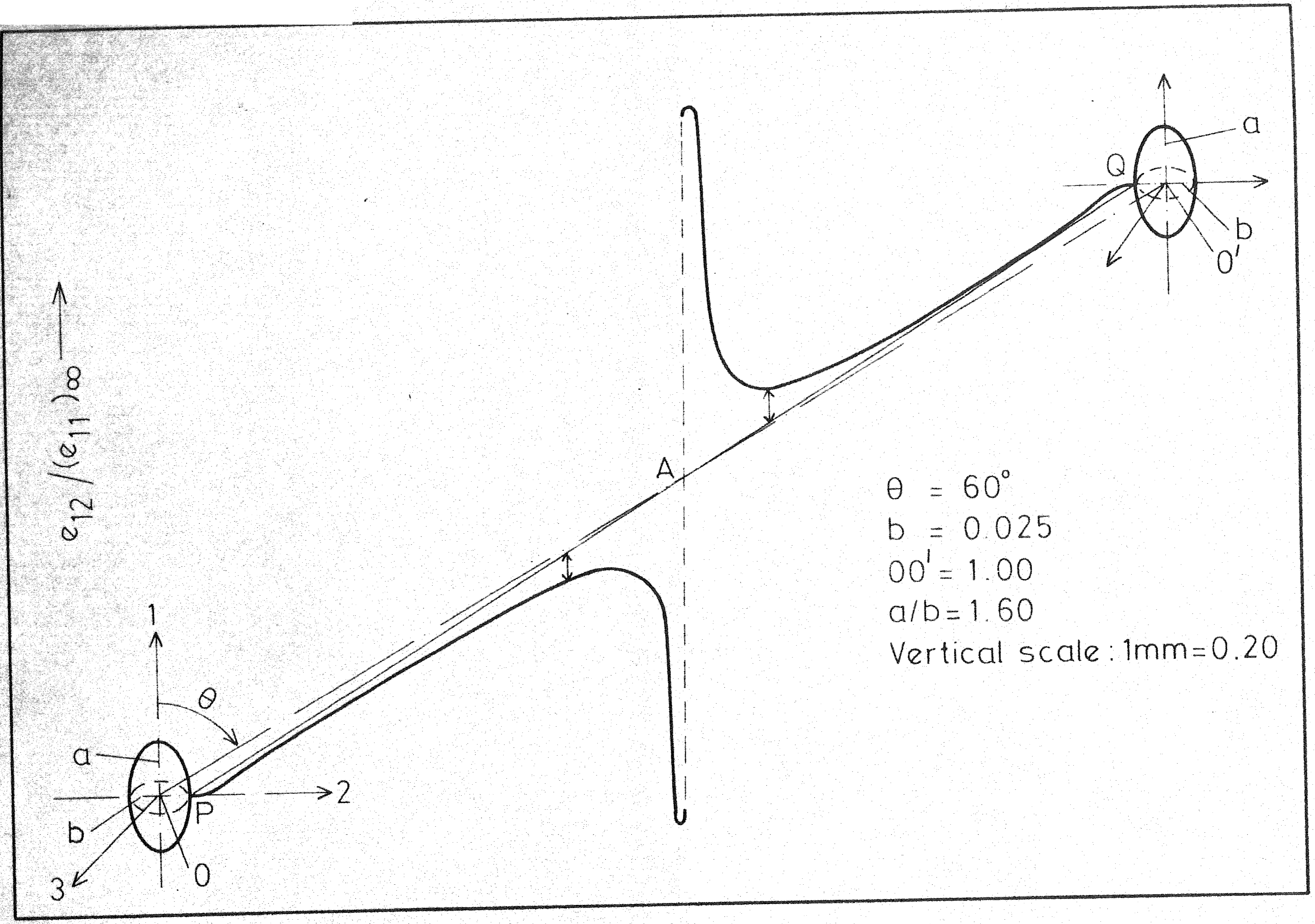

FIG. 5.8 SHEAR STRAIN LOCALIZATION ON LIGAMENT LINE PQ IN $X_3 = 0$ PLANE BETWEEN TWO PROLATE SPHEROIDAL HOLES UNDER UNIAXIAL TENSION.

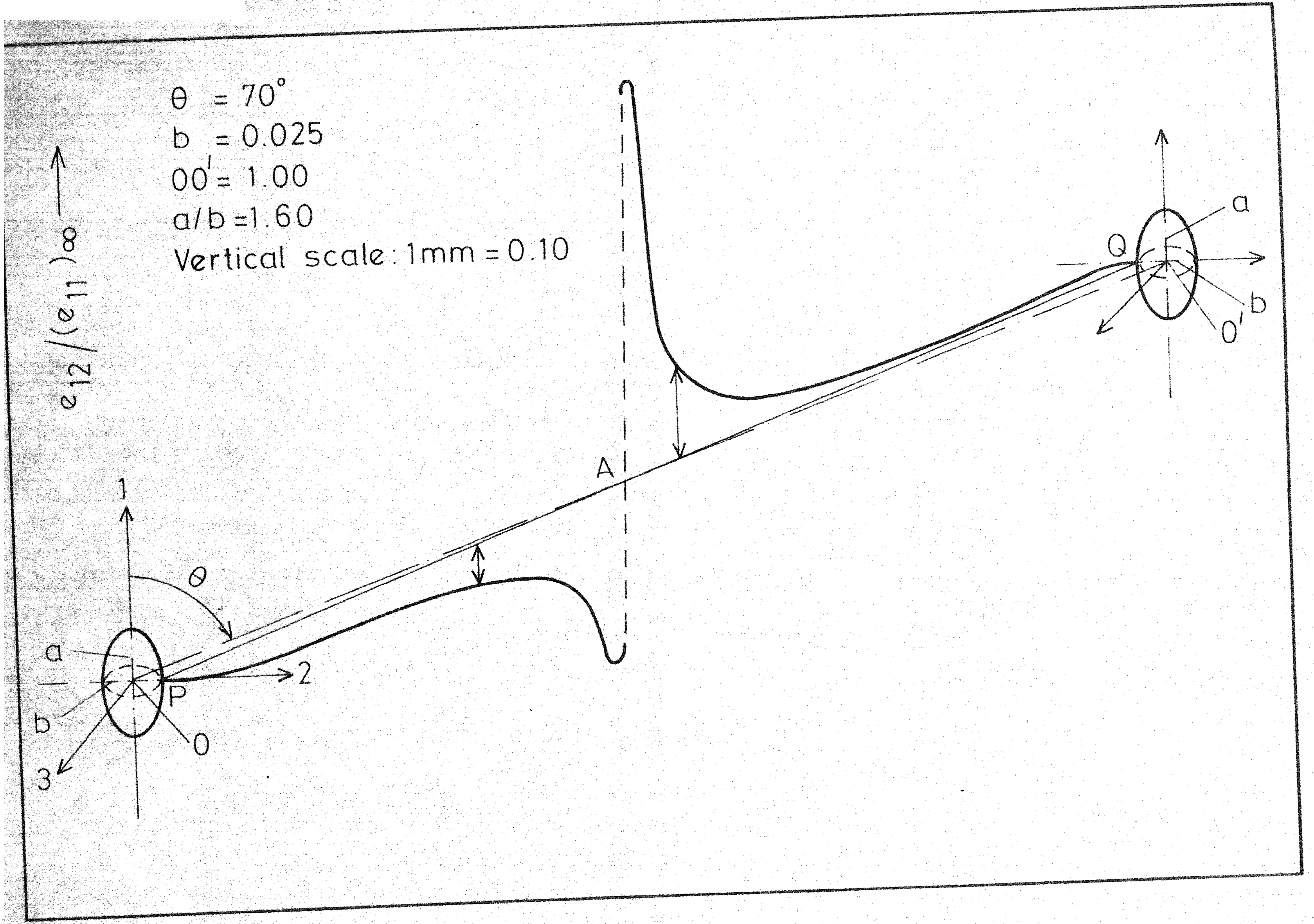

FIG. 5.9 SHEAR STRAIN LOCALIZATION ON LIGAMENT LINE PQ IN $X_3 = 0$ PLANE BETWEEN TWO PROLATE SPHEROIDAL HOLES UNDER UNIAXIAL TENSION.

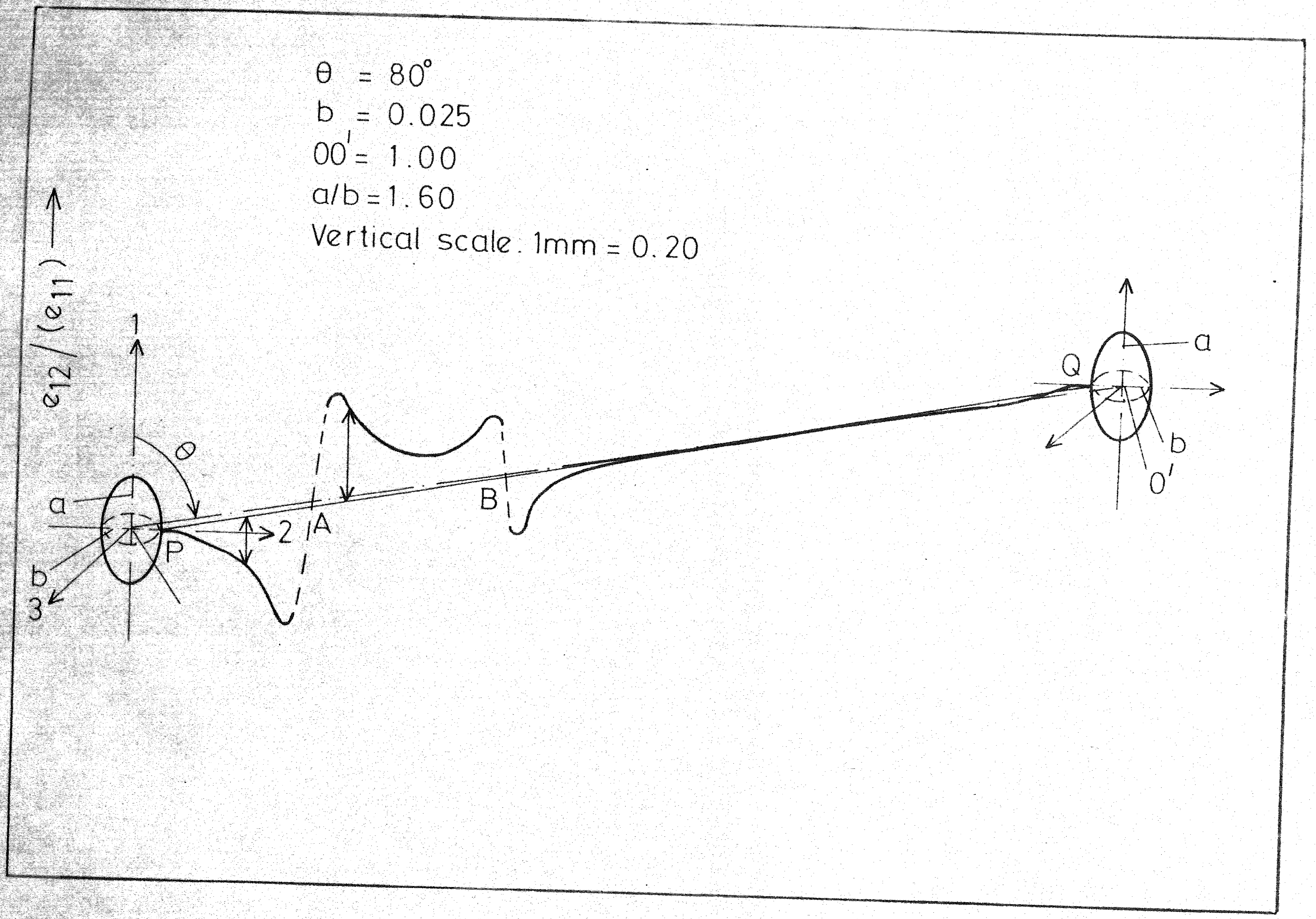

FIG. 5.10 SHEAR STRAIN LOCALIZATION ON LIGAMENT LINE PQ IN $X_3 = 0$ PLANE BETWEEN TWO PROLATE SPHEROIDAL HOLES UNDER UNIAXIAL TENSION.

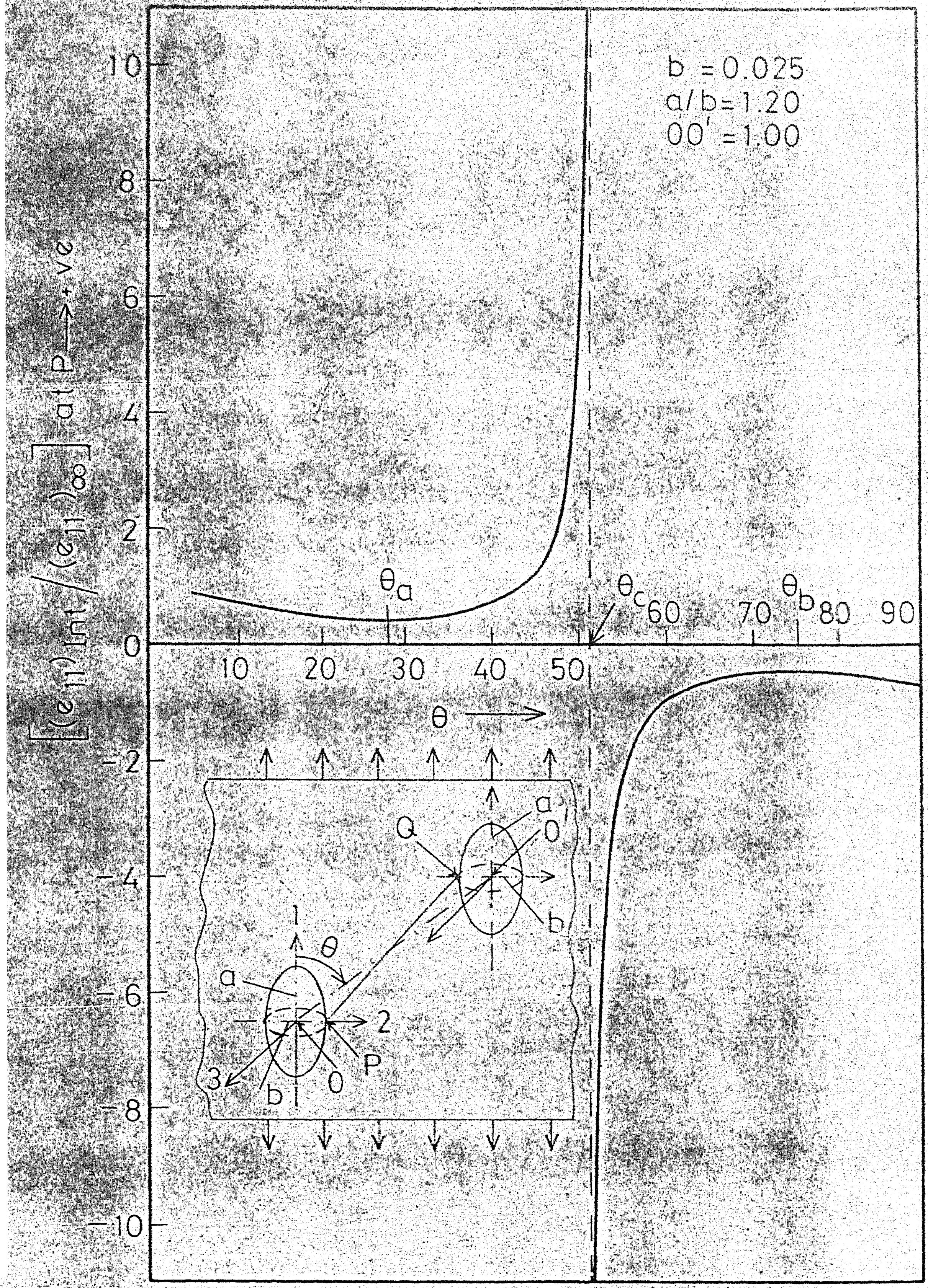

FIG. 5.11 INTERACTION NORMAL TENSILE STRAIN $(e_{11})_{Int.}$ AT P PER UNIT REMOTELY APPLIED TENSILE STRAIN PLOTTED AGAINST VOID POSITION ANGLE θ IN DEGREES.

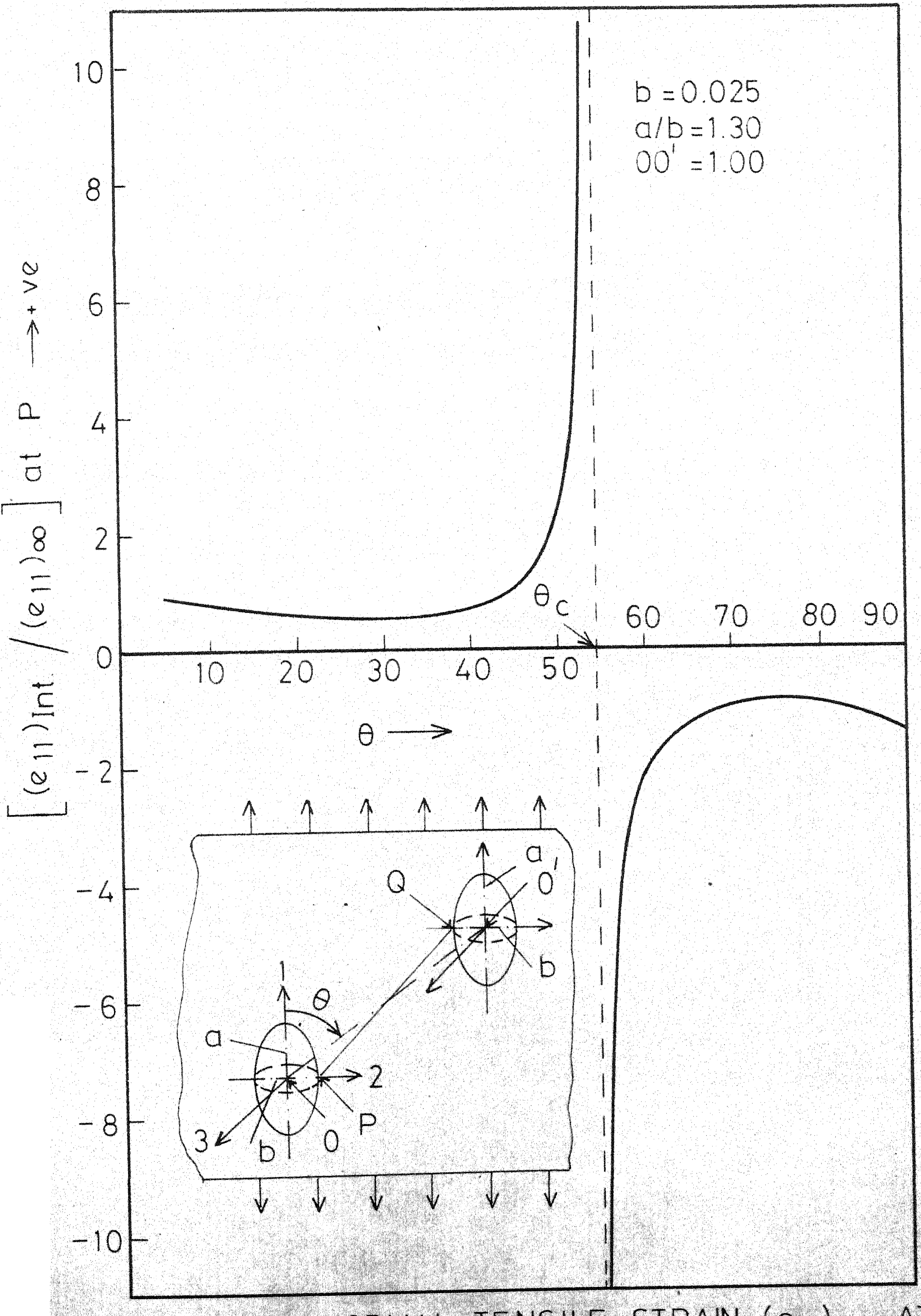

FIG.5.12 INTERACTION NORMAL TENSILE STRAIN $(e_{11})_{Int.}$ AT P PER UNIT REMOTELY APPLIED TENSILE STRAIN PLOTTED AGAINST VOID POSITION ANGLE θ IN DEGREES.

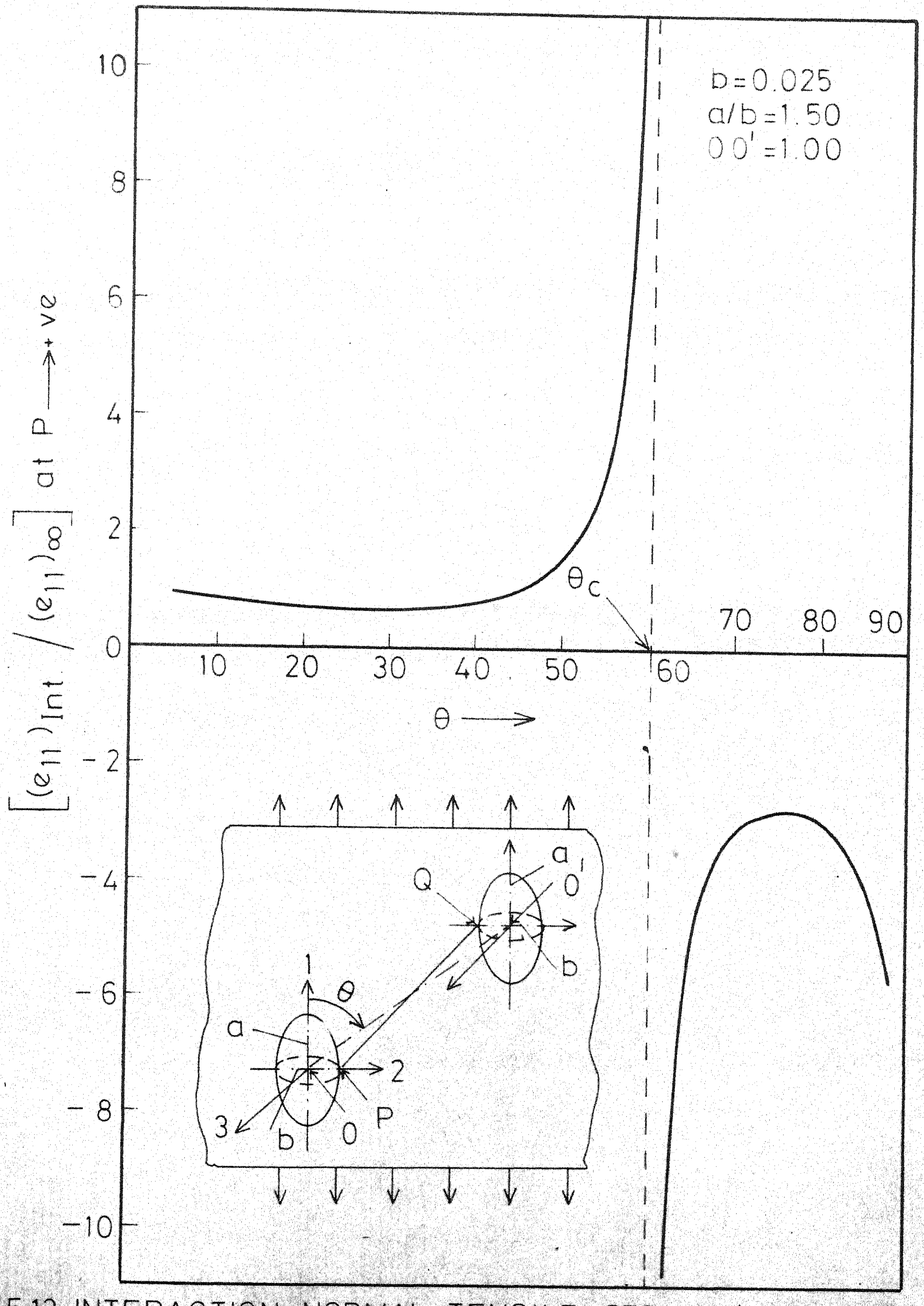

FIG.5.13 INTERACTION NORMAL TENSILE STRAIN $(e_{11})_{Int.}$ AT P PER UNIT REMOTELY APPLIED TENSILE STRAIN PLOTTED AGAINST VOID POSITION ANGLE θ IN DEGREES.

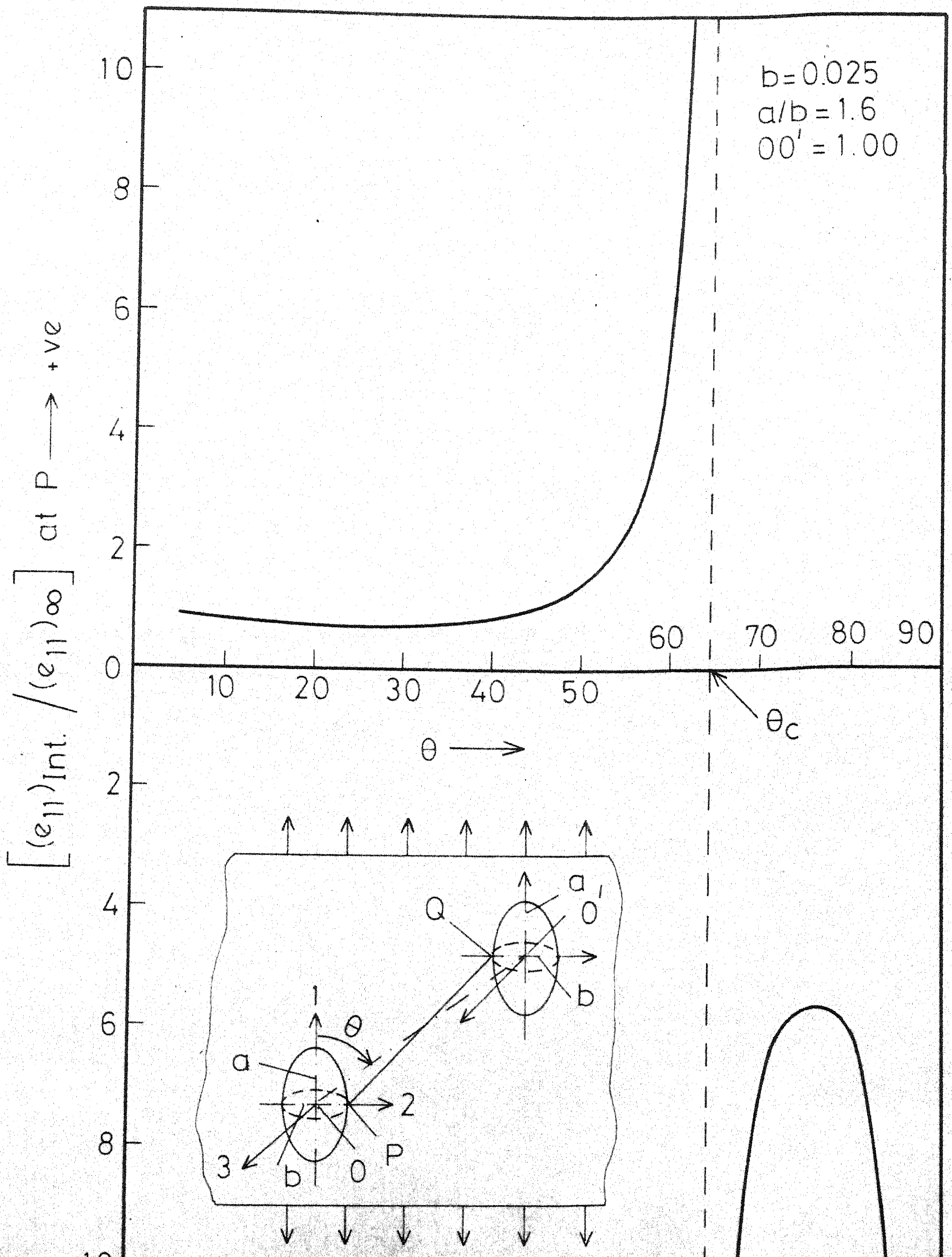

FIG.5.14 INTERACTION NORMAL TENSILE STRAIN $(e_{11})_{Int.}$ AT P PER UNIT REMOTELY APPLIED TENSILE STRAIN PLOTTED AGAINST VOID POSITION ANGLE θ IN DEGREES.

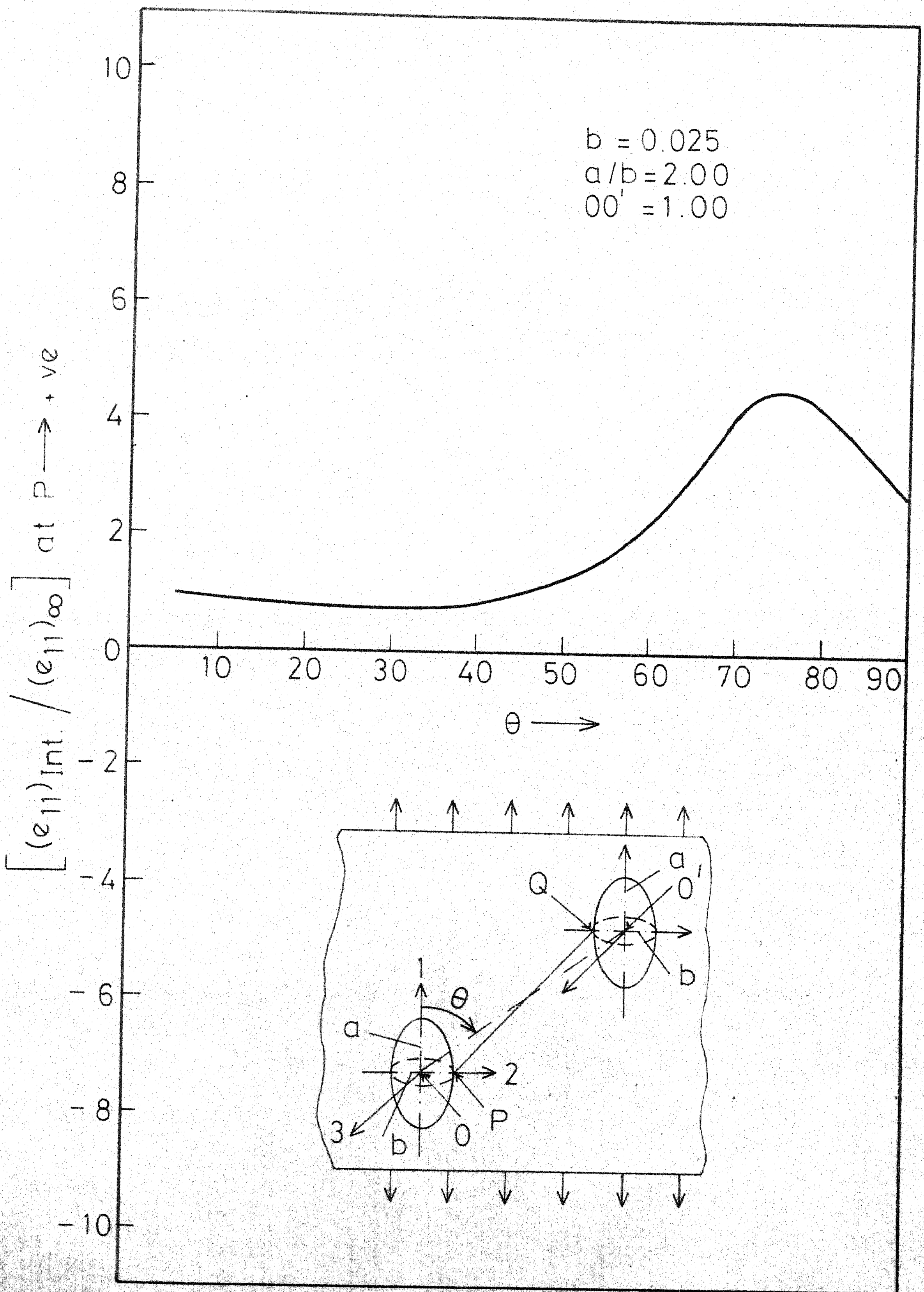

FIG. 5.15 INTERACTION NORMAL TENSILE STRAIN $(e_{11})_{Int.}$ AT P PER UNIT REMOTELY APPLIED TENSILE STRAIN PLOTTED AGAINST VOID POSITION ANGLE θ IN DEGREES.

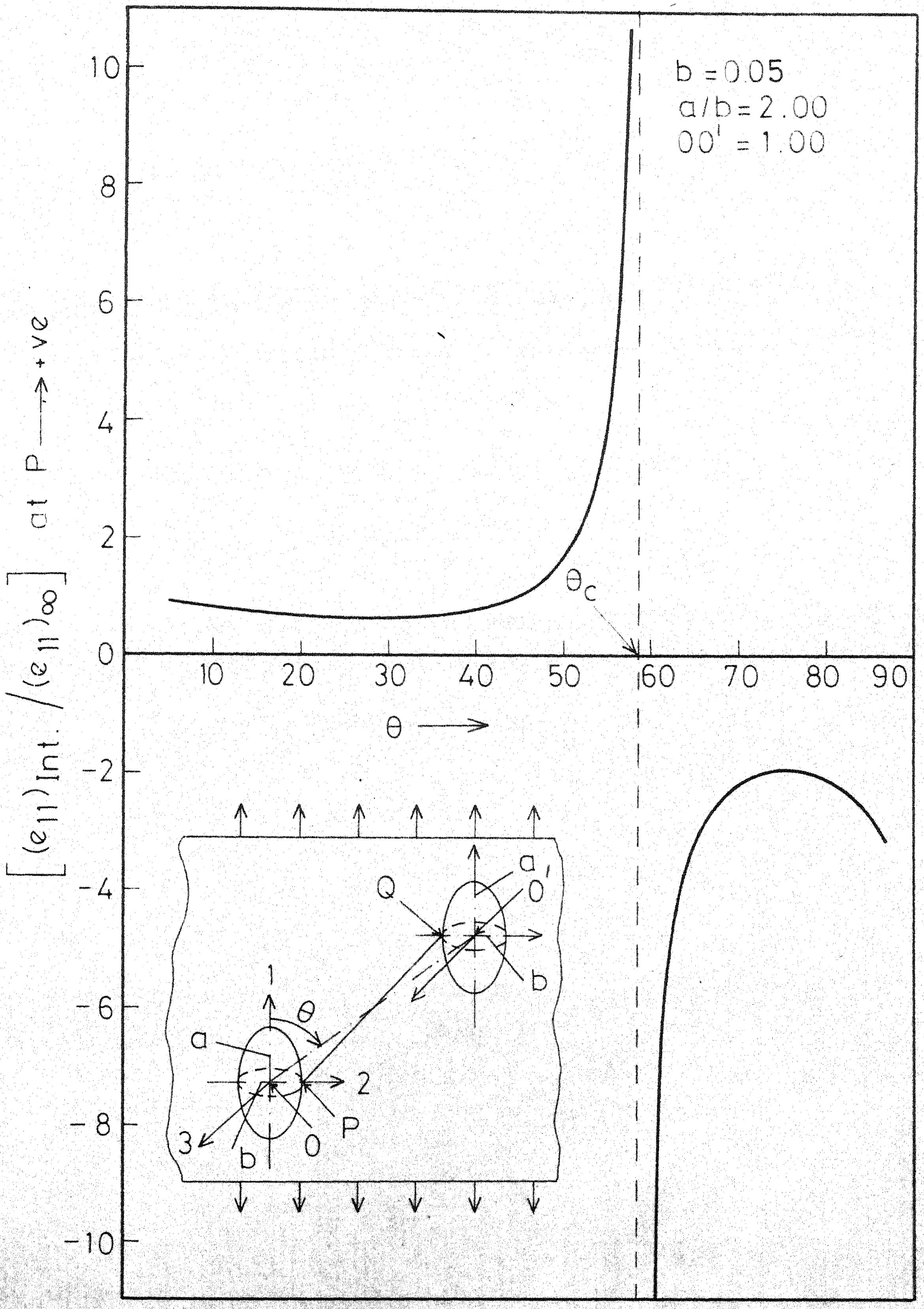

FIG. 5.16 INTERACTION NORMAL TENSILE STRAIN $(e_{11})_{Int.}$ AT P PER UNIT REMOTELY APPLIED TENSILE STRAIN PLOTTED AGAINST VOID POSITION ANGLE θ IN DEGREES.

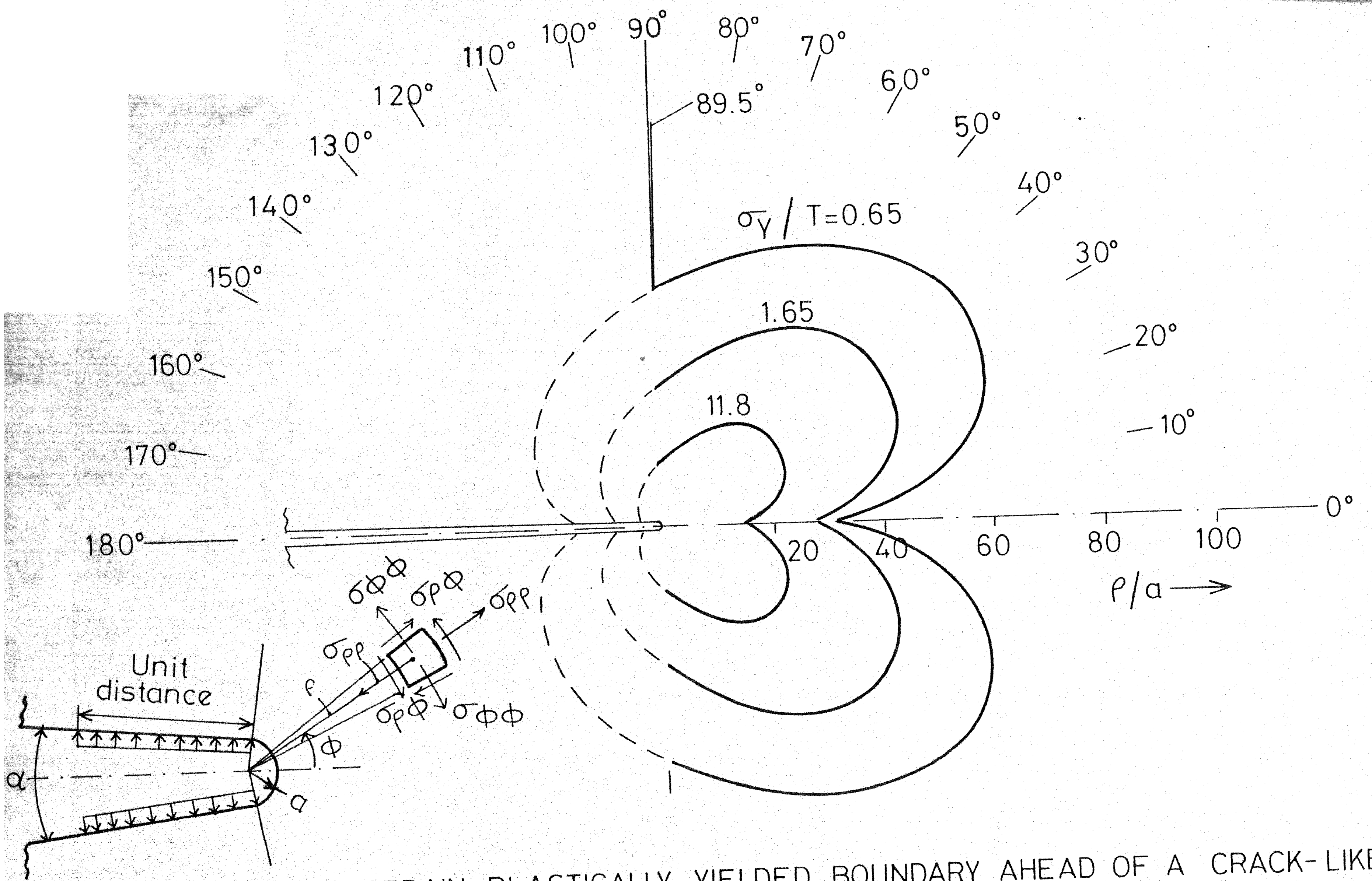

FIG. 6.1 PLANE STRAIN PLASTICALLY YIELDED BOUNDARY AHEAD OF A CRACK-LIKE-NOTCH FOR AN IDEALLY PLASTIC VON-MISES MATERIAL FOR DIFFERENT YIELD STRENGTHS. $\alpha = 1°, a = 0.01$

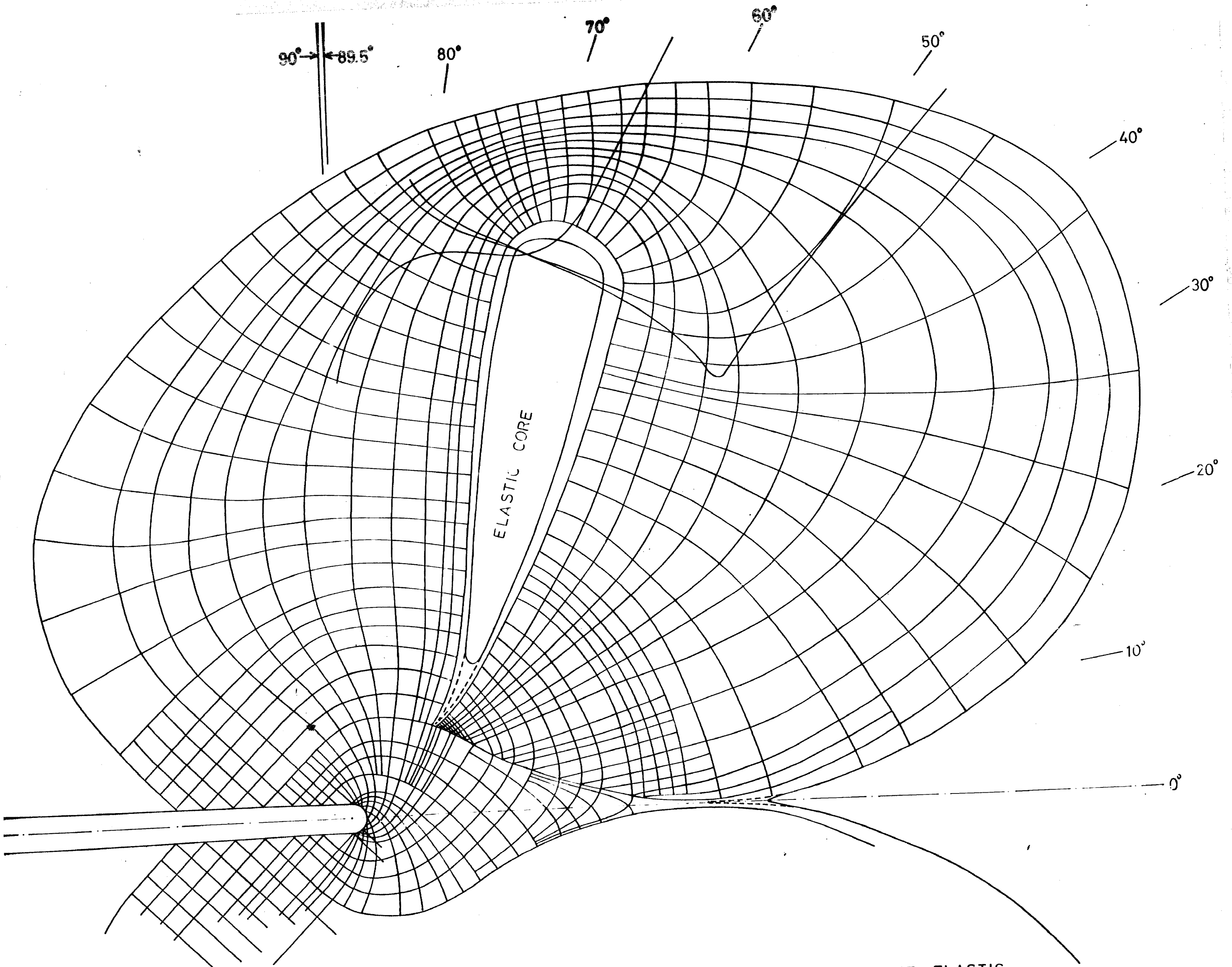
90°
89.5°
80°
70°
60°
50°
40°
30°
20°
10°
0°
ELASTIC CORE

FIG. 6.2 SLIP-LINE FIELD FOR 1° CRACK-LIKE-NOTCH WITH COMPRESSIVE STRESSES AT ELASTIC-PLASTIC INTERFACE.

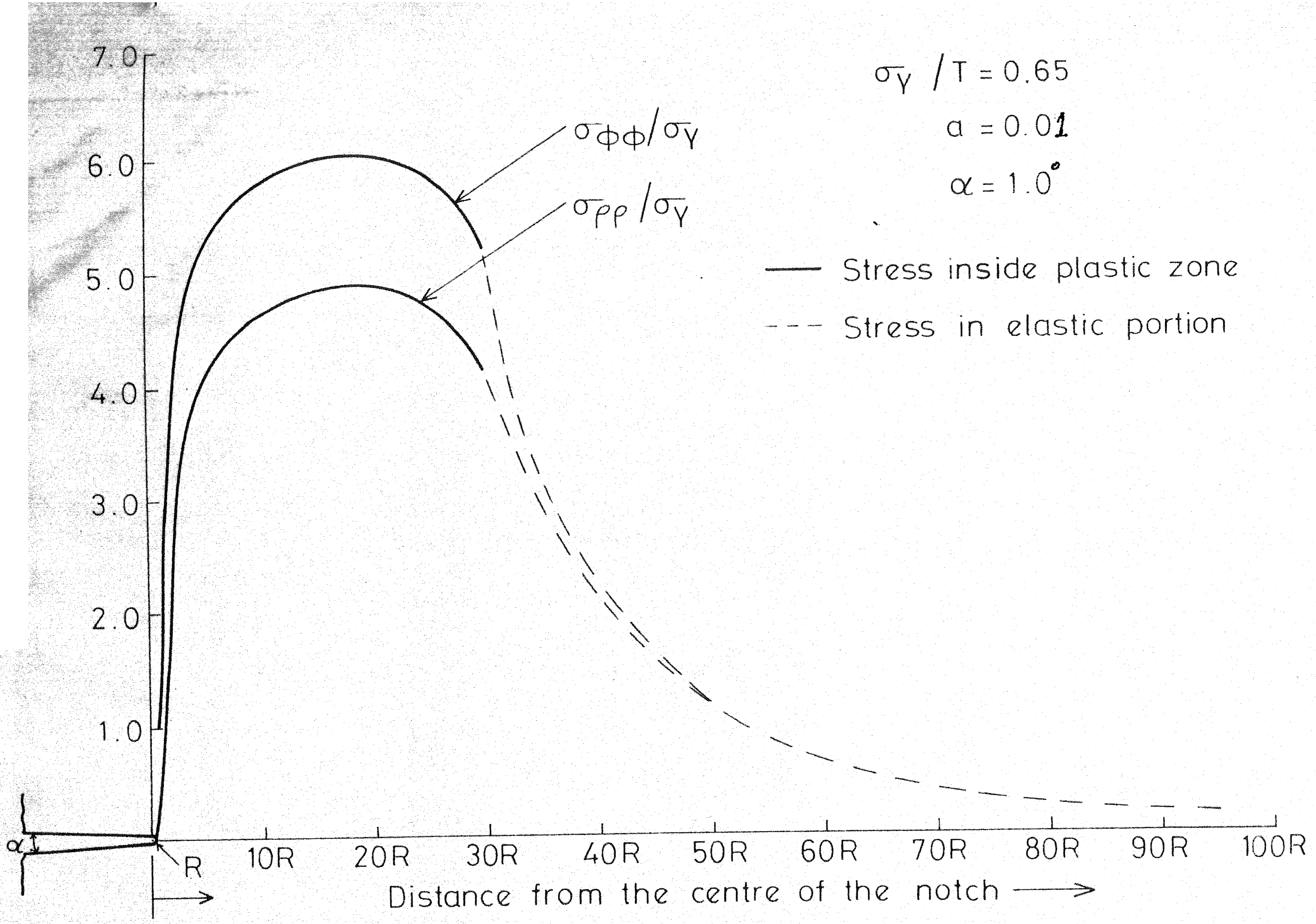

FIG.6.3 ELASTIC-PLASTIC STRESS DISTRIBUTION BELOW THE ROOT OF A CRACK-LIKE-NOTCH ON 0° PLANE FOR A VON MISES YIELDING IDEALLY PLASTIC MATERIAL.

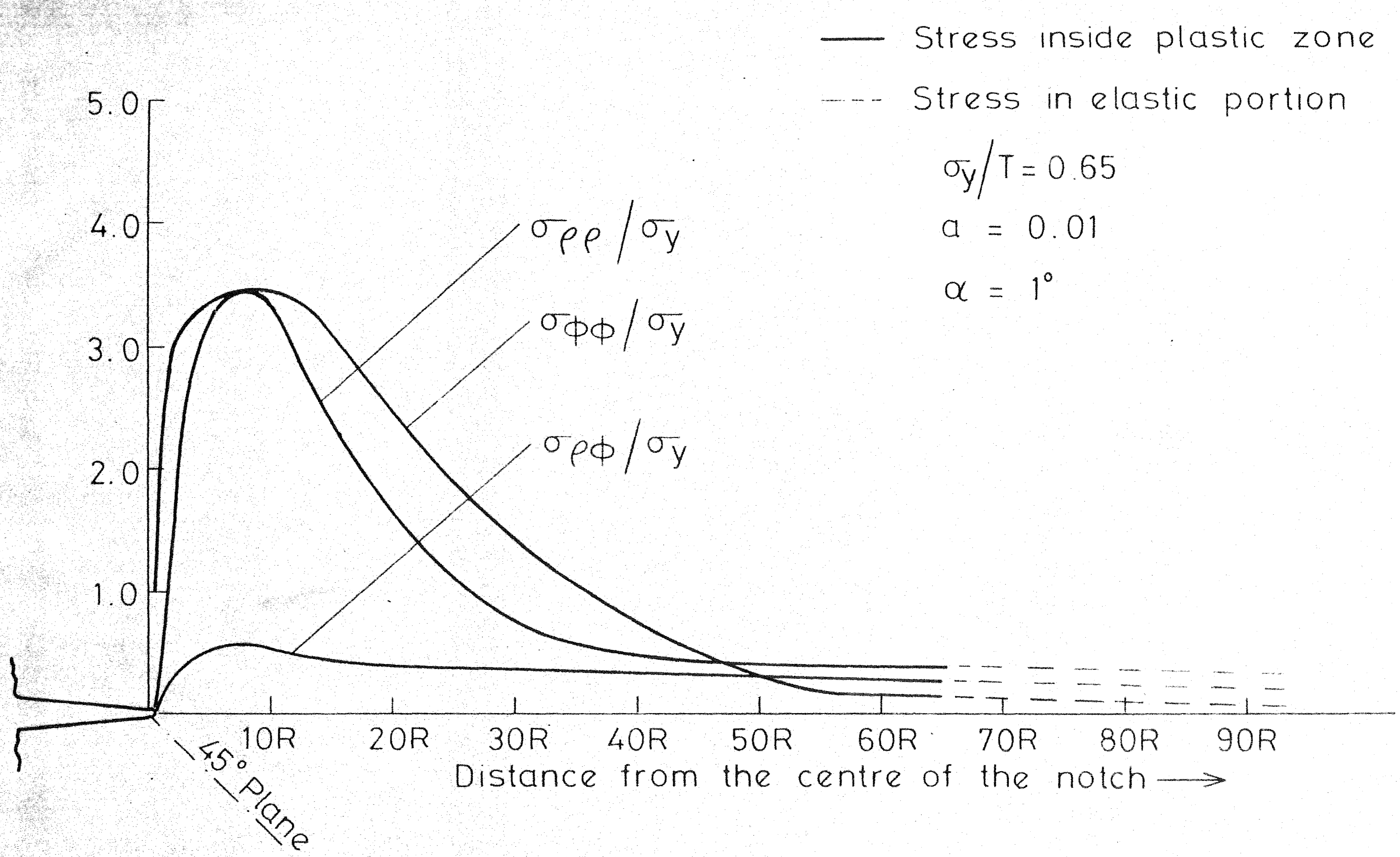

FIG.6.4 ELASTIC-PLASTIC STRESS DISTRIBUTION AHEAD OF A CRACK LIKE NOTCH ON 45° PLANE FOR A VON MISES YIELDING IDEALLY PLASTIC MATERIAL.

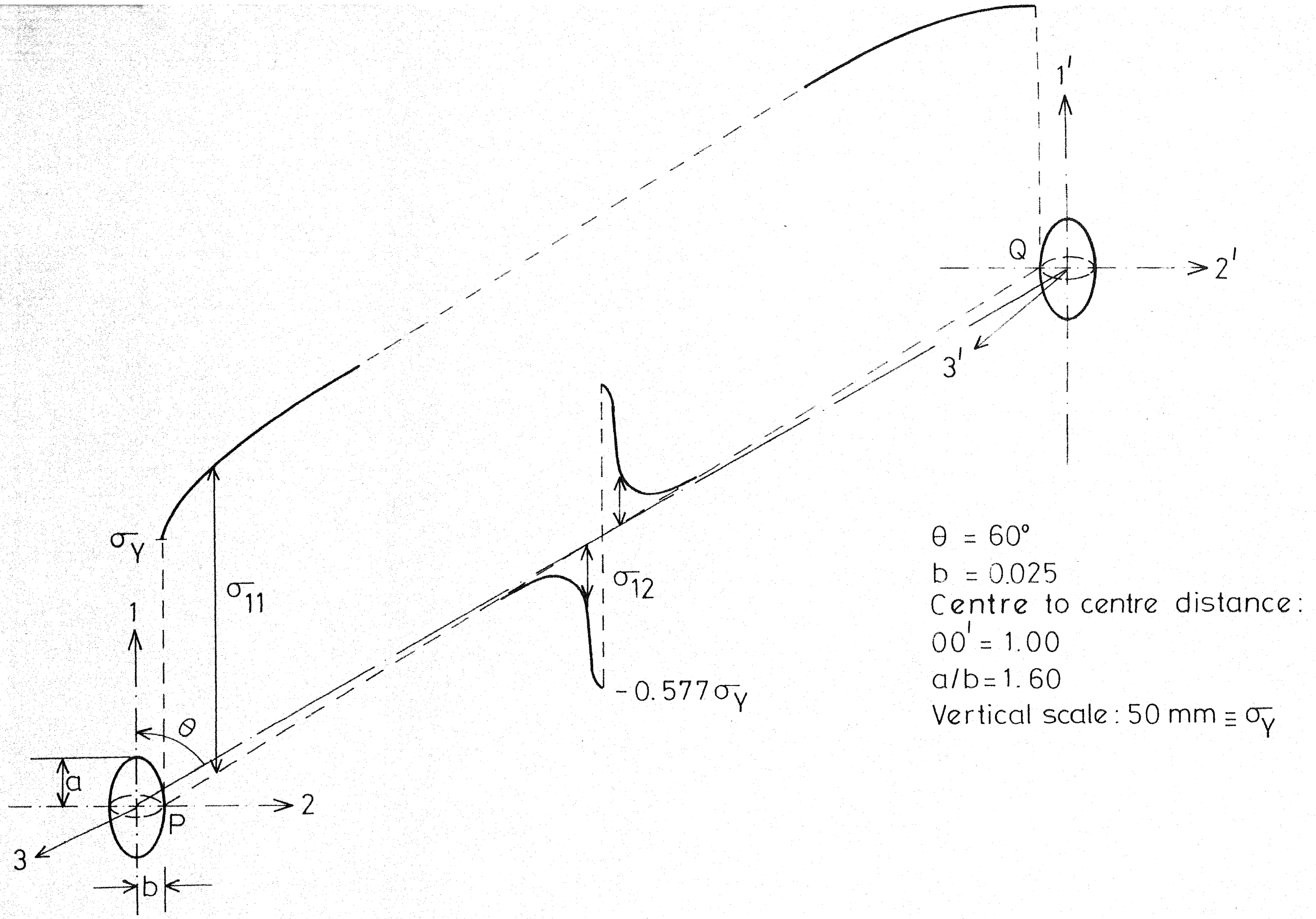
1'
Q
2'
3'
σ_Y
σ_{11}
σ_{12}
$-0.577\sigma_Y$
1
θ
a
2
P
3
b
$\theta = 60°$
b = 0.025
Centre to centre distance:
$00' = 1.00$
a/b = 1.60
Vertical scale: 50 mm $\equiv \sigma_Y$

FIG. 6.6 STRESS ON $X_3 = 0$ PLANE ALONG LINE PQ BETWEEN TWO PROLATE SPHEROIDAL HOLES IN AN IDEALLY VON MISES YIELDING PLASTIC MATERIAL.

BIBLIOGRAPHY

1. Griffith, A.A., The Phenomena of Rupture and Flow in Solids, Philosophical Transactions Royal Soc. of London, Ser.A., Vol. 221, pp. 163-198 (1920).

2. Griffith, A.A., The Theory of Rupture, Proceedings of the Ist International Congress for Applied Mechanics, Delft, Holland, pp. 55-63 (1925).

3. Cottrell, A.H., Fracture, The Physics of Metals, Vol. 2, Chapter 6, pp. 247, ed. by P.B. Hirsch, Cambridge Univ. Press (1975).

4. Mott, N.F., Atomic Structure and the Strength of Metals, Pergamon Press, (1956).

5. Bailey, A.I., Second International Congress on Surface Activity, Vol. 3, pp. 406 (1957).

6. Obreimov, I.V., The Splitting Strength of Mica, Proc. of the Royal Soc. of London, Ser. A., Vol.127, pp. 290-297 (1930).

7. Benbow, J.J., and Roesler, F.C., Experiments on Controlled Fractures, Proc. Phys. Soc. B70, pp.201-211 (1957).

8. Wells, A.A., Strain Energy Release Rates for Fractures Caused by Wedge Action, NRL Report No. 4705 (1956).

9. Barenblatt, G.I., The Mathematical Theory of Equilibrium Cracks in Brittle Fracture, Advances in Applied Mechanics, Vol. 7, pp. 55-129, (1962), Academic Press, New York.

10. Eshelby, J.D., The Continuum Theory of Lattice Defects, Solid State Physics (ed.by F.Seitz and D. Turnbull), Vol. 3, pp. 79 (1956).

11. Bilby, B.A. and Eshelby, J.D. , Dislocations and the Theory of Fracture, Chapter 2, Vol. 1, FRACTURE - An Advanced Treatise, Ed. by H. Liebowitz, Academic Press, (1968).

12. Thomas, T.Y., Plastic Flow and Fracture in Solids, Academic Press, New York (1961).

13. Hill, R., Discontinuity Relations in Mechanics of Solids, Progress in Solid Mechanics, ed. by I.N. Sneddon and R. Hill, North-Holland, Amsterdam, Vol. 2, pp. 247-276 (1961).

14. Sneddon, I.N., Fourier Transforms, New York, McGraw-Hill (1951).

15. Naylor, D., On a Mellin Type Integral Transform, Journal of Mathematics and Mechanics, Vol.12,No.2, pp.265-274 (1963).

16. Tranter, C.J., Integral Transforms in Mathematical Physics, London : Methuen and Co. Ltd., 3rd Edn. (1966).

17. Sneddon, I.N., and Lowengrub, M., 'Crack Problems in the Classical Theory of Elasticity, John Wiley and Sons, Inc., New York (1969).

18. Oberhettinger, F., 'Tables of Mellin Transforms, Springer-Verlag, Berlin, pp. 7(1974).

19. Neuber, H., Theory of Notch Stresses, Edward Publisher, Michigan, U.S.A. (1946).

20. Muskhelishvilli, N.I., Some Basic Problems of the Mathematical Theory of Elasticity, 4th ed. Izd. AN SSSR, M.-L., (1954), (Translated from Russian 3rd ed., Noordhoof, Holland, 1953).

21. Westergaard, H.M., Bearing Pressures and Cracks, Journal of Applied Mechanics, Vol.6, No.2, Ser.A., pp. 49 (1939).

22. Williams, M.L., On the Stress Distribution at the Base of a Stationary Crack, Journal of Applied Mechanics, Vol.24, No.1, Trans. A.S.M.E., Ser. E, pp. 109, (1957).

23. Sternberg, E. and Koiter, W.T., The Wedge Under a Concentrated Couple: A Paradox in the Two-dimensional Theory of Elasticity, Journal of Applied Mechanics, Trans., A.S.M.E. Ser. E., Vol. 25, pp. 575-581, (1958).

24. Wigglesworth, L.A., Stress Distribution in a Notched Plate, Mathematica, Vol.4, pp. 76-96 (1957).

25. Koiter, W.T., Flexural Rigidity of a Beam Weakened by Transverse Saw Cuts, II Proc. Kon. Nederland, Akademy V. Wetenseh, Ser.B, Vol. 59, pp. 635 (1956).

26. Sih, G.C. and Liebowitz, H., Mathematical Theories of Brittle Fracture, Chapter 2, Vol. 2, FRACTURE, - An Advanced Treatise, Ed. by H. Liebowitz, Academic Press (1968).

27. Doran, H.E., and Buchwald, V.T., The Half-plane with an Edge Crack in Plane Elastostatics, Journal of the Institute of Maths and its Applications, Vol.5, pp. 91-112 (1969).

28. Sih, G.C., The Mechanics Aspects of Ductile Fracture, ICF4, Vol.4, pp. 361, ed. by D.M.R. Taplin, University of Waterloo Press, Canada (1977).

29. Frenkel, Y . I., The Theory of Reversible and Irreversible Cracks in Solids, Z hurn. Tekhn. fiz. Vol. 22, pp. 1857-1866 (1952).

30. Khristianovitch, S.A., et al., On the Mechanism of Hydraulic Fracture of an Oil-bearing Stratum, Izvestiya AN SSSR, OTN, No.5, pp.3-41 (1955).

31. Cottrell, A.H., Mechanisms of Fracture, Tewksbury Symposium on Fracture, pp.1, University of Melbourn (1963).

32. Bowie, O.L., Analysis of an Infinite Plate Containing Radial Cracks Originating at the Boundary of an Internal Circular Hole, Journal of Mathematics and Physics, Vol.35, pp. 60 (1956).

33. Koehler, J.S., On the Dislocation Theory of Plastic Deformation, Physical Review, Vol.60,pp.397 (1941).

34. Newman, J.C., An Improved Method of Collocation for the Stress Analysis of Cracked Plates with Various Shaped Boundaries, National Aeronautics and Space Administration, T.N., D-6376 (1971).

35. Miller, K.J., Application of Fracture Mechanics to Fatigue at Notches, International Journal of Fracture, Vol. 9, pp. 326 (1973).

36. Nisitani, H., and Takao, K.I., Behaviour of a Tip of Non-Propagating Fatigue Crack during one Stress Cycle, Engineering Fracture Mechanics, Vol.6,No.2, pp. 253 (1974).

37. Smith, R.A., Jerram, K., and Miller, K.J., Experimental and Theoretical Fatigue Crack Propagation Laws of Variously Notched Plate, Journal of Strain Analysis, Vol.9, No.2, pp. 161 (1974).

38. Titchmarsh, E.C., Introduction to the Theory of Fourier Integrals, Oxford (1937).

39. Dugdale, D.S., Yielding of Steel Sheets Containing Slits, Journal of Mechanics and Physics of Solids, Vol. 8, pp. 100 (1960).

40. Green, A.P., and Hundy, B.B., Initial Plastic Yielding in a Notch Bend Test, Journal of Mechanics and Physics of Solids , Vol. 4, pp. 128 (1956).

41. Hahn, G.T., and Rosenfield, A.R., Local Yields and Extension of Crack Under Plane Stress, Acta Metallurgica, Vol. 13, pp. 293 (1965).

42. McClintock, F.A., and Irwin, G.R., Plasticity Aspects of Fracture Mechanics, A.S.T.M., S.T.P.,No. 381, pp. 84 (1964).

43. Bilby, B.A., Cottrell, A.H., and Swinden, K.H., The Spread of Plastic Yield from a Notch, Proc. of the Royal Soc., of London, Ser. A, Vol. 272, pp. 304 (1963).

44. Gross, B., and Srawley, J.E., Stress Intensity Factor for Three point Bend Specimens by Boundary Collocation, N.A.S.A. Report, T.N., D-3092 (1965),.

45. Irwin, G.R., Fracturing of Metals, Trans. American Soc. of Metals, Vol. 40, pp.147,(1948).

46. Orowan, E., Fracture and Notch-Brittleness in Ductile Metals- A Discussion on Brittle Fracture in Mild Steel Plates, Engineering, Vol. 164, pp. 581-605 (1947).

47. Irwin, G.R., Plastic Zone Near a Crack and Fracture Toughness, Seventh Sagamore Ordnance Materials Conference, Aug. (1960).

48. Orowan, E., et al., Theoretical Research Report, 16/45, Ministry of Supply, Armament Research Department, (1945).

49. Mott, N.F., Fracture of Metals : Theoretical Considerations, Engineering, Vol. 165, pp. 16-18 (1948).

50. Hill, R., The Mathematical Theory of Plasticity, University Press, Oxford (1950).

51. Bandyopadhyay, S.N. and Griffiths, J.R., Effects of Specimen Dimensions on the Fracture Strength of Gauge Plate, (Unpublished Report), Materials Division, C.E.R.L., Leatherhead, Central Electricity Generating Board, England (1970).

52. Bandyopadhyay, S.N., and Mubeen, A., Plasticity Spread in Mild Steel Pre-Cracked Charpy Bars, Engineering Fracture Mechanics, Vol. 12, No.2(1979).

53. Singh, N., Bandyopadhyay, S.N. and Murthy, G.S., Fracture Strength of Short Cracked Beams in the Non-valid Crack toughness Testing Regime, (Paper Submitted for Publication) in Journal of Materials and Technology, Trans. A.S.M.E. Ser. H, (1979).

54. Ritchie, R.O., Rice, J.R., and Knott, J.F., On the Relationship Between Critical Tensile Stress and Fracture-Toughness in Mild Steel, Journal of Mechanics and Physics of Solids, Vol. 21, pp. 395 (1973).

55. McClintock, F.A., Effects of Root Radius,Stress, Crack Growth and Rate on Fracture Instability, Proc. of the Royal Soc. of London, Ser. A., Vol.285, pp. 58 (1965).

56. Knott, J.F., and Cottrell, A.H., Notch Brittleness in Mild Steel, Journal of the Iron and Steel Institute, Vol. 201, pp. 249 (1963).

57. Griffiths, J.R., and Cottrell, A.H., Elastic Failure at Notches in Silicon Steel, Journal of Mechanics and Physics of Solids, Vol. 13, pp. 135 (1965).

58. Oates, G., Influence of Fatigue on Brittle Fracture in Mild Steel, Journal of the Iron and Steel Institute, Vol. 204, pp. 991 (1966).

59. Griffiths, J.R., and Owen, D.R.J., An Elastic-Plastic Stress Analysis for a Notched Bar in Plane Strain Bending, Journal of Mechanics and Physics of Solids, Vol.19, pp. 419-431 (1971).

60. Miller, K.J., and Kfouri, A.P., An Elastic-Plastic Finite Element Analysis of Crack Tip Fields Under Biaxial Loading Conditions, International Journal of Fracture, Vol.10, No. 3, pp. 393 (1974).

61. Rice, J.R., McMeeking, R.M., Parks, D.M. and Sorënsen, E.P., Recent Finite Element Studies in Plasticity and Fracture Mechanics, Computer Methods in Applied Mechanics and Engineering, Vol.17/18, pp.411, Feb.(1979).

62. Rice, J.R., and Johnson, M.A., Inelastic Behaviour of Solids, (edited by Kanninen, M.F., Adler, W.F., Rosenfield, A.R., and Jaffee, R.I.), pp. 641, McGraw-Hill, New York (1970).

63. Knott, J.F., Fundamentals of Fracture Mechanics, Butterworths, London (1973).

64. Argon, A.S., and Im, J., Separation of Second Phase Particles in Spheroidized 1045 Steel, Cu-0.6 percent Cr Alloy and Maraging Steel in Plastic Straining, Metallurgical Transactions, Vol.6, Ser.A, pp. 839-851 (1975).

65. Sokolovsky, V.V., The Theory of Plasticity - An outline of Work Done in Russia, J. of Applied Mechanics, Trans. A.S.M.E. Ser.E., Vol. 13, No.1, pp. A-1 (1946).

66. Prager, W., Hodge, P.G., JR., Theory of Perfectly Plastic Solids, Dover Publications, INC, New York (1968).

67. Nadai, A., Theory of Flow and Fracture of Solids, (Revision of Plasticity) Vol.I (1950); and Vol.II (1963), McGraw-Hill, INC., N.Y.

68. Brown, JR., W.F. and Srawley, J.E., Plane Strain Crack Toughness Testing of High Strength Metallic Materials, A.S.T.M., S. T. P., No. 410 (1966).

69. Rice, J.R., Mathematical Analysis in the Mechanics of Fracture, Fracture, Vol. II, Chap. 3, - An Advanced Treatise, ed. by H. Liebowitz, Academic Press, (1968).

70. Knott, J.F., Micro-Mechanisms of Fracture and the Fracture Toughness of Engineering Alloys, Proc. of the Fourth International Conference on Fracture. Fracture ed. by D.M.R. Taplin, Vol. I, pp.61-92, June (1977).

71. Smith, E., Cook, T.S., and Rau, C.A., Flow Localization and the Fracture Toughness of High Strength Materials, Proceedings of the Fourth International Conference on Fracture. Fracture ed. by D.M.R. Taplin, Vol.I, pp. 215-236, June (1977).

72. Begley, J.A., and Landes, J.D., The Effect of Specimen Geometry on J_{1c} , A.S.T.M., S.T.P., No. 514 (1972).

73. Rice, J.R., and Sorensen, E.P., Continuing Crack-tip Deformation and Fracture for Plane-Strain Crack Growth in Elastic-Plastic Solids, Journal of Mechanics and Physics of Solids, Vol.26, pp. 163-186 (1978).

74. Kachanov, L.M., Foundations of the Theory of Plasticity, North-Holland, Amsterdam (1971).

75. Goodier, J.N., Slow Viscous Flow and Plastic Deformation, Philosophical Magazine, Vol. 22, p. 678 (1936).

76. Mott, N.F., Fracture in Metals, Journal of the Iron and Steel Institute, Vol. 183, pp. 233 (1956).

77. Stroh, A.N. , A Theory of the Fracture of Metals, Advances in Physics, Vol. 6, pp. 418-465 (1957).

78. Smith, R.A., A Simplified Method of Predicting the Rates of Growth of Cracks initiated at Notches, Fracture Mechanics in Engineering Practice, ed. by P. Stanley, Allied Science Publishers Ltd., London (1977).

79. Orowan, E., Fracture and Strength of Solids, Reports on Progress of Physics, Vol. 12, pp.185 (1949).

80. Singh, N., and Bandyopadhyay, S.N., Stability of Void Growth in an Incompressible Solid, Abstracts of Papers for presentation at Semi-annual Paper Meeting, Institution of Engineers (India), held at Jamshedpur, July, (1979).

81. Perra, M. and Finnie, I., Void Growth and Localization of Shear in Plane Strain Tension, FRACTURE 1977, Vol.II, pp. 415, ICF 4, ed. by D.M.R. Taplin, Univ. of Waterloo Press, Canada, (1977).

82. Singh, N. and Bandyopadhyay, S.N., Stability of Void Growth in an Incompressible Solid Under Uniaxial Tension and Shear, Engg. Fracture Mechanics, pp.635, Vol.11, No. 4, (1979).

83. McClintock, F.A., A Criterion for Ductile Fracture by the Growth of Holes, Journal of Applied Mechanics, Vol. 35, Trans. A.S.M.E., Ser. E, (1968).

84. Berg, C.A., Plastic Dilatation and Void Interaction, Inelastic Behaviour of Solids, M.F. Kanninen et al. (eds.), McGraw-Hill, New York, pp. 171-210 (1970).

85. Nagpal, V., McClintock, F.A., Berg, C.A., and Subudhi, M., Traction-displacement Boundary Conditions for Plastic Fracture by Hole-Growth, Foundations of Plasticity, International Symposium held at Warsaw, Ed. by A. Sawczuk, Noordhoff, Leyden pp. 365, (1972).

86. Brown, L.M., and Embury, J.D., The Initiation and Growth of Voids at Second Phase Particles, The Microstructure and Design of Alloys, Proc. of the Third International Conference on the Strength of Metals and Alloys, Cambridge, Paper 33, pp. 164-169, (1973).

87. Bluhm, J.I., and Morrissey, R.J., Fracture in a Tensile Specimen, Proc. of the First International Conference on Fracture, Sendai, Japanese Society for Strength and Fracture of Materials, Vol.3, pp. 1739-1780 (1966).

88. Eshelby, J.D., Scope and Limitations of the Continuum Approach, Proc. of the Symposium on Internal Stresses and Fatigue in Metals, Ed. by G.M. Rassweiler and W.L. Grube,Elsvier Publishing Co., Amsterdam, pp. 51-58, (1959).

89. Cherepanov, G.P., Mechanics of Brittle Fracture, (In Russian), Gos. Izdat, Moscow (1974).

90. Cook, T.S., Rau, C.A., and Smith, E., The Modelling of Flow Concentration in Two-Phase Materials, Jl. of Engineering Materials and Technology, Vol. 98, Ser. H, Trans. A.S.M.E., pp. 180-189, April (1976).

91. Bilby, B.A., Plenary Session Lecture at ICF4, Fourth International Conference on Fracture, FRACTURE-1977, Vol. IV, ed. by D.M.R. Taplin, Univ. of Waterloo Press, Canada (1977).

92. Winnie, D.H., and Wundt, B.M., Application of Griffith-Irwin Theory of Crack Propagation to Bursting Behaviour of Discs Including Analytical and Experimental Studies, Trans. of the A.S.M.E., Vol. 80, pp. 1643-1658 (1958).

93. Hinkleypoint, A-Report, Proc. of the Institution of Mechanical Engineers (London), Vol. 186, pp.341 (1972).

94. Isida, M., and Nisitani, H., Preprint at Lecture Meeting of Japan Society of Mechanical Engineers, No. 212, pp. 131 (1969).

95. Yokobori, T.A., Kamei and Konosu, S., The Stress Intensity Factors for an Elliptic Notch with Two Collinear Cracks at its Tips, Report of Research Institute of Strength and Fracture of Materials, Tohoku University, Vol. 7, No.2, pp.57 (1971).

96. Rooke, D.P., and Cartwright, D.J., Compendium of Stress Intensity Factor, Her Majesty's Stationary Office, High Holborn, London (1976).

97. Smith, R.A., and Miller, K.J., Prediction of Fatigue Regimes in Notched Components, International Journal of Mechanical Science, Vol. 20, pp. 201-206 (1978).

98. Broek, D., The Propagation of Fatigue Cracks Emanating from Holes, National Aerospace Laboratory, Report NLR TR 72134 U, Amsterdam.

99. Broek, D., Elementary Engineering Fracture Mechanics, Noordhoff Publishers, Holland (1974).

100. Bowie, O.L., and Neal, D.M., The Effective Crack Length of an Edge Slot in a Semi-Infinite Sheet Under Tension, Int. J. of Fracture Mechanics, pp.111, Vol. 3, (1967).

101. Kutter, H.K., International Journal of Fracture Mechanics, Vol. 6, pp. 233, (1970).

102. Sumpter, J.D.J., and Turner, C.E., Proc. of the Second International Conference on Pressure Vessel Technology, San Antonio, ASME, Vol.2, pp.1095, (1973).

103. Wells, A.A., and Post, D., The Dynamic Stress Distribution Surrounding a Running Crack, Proc. of the Soc. of Experimental Stress Analysis, Vol.16, No.1, pp.69, (1958).

104. Pratt, P.L., and Stock, T.A., The Distribution of Stress About a Running Crack, Proc. of the Royal Soc.of London, Ser.A., Vol. 285, pp. 73, (1965).

105. Kobayashi, A.S., Harris, D.O., and Engstrom, W.L., Transient Analysis in Fracturing Magnesium Plate, Proc. of the Soc. of Experimental Stress Analysis, Vol. 24, No.2, pp. 434 (1967).

106. Dixon, J.R., and Visser, W., The Elastic-Plastic Strain Distribution, Symposium on Photoelasticity (1961), Ed. by M.M. Frocht, Pergamon Press (1963).

107. Gerberich, W.W., Plastic Strains and Energy Density in Cracked Plates, Experimental Mechanics, Vol. 4, No. 11, pp. 335 (1964).

108. Kobayashi, A.S., Experimental Techniques in Fracture Mechanics, SESA Monograph No.1, Iowa State Univ. Press (1973).

109. Theocaris, P.S., Local Yielding Around a Crack Tip in Plexiglass, Journal of Applied Mechanics, Trans. ASME, Ser. E., Vol. 37, pp. 409-415, June, (1970).

110. Theocaris, P.S., and Gdoutos, E.E., A Photoelastic Determination of K_I Stress Intensity Factors, Engineering Fracture Mechanics, Vol. 7, pp. 331-339, (1975).

111. Vitvitskii, P.M., Panasyuk, V.V., and Yarema, S. Ya., Plastic Deformation Around Crack and Fracture Criteria, A Review Article, Engineering Fracture Mechanics, Vol. 7, pp. 305 (1975).

112. Irwin, G.R., A Discussion on the Paper, The Dynamic Stress Distribution Surrounding A Running Crack - A Photoelastic Analysis - by Wells and Post, Proc. of the Soc. of Experimental Stress Analysis, Vol. 16, No.1, pp. 93-96 (1958).

113. Raju, K.N., Plastic Energy Dissipation Rate for Stable Crack Growth on a Plate of Finite Thickness Under Biaxial Loading, International Conf. on Fracture Mechanics in Engineering Application, held in Bangalore March, (1979).

114. Dally, J.W. and Riley, W.F., Experimental Stress Analysis, 2nd Edn., McGraw-Hill Book Co. N.Y., (1978).

115. McClintock, F.A., Plasticity Aspects of Fracture, Fracture, Vol.3, H. Liebowitz, ed., Academic Press, N.Y., pp. 24-225 (1971).

116. Rice, J.R., and Rosengren, G.F., Plane Strain Deformation Near a Crack Tip in a Power Law Hardening Materials, Journal of Mechanics and Physics of Solids, Vol. 16, pp. 1-12, (1968).

117. Rice, J.R. and Hutchinson, J.W., Discussion Session-On Elastic-Plastic Fracture Mechanisms at ICF4, Fourth International Conference on Fracture, held at the Univ. of Waterloo, June, (1977).

118. Koning, DE., A.U., A Contribution to the Analysis of Quasi-Static Crack Growth in Sheet Materials, Vol.3, pp. 25, ICF4, Fracture 1977, ed. by D.M.R. Taplin, Univ. of Waterloo Press, (1977).

119. Anderson, H., Analysis of A Model For Void Growth And Coalescence Ahead of A Moving Crack Tip, Journal of Mechanics and Physics of Solids, Vol. 25, pp.217-233 (1977).

120. Ewing, D.J.F., and Griffiths, J.R., The Applicability of Slip-line Field Theory to Contained Elastic-Plastic Flow Around a Notch, Journal of Mechanics and Physics of Solids, Vol.19, pp. 389, (1971).

121. D.J.F. Ewing and C.E. Richards, The Yield Point Loads of Singly-Notched Pin-Loaded Tensile Strips, Jl. of Mechanics and Physics of Solids, Vol.22, pp. 27, (1974).

122. Hill, R., and Hutchinson, J.W., Bifurcation Phenomena in the Plane Tension Test, J. of Mechanics and Physics Solids, Vol.23, pp. 239, (1975).

123. Thomason, P.F., Plane Stress Slip-line Fields For Crack-Tip Plastic Zones in Thin-sheet Materials, ICFMEA, held in Bangalore, India, March (1979), to be published by Noordhoff, Holland, ed. by G.C. Sih and S.R. Valluri.

124. Kfouri, A.P., and Miller, K.J., Proc. of the Institutions of Mechanical Engineers (London), Vol. 190, pp. 571, (1976).

125. Green, G., and Knott, J.F., The Initiation and Propagation of Ductile Fracture in Low Strength Steels, Journal of Engineering Materials and Technology, Trans. ASME, Vol. 98, Ser. H, pp. 37-46 (1976).

126. Rice, J.R., and Tracey, D.M., Computational Fracture Mechanics, Numerical and Computer Methods in Structural Mechanics, eds Fenves, S.J. et al., Academic Press, N.Y., pp. 585, (1973).

127. Hahn, G.T., Kanninen, M.F., and Rosenfield, A.R., Ductile Crack Extension and Propagation in Steel Foil, FRACTURE 1969, pp. 58, ed. by P.L. Pratt, Chapman and Hall Ltd., London, (1969).

128. Paris, P.C., Tada, H., Z ahoor, A., and Ernst, H., A Treatment on the Subject of Tearing Instability, U.S. Nuclear Regularity Commission Report NUREG-0311, Aug. (1977).

129. Krafft, J.M., Sullivan, A.M., and Boyle, R.W., Effects of Dimensions on Fast Fracture Instability of Notched Sheets, Proc. on the Symposium on Crack Propagation, Cranfield, pp. 8, (1961).

130. Boit, M.A., Mechanics of Incremental Deformations, John Wiley, New York (1965).

131. Hull, D. and Cottrell, A.H., Extrusion and intrusion by cyclic slip in copper, A discussion on work hardening and fatigue in metals, Proceedings of the Royal Society of London, Ser. A., Vol. 242, pp. 211, (1957).

132. Cottrell, A.H., Mechanics of Fracture in Large Structures, A discussion on Damage and Failure Mechanisms of Heavy Section Steels, Proceedings of the Royal Society of London, Ser. A., Vol.285, pp.10, (1965).

133. Francois, D., Micromechanisms of Slow Stable Crack Growth, International Conference on Fracture Mechanics in Engineering Applications, held in Bangalore, March (1979).

134. McClintock, F.A., On the Mechanics of Fracture From Inclusions, Ductility, American Society For Metals, Metals Park, Ohio, pp. 255-277 (1968).

135. Rice J.R., and Tracey, D.M., On the ductile enlargement of voids in triaxial stress fields, Journal of the Mechanics and Physics of Solids, Vol. 17, pp. 201, (1969).

136. Brown, L.M. , The Initiation and Growth of Voids by Plastic Flow Near Second Phase Particles, Research Report, Cavendish Laboratory, Cambridge, England.

137. Nix, W.D., and Goods, S.H., 'The Coalescence of Large Grain Boundary Cavities in Silver During Tension Creep, Acta Metallurgica, Vol. 26, pp. 753, (1978).

138. Jaeger, J.C. , 'Elasticity, Fracture and Flow ' 3rd Edn. , Mathuen Publisher, London (1969).

139. Eshelby, J.D., Comments on the paper by N. Singh and S.N. Bandyopadhyay - Unstable Void Growth in an Incompressible Solid, Private Communication, (1979).

140. McClintock, F.A., Discussion on Perra-Finnie's paper on unstable plane strain void growth ; at ICF4, Waterloo, Canada, June (1977) , (FRACTURE-1977, ed. by D.M.R. Taplin, Univ. of Waterloo Press).

141. Raj, R. and Ashbey, M.F., Intergranular Fracture at Elevated Temperature, Acta Metallurgica, Vol. 23, (1975).

142. Tait, R.A. and Taplin, D.M.R., 'Interaction Effects During the Growth of holes in a Superplastically Deforming Medium', Scripta Metallurgica, Vol.13, pp. 77 (1979).

143. El-Sudani, and Knott, J.F., Research Report, Department of Metallurgy, University of Cambridge (1977).

144. Bilby, B.A, Eshelby, J.D., Kundu, A.K., and Kolbuszewsky, M.I., The change of shape of a viscous ellipsoidal region embedded in slowly deformed matrix having a different viscosity, Techtonophysics, Vol. 35, p. 408 (1976).

145. Rudnicki, J.W. and Rice, J.R., Conditions for the localization of deformation in pressure sensitive dilatant materials, Jl. of Mechanics and Physics of Solids, Vol. 23, pp. 371, (1975).

146. Asaro, R.J. and Rice, J.R., Strain Localization in Ductile single crystals, Jl. of Mechanics and Physics of Solids, Vol. 25, pp. 309 (1977).

147. Yamamoto, H., Conditions for Shear Localization in the ductile Fracture of void containing materials, International Journal of Fracture, Vol.14, No. 4, pp. 347 (1978).

148. Argon, A.S., Formation of Cavities From Non-deformable Second-Phase Particles in Low Temperature Ductile Fracture, J. of Materials and Technology, Trans. A.S.M.E., Ser. H., pp. 60, January (1976).

149. Backofen, W.A., Deformation Processing, Addison-Wesley, Reading, Massachusetts (1972).

150. Blackburn, M.J., and Williams, J.C., Strength, Deformation Modes, and Fracture in Titanium-Aluminium Alloys, Transactions of the American Society for Metals, Vol. 62, pp. 398-409 (1969).

151. Cottrell, A.H. and Stokes, R.J., Effects of Temperature on the Plastic Properties of Aluminium Crystals, Proceedings of the Royal Society of London, Ser. A, Vol. 233, p. 17, (1955).

152. Beevers, C.J., and Honeycombe, R.W.K., Ductile Fracture of Single Crystals, Fracture, B.L. Averbach, et al.,eds. Wiley, New York, pp. 474-497 (1959).

153. Price, R.J., and Kelly, A., Deformation of Age-Hardened Aluminium Alloy Crystals-II, Fracture, Acta Metallurgica, Vol. 12, No. 9, pp. 979-992 (1964).

154. Dubey, R.N. and Ariaratnam, S.T., Some cases of Bifurcation in Elastic-Plastic Solids in Plane Strain, Quart. of Applied Mathematics, XXVII, p.349, (1969).

155. Sih, G.C., Elastic-Plastic Fracture and Mechanisms of Hole Growth during Ductile Metals, Private Communications, during ICMEA, Bangalore, 1979.

156. Thomason, P.F., A Theory of Ductile Fracture by Internal Necking of Cavities, Journal of the Institute of Metals, Vol. 96, p. 360 (1968).

157. Hancock, J.W. and MacKenzie, A.C., On the mechanism of ductile failure in high strength steels subjected to multiaxial stress-states, J. Mechanics and Physics of Solids, Vol. 24, pp. 147, (1976).

158. Bridgman, P.W., Studies in Large Plastic Flow and Fracture, Cambridge, Mass., Harvard University Press (1964).

159. Norris, D.M., Moran, Jr., B., Scudder, J.K., and Quinones, D.F., A Computer Simulation of the Tension Test, Journal of Mechanics and Physics of Solids, Vol. 26, No. 1, pp. 1-19 (1978).

160. Rogers, H.C., The Effect of Material Variables on Ductility, American Society for Metals, Metals Park, Ohio, pp. 31-61 (1968).

161. Eshelby, J.D., The determination of the elastic field of an ellipsoidal inclusion, and related problems, Proceedings of the Royal Society of London, Ser. A., Vol. 241, pp. 376, (1957).

162. Eshelby, J.D., The Elastic Field outside An Ellipsoidal Inclusion, Proceedings of the Royal Society of London, Ser. A., Vol. 252, pp. 561, (1959).

163. Tranter, C.J., The use of the Mellin Transform in finding the stress distribution in an infinite wedge, Quart. J. Mech. and Applied Maths., Vol.I, pp. 125, (1948).

164. Green, A.E., and Zerna, W., Theoretical Elasticity, Clarendon Press, Oxford (1954).

165. Miyamoto, H., On the problem of Elasticity Theory for an infinite region containing two spherical cavities, Proceedings of the 5th Japan National Congress of Applied Mechanics, pp. 125 (1955).

166. Hashin, Z., The moduli of an elastic solid containing spherical particles of another elastic material, IUTAM, Non-Homogeneity in Elasticity and Plasticity, Symposium, Warsaw, Ed. by W. Olszak, pp. 463 (1959).

167. Chen, H.S., and Acrivos, A., The Solution of the Equations of Linear Elasticity for an Infinite Region Containing two Spherical Inclusions, Int. J. of Solids and Structures, Vol.14, pp. 331, (1978).

168. Rice, J.R., and Drucker, D.C., Energy Changes in Stressed Bodies Due to Void and Crack Growth, International Journal of Fracture Mechanics, Vol. 3, No. 1 (1967).

169. Owen, D.R., Nayak, G.C., Kfouri, A.P., and Griffiths, J.R., Stresses in a Partly Yielded Notched Bar - An Assessment of Three Alternative Programmes, International Journal for Numerical Methods in Engineering, Vol. 6, pp. 63-73 (1973).

170. Chell, G. G., Milne, I., and Kirby, J.H., Practical Fracture Mechanics in the Post-Yielded Regime, Metals Technology, Vol. 2, Pt. 12, pp. 549, Dec.(1975).

171. Chell, G.G., Semi-empirical Solutions for a Crack in a Body of Arbitrary, Shape with Yielding Ahead of Its Tip, Materials Science and Engineering , Vol. 17, No. 2, pp. 227, Feb. (1975).

172. Heald, P.T., Spink, G.M., and Worthington, P.J., Post- Yield Fracture Mechanics, Materials Science and Engineering, Vol. 10, pp. 129 (1972).

173. Tetelman, A.S., and McEvily, A.J., Jr., Fracture of Structural Materials, John Wiley Publisher, New York (1967).

174. Swedlow, J.L., et.al. A Case of Elasto-plastic Flow Using a new Special Element, Plenery Session Lecture at ICF4, Waterloo, FRACTURE 1977, Vol.I, pp. 117, ed. by D.M.R. Taplin, University of Waterloo Press.

175. Garg, K.G., Plastic Deformation Ahead of Charpy - Notch and Sharp Crack, Master of Technology Thesis, I.I.T. Kanpur (India), (1974), (Under the Supervision of Dr. S.N. Bandyopadhyay).

176. Mubeen, A., Fracture of A Beam When A Small Fatigue Crack Exists Ahead of A Notch, Doctor of Philosophy Thesis, I.I.T. Kanpur (India), (1977), (Under the Supervision of Dr. S.N. Bandyopadhyay).

177. Mubeen, A., and Bandyopadhyay, S.N. , Fracture Strength of a Notched Beam When a Small Fatigue Crack Emanates From The Notch Root, Proceedings of the Fourth International Conference on Fracture. Fracture edited by D.M.R. Taplin, Vol.3, Waterloo, Canada, pp. 741-749 (1977).

178. Singh, N., Ph.D. thesis, Department of Metallurgy, I.I.T. Kanpur (India), (1979), (Under the joint Supervisions of Dr. S.N. Bandyopadhyay and Dr.G.S. Murty).

179. Timoshenko, S.P., and Goodier, J.N., Theory of Elasticity, McGraw-Hill Kogakusha Ltd. (1970).

180. Love, A.E.H., A Treatise on the Mathematical Theory of Elasticity, Cambridge University Press (1952).

181. Maunsell, F.G., Stresses in a Notch Plate Under Tension, Philosophical Magazines, Vol. 21, pp.765 (1936).

182. Ling, Chi , Bi , On the Stresses in a Notched Plate Under Tension, Journal of Mathematics and Physics, Vol. 26, pp. 284 (1947).

183. Mitchell, L.H., Stress Concentration at Semi-Circular Notch, J. of Applied Mechanics, Vol. 32, pp. 938, Trans. ASME, Ser. E., (1965).

184. Bowie, O.L., Analysis of Edge Notches in a Semi-infinite Region, Journal of Mathematics and Physics, Vol. 45, pp. 356 (1966).

185. Buchwald, V.T., and Doran, H. E., Eigen Functions of Plane Elastostatics etc, Proceedings of the Royal Society of London, Ser. A., Vol. 284, p. 69, (1965).

186. Whittaker, E.T. and Watson, G.N., A Course on Modern Analysis, Cambridge University Press (1952).

187. Eshelby, J.D., Elastic Inclusions and Inhomogeneities, Progress in Solid Mechanics, Vol.2, edited by I.N. Sneddon and R. Hill, North-Holland, pp. 89-139 (1961).

188. Band, B. , Introduction to Mathematical Physics, Van Nostrand, Princeton, N.J., U.S.A., pp. 191-203 (1959).

189. Kellogg, O.D., Foundations of Potential Theory, Springer-Verlag, Berlin, pp. 195 (1967).

190. Rooke, D.P. and Tweed, J., The distribution of Stress Near the tip of a Radial Crack at the edge of a Circular hole, International Journal of Engineering Science, Vol.11, pp. 1185 (1973).

191. Landau, L.D. and Lifshitz, E. M., The Classical Theory of Fields, Pergamon Press, pp. 97 (1971).

192. Carnahan, B., Luther, H.A., and Wilkes, J.O., Applied Numerical Methods, John Wiley and Sons, Inc., New York, (1969).

193. Noble, B., Methods based on the Weiner-Hopf Technique for the solution of partial differential equations, Pergamon Press (1958).

194. Burke, M.A. and Nix, W.D., A Numerical Analysis of Void Growth in Tension Creep, Int. J. of Solids and Structures, No.1, Vol.15, pp.55 (1979).

195. Deysarker, H.K. and Bandyopadhyay, S. N., A Comparison Between Critical Strain-Energy-Density and Maximum Shear Strain Localization Criteria for Fracture in an Elastic-Plastic Solid, International Symposium on the Energy Density Criterion for Fracture, Paper accepted for publication in the Proceedings of the symposium, Ed. by G.C. Sih, Sijthoff and Noordhoff, Holland.

196. Dey Sarker, H.K., and Bandyopadhyay, S.N., Criteria for Fracture of a Crack-Like-Notch in Brittle and Ductile Materials, Paper submitted for publication, ICF5, Fifth International Conference on Fracture, To be held in Cannes, France, March (1981).

197. Dey Sarker, H.K., and Bandyopadhyay, S.N., Ductile Fracture due to shear Localization between two Spheroidal Holes, Paper submitted for publication, ICF5, Fifth International Conference on Fracture, To be held in Cannes, France, March (1981).

198. Dey Sarker, H.K., and Bandyopadhyay, S.N., Stresses and Misfit at the root of a Crack-Like-Notch, (Paper submitted for publication) in International Journal of Fracture.

199. Dey Sarker, H.K., and Bandyopadhyay, S.N., Interaction Strain Field and Ligament Instability between two Prolate Spheroidal Holes under Uniaxial Tension, (Paper submitted for publication) in International Journal of Fracture.

200. Dey Sarker, H.K., and Bandyopadhyay, S.N., Application of Finite Mellin Transform to Notch Problems, (Paper submitted for Publication) in International Journal of Fracture.

APPENDIX A

APPLICATION OF FINITE MELLIN TRANSFORM IN PLANE PROBLEMS OF ELASTICITY

Mellin transform in the infinite range, and particularly its advantage for wedge region on plane elasticity problems are well known. The definition of finite Mellin transform and its application to the various fields of engineering have also become popular in recent years [14, 15, 190]. By making a finite Mellin transform, all the boundary conditions for a semi-circular edge notch cut-out in a semi-infinite plate or in a notched wedge can be resolved more easily. We define our finite Mellin transform as :

Let, $\bar{f}(s,\theta) = \int_0^\infty f(r,\theta)\, r^{s-1}\, dr$, for $a < r < \infty$ region only, (A.1)

and $I_n = \int_a^\infty r^n\, r^{s-1} \frac{\partial^n f}{\partial r^n}\, dr$, for the entire $a \leq r \leq \infty$ region with $n = 1,2,3,4,\ldots$ (A.2)

Then, we have, for $n = 1$

$$I_1 = \int_a^\infty r^s \frac{\partial f}{\partial r}\, dr = \Big[r^s f\Big]_a^\infty - s \int_0^\infty f\, r^{s-1}\, dr \quad \text{(for } r > a\text{)}$$

$$= - a^s (f)_a - s\,\bar{f}$$

Proceeding in the same manner, for $n = 2$ one gets,

$$I_2 = - a^{s+1} (\partial f/\partial r)_a + (s+1)\, a^s (f)_a + s(s+1)\,\bar{f}$$

Similarly for I_3, I_4 and so on.

Thus, the function f is actually transformed in the region $a < r < \infty$, and at $r = a$, the value of the function plus its derivatives are written separately.

The biharmonic equation in two-dimensional plane problems of elasticity, in r, θ polar coordinate is,

$$\left(\frac{\partial^2}{\partial r^2} + \frac{1}{r} \frac{\partial}{\partial r} + \frac{1}{r^2} \frac{\partial^2}{\partial \theta^2} \right) \left(\frac{\partial^2 f}{\partial r^2} + \frac{1}{r} \frac{\partial f}{\partial r} + \frac{1}{r^2} \frac{\partial^2 f}{\partial \theta^2} \right) = 0$$

or,

$$r^4 \frac{\partial^4 f}{\partial r^4} + 2r^3 \frac{\partial^3 f}{2r^3} - r^2 \frac{\partial^2 f}{\partial r^2} + r \frac{\partial f}{\partial r} - 2r \frac{\partial^3 f}{\partial r \partial \theta^2}$$

$$+ 2r^2 \frac{\partial^4 f}{\partial r^2 \partial \theta^2} + 4 \frac{\partial^2 f}{\partial \theta^2} + \frac{\partial^4 f}{\partial \theta^4} = 0 \qquad (A.3)$$

where, $f(r,\theta)$ is the Airy stress function, r and θ being the usual polar coordinates shown in Fig. 3.1(a). Let "a" be the radius of the semi-circular cut-out rim with 0 as its origin on the vertex edge of the plate. Multiplying Eqn.(A.3) by $r^{s-1}\,dr$ and integrating in the range of $a \leq r < \infty$, one gets,

$$\frac{d^4\bar{f}}{d\theta^4} + \frac{d^2}{d\theta^2}(4 - 2I_1 + 2I_2) + (I_4 + 2I_3 - I_2 + I_1) = 0$$

or,

$$\begin{aligned}
\frac{d^4\bar{f}}{d\theta^4} + \frac{d^2}{d\theta^2}\Big[& 4\bar{f} + 2a^s(f)_a + 2s\bar{f} - 2a^{s+1}(\partial f/\partial r)_a \\
& + 2(s+1)\, a^s(f)_a + 2s(s+1)\,\bar{f}\Big] \\
+ \Big[& - a^{s+3}(\partial^3 f/\partial r^3)_a + (s+3)\, a^{s+2}(\partial^2 f/\partial r^2)_a \\
& - (s+3)(s+2)\, a^{s+1}(\partial f/\partial r)_a + (s+3)(s+2)(s+1)a^s(f)_a \\
& + (s+3)(s+2)(s+1)s\bar{f} - 2a^{s+2}(\partial^2 f/\partial r^2)_a \\
& + 2a^{s+1}(s+2)\,(\partial f/\partial r)_a - 2(s+2)(s+1)\, a^s(f)_a \\
& - 2(s+2)(s+1)s\,\bar{f} + a^{s+1}(\partial f/\partial r)_a - (s+1)\, a^s(f)_a \\
& - (s+1)\, s\bar{f} - a^s(f)_a - s\bar{f}\Big] = 0 \qquad (A.4)
\end{aligned}$$

Making an assumption that the nature of our Airy stress function $f(r,\theta)$ is similar to χ Airy stress function chosen by Green and Zerna [164] for a semi-circular edge notch, having property on the traction-free semi-circular rim boundary $r = a$, as, $(\chi)_a = (\partial\chi/\partial r)_a = 0$, but tangential stress $(\partial^2\chi/\partial r^2)_{r=a}$ exists on the rim. Thus, for a traction-free semi-circular type edge notched plate, following Green and Zerna, we make an assumption that the nature of the unknown Airy stress function is,

$$(f)_a = (\partial f/\partial r)_a = (\partial^3 f/\partial r^3)_a = 0 \qquad (A.5)$$

Hence, by making finite Mellin transform for traction-free semi-circular cut-out edge notched plate, the transformed form of the biharmonic equation reduces to

$$\frac{d^4\bar{f}}{d\theta^4} + [(s+2)^2 + s^2]\frac{\partial^2\bar{f}}{\partial\theta^2} + s^2(s+2)^2\bar{f} + (s+1)\,a^{s+2}(\sigma_{\theta\theta})_a = 0 \qquad (A.6)$$

It is interesting to note that the solution of this differential equation has a particular integral in terms of an unknown rim stress $(\sigma_{\phi\phi})_a$ plus a well known complementary function [163] .

Therefore, the solution of the differential equation gives the transformed Airy stress function as

$$\begin{aligned}\bar{f}(s,\theta) = {} & A(s)\cos s\theta + B(s)\sin s\theta + C(s)\cos(s+2)\theta + \\ & + D(s)\sin(s+2)\theta + \frac{a^{s+2}}{4}\Big[\frac{1}{s}\cos s\theta \int(\sigma_{\theta\theta})_a \sin s\theta\, d\theta \\ & - \frac{1}{s}\sin s\theta \int(\sigma_{\theta\theta})_a \cos s\theta\, d\theta \\ & - \frac{\cos(s+2)\theta}{s+2}\int(\sigma_{\theta\theta})_a \sin(s+2)\theta\, d\theta \\ & + \frac{\sin(s+2)\theta}{s+2}\int(\sigma_{\theta\theta})_a \cos(s+2)\theta\, d\theta\Big]\end{aligned} \qquad (A.7)$$

Integrating by parts, the particular integral of the transformed Airy stress function can be written in an asymptotic form and is,

$$\bar{f}(s,\theta) = \Big[A(s)\cos s\theta + B(s)\sin s\theta + C(s)\cos(s+2)\theta + D(s)\sin(s+2)\theta \Big] + \Big[\sigma_{\theta\theta_a}/(s+2)^2 - \frac{\sigma_{\theta\theta_a}^{ii}}{(s+2)^4} + \frac{\sigma_{\theta\theta_a}^{iv}}{(s+2)^6} - \frac{\sigma_{\theta\theta_a}^{vi}}{(s+2)^8} + \ldots - \frac{\sigma_{\theta\theta_a}}{s^2} + \frac{\sigma_{\theta\theta_a}^{ii}}{s^4} - \frac{\sigma_{\theta\theta_a}^{iv}}{s^6} + \frac{\sigma_{\theta\theta_a}^{vi}}{s^8} \ldots \Big] \quad \ldots (A.8)$$

where, $\sigma_{\theta\theta_a}$ = tangential stress on the semi-circular rim $r = a$, and $\sigma_{\theta\theta_a}^{n} = d^n\sigma_{\theta\theta_a}/d\theta^n$.

This solution will be useful for a wedge with radiused cut-out at the vertex. So the included angle could be $0 < \theta < 2\pi$. It is clear that the solution has two distinct parts: - the first part is the usual field solution, and the second part gives an azimuthal solution for the core stress field very close to the rim $r = a$. If there is no cut-out at the vertex of the wedge plate, then the second part does not exist and our result agrees with usual solutions. Selecting a suitable strip in the complex plane, $\mu_o < \gamma < \mu_1$, for which the function is analytic, then from the inversion formula of Mellin transform [14, 16, 38], Airy stress function becomes,

$$f(r,\theta) = \frac{1}{2\pi i} \int_{\gamma - i\infty}^{\gamma + i\infty} \{ [A(s) \cos s\theta + B(s) \sin s\theta + C(s)\cos(s+2)\theta + D(s)\sin(s+2)\theta]$$

$$+ \left[\frac{\sigma_{\theta\theta_a}}{(s+2)^2} - \frac{\sigma_{\theta\theta_a}^{ii}}{(s+2)^4} + \frac{\sigma_{\theta\theta_a}^{iv}}{(s+2)^6} - \frac{\sigma_{\theta\theta_a}^{vi}}{(s+2)^8} + \dots \right.$$

$$\left. - \frac{\sigma_{\theta\theta_a}}{s^2} + \frac{\sigma_{\theta\theta_a}^{ii}}{s^4} - \frac{\sigma_{\theta\theta_a}^{iv}}{s^6} + \frac{\sigma_{\theta\theta_a}^{vi}}{s^8} \dots \right] \} r^{-s} ds$$

...(A.9)

Applying Doetsch's theorem given by Oberhettinger [18] on the second part and separating the azimuthal solution, one gets the Airy stress function as,

$$f(r,\theta) = \chi_f(r,\theta) + \chi_c(r,\theta) \qquad (A.10)$$

where, $\chi_f(r,\theta)$ = Airy stress function for the field region and χ_c = Airy stress function for the core region.

$$\chi_f(r,\theta) = \frac{1}{2\pi i} \int_{\gamma - i\infty}^{\gamma + i\infty} [A(s) \cos s\theta + B(s) \sin s\theta + C(s) \cos(s+2)\theta + D(s)\sin(s+2)\theta] r^{-s} ds$$

...(A.11)

and $\chi_{core}(r,\theta)$ = Airy stress function for core region i.e. very close to the notch rim,

$$\chi_c(r,\theta) = \frac{1}{4}(r^2 - a^2)\Big[\sigma_{\theta\theta_a}(\ln r/a) + \frac{\sigma_{\theta\theta_a}^{ii}}{3!}(\ln r/a)^3 - \frac{\sigma_{\theta\theta a}^{iv}}{5!}(\ln r/a)^5 + \ldots + \ldots (-1)^n \frac{\sigma_{\theta\theta_a}^{2n-2}}{(2n-1)!}(\ln r/a)^{2n-1} + \ldots \Big] \quad \ldots (A.12)$$

i.e. $$\chi_c(r,\theta) = -\frac{1}{4} a^2 \left(\frac{r^2}{a^2} - 1\right) \sum_{m=0,1,2,3} (-1)^m \frac{(\ln r/a)^{2m+1}}{(2m+1)!} \frac{d^{2m}\sigma_{\theta\theta_a}}{d\theta^{2m}}$$

Airy stress function $\chi_{core}(r,\theta)$ is used to determine stresses very close to the rim, and $\chi_{field}(r,\theta)$ solution will be used to find the stresses in the near and far field regions.

APPENDIX B

ELASTIC STRESSES AT THE ROOT OF A CRACK-LIKE-NOTCH

The basic formulation of the problem is given in Chapter IV. After solving Eqns. (4.11) and (4.12), one gets the following expressions for

$$\frac{F}{T} = - \frac{2w(\sin 2w\ (\pi-\alpha) + 2w \sin \alpha\ )}{(2w+1)\ \phi(\alpha,\ w)} \Big[(4w^2 - \sin^2 \pi w) L(w,\alpha)$$

$$+ (\sin 2w(\pi-\alpha) + 2w \sin \alpha) K(w,\alpha) \Big] + \frac{(4w^2 - \sin^2 \pi w)}{(2w+1)\ \phi(\alpha, w)}$$

$$a^{2w+1}_{\ \ \beta} \Big[(4w^2 - \sin^2 \pi w)\ M(w,\alpha) - (\sin 2w(\pi-\alpha)$$

$$+ 2w \sin \alpha)\ N(w,\ \alpha) \Big]$$

$$\ldots(\text{B.1})$$

$$\frac{S}{T} = \frac{4w(2w+1)(\sin 2w(\pi-\alpha) + 2w \sin \alpha)}{\phi(\alpha,\ w)} \Big[(4w^2 - \sin^2 \pi\ w) P(w,\alpha)$$

$$(\sin 2w\ (\pi-\alpha) + 2w \sin \alpha)\ Q(w,\alpha) \Big]$$

$$+ a^{2w+1} \frac{(2w+1)(4w^2 - \sin^2 \pi w)}{\phi(\alpha,\ w)} \beta \Big[(\sin 2w(\pi-\alpha) + 2w \sin \alpha)$$

$$R(w,\ \alpha) \Big] \quad (\text{B.2})$$

where β is a function of a and α. $\beta = (\sigma_{\phi\phi})_a / T$.

Therefore,

$$\frac{\sigma}{T} = \frac{1}{\pi i} \int_{\gamma - i\infty}^{\gamma + i\infty} - \frac{2w(\sin 2w(\pi-\alpha) + 2w \sin \alpha}{(2w+1)\ \phi(\alpha,\ w)}$$

$$\Big[(4w^2 - \sin^2 \pi w) L(w,\alpha) + (\sin 2w(\pi-\alpha) + 2w \sin \alpha)$$

$$K(w,\alpha) \Big] \ . \ (\rho)^{-2w-1} \ dw \ + \frac{\beta}{\pi i} \int_{\gamma - i\infty}^{\gamma + i\infty} \frac{(4w^2 - \sin^2 \pi w)}{(2w+1)\ \phi(\alpha, w)}$$

$$\Big[(4w^2 - \sin^2 \pi w)\ M(w,\alpha) - (\sin 2w(\pi-\alpha) + 2w \sin \alpha)$$

$$N(w,\alpha) \Big] \ (\rho/a)^{-2w-1} \ dw \qquad \ldots (B.3)$$

$$\frac{\tau}{T} = \frac{1}{\pi i} \int_{\gamma - i\infty}^{\gamma + i\infty} \frac{4w(2w+1)(\sin 2w(\pi-\alpha) + 2w \sin \alpha)}{\phi\ (\alpha,\ w)}$$

$$\Big[(4w^2 - \sin^2 \pi w)\ P(w,\alpha) + (\sin 2w(\pi-\alpha) + 2w \sin\alpha)$$

$$Q(w,\alpha) \Big] \ . \ (\rho)^{-2w-1} \ dw \ + \frac{\beta}{\pi i} \int_{\gamma - i\infty}^{\gamma + i\infty} \frac{(2w+1)}{\phi(\alpha, w)}$$

$$. (4w^2 - \sin^2 \pi w) \Big[\sin 2w(\pi-\alpha) + 2w \sin \alpha \Big] R(w,\alpha)$$

$$. \ (\rho/a)^{-2w-1} \ dw \qquad (B.4)$$

The roots of $\phi(z) = 0$, **were** investigated in the complex plane. It is interesting to note that for $\alpha \leq 2^\circ$, the equation has real roots first. In the range of

$\frac{1}{2} < w_n < 10$ for $\alpha \leq 1^{\circ}$ the real roots of $\phi(z) = 0$ are given in Table B.1. There is always a real root $\frac{1}{2} + \lambda(\alpha)$ of $\phi(z)$ equation, where $\lambda(\alpha)$ is a fixed real quantity, and $\lambda > 0$ always. So, the strip of integration is chosen in the range of $\frac{1}{2} + \epsilon < \gamma < \frac{1}{2} + \lambda - \delta$, so that the line integral is taken along $\frac{1}{2} < \gamma < \frac{1}{2} + \lambda$. The function is analytic in this strip. Furthermore, it is also noticed that along the semi-circular path the integration in the complex plane vanishes. Thus, on plane $\phi = \pi/2 - \alpha/2$ the normal and shear stresses are,

$$\sigma = \sum_{n=1,2,3} T \beta X_n . (\rho/a)^{-2w_n-1} \qquad \text{for } a < \rho < 1$$

$$= \sum_{n=1,2,3} T \beta X_n (\rho/a)^{-2w_n - 1} + \sum_{n=1,2,3..} T Y_n \rho^{-2w_n-1} \qquad \text{for } \rho \geq 1 \qquad (B.5)$$

and similarly,

$$\tau = \sum_{n=1,2,3} T \beta B_n . (\rho/a)^{-2w_n - 1} \qquad \text{for } a < \rho < 1$$

$$= \sum_{n=1,2,3} T \beta B_n (\rho/a)^{-2w_n-1} + \sum_{n=1,2,3} T A_n . \rho^{-2w_a-1} \qquad \text{for } \rho \geq 1 \qquad (B.6)$$

The coefficients A_n, B_n, X_n and Y_n are determined from the residue theorem, for $n = 1,2,3,4,\ldots$.

TABLE B.1 First Few Real Roots of $\phi(z) = 0$; $\mathrm{Re}(z) > \frac{1}{2}$
For Three Different Flank Angles. $\alpha \leq 1^{\circ}$

Sl.No.	Roots for flank opening angles, α in degrees		
	0.2°	0.6°	1.0°
1	0.501	0.503	0.505
2	0.502	0.505	0.508
3	0.999	0.999	0.999
4	1.001	1.003	1.005
5	1.503	1.506	1.511
6	1.503	1.510	1.516
7	1.999	1.999	1.999
8	2.002	2.006	2.011
9	2.503	2.509	2.516
10	2.505	2.516	2.528
11	2.999	2.999	2.999
12	3.003	3.010	3.016
13	3.504	3.512	3.521
14	3.507	3.523	3.539
15	3.999	3.999	3.999
16	4.004	4.013	4.022
17	4.505	4.515	4.526
18	4.510	4.530	4.549
19	4.999	4.999	4.999
20	5.005	5.016	5.027
21	5.506	5.519	5.531
22	5.512	5.536	5.561
23	5.999	5.999	5.999
24	6.006	6.020	6.033
25	6.507	6.522	6.537
26	6.514	6.543	6.573
27	6.999	6.999	6.999
28	7.007	7.023	7.039
29	7.508	7.525	7.542
30	7.516	7.550	7.584
31	7.999	7.999	7.999
32	8.008	8.026	8.044
33	8.509	8.528	8.548
34	8.518	8.557	8.596
35	8.999	8.999	8.999
36	9.010	9.030	9.049
37	9.510	9.532	9.553
38	9.521	9.563	9.607
39	9.999	9.999	9.998
40	10.011	10.033	10.055

The constant β is determined from the equilibrium condition of the 90°- wedge as follows :

Equating the horizontal forces along the direction of applied tension T,

$$T = \int_a^\infty \tau \, d\rho$$

$$\text{or,} \quad 1 = \frac{\beta a}{2} \sum_{n=1,2,3} \frac{B_n}{w_n} + \frac{1}{2} \sum_{n=1,2,3} \frac{A_n}{w_n}$$

$$\text{or,} \quad \beta = \frac{2}{a} \cdot \frac{1 - \frac{1}{2} \sum_{n=1,2,3,\ldots} A_n/w_n}{\sum_{n=1,2,3} B_n/w_n} \qquad \text{(B.7)}$$

For $\alpha = 1^\circ$ and $a = 0.01$, β comes out to be 595.00 approximately.

The functions used in the above expressions are,

$$L(w,\alpha) = 2 \left[\cos \pi w \, \{\cos 2w(\pi-\alpha) - \cos\alpha\} - \sin \pi w \, \{2w(3+4w^2) \sin\alpha + (12w^2+1) \sin 2w(\pi-\alpha)\} \right]$$

$$K(w,\alpha) = 4w \sin\pi w \left[(3+4w^2) \sin^2\pi w - (12w^2+1) \right] - \sin 2\pi w \cos \pi w \, .$$

$$M(w,\alpha) = 2(\cos^2 2w(\pi-\alpha) - \cos^2\alpha) + (\sin 2w(\pi-\alpha) - 2w \sin\alpha) \{2w(4w^2+3) \sin\alpha + (12w^2+1) \sin 2w(\pi-\alpha)\}$$

$$N(w,\alpha) = \sin 2\pi w \{\cos 2w(\pi-\alpha) + \cos\alpha\} + 2w(\sin 2w(\pi-\alpha) - 2w \sin\alpha) \{(3+4w^2) \sin^2\pi w - (12w^2+1)\}$$

$$P(w, \alpha) = 2 \sin \pi w \, (\cos 2w \, (\pi-\alpha) + \cos \alpha) + \cos \pi w (\sin 2w \, (\pi-\alpha) - 2 \, w \sin \alpha)$$

$$Q(w,\alpha) = \sin 2\pi \, w \sin \pi w + \cos \pi w \, (4w^2 + \sin^2 \pi \, w)$$

$$R(w, \alpha) = \sin 2\pi w \, (\sin 2w(\pi-\alpha) - 2w \sin \alpha) - 2(4w^2+\sin^2 \pi w) (\cos 2w \, (\pi-\alpha) + \cos \alpha)$$

$$I(w, \phi, \alpha) = (2w+1) \sin (2w+1)(\pi/2 - \alpha/2) \cos (2w-1)\phi - (2w-1) \sin (2w-1) (\pi/2 - \alpha/2) \cos(2w+1) \phi$$

$$J(w,\phi,\alpha) = \cos (2w+1) (\pi/2 - \alpha/2) \cos (2w-1)\phi - \cos (2w-1) (\pi/2 - \alpha/2) \cos (2w+1) \phi$$

when $\phi = \pi/2 - \alpha/2$, $J = 0$, and $I = \sin 2w \, (\pi - \alpha) + 2w \sin \alpha$

$$\begin{aligned}
\phi(\alpha,w) = {} & \Big[(4w^2+ \sin^2 \pi w) (\sin 2w(\pi-\alpha) + 2w \sin \alpha) \\
& + (4w^2- \sin^2 \pi w) (\sin 2w \, (\pi-\alpha) - 2w \sin \alpha) \Big] \cdot \\
& \Big[2w(\sin 2w(\pi-\alpha) + 2w \sin \alpha) \{(4w^2 +3) \sin^2 \pi w \\
& - (12w^2+ 1)\} - (4w^2 - \sin^2 \pi w) \{2w(4w^2 +3) \sin \alpha \\
& + (12w^2+1) \sin 2w(\pi-\alpha) \} \Big] - 4 w^2 \Big[\sin 2\pi w \\
& (\sin 2w(\pi-\alpha) + 2w \sin \alpha) + 2(4w^2- \sin^2 \pi w) \\
& (\cos 2w(\pi-\alpha) + \cos \alpha) \Big] \cdot \Big[2(4w^2- \sin^2 \pi w) \\
& (\cos 2w(\pi-\alpha) - \cos \alpha) - \sin 2\pi w \, (\sin 2w(\pi-\alpha) \\
& + 2w \sin \alpha) \Big]
\end{aligned}$$

when $1 < \rho/a < 2$, $\chi_{core}(\rho, \phi)$ Airy stress function can be used to find the stresses near the core region of a notch.

For example,

$$
\begin{aligned}
(\sigma_{\phi\phi})_{\text{core}} &= \frac{\partial^2 \chi_c}{\partial \rho^2} \\
&= \frac{1}{4}\left(1 - a^2/\rho^2\right)\Big[(\ln \rho/a)\, \sigma_{\phi\phi_a}^{ii} - \frac{(\ln \rho/a)^3}{3!}\, \sigma_{\phi\phi_a}^{iv} + \frac{(\ln \rho/a)^5}{5!}\, \sigma_{\phi\phi_a}^{vi} - \ldots\Big] \\
&\quad + \frac{1}{4}\left(1 + a^2/\rho^2\right)\Big[- \sigma_{\phi\phi_a} + \frac{(\ln \rho/a)^2}{2!}\, \sigma_{\phi\phi_a}^{ii} - \frac{(\ln \rho/a)^4}{4!}\, \sigma_{\phi\phi_a}^{iv} + \frac{(\ln \rho/a)^6}{6!}\, \sigma_{\phi\phi_a}^{vi} - \ldots\Big] \\
&\quad + \frac{1}{2}\Big[- \sigma_{\phi\phi_a} + \frac{(\ln \rho/a)^2}{2!}\, \sigma_{\phi\phi_a}^{ii} - \frac{(\ln \rho/a)^4}{4!}\, \sigma_{\phi\phi_a}^{iv} + \frac{(\ln \rho/a)^6}{6!}\, \sigma_{\phi\phi_a}^{vi} - \ldots\Big] \\
&\quad + \frac{1}{2}\Big[-(\ln \rho/a)\, \sigma_{\phi\phi_a} + \frac{(\ln \rho/a)^3}{3!}\, \sigma_{\phi\phi_a}^{ii} - \frac{(\ln \rho/a)^5}{5!}\, \sigma_{\phi\phi_a}^{iv} + \frac{(\ln \rho/a)^7}{7!}\, \sigma_{\phi\phi_a}^{vi} - \ldots\Big]
\end{aligned}
\quad \ldots\text{(B.8)}
$$

and similarly, $\sigma_{\rho\rho}$ and $\sigma_{\rho\phi}$ can easily be determined. Applying Green and Zerna's condition,

$$\chi(a, \phi) = \chi_f(a,\phi) + \chi_c(a,\phi) = 0 \qquad \text{(B.9)}$$

One determines the notch stress on the rim as,

$$(\sigma_{\phi\phi})_a/T = \frac{\beta}{\pi I}\int_{\gamma-i\infty}^{\gamma+i\infty}\{\left[\frac{4w^2-\sin^2\pi w)^2 M}{(2w+1)\phi(\alpha,w)[\sin 2w(\pi-\alpha)+2w\sin\alpha]} - \frac{(4w^2-\sin^2\pi w)N}{(2w+1)\phi(\alpha,w)}\right] I(\phi) + \frac{(4w^2-1)[4w^2-\sin^2\pi w)R}{\phi(\alpha,w)} J(\phi) + \frac{I(\phi)}{(2w+1)[\sin 2w(\pi-\alpha)+2w\sin\alpha]}\}\,dw \qquad ..(B.10)$$

Writing in terms of real quantity, it is possible to evaluate this integral by Simpson's rule. The tangential, radial and shear stresses are determined from the properties of Mellin transform inversion as,

$$(\sigma_{\phi\phi})_f/T = \frac{1}{\pi i}\int_{\gamma-i\infty}^{\gamma+i\infty}\frac{2w}{2w+1}\{2(2w+1)(4w^2-1)\,.\left[\frac{4w^2-\sin^2\pi w}{\phi(\alpha,w)}P + \frac{\sin 2w(\pi-\alpha)+2w\sin\alpha}{\phi(\alpha,w)}Q\right].\,J(\phi) - \left[\frac{4w^2-\sin^2\pi w}{\phi(\alpha,w)}L + \frac{\sin 2w(\pi-\alpha)+2w\sin\alpha}{\phi(\alpha,w)}K\right].\,I(\phi)\}\,(\rho)^{-2w-1}\,dw$$

$$+\frac{\beta}{\pi i}\int_{\gamma-i\infty}^{\gamma+i\infty}\{\left[\frac{(4w^2-\sin^2\pi w)^2 M}{(2w+1)[\sin 2w(\pi-\alpha)+2w\sin\alpha]\phi(\alpha,w)}\right.$$

$$\begin{aligned}
(\sigma_{\rho\phi})_f/T = {} & \frac{1}{\pi i} \int_{\gamma-i\infty}^{\gamma+i\infty} \Big\{ 4w(2w+1) \Big[\frac{(4w^2-\sin^2\pi w)\,P}{\phi(\alpha,w)} \\
& + \frac{(\sin 2w(\pi-\alpha) + 2w\sin\alpha)\,Q}{\phi(\alpha,w)} \Big] J_1(\phi) \\
& - 2w \Big[\frac{(4w^2-\sin^2\pi w)L}{\phi(\alpha,w)\,(4w^2-1)} + \frac{(\sin 2w(\pi-\alpha)+2w\sin\alpha)K}{(4w^2-1)\,\phi(\alpha,w)} \Big] \\
& I_1(\phi) \Big\} \; (\rho)^{-2w-1}\, dw \\
& + \frac{\beta}{\pi i} \int_{-i\infty}^{+i\infty} \Big\{ \Big[\frac{(4w^2-\sin^2\pi w)\,(4w^2-\sin^2\pi w)\,M}{(4w^2-1)\,\phi(\alpha,w)\,\big[\sin 2w(\pi-\alpha) + 2w\sin\alpha\big]} \\
& - \frac{(4w^2-\sin^2\pi w)\,N}{(4w^2-1)\,\phi(\alpha,w)} \Big] I_1(\phi) \\
& + \frac{(2w+1)\,(4w^2-\sin^2\pi w)\,R}{\phi(\alpha,w)} \; J_1(\phi) \\
& + \frac{I_1(\phi)}{(4w^2-1)\,\big[\sin 2w\,(\pi-\alpha) + 2w\sin\alpha\big]} \Big\} \; (\rho/a)^{-2w-1}\, dw
\end{aligned}$$

...(B.13)

I_n stands for $d^nI/d\phi^n$ and J_n for $d^n J/d\phi^n$ in the above expressions. The roots of the equation $\sin 2w(\pi-\alpha) + 2w\sin\alpha = 0$ are also determined and given in Table B.2. The line integral was chosen in such a manner that, $\frac{1}{2} < \gamma < \frac{1}{2} + \lambda(\alpha)$, where $\frac{1}{2} + \lambda(\alpha)$ is the first real root of the equation $\phi(z) = 0$ for $z > 1/2$. Therefore, at any given angle ϕ , by applying residue theorem the stresses can be calculated from the above expressions.

TABLE B.2 First Few Real Roots of $\sin 2w(\pi-\alpha) + 2w \sin\alpha = 0$; $\mathrm{Re}(w) > 1/2$ for Notch opening Angle, $\alpha = 1^{\circ}$

Sl. No.	Roots
1	0.5056
2	0.9999
3	1.5169
4	1.9999
5	2.5281
6	2.9999
7	3.5394
8	3.9999
9	4.5507
10	4.9998
11	5.5620
12	5.9997
13	6.5734
14	6.9996
15	7.5848
16	7.9994
17	8.5963
18	8.9991
19	9.6078
20	9.9988
21	10.6194
22	10.9984
23	11.6312
24	11.9979
25	12.6430
26	12.9973
27	13.6549
28	13.9965
29	14.6670
30	14.9956
31	15.6793
32	15.9946
33	16.6917
34	16.9934
35	17.7044

APPENDIX C

MULTIPOLE STRUCTURE ASYMPTOTIC EXPANSION FOR EXTERIOR POTENTIAL FIELD OF AN ELLIPSOIDAL REGION

"Multipole expansion" method is well established in gravitational, electromagnetic and nuclear charge field theories. Recently, considerable attention has been focussed on finding out the Boussinesq - Neuber- Papkovitch displacement potentials of spherical and, ellipsoidal regions at an external point by applying 'multipole structure' field theory. Miyamoto [165], Hashin [166] and Chen [167] made successful attempts to solve spherical region problems by using multipole asymptotic expansion for a row of spheres. For a three-dimensional closed surface occupying a region inside an infinite continuum can be regarded as the sum of a large number of components of equivalent potentials at the origin. Thus, the closed body like ellipsoid can be replaced by a series of strengths: monopole, dipole, quadrupole, octupole etc. charges at the origin. As Newtonian potentials are always additive at an exterior point, the potential due to identical density distribution bodies with these multipole-components can be added at that point for both the first and second bodies.

Therefore, with respect to the origin of the first body O, a multipole expansion is obtained for each potential term. Fig. 5.1 shows an illustration of multipole charge distribution for an ellipsoid concerning the Taylor's expansion in three dimensions.

Let
$$\frac{1}{R} = \frac{1}{|\mathbf{r}-\mathbf{r}_0|} = \sum_{n=0} (-1)^n (1/n!) \left(x_0 \frac{\partial}{\partial x} + y_0 \frac{\partial}{\partial y} + z_0 \frac{\partial}{\partial z}\right)^n . (1/r) \qquad (C.1)$$

where , (1/r) is the Newtonian exterior potential for an ellipsoidal region, obtained by solving Laplace's equation in three dimensions.

Kellog [189] in his book on classical field theory has given the exterior (1/r) field potentials for an ellipsoid as well as oblate and prolate spheroids. From Kellog's result, for a prolate spheroid of $a > b(= c)$, having 'a' as semi-major and 'b' as semi-minor axes, the exterior potential at a point (x_1, x_2, x_3) is given as :

For the first cavity with respect to the origin O,

$$(1/r) \equiv \phi(x_1, x_2, x_3) \text{ per unit volume of the cavity}$$

$$\phi(x_1,x_2,x_3) = \frac{3}{2} \cdot \frac{1}{a^2 b^2} \left[\frac{4x_1^2 - 2x_2^2 - 2x_3^2 - 4(a^2-b^2)}{4\sqrt{a^2 - b^2}} \right.$$
$$. \log_e \sqrt{\left(\frac{s - 2\sqrt{a^2 - b^2}}{s+2\sqrt{a^2 - b^2}}\right)}$$
$$\left. + \frac{(2x_1^2 - x_2^2 - x_3^2)\, s^2 - 8x_1^2 (a^2 - b^2)}{s\,\{s^2 - 4(a^2 - b^2)\}} \right] \quad ...(C.2)$$

where,
$$s = x_1 + \sqrt{(x_2^2 + x_3^2)} + \sqrt{\{x_1^2 + x_2^2 + x_3^2 + a^2 - b^2 + 2x_1\sqrt{(a^2 - b^2)}\}} + \sqrt{\{x_1^2 + x_2^2 + x_3^2 + a^2 - b^2 - 2x_1\sqrt{(a^2 - b^2)}\}}$$

For the second cavity with respect to the origin of the first cavity, 0, the potential $(1/r) \equiv \Omega(x_1, x_2, x_3)$ per unit volume can be written as

$$\Omega = \phi(x_1 - \alpha, \ x_2 - \beta, x_3) \qquad (C.3)$$

Thus, both the origins of the spheroids are situated on $x_3 = 0$ plane, but their equatorial and meridian planes are at α and β distances apart respectively (Fig. 1.14).

As we are given some distribution of charge inside a finite spheroidal region, and that we have represented by a density function $\rho(x_0, y_0, z_0)$ of position inside the region, then the potential at an exterior point due to this charge distribution can be expressed as

$$\Theta_P = \iiint (1/R) \ \rho(x_0, y_0, z_0) \, dx_0 \, dy_0 \, dz_0 \, . \qquad \ldots (C.4)$$

Applying multinomial theorem on Eqn. (C.1), we get,

$$\frac{1}{R} = \sum_n \sum_j \sum_k \frac{(-1)^n x_0^j y_0^k z_0^{n-j-k}}{(n-j-k)! \ j! \ k!} \frac{\partial^n}{\partial x^j \, dy^k \, dz^{n-j-k}} (1/r) \qquad \ldots (C.5)$$

Thus, we have been able to replace the total potential by a series of multipole asymptotic equivalent moment structures. The details of the method of evaluating dipole, quadrupole, octupole moment tensor triple integrals over spheroidal region are given by Band [188] and Landau and Lifshitz [191]. Thus, in our problem, this method has been used to obtain additive potential expressions for $\bar{\phi}$, $\bar{\phi}_{x_o}$, $\bar{\phi}_{y_o}$, $\bar{\phi}_{z_o}$, $\bar{\phi}_{x_o^2}$, $\bar{\phi}_{y_o^2}$ and $\bar{\phi}_{z_o^2}$. All moment coefficients are determined with respect to the origin of the first cavity. Hence, the final expressions obtained are as follows:

$$
\begin{aligned}
\bar{\phi}/V = {} & \phi + \tfrac{1}{2}(a^2/5 \,.\, \phi_{,11} + 2b^2/5 \,.\, \phi_{,22}) + \frac{1}{24}\big[3/35.\ a^4\phi_{,1111} \\
& + 12/35.b^4\phi_{,2222} + 12/35.a^2b^2\,\phi_{,1122}\big] + \Omega - \\
& (\alpha\,\Omega_{,1} + \beta\,\Omega_{,2}) + \tfrac{1}{2}\big[\alpha^2\,\Omega_{,11} + \beta^2\,\Omega_{,22} + 2\alpha\beta\,\Omega_{,12}\big] \\
& - \frac{1}{6}\big[(\alpha^3 + 3/5.\,\alpha a^2)\,\Omega_{,111} + (3/5.\beta b^2 + \beta^3)\Omega_{,222} \\
& + 3/5.\alpha b^2(\Omega_{,122} + \Omega_{,133}) + 3/5.\beta(a^2\,\Omega_{,112} + b^2\Omega_{,233})\big] \\
& + 1/24.\big[3/35.\ a^4\,\Omega_{,1111} + 3/35.b^4(\Omega_{,2222} + 2\Omega_{,2233} \\
& + \Omega_{,3333}) + \frac{6}{35}\,a^2b^2(\Omega_{,1122} + \Omega_{,2233}) \\
& + \frac{6}{5}\alpha^2a^2\,\Omega_{,1111} + \alpha^4\,\Omega_{,1111} + \frac{6}{5}\beta^2b^2\,\Omega_{,2222} \\
& + \beta^4\,\Omega_{,2222} + 6(\alpha^2b^2/5. + a^2\beta^2/5 + \alpha^2\beta^2)\,\Omega_{,1122}
\end{aligned}
$$

$$+ \frac{6}{5}\alpha^2 b^2 \Omega_{,1133} + \frac{6}{5}\beta^2 b^2 \Omega_{,2233} + 4\left(\frac{3}{5} a^2\alpha\beta + \alpha^3\beta\right)\Omega_{,1112}$$

$$+ 4\left(\frac{3}{5} b^2\alpha\beta + \alpha\beta^3\right)\Omega_{,1333} + \frac{12}{5}\alpha\beta\, b^2 \Omega_{,1233}\Big] - \frac{1}{120}\Big[\left(\frac{3}{7}\alpha a^4\right.$$

$$\left. + 2\alpha^3 a^2 + \alpha^5\right)\Omega_{,11111} + \left(\frac{3}{7}\beta b^4 + 2b^2\beta^3 + \beta^5\right)\Omega_{,22222}$$

$$+ 5\left(\frac{3}{35}\alpha b^4 + \frac{6}{5}\alpha\beta^2 b^2 + \alpha\beta^4\right)\Omega_{,12222} + 5\left(\frac{3}{35} a^4\beta +\right.$$

$$\left. + \frac{6}{5}\alpha^2\beta a^2 + \beta\alpha^4\right)\Omega_{,11112} + \frac{3}{7}\beta b^4 \Omega_{,23333} + \frac{3}{7}\alpha b^4 \Omega_{,13333}$$

$$+ 10\left(\frac{3}{35} a^2 b^2\beta + \frac{a^2\beta^3}{5} + \frac{3}{5}\alpha^2\beta b^2 + \alpha^2\beta^3\right)\Omega_{,11222}$$

$$+ 10\left(\frac{3}{35} a^2 b^2\alpha + \frac{\alpha^3 b^2}{5} + \frac{3}{5}\alpha\beta^2 a^2 + \alpha^3\beta^2\right)\Omega_{,11122}$$

$$+ 10\left(\frac{3}{35} b^4\beta + \frac{\beta^3 b^2}{5}\right)\Omega_{,22233} + 10\left(\frac{3}{35} a^2 b^2\alpha + \frac{\alpha^3 b^2}{5}\right.$$

$$\left. + \frac{3}{5}\alpha\beta^2 a^2 + \alpha^3\beta^2\right)\Omega_{,11133} + 30\left(\frac{\alpha^2\beta b^2}{5} + \frac{\beta a^2 b^2}{35}\right)\Omega_{,11233}\Big]$$

$$+ O(d^{-6})$$

$$\ldots\text{(C.6)}$$

$$
\begin{aligned}
\frac{\bar{\phi}_{x_o}}{V} = & -\frac{a^2}{5}\phi_{,1} - \frac{1}{6}\Big[\frac{3}{35}a^4\phi_{,111} + \frac{6}{35}a^2b^2\phi_{,122}\Big] \\
& + \alpha\Omega - \Big[\big(\frac{a^2}{5} + \alpha^2\big)\Omega_{,1} + \alpha\beta\Omega_{,2}\Big] \\
& + \frac{1}{2}\Big[\big(\frac{3}{5}\alpha a^2 + \alpha^3\big)\Omega_{,11} + \big(\alpha\beta^2 + \frac{\alpha b^2}{5}\big)\Omega_{,22} \\
& + \frac{\alpha b^2}{5}\Omega_{,33} + 2\big(\alpha^2\beta + \beta a^2/5\big)\Omega_{,12}\Big] \\
& - \frac{1}{6}\Big[\frac{3}{35}a^4\Omega_{,111} + \frac{3}{35}a^2b^2\big(\Omega_{,122} + \Omega_{,133}\big) \\
& + \big(\frac{6}{5}\alpha^2a^2 + \alpha^4\big)\Omega_{,111} + \big(\frac{3}{5}\alpha\beta b^2 + \alpha\beta^3\big)\Omega_{,222} \\
& + 3\big(\alpha^3\beta + \frac{3}{5}\alpha\beta a^2\big)\Omega_{,112} + 3\big(\alpha^2b^2/5 + \frac{\beta^2a^2}{5} + \alpha^2\beta^2\big)\Omega_{,122} \\
& + \frac{3}{5}\big(\alpha\beta a^2\Omega_{,233} + \frac{3}{5}\alpha^2b^2\Omega_{,133}\Big] + \frac{1}{24}\Big[\big(\frac{3}{7}\alpha a^4 \\
& + 2\alpha^3a^2 + \alpha^5\big)\Omega_{,1111} + \big(\frac{3}{35}\alpha b^4 + \frac{6}{5}\alpha\beta^2b^2 + \alpha\beta^4\big)\Omega_{,2222} \\
& + 3\alpha b^4\Omega_{,3333}/35 \\
& + 6\big(\frac{3}{35}\alpha a^2b^2 + \alpha^3b^2/5 + \frac{3}{5}\alpha\beta^2a^2 + \alpha^3\beta^2\big)\Omega_{,1122} \\
& + 6\big(\frac{3}{35}\alpha a^2b^2 + \frac{\alpha^3b^2}{5}\big)\Omega_{,1133} + 4\big(\frac{3}{35}\beta a^2b^2 + \frac{3}{5}\alpha^2\beta b^2 \\
& + a^2\beta^3/5 + \alpha^2\beta^3\big)\Omega_{,1333} + 4\big(\frac{3}{35}\beta a^4 + \frac{6}{5}\alpha^2\beta a^2 + \alpha^4\beta\big)\Omega_{,1112} \\
& + 6\big(\alpha b^4/35 + \alpha\beta^2b^2/5\big)\Omega_{,2233} + 12\big(a^2b^2\beta/35 \\
& + \alpha^2\beta b^2/5\big)\Omega_{,1233}\Big] + 0(d^{-6})
\end{aligned}
\tag{C.7}
$$

$$
\begin{aligned}
\frac{\bar{\phi}_{y_o}}{V} = & - \frac{b^2}{5}\phi_{,2} - \frac{1}{6}\left[\frac{6}{35} b^4 \phi_{,222} + \frac{3}{35} a^2 b^2 \phi_{,112} \right] \\
& + \beta\Omega - \left[\left(\frac{b^2}{5} + \beta^2 \right) \Omega_{,2} \right] + \frac{1}{2}\Big[(a^2/5 + \alpha^2)\beta\Omega_{,11} \\
& + \left(\beta^3 + \frac{3}{5}\beta b^2 \right)\Omega_{,22} + \beta b^2/5 . \Omega_{,33} + 2\alpha\, (\beta^2 + b^2/5)\Omega_{,12} \Big] \\
& - \frac{1}{6}\Big[\beta \left(\alpha^3 + \frac{3}{5}\alpha\, a^2 \right)\Omega_{,111} + \left(\frac{3}{35} b^4 + \frac{6}{5}\beta^2 b^2 + \beta^4 \right)\Omega_{,222} \\
& + 3\alpha \left(\beta^3 + \frac{3}{5}\beta b^2 \right)\Omega_{,122} + 3(a^2 b^2/35 + \alpha^2 b^2/5 \\
& + \beta^2 a^2/5 + \alpha^2\beta^2)\Omega_{,112} + 3(b^4/35 + \beta^2 b^2/5)\Omega_{,233} \\
& + \frac{3}{5}\alpha\beta b^2 \Omega_{,133} \Big] + \frac{1}{24}\Big[\left(\frac{3}{35}\beta a^4 + \frac{6}{5}\alpha^2\beta\, a^2 + \alpha^4 \right)\Omega_{,1111} \\
& + \left(\frac{3}{7} b^4 + 2\beta^3 b^2 + \beta^5 \right)\Omega_{,2222} + \frac{3}{35}\beta\, b^4 \Omega_{,3333} \\
& + 6\left(a^2\beta^3/5 + \frac{3}{35} a^2 b^2 \beta + \frac{3}{5}\alpha^2\beta b^2 + \alpha^2\beta^3 \right)\Omega_{,1122} \\
& + 6\beta \left(\alpha^2 b^2/5 + \frac{3}{35} a^2 b^2 \right)\Omega_{,1133} + 6\left(\frac{3}{35}\beta b^4 + \beta^3 b^2/5 \right) \\
& \Omega_{,2233} + 4\left(\frac{3}{35}\alpha\, a^2 b^2 + \frac{3}{5}\alpha\beta^2 a^2 + \alpha^3 b^2/5 + \alpha^3\beta^2 \right) \\
& \Omega_{,22333} + 4\alpha \left(\frac{3}{35} b^4 + \frac{6}{5}\beta^2 b^2 + \beta^4 \right)\Omega_{,1333} \\
& + \left(\frac{12}{35}\alpha\, b^4 + \frac{12}{5}\alpha\,\beta\, b^2 \right)\Omega_{,1233} \Big] + 0\,(d^{-6})
\end{aligned}
\qquad \ldots(C.8)
$$

$$
\begin{aligned}
\frac{\bar{\Phi}_{z_o}}{V} = & - \frac{b^2}{5}\phi_{,3} - \frac{1}{6}\Big[\frac{6}{35} b^4 \phi_{,333} + \frac{3}{35} a^2 b^2 \phi_{,113} \Big] \\
& - \frac{b^2}{5}\Omega_{,3} + \frac{1}{2}\Big[\frac{2}{5}\beta b^2 \Omega_{,23} + \frac{2}{5}\alpha b^2 \Omega_{,13} \Big] \\
& - \frac{1}{6}\Big[\frac{3}{35} b^4 \Omega_{,333} + \frac{6}{5}\alpha\beta b^2 \Omega_{,123} \\
& ++ \Big(\frac{\beta^2 b^2}{5} + \frac{b^4}{35} \Big)\Omega_{,223} + \Big(\frac{\alpha^2 b^2}{5} + \frac{a^2 b^2}{35} \Big)\Omega_{,1133} \Big] \\
& + \frac{1}{24}\Big[\Big(\frac{12}{35}\beta b^4 + \frac{4}{5}\beta^3 b^2 \Big)\Omega_{,2223} \\
& + \frac{12}{35}\beta b^4 \Omega_{,2333} + \frac{12}{35}\alpha b^4 \Omega_{,1333} \\
& + 4\Big(\frac{3}{35}\alpha a^2 b^2 + \frac{\alpha^3 b^2}{5} \Big)\Omega_{,1113} \\
& + \Big(\frac{12}{35}\alpha b^4 + \frac{12}{5}\alpha\beta^2 b^2 \Big)\Omega_{,1223} \\
& + 12\beta\Big(\frac{a^2 b^2}{35} + \frac{\alpha^2 b^2}{5} + \frac{a^2\beta^2}{5} + \alpha^2\beta^2 \Big)\Omega_{,1123} \Big] \\
& + O(d^{-6}) \\
= & \ 0 \qquad \text{(C.9)}
\end{aligned}
$$

$$
\begin{aligned}
\frac{\bar{\phi}_{x_o^2}}{V} = {} & \frac{a^2}{5}\phi + \frac{1}{2}\left[\frac{3}{35} a^4 \phi_{,11} + \frac{2}{35} a^2 b^2 \phi_{,22} \right] \\
& + \left(\alpha^2 + \frac{a^2}{5} \right) \Omega - \left[\left(\frac{3}{5} \alpha a^2 + \alpha^3 \right) \Omega_{,1} + \right. \\
& + \left. (\beta a^2/5 + \alpha^2 \beta)\, \Omega_{,2} \right] + \frac{1}{2} \left[\left(\frac{3}{35} a^4 \right. \right. \\
& + \left. \frac{6}{5} a^2 \alpha^2 + \alpha^4 \right) \Omega_{,11} + (\alpha^2 \beta^2 + a^2 b^2/35 + \alpha^2 b^2/5 \\
& + \beta^2 a^2/5)\Omega_{,22} + (a^2 b^2/35 + \alpha^2 b^2/5)\, \Omega_{,33} \\
& + \left. \left(\frac{6}{5} \alpha \beta a^2 + 2 \alpha^3 \beta \right) \Omega_{,12} \right] - \frac{1}{6} \left[\left(\frac{3}{7} a^4 \alpha \right. \right. \\
& + \left. 2a^2 \alpha^3 + \alpha^5 \right) \Omega_{,111} + \left(\frac{3}{35} a^2 b^2 \beta + a^2 \beta^3/5 \right. \\
& + \left. \frac{3}{5} \alpha^2 \beta b^2 + \alpha^2 \beta^3 \right) \Omega_{,222} + 3\left(\frac{3}{35} a^4 \beta + \frac{6}{5} \alpha^2 \beta a^2 \right. \\
& + \left. \alpha^4 \beta \right) \Omega_{,112} + 3\left(\frac{3}{35} \alpha a^2 b^2 + \alpha^3 b^2/5 + \frac{3}{5} \alpha \beta^2 a^2 \right. \\
& + \left. \alpha^3 \beta^2 \right) \Omega_{,122} + 3(\beta a^2 b^2/35 + \alpha^2 \beta b^2/5)\, \Omega_{,233} \\
& + \left. 3\left(\frac{3}{35} \alpha a^2 b^2 + \alpha^3 b^2/5 \right) \Omega_{,133} \right] + 0(d^{-6})
\end{aligned}
\qquad \ldots \text{(C.10)}
$$

$$
\begin{aligned}
\frac{\bar{\phi}_{y_o^2}}{V} = {} & \frac{b^2}{5}\phi + \frac{1}{2}\left[\frac{a^2 b^2}{35} \phi_{,11} + \frac{4}{35} b^4 \phi_{,22} \right] + \left(\frac{b^2}{5} + \beta^2 \right) \Omega \\
& - \left[\alpha (b^2/5 + \beta^2)\, \Omega_{,1} + \left(\frac{3}{5} \beta b^2 + \beta^3 \right) \Omega_{,2} \right] \\
& + \frac{1}{2} \left[(a^2 b^2/35 + \alpha^2 b^2/5 + \beta^2 a^2/5 + \alpha^2 \beta^2)\, \Omega_{,11} \right. \\
& + \left(\frac{3}{35} b^4 + \frac{6}{5} \beta^2 b^2 + \beta^4 \right) \Omega_{,22} + \left(\frac{b^4}{35} + \frac{\beta^2 b^2}{5} \right) \Omega_{,33}
\end{aligned}
$$

$$+ 2\alpha\left(\frac{3}{5}\beta b^2 + \beta^3\right)\Omega_{,12}\Big] - \frac{1}{6}\Big[\left(\frac{3}{5}\alpha\beta^2 a^2 + \alpha^3\beta^2\right.$$

$$\left. + \frac{3}{35}\alpha a^2 b^2 + \alpha^3 b^2/5\right)\Omega_{,111} + \left(\frac{3}{7}\beta b^4 + 2\beta^3 b^2 + \beta^5\right).$$

$$\Omega_{,222} + 3\left(\frac{3}{35}a^2 b^2 \beta + \frac{3}{5}\alpha^2\beta b^2 + a^2\beta^3/5 + \alpha^2\beta^3\right).$$

$$\Omega_{,112} + 3\alpha\left(\frac{3}{35}b^4 + \frac{6}{5}\beta^2 b^2 + \beta^4\right)\Omega_{,122}$$

$$+ 3\left(\frac{3}{35}\beta b^4 + \beta^3 b^2/5\right)\Omega_{,233} + 3\alpha\left(b^4/35 + \beta^2 b^2/5\right).$$

$$\Omega_{,133}\Big] + O(d^{-6}) \qquad \text{(C.11)}$$

$$\frac{\bar{\Phi}_{z_o^2}}{V} = \frac{b^2}{5}\phi + \frac{1}{2}\Big[\frac{a^2 b^2}{35}\phi_{,11} + \frac{4}{35}b^4\phi_{,33}\Big] + \frac{b^2}{5}\Omega$$

$$- \Big[\alpha b^2\Omega_{,1} + \frac{\beta b^2}{5}\Omega_{,2}\Big] + \frac{1}{2}\Big[\left(a^2 b^2/35 + \alpha^2 b^2/5\right)$$

$$\Omega_{,11} + \left(b^4/35 + \beta^2 b^2/5\right)\Omega_{,22} + \frac{3}{35}b^4\Omega_{,33} +$$

$$\frac{2}{5}\alpha\beta b^2\Omega_{,12}\Big] - \frac{1}{6}\Big[\left(\frac{3}{35}\alpha a^2 b^2 + \alpha^3 b^2/5\right)\Omega_{,111}$$

$$+ \left(\frac{3}{35}\beta b^4 + \beta^3 b^2/5\right)\Omega_{,222} + 3\beta\left(\alpha^2 b^2/5 + a^2 b^2/35\right)$$

$$\Omega_{,112} + 3\alpha\left(b^4/35 + \beta^2 b^2/5\right)\Omega_{,122} + \frac{3}{35}\beta b^4\Omega_{,233}$$

$$+ \frac{3}{35}\alpha b^4\Omega_{,133}\Big] + O(d^{-6})$$

$$\ldots\text{(C.12)}$$